Detection and quantification of caffeine in the coffee industry using imprinted polymers and bare carbon electrodes

A thesis submitted in partial fulfilment of the requirements of the Degree of Doctor of Philosophy

Luca Redivo

School of Biological and Chemical Science,
Queen Mary University of London

Supervisor: Professor Marina Resmini

2018

Statement of originality

I, Luca Redivo, confirm that the research included within this thesis is my own work or that where it has been carried out in collaboration with, or supported by others, that this is duly acknowledged below and my contribution indicated. Previously published material is also acknowledged below.

I attest that I have exercised reasonable care to ensure that the work is original, and does not to the best of my knowledge break any UK law, infringe any third party's copyright or other Intellectual Property Right, or contain any confidential material.

I accept that the College has the right to use plagiarism detection software to check the electronic version of the thesis.

I confirm that this thesis has not been previously submitted for the award of a degree by this or any other university.

The copyright of this thesis rests with the author and no quotation from it or information derived from it may be published without the prior written consent of the author.

Signature: 

Date: 28/08/2018

Details of collaboration and publications:

The computational work described in chapter 2 was done in collaboration with Dr D. Di Tommaso (Queen Mary University of London), Professor F. Berti (Università degli Studi di Trieste) and Professor M. Peressi (Università degli Studi di Trieste). The experimental validation of the computational data was carried out by Ms R. Anastasiadi (Queen Mary University of London), and her data were included for completeness of chapter 2. This work has resulted in a manuscript currently under submission with the following authorships and title: L. Redivo, R. Anastasiadi, M. Pividori, F. Berti, M. Peressi, D. Di Tommaso, M. Resmini. Self-association of adenosine analogues: combined computational and isothermal titration calorimetry studies of caffeine and paraxanthine.

The work described in chapter 4 was done in collaboration with Dr M. Stredanský (Biorealis Ltd.), Professor L'. Svorc (Slovak University of Technology in Bratislava) Dr L. Navarini (illy caffè S.p.A.) and Ms E. De Angelis (illy caffè S.p.A.). Part of the work

is published in RS open science: L. Redivo, M. Stredansky, E. De Angelis, L. Navarini, M. Resmini, Ĺ Švorc. Bare carbon electrodes as simple and efficient sensors for the quantification of caffeine in commercial beverages. *Royal Society open science*, **2018**, 5, 172146.

During my placement at Biorealis Ltd. I have contributed to the preparation of a short communication which is now published in Food Chemistry:

M. Stredansky, L. Redivo, P. Magdolen, A. Stredansky, L. Navarini. Rapid sucrose monitoring in green coffee samples using multienzymatic biosensor. *Food Chemistry*, **2018**, 254, 8-12.

This thesis is dedicated to my beloved **Chiara** for having changed my life in better and for always being supportive.

And to my wonderful **family** especially because they have taught me to be an independent thinker.

Abstract

Food quality control is a mandatory task in the food industry, and for coffee manufacturers, one of the key target compounds is caffeine, because of its well-known biological effects and currently expensive analytical methods are employed for caffeine quantification. This project was thought with the aim of developing a cost-effective caffeine sensor for application in industrial environments. Two main approaches were investigated: i) the use of imprinted polymers; ii) electrochemical using bare carbon electrodes.

Chapter 1 is the main introduction, it focuses on the importance of food quality control, the limitation of the methodologies currently employed and it presents the advantages of using imprinted polymers recognition and electrochemistry signal transduction.

Chapter 2 presents data related to studies of self-association of caffeine in water using a novel computational approach. The wider applicability of the method was assessed by studying self-association of paraxanthine and the results were validated via a collaboration with Miss R. Anastasiadi who employed isothermal titration calorimetry.

Chapter 3 describes the synthesis of MIPs in water, starting with the selection of the functional monomers: HPTS (8-hydroxypyrene-1,3,6-trisulfonic acid, trisodium salt). The polymerisation conditions were optimised in terms of solvent to be used, initiator content, temperature and total monomer concentration. Afterwards, the polymers were synthesised, characterised, and preliminary data on the rebinding ability towards caffeine were presented.

Chapter 4 focuses on electrochemical methods for the detection of caffeine using bare carbon electrodes. A voltammetric method for accurate determination of caffeine in beverages was developed. Based on the encouraging results obtained, further studies on the applicability of electrochemical methods for coffee quality analysis were done. A second method was developed for simultaneous detection of caffeine and polyphenols and an amperometric chemosensor for sucrose determination was acquired and its applicability for the analysis of green coffee beans was evaluated.

Acknowledgements

This work was possible thanks to the help and constant support of many people: professors from different universities, industrial supervisors and friends. Among them Professor Marina Resmini deserves my greatest thankfulness for having selected me for this PhD student position, for her constant supervision also during the numerous placements outside London, and her training not only in scientific subjects but also in many transferable skills. She has contributed significantly to my personal growth at this early stage of my professional carrier and she gave me a solid base of skills which will help me to build my future.

Given the peculiar structure and multidisciplinarity of the project I was fortunate to carry out my research in different places and under the co-supervision of many experts. During the first months of this project, I worked in close collaboration with Professor Federico Berti and Professor Maria Peressi. Before this experience, computational chemistry was a mystery to me, but thanks to their training, support and by directly applying computational methods for my research, I started understanding it and appreciating its utility. The intriguing preliminary results accomplished, led to further exploration of this area of chemistry by collaborating with Dr. Di Tommaso at Queen Mary University of London who has also considerably contributed to my development in computational chemistry. During the last year and a half, I have experienced scientific research in the industrial sector. Initially, in Bratislava, under the supervision of Dr Miroslav Stredanský, I was introduced to the world of electrochemical sensors. Thanks to his passion for electrochemistry and the collaboration with Professor Lubomir Svorc, I was captured by the simplicity and reliability of electrochemical sensing devices. Moreover, I am grateful to Dr. Luciano Navarini. He supervised me during my 9 months of work at illy caffè and allowed me to further explore the applicability of electrochemistry for coffee quality analysis; which was not a technique previously employed at illy caffè.

All the work carried out during this three years was also achieved thanks to the friendship and companionship of many friends and colleagues. Starting from my friends in London, I want to thank the members of Professor Resmini's group: Katarzyna, Paolo, Ana, Gabriele, Giorgio, Fosca, Angelo, Rosemarie, Charlie (in particular for proofreading part of the thesis) and Fei for their helpful discussions and happy moments in the lab and outside. I would like to acknowledge all the IPCOS team: Dr. Matjaz Peterka, Dr.

Adriano Savoini, Dr. Max Fabian, Ana Oreski, Dr. Annabelle Scott, Ms. Claire Diot-Lefebvre. I am thankful to all the people working in Aroma Lab of illy caffè including, Elisabetta, Silvia, Valentina, Marianna, Veronica, Lorenzo and Delvana for their contagious love for coffee, their scientific knowledge, and making the working place a welcoming and friendly environment. My special thanks go to the current and previous students of lab 330-333 of the Dipartimento di Chimica of the Università degli studi di Trieste and in particular Giorgia, Martina, Anggy and the two Elene who have seen my professional growth from being a Master student up to now. During all this time, they have been genuine friends to share happy moments and difficulties.

The financial support from European Union's Horizon 2020 research and innovation programme (grant agreement number 642014 IPCOS) is gratefully acknowledged.

Contents

Statement of originality 2

Abstract 5

Acknowledgements 6

List of abbreviations 13

Premise 18

CHAPTER 1 Introduction 21

1.1 Food safety and quality 22

1.2 Coffee safety and quality 23

1.3 Coffee, the plant and the steps towards the final cup 25

1.4 Sensor and food analysis 28

1.5 Electrochemical sensor development and application for food analysis 30

1.6 Molecular Imprinted Polymers (MIPs) 34

1.6.1 MIPs in sensor technology 38

1.7 Conclusion 39

1.8 Aims and objectives 40

1.9 References 41

CHAPTER 2 45

Computational studies on the self-association process of caffeine and paraxanthine 45

2.1 Introduction 46

2.2 Results and discussion 50

2.2.1 Assessment of the method 51

2.2.2 Computational results on self-association of caffeine 63

2.2.3 Computational results on paraxanthine self-association process 71

2.2.4 Comparative experimental studies on caffeine and paraxanthine self-association in aqueous solutions. 78

2.3 Conclusion and future work..... 85

2.4 Computational details 87

2.4.1 Density functional theory methods 87

2.4.2 Assessment of the method 88

2.4.3 Probing the potential energy surface of caffeine and paraxanthine dimer 88

2.4.4 Generation of caffeine trimer and tetramer 89

2.5 Experimental details 89

2.5.1 Reagents and instrumentations 89

2.5.2 X-ray crystallographic analysis of paraxanthine 89

2.5.3 Dissociation experiments by isothermal titration calorimetry (ITC) 90

2.6 References..... 91

CHAPTER 3 94

Synthesis and characterisation of MIPs specific for caffeine 94

3.1 Introduction..... 95

3.2 Results and discussion 95

3.2.1 Selection of the functional monomer..... 95

3.2.2 Optimisation of the polymerisation conditions 116

3.2.3 Studies of the analyte binding properties of the nanogels 127

3.3 Conclusion and future work 137

3.4 Materials and Methods 137

3.4.1 Reagents 137

3.4.2 Apparatus 138

3.4.3 General procedures 140

3.4.4 Proton NMR peak assignation 142

3.4.5 Synthesis of a polymerizable analogue of HPTS 143

3.4.6 General procedure of polymer synthesis and composition calculations 145

3.4.7 Reactivity of caffeine during radical polymerisation 146

3.4.8 Optimisation of initiator concentration 147

3.4.9 Polymer synthesis LR5, 6, 7, 8, 9, 10 148

3.4.10 Sample preparation for DLS and ζ-potential measurements 149

3.4.11 UV-vis calibration curve of MIP and NIP 149

3.4.12 Precipitation of polymer using centrifugation 150

3.4.13 Separation of polymer from dispersion using centrifugal filters 150

3.4.14 Analyte rebinding experiment procedure 150

3.5 References 152

CHAPTER 4 154

Electrochemical sensor for coffee analysis 154

4.1 Bare glassy carbon electrode as sensing platform for caffeine determination 155

4.1.1 Introduction 155

4.1.2 Results and discussion 158

4.1.3 Conclusion and future work 185

4.2 Screen-printed carbon paste electrode for simultaneous determination of polyphenols and caffeine in coffee brews 187

4.2.1 Introduction 187

4.2.2 Results and discussion 194

4.2.3 Conclusion and future work 228

4.3 Sucrose in green coffee beans 229

4.3.1 Introduction 229

4.3.2 Results and discussion 231

4.3.3 Conclusion 235

4.4 Chapter conclusion and future work 236

4.5 Materials and methods 237

4.5.1 Chemicals and reagents 237

4.5.2 Apparatus 237

4.5.3 Sample preparation 239

4.5.4 Electrochemical Measurements 240

4.5.5 Comparative UHPLC and HPLC method 245

4.5.6 Measurement procedures for the determination of sucrose in green coffee beans. 245

4.5.7 Data analysis and statistical evaluation 245

4.6 References 246

Chapter 5 251

General conclusion and future work 251

Annex I 255

More details on the computational study presented in chapter 2 255

Computational studies using quantum mechanics 256

Quantum Mechanics calculations 256

Computational studies of chemical processes in solution. 263

Computational study on the self-association process of organic molecules 266

References 269

Annex II 270

Published articles and manuscript submitted 270

List of abbreviations

1-MA-3MI-Br	1-Methylacrylate-3-methylimidazolium bromide
3-CQA	3-Caffeoylquinic acid
3-D	Three dimensional
3-TAA	3-Tiopheneacetic acid
3,4-DiCQA	3,4-Dicaffeoylquinic acid
3,5-DiCQA	3,5-Dicaffeoylquinic acid
3-FQA	3-Ferruloylquinic acid
4-CQA	4-Caffeoylquinic acid
4,5-DiCQA	4,5-Dicaffeoylquinic acid
4-FQA	4-Ferruloylquinic acid
5-CQA	5-Caffeoylquinic acid
5-FQA	5-Ferruloylquinic acid
AA	Acrylic acid
ACN	Acetonitrile
Am	Acrylamide
Amp	Amperometry
APS	Ammonium persulfate
AuNPs	Gold nanoparticles
BAP	2,6-Bis(acrylamido)pyridine
$\mathbf{a_x}$	Activity of the X chemical species

CAF	Caffeine
CAF_{ox}	Oxidised product of caffeine
CGA(s)	Chlorogenic acid(s)
Cm	Total monomer concentration
CP	Chronopotentiometry
CPE	Carbon paste electrode
CV	Cyclic voltammetry
DFT	Density functional theory
DLS	Dynamic light scattering
DMF	Dimethylformamide
DP	Differential pulse
DPV	Differential pulse voltammetry
DVB	Divinylbenzene
E	Oxidation potential for a chemical process (V)
E_0	Standard oxidation potential for a chemical process (V)
EDOT	3,4-Ethylenedioxythiophene
EFSA	European Food Safety Authority
EGDMA	Ethylene glycol dimethylacrylate
F	Faraday constant (96485 C mol^{-1})
FM	Functional monomer
GCE	Glassy carbon electrode
GGA	Generalized gradient approximation

GLU	D-(+)-Glucose
GO	Graphene oxide
HDFT	Hybrid density functional theory
HMDFT	Hybrid meta density functional theory
HPLC	High-performance liquid chromatography
HPTS	8-Hydroxypyrene-1,3,6-trisulfonic acid trisodium salt
IPCOS	Imprinted polymers as coffee sensors
IUPAC	International Union of Pure and Applied Chemistry
ITC	Isothermal titration calorimetry
LOD	Limit of detection
LOQ	Limit of quantification
MAA	Methacrylic acid
MBA	*N,N′*-Methylenebis(acrylamide)
MD	Molecular dynamics
MeOH	Methanol
MIS	Molecularly imprinted siloxane
MIPs	Molecularly imprinted polymers
MTES	methyltriethoxysilane
MWCNT	Multi-walled carbon nano tubes
NMR	Nuclear magnetic resonance
NIP	Non imprinted polymer
Ox	Oxidation reaction

ox	Oxidised form of a chemical species
PBS	Phosphate-buffered saline
PCR	Polymerise chain reaction
PEDOT	Poly(3,4-ethylenedioxy thiophene)
PGE	Pencil graphite electrode
PSS	Poly(4-styrenesulfonic acid)
PTES	Triethoxyphenylsilane
PTFE	Polytetrafluoroethylene
PX	Paraxanthine
ppm	Part per million
QMUL	Queen Mary University of London
R	Universal gas constant
RSD	Relative standard deviation
rpm	revolutions per minute
r.m.m.	Relative molecular mass
Red	Reduction reaction
red	Reduced form of a chemical species
s	Second(s)
SPCE	Screen-printed carbon paste electrode
SUC	Sucrose
SW	Square wave
SWAdSV	Square wave adsorption stripping voltammetry

SWV	Square wave voltammetry
T	Absolute temperature (K)
TB	Theobromine
TEMED	Tetramethylethylenediamine
TEOS	Tetraethylorthosilicate
THEO	Theophylline
THF	Tetrahydrofuran
TLC	Thin-layer chromatography
TMPTA	Trimethylolpropane triacrylate
TRIM	trimethylolpropane trmethacrylate
UHPLC	Ultra high-performance liquid chromatography
UNITS	Università degli studi di Trieste
UV-Vis	Ultraviolet-visible
V	Volt
Z	Number of electrons exchanged in an electrochemical process

Premise

The following thesis reports the key scientific findings achieved during the research conducted as an early-stage researcher of the IPCOS project (www.ipcos.qmul.ac.uk). This project was funded by the European Commission (grant agreement number 642014) as a European industrial doctorate programme, targeting the development of novel sensing platforms to be applied in the coffee industry. A multidisciplinary approach and a strong collaboration between 3 academic and 3 industrial partners were key in bringing innovation to this sector. A total of 5 researchers were involved and several target compounds present in coffee, and responsible for its quality, were identified. My work focused, in particular, on caffeine as the main target. A requirement of a European industrial doctorate program is that the researchers have to experience both the academic and industrial research environment for an equal amount of time. Therefore, as part of the 36 months project I was seconded to the industrial partners for a total of 18 months; more specifically 9 months with Biorealis, in Bratislava (Slovakia) and 9 months with illy caffè in Trieste (Italy). In addition, I spent 6 months at the start of the project based at the University of Trieste.

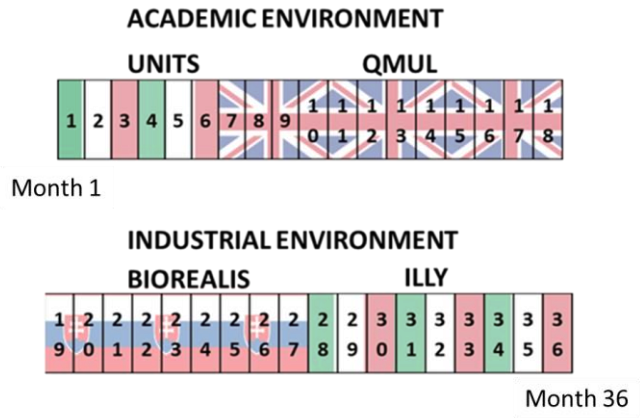

Figure 0.1. Time table of the research project as part of a European industrial doctorate program requiring to experience both the academic and industrial research environment for 18 months each. UNITS is the Università degli studi di Trieste in Italy. QMUL is Queen Mary University of London based in the United Kingdom. The industrial secondments were at Biorealis (located in Slovakia) and illy Caffè base in Italy.

As the figure above clearly shows, the research was carried out in academic environments (Università degli Studi di Trieste (Italy) and Queen Mary University of London) as well as that industrial (Biorealis Ltd and illy Caffè). Each placement involved a different field of research, with the first secondment in Italy focusing on computational methodos for studying the interaction between caffeine and small organic molecules. The application of computational studies was subsequently further explored during the work done at QMUL, where also the synthesis of molecularly imprinted polymers selective to caffeine was studied. On the other hand, during the secondments at the two industrial partners, the application of an electrochemical sensor for the determination of caffeine and other key target compounds present in coffee was explored. Given the multidisciplinary aspects of the project, each placement required dedicated training for specific methodologies (computational chemistry, polymer synthesis and characterisation, electrochemistry and chemical analysis of food products). The tight schedule that had to be followed did limit in some cases the depth of the study and did not allow for further investigations. Nevertheless, two articles were published as a result of the work carried out. The first one reported the development of a simple procedure for caffeine determination using a bare carbon electrode (L. Redivo, M. Stredansky, E. De Angelis, L. Navarini, M. Resmini, Ĺ Švorc. *R.Soc.Opensci;* **2018**, 5, 172146-172150.). A second communication describing the applicability of an amperometric sensor for sucrose determination in green coffee was also published this year (M. Stredansky, L. Redivo, P. Magdolen, A. Stredansky, L. Navarini; *Food chemistry* **2018**, 254, 8-12); this article was the result of an ongoing collaboration between illy Caffè and Biorealis. The data obtained using this sensor are presented in Chapter 4 of this thesis. Moreover, a second full paper on the application of quantum mechanical DFT studies to understand the self-aggregation process of caffeine in solution (L. Redivo, R.

Anastasiadi, M. Pividori, F. Berti, M. Peressi, D. Di Tommaso, M. Resmini. Self-association of adenosine analogues: combined computational and isothermal titration calorimetry studies of caffeine and paraxanthine) is currently submitted. The manuscripts are attached at the end of this thesis in annex II.

CHAPTER 1 Introduction

1.1 Food safety and quality

Food quality and safety are topics that have been gaining prominence in recent years, mainly as a result of increased public awareness and expectations.[1] Consequently, local and international authorities have continued to raise the number of regulations and directives that must be followed in order to ensure that traded food products fulfil safety requirements, before reaching the final consumer.[1,2] The words 'safety' and 'quality' in relation to a product are sometimes used as synonyms, although in fact *food safety* specifically refers to the healthiness of the product, while *quality* refers to its appearance (i.e. colour, shape, presence of defects), smell, taste, authenticity (origin, variety) and is not related to the possible toxicity of the product.[3] Ensuring that food has high quality and safety is a key priority also from an economics point of view, given that unhealthy food can result in high medical costs (for example due to poisoning). Furthermore it can have an impact on exports and tourism, since countries linked with unhealthy foods are less prone to be import-export partners and tourism destinations.[1] With regards to food safety in particular, there is a key requirement based on the identification of toxic agents which can be both biological (bacteria, fungi and viruses) and chemical (pesticides, herbicides, antibiotics, etc.), and can arise from problems in the manufacturing processes but also from poor environmental hygiene.[1] The spectra of targets is wide, and different techniques are required for the identification of the diverse compounds and toxins. In addition, due to globalisation, the origin of any product can be thousands of kilometres away from the final consumer therefore, ensuring high standards in the whole food supply chain has become even more challenging.[4] To identify biological hazards, the most common techniques employed are polymerase chain reaction (PCR) panels and antigen-based assays[5], while in the case of toxic chemicals the preferred analytical tool is chromatography, commonly coupled with UV-vis detectors.[6–9] These techniques are accurate, sensitive, robust and can be applied to a broad range of compounds. However,

these techniques are often expensive in terms of initial purchase and maintenance costs. In many cases they require sample pre-treatments, which can be performed only by highly trained personnel. Inevitably, the costs associated with food quality certification are high and, not surprisingly, there is a demand for more cost-effective sensing devices and simple procedures.[10] The substantial interest and need for the development of cost-effective sensors has also been recently highlighted by a number of published reviews covering the topic of sensors developed for food analysis.[11–15] The triggers of food safety and their implications on the industrial and scientific sectors are summarised in Scheme 1.1, below.

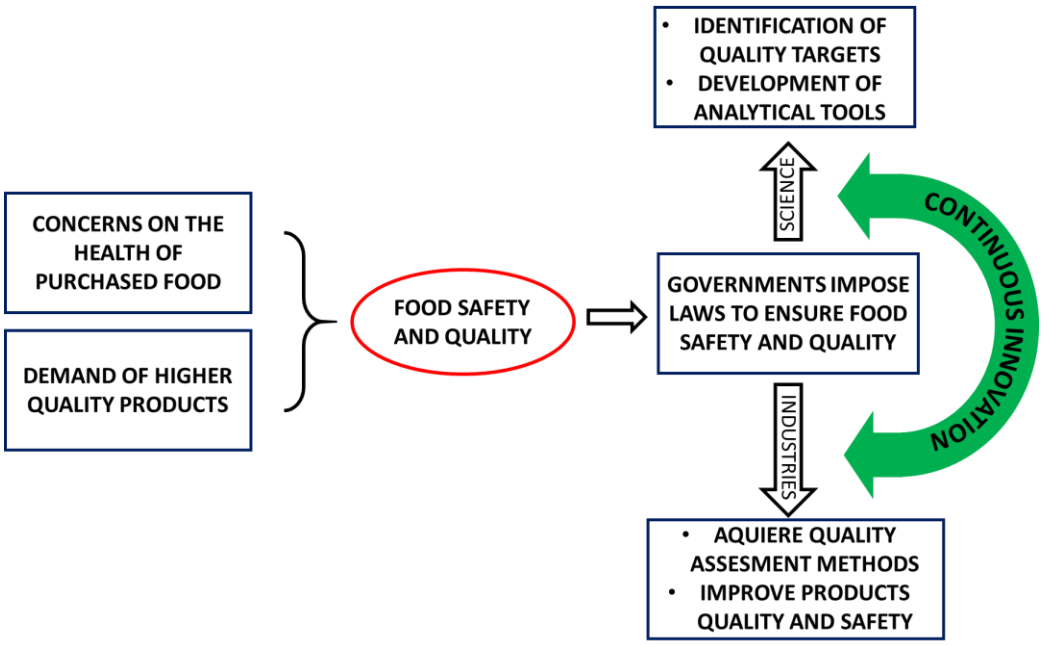

Scheme 1.1. Diagram summarising the importance of food safety and how the industrial and scientific sectors collaborate to ensure high quality and safety standards for commercialised food products.

1.2 Coffee safety and quality

In the case of coffee containing products, there are both health and quality concerns linked to its commercialisation and intake. Regarding safety assessment, it is fundamental to ensure that coffee is cultivated and stored in the correct environment to avoid the formation of moulds and toxins (such as Ochratoxin A).[16,17] In addition, the

European Food Safety Authority (EFSA) established that coffee is one of the primary sources of acrylamide (Am) intake in the human diet; although Am levels in coffee are considerably lower than the legislation limits, its content must still be monitored.[18,19] Coffee quality has been gaining increased levels of attention over the past decade thanks also to the consumers' increased knowledge of coffee varieties, brewing methods and coffee benefits.[20] Scientific research has identified many compounds present in coffee and their beneficial biological effects (antioxidant activity, glucose level regulation, stimulant). In the past, coffee was primarily linked to caffeine and its stimulating activity and when overused, heart disease.[21,22] The structural formula of caffeine is reported in Scheme 1.2.

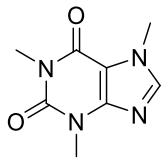

Scheme 1.2.Structural formula of caffeine.

However, the coffee brew contains hundreds of biologically active compounds, with polyphenols being the most abundant, showing antioxidant, hepatoprotective properties, and they are also glucose regulators that help to prevent diabetes.[23,24] In particular, green coffee is rich in 5-caffeoylquinic acid (Scheme 1.3) which is subsequently degraded during the roasting process.

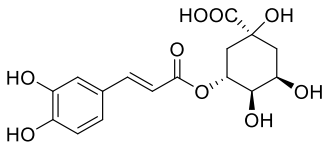

Scheme 1.3. Structural formula of 5-caffeoylquinic acid the most abundant polyphenol present in green coffee beans.

Therefore, given the recent discoveries on the additional benefits of drinking coffee, the increase in popularity of coffee brews, together with a demand for high-quality products,

it is not surprising that the request for cost-effective sensors to be used routinely for quality assessment has become a priority within the coffee industry. In the next section, a brief description of coffee plants and the typical manufacturing process used to obtain the final product are presented to facilitate the understanding of the principal factors of the production process that affect the final quality of the product.

1.3 Coffee, the plant and the steps towards the final cup

Coffee is a commodity with a worldwide production of hundreds of millions of bags yearly.[25] The brew is obtained from the seed of *Coffea* plants which are cultivated in tropical regions. Even though nowadays Brazil is the greatest coffee producer, coffee's origins are from Africa and the discovery of its properties can be dated back to the ninth century. Until the beginning of the 17th century the consumption of coffee brews was limited to Arabic communities, who then exported this tradition to Europe and subsequently a more worldwide cultivation of coffee plants started and diffused.[26,27] There are more than 100 varieties of coffee plants, however, only *Coffea* Canephora and *Coffea* Arabica have a considerable economic importance, contributing more than 90 % of the total coffee trade market.[27] There are some differences between the two plants from a morphological point of view and regarding the quality of the final brew. Arabica plants grow at higher altitude (between 1200 and 2000 meters), prefer soils with higher acidity ($4 \leq pH \geq 6$), and the seeds are usually oval (Figure 1.1A). Canephora plant is also called Robusta given the higher resistance to environmental stress and diseases, it is cultivated at lower altitude and the seeds are more rounded (Figure 1.1B).[28,29]

Figure 1.1. Example of Arabica (A) and Robusta (B) green coffee beans.

From a chemical point of view, Arabica seeds contain a lower amount of caffeine and chlorogenic acids compared with Robusta. However Arabica has almost double the amount of sucrose, and a higher content of trigonelline.[30–33] The structural formulae of the mentioned compounds are reported in Scheme 1.4.

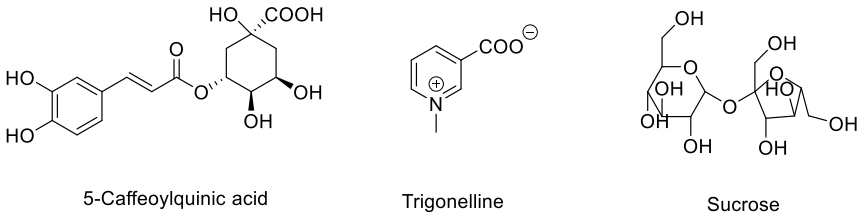

Scheme 1.4. Structural formulae of 5-Caffeoyl quinic acid (the most abundant chlorogenic acid present in green coffee), trigonelline and sucrose.

A coffee plant can produce fruits for 30 years and one single plant can lead up to 1 kg of green beans yearly. The coffee fruit, also called the cherry, changes colour during maturation from green to red, and inside each cherry two green beans can be found, covered by a protective layer (called silver skin), and the cherry pulp. After being harvested, the fruits are depulped and washed to obtain the coffee beans, which are then dried until the moisture level is below 12% (to prevent the formation of mould during transportation). Subsequently, coffee roasters purchase coffee beans and ship the product to their factories where the beans are roasted. The roasting stage is one of the most crucial steps since it is responsible for the development of the aroma and final taste of coffee (more information about the roasting process is presented in Chapter 4). The progressive

change in colour during roasting is shown in the Figure 1.2. Once roasted, coffee beans are ground, packed and shipped to reach the final consumer.[34]

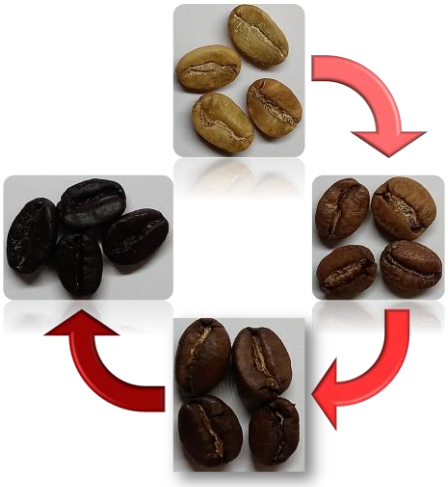

Figure 1.2. Change in colour of coffee beans during the roasting process. At the top green coffee beans and clockwise different steps during roasting.

From the coffee plant to the final brew there is a long journey and many factors may affect the final quality of the beverage. Starting from the raw beans, the first factor affecting the cup quality is the variety of coffee employed. Arabica beans are higher in quality and lead to a final brew with lower acidity and a richer aroma, probably thanks to the higher content of sucrose and trigonelline.[35–37] On the other hand Robusta, although inferior in quality, has a lower price and most of coffee roasters prefer to sell a mixture of Robusta and Arabica to maintain a low price. In contrast, some other roasters like illy Caffè are proud to sell 100 % Arabica products with a higher quality and price. Besides the plant species, a second important factor is the local soil composition and climate, which influences year by year the production and quality. Interestingly, in recent years, coffee consumers have shown an increased interest in mono-origin coffee products, which now have a significant market importance.[34] Although all these factors play an important role in the quality of the coffee cup, there are no doubts that without proper manufacturing processes, high coffee quality cannot be achieved. Cultivation techniques play a key role; for example the amount of sun/shade impacts the coffee

cherry growth and the properties of the obtained beans. For high quality, it is important to ensure a proper amount of shade since this leads to a more constant temperature throughout the day and also allows the development of local fauna, which acts as a natural insecticide.[38,39] Nevertheless, in some places coffee plants are exposed to full sun to accelerate the maturation of the coffee cherries. In addition, once the cherries are ripe, there are numerous procedures to harvest and remove the beans out of the cherries, leading to variability in quality (a more detailed discussion is presented in Chapter 4).[40,41] Once the green beans are shipped to the roasting companies, it is essential to ensure that the roasting stage is performed properly, as it is responsible for the flavour and aroma of the roasted beans. Moreover, care has to be taken to ensure that the product is not burnt due to overroasting.[42–44] Finally, the grinding stage plays the key role to ensure that there is the correct contact between hot water and coffee powder during the brewing stage.[34]

To summarise, coffee quality can be affected at different stages. Given the increased demand for high-quality products, it is important that coffee producers ensure high quality and have analytical methods for its assessment. There is a tendency to improve quality and monitor closely all production stages, from when the green coffee bean has harvested to the final roasting step. This type of research is often based on a trial and error approach involving also the work of a sensory panel. Although sensory panel members are trained and work to provide a reliable opinion, it is not an objective approach. Therefore, analytical instrumentations measuring key compounds responsible for coffee quality are an important target.[13]

1.4 Sensor and food analysis

Based on the International Union of Pure and Applied Chemistry (IUPAC) a chemical sensor is: *"a device that transforms chemical information, ranging from the concentration of a specific sample component to total composition analysis, into an*

analytically useful signal".[45] The structure of a generic sensor can be divided into three essential components: (i) the signalling unit which is responsible for giving rise to an analytical signal once the analyte is recognised; (ii) the recognition unit which is able to bind the analyte; and (iii) the transducer which connects the two units. A simplified representation of a chemical sensor and its components is depicted in Scheme 1.5 below.

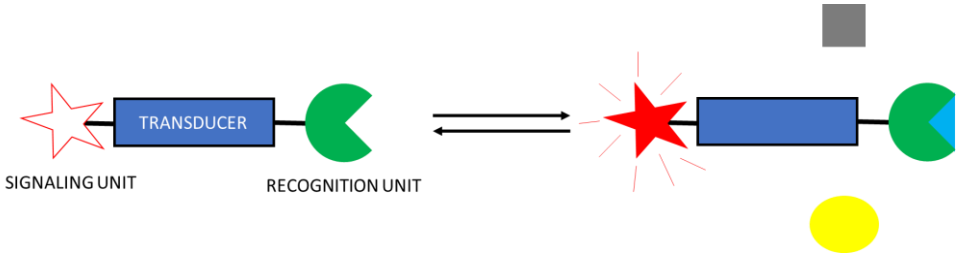

Scheme 1.5. Representation of a chemical sensor and its major components, namely the signalling, transducer and recognition units.

Some examples of the type of signal generated are reported below. [45]

- Optical: where a change in absorbance, fluorescence, refractive index, light scattering is measured.
- Electrochemical: in which a change in current, or capacity is measured.
- Mass-sensitive: for instance, piezoelectric or acoustic waves devices, where the small change in mass upon analyte binding leads to a change in resonance frequency of the bulk or surface acoustic wave.
- Magnetic: where a change in magnetic properties is observed in the presence of the analyte.
- Heat measuring device: where a change in heat is measured as the signal.

Among these different signalling units, the most studied are optical and electrochemical devices, given the relatively low costs of the components, their demonstrated high sensitivity, easy miniaturisation and wide applicability for different analytes. The recognition unit is responsible for the selectivity of the device, preferably binding only the target analyte and, ideally, no possible interferences. Several biological examples of recognition units have been reported, including small peptides[46–48] and enzymes[49–51] as

well as chemical, e.g. molecularly imprinted polymers (MIPs)[52–54]. Across this variety of sesnors, it is possible to categorise them into two classes; general sensors, showing wide applicability for different analytes, and specific systems, which are developed towards a particular target molecule. General sensors have the advantages of being simple, cost-convenient and the time required to develop the sensor is usually shorter. In this thesis an example of this sensor type is presented in Chapter 4 where the applicability of bare carbon electrode is described for the detection of caffeine and polyphenols. One of the drawbacks of this approach is that the target compound must be detectable by itself, for example in the case of an electrochemical sensor, it must be electrochemically active. On the other hand, selective sensors can also be applied for molecules which are not detectable by themselves. However, this selectivity requires longer time for its development and the associated cost of the final devices is higher. One of the techniques to achieve selectivity is the use of MIPs, which can bind and selectivelly detect a target compound.

1.5 Electrochemical sensor development and application for food analysis

Among different electrochemical techniques, voltammetry and amperometry are the most employed for the development of electrochemical analytical tools. In the case of voltammetry, the flow of current is measured while the potential is linearly varied. When the appropriate potential is reached, the oxidation/reduction of the target analyte occurs and current is recorded (Figure 1.3). Three electrodes are necessary to perform the experiments: (i) a working electrode (where the oxidation or reduction of the analyte is occurring); (ii) a reference electrode which is employed to measure the potential between it and the working electrode; (iii) a counter electrode which measures current between it and the working electrode. A potentiostat is then responsible to vary the potential,

measure the current and send the data to a computer, which is used to process and analyse the data. A schematic representation of an electrochemical cell set-up is reported in Figure 1.3.

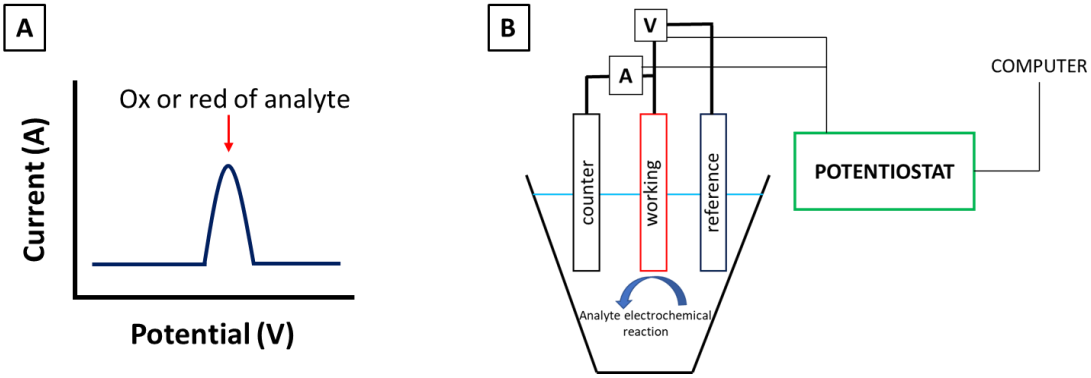

Figure 1.3. (A) A typical differential pulse voltammogram. Current is observed when the oxidation or reduction potential of the target compound is reached. (B) A schematic representation of an electrochemical cell with counter, working and reference electrodes connected to the potentiostat which is linked to a computer for data handling. The flow of current (A) is measured between the counter and working electrode (where the electrochemical reaction occurs). The potential (V) is measured between the working and reference electrode.

The analyte molecule must reach the electrode surface to be oxidised/reduced. When voltammetry is performed in the presence of a supporting electrolyte under stagnant solutions, molecule transport is only possible by diffusion. As a consequence, at the beginning, the concentration of the analyte in proximity to the working electrode is equal to the concentration of the bulk solution (Figure 1.4 (1)). In Figure 1.4 B the change in analyte concentration near the electrode is depicted, using as example an oxidation reaction process.

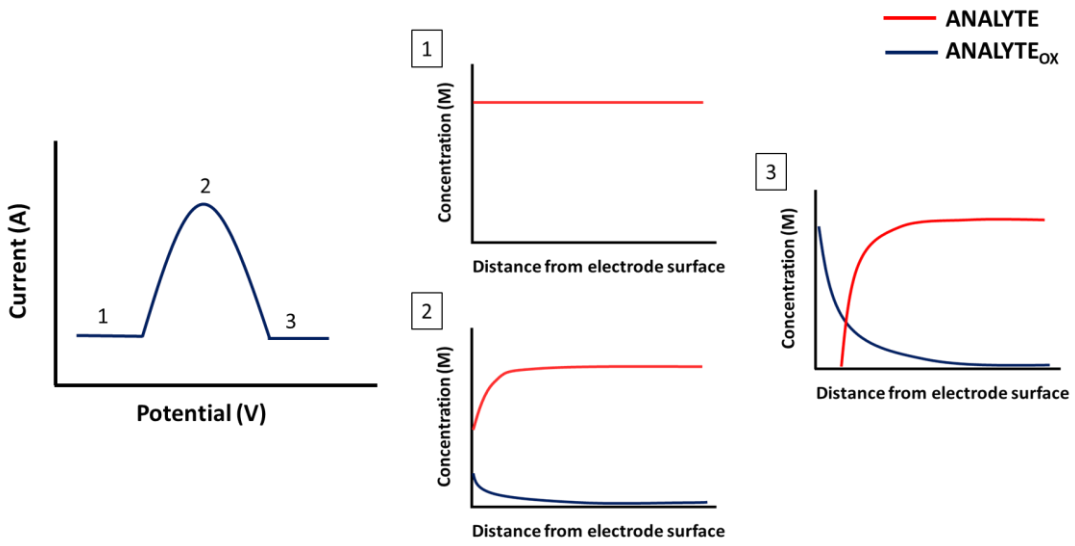

Figure 1.4.Graphical representation on how the concentration profile of analyte and the oxide product changes during the voltammogram profile. At point 1 the potential is not sufficient to trigger the reaction and the concentration at the electrode surface is equal to the concentration in the bulk solution (point 1). When the appropriate potential is reached the analyte concentration in proximity to the electrode is reduced and no current is produced anymore (point 3).

With regards to amperometric measurements, a three electrode set up (Figure 1.4 B) is also employed, however, during amperometry the current is measured over time at a constant potential. In this thesis, amperometric measurements were performed under stirring conditions in which case the current increased until a steady-state value was reached. No matter which electrochemical technique is employed, current is proportional to the amount of electrons exchanged during the electrochemical reaction and, therefore, it is directly proportional to the amount of analyte present in solution (see scheme below).

$$Analyte_{red} \leftrightarrows Analyte_{ox} + n\,electron$$

Scheme 1.6.General reaction scheme of a redox process.

As a consequence, a calibration curve constructed as a dependence of current intensity on the analyte concentration can be obtained and used for analytical purposes. Moreover, the area under the peak (Figure 1.4 A) is directly related to the analyte concentration and can be employed to determine the amount of the target compound. During the

development of an electrochemical sensor, it is important to find an appropriate material to be used as the working electrode. This is because this material must be suitable to reach the potential required for the electrochemical reaction to occur. Furthermore, it is essential to find experimental conditions and instrumental parameters that would allow for recording of a well pronounced signal (regarding for instance, width, signal-to-noise ratio, etc).

The most straightforward application of electrochemistry as an analytical tool is when the analyte is an electrochemically active compound. However, when the electroactive analyte cannot directly be reduced or oxidised at the electrode, it is necessary to use a different approach. For instance, it is in some cases possible to use enzymatic reactions to oxidise the analyte in the mediator presence. Subsequently, the mediator is reduced by the enzyme and the reduced form of the mediator is oxidised at the working electrode surface thus generating an electrochemical signal.[55–57] The amperometric biosensor that was employed for monitoring sucrose in green coffee beans (Chapter 4) was based on the above-described approach and a graphical representation of a general biosensor mechanism is presented below in Scheme 1.7.

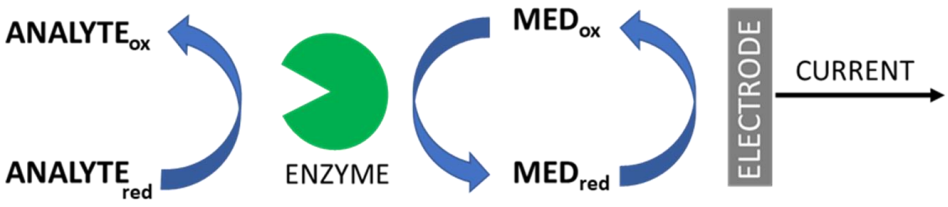

Scheme 1.7.Schematic representation of an electrochemical biosensor, where the oxidation of the analyte is catalysed by an enzyme which is also responsible for the reduction of a mediator which is then oxidised on the electrode surface, thus generating a measurable signal.

When no enzymes are available to catalyse the oxidation of the analyte, other strategies can be used. For instance, it is possible to electrodeposit a molecularly imprinted polymer film and monitor the electrochemical signal of a mediator. In this case, when

the analyte is present, it will bind to the cavities of the imprinted material, thus blocking the mediator from reaching the surface of the electrode. Then a decrease in the current signal is observed.[58,59] The above are just some examples to show how the working electrode can be modified and how electrochemistry can be widely applied for electrochemically inactive compounds.

In the literature, several recent examples can be found on the application of electrochemical sensors for the analysis of food samples. In many cases the targets are compounds with important biological effects (vitamins[60,61], carcinoges compounds[62–65]), dyes[66,67] and flavouring compounds[68,69]. The applicability has been demonstrated both for solid food and beverages, and in most of the cases carbon-based electrodes were employed, given their relatively low cost and wide anodic and cathodic potential range. If required the electrode surface can be modified to increase sensitivity or to ensure selectivity.[72] The development of innovative electrochemical sensors is therefore a vibrant research field. It can be envisaged that in the coming years it will remain a hot topic in scientific research.

1.6 Molecular Imprinted Polymers (MIPs)

The idea behind molecular imprinting in polymers is to build three-dimensional cavities inside a polymer matrix, which are complementary in size and shape to a target compound. To achieve molecular recognition that way, a target molecule is used as the template during the polymer synthesis. During the polymerisation two different monomers are essential: (i) the functional monomer, which is responsible for interacting with the template molecule; (ii) the crosslinker, which allows forming of a 3 D network and incurring rigidity to the polymer. The general synthetic scheme is depicted in Scheme 1.8.

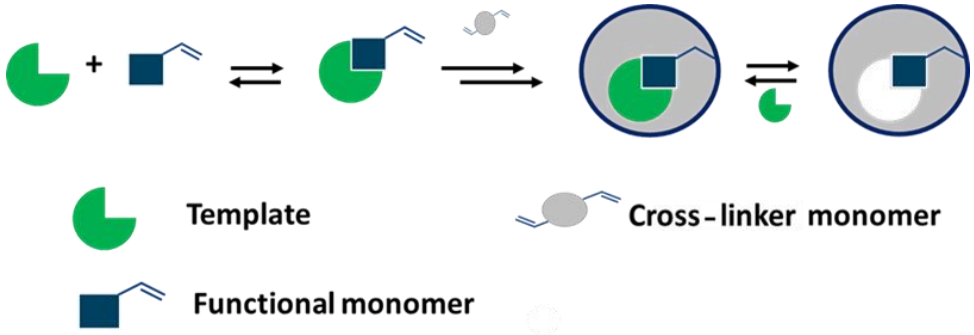

Scheme 1.8.General reaction scheme for the MIP synthesis.

During the polymerisation, three main synthetic steps can be distinguished. The first one is the pre-polymerisation stage in which the functional monomer and the template react to form the pre-polymerisation complex. Two major types of interaction can be defined: (i) the covalent one (where a chemical bond is formed between the template and the functional monomer); and (ii) non-covalent (where non-covalent interaction like hydrogen, ionic bond or hydrophobic interactions, are formed). Based on the types of interaction, two processes can be defined, called covalent and non-covalent imprinting. In recent years, most of the interest has focused towards the non-covalent approach, because the removal of the template after polymerisation is easier and a wider range of compounds can be imprinted with less limitations on the functional groups present.[73] In the second step, the functional monomer is copolymerised with a cross-linker using an initiator triggered by thermal or photochemical activation.[74,75] The last step is the template removal from the polymer matrix, which leaves vacant cavities in the polymer that are complementary to the target molecules in size, shape and position of recognising sites, so that they can specifically rebind. When compared to their biological analogues (enzymes, antibodies or peptide) the advantages of MIPs are: lower cost, higher stability (to extreme pH, temperature, etc.), remarkable mechanical stability, longer lifetime, easier regeneration and sterilisation. Moreover, they can be applied to a wider range of analytes.[76] The first example of MIPs was reported by Wulff and Sarhan in 1972,[76] and

since then the synthesis of imprinted materials has attracted attention of many researchers. Different synthetic strategies have been proposed including bulk, high dilution, emulsion and solid-state polymerisation just to name the most common approaches.[74] Among the different approaches, high dilution radical polymerisation was employed in this thesis (Chapter 3) giving its advantages regarding simplicity of the synthesis, homogeneity of the obtained material and possibility to obtain nanogels of high active surface area forming stable colloidal systems in solution.[77–79] No matter what synthetic approach is investigated, the high selectivity of the imprinted material can be achieved through the optimisation of some key conditions. Firstly, it is fundamental to ensure the formation of the pre-polymerisation complex in solution. In fact, if non-complexed template and functional monomer are present during polymerisation, these can form binding sites with lower affinity and selectivity, leading to low homogeneity of the recognising sites and a decrease in the molecular recognition properties. Scheme 1.9 below, represents visually the effect of low complexation between functional monomer and template molecule, using a simplified description where the pre-polymerisation complex formation is the only parameter affecting the binding sites obtained.

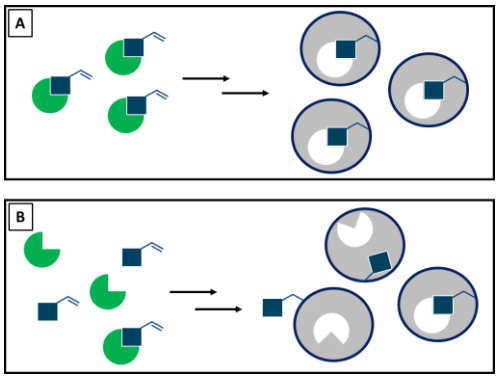

Scheme 1.9. Graphical representation of the effect of the degree of pre-polymerisation complex formation on the homogeneity of the obtained MIP. In case A, all template molecules form a stable pre-polymerisation complex with the functional monomer and the obtained polymer shows homogeneous recognising sites and of correct orientation. In case B, unbound functional monomer and template molecule are present during the synthesis and the homogeneity of the final polymers is lower.

It is therefore essential to select an appropriate functional monomer that is able to form a thermodynamically stable complex with the template. For this purpose, several experimental and computational approaches are available.[80,81] For instance, isothermal titration calorimetry (ITC) experiments can be employed to determine in one single experiment the thermodynamic stability and the stoichiometry of the pre-polymerisation complex.[82] Alternatively, titration experiments can be performed using UV-vis, fluorescence, or NMR spectroscopy [83]. In particular, the latter was applied herein and is described in Chapter 3 for the selection of the functional monomer.

Beside the pre-polymerisation complex, the polymer formulation plays an important role in the recognition ability of the MIPs. In fact, the ratio of the functional monomer to the cross-linker will affect the rigidity of the synthesised polymer. More rigid polymers are obtained with a higher degree of cross-linking.[79] As a consequence, the recognising site will be more selective towards the template because other compounds cannot adapt to this site. On the other hand, highly cross-linked polymers will limit the release of the template molecules after polymerisation as well as the rebinding.[79] With regards to the size of the polymer, it is possible to control it by varying the total monomer concentration, with more diluted conditions leading to smaller particles. Moreover, the amount of the initiator plays a role in the polymer size since higher amounts of the initiator will favour the formation of shorter-chain polymers. In conclusion, specific recognition properties depicted in Scheme 1.9 are obtained only after a careful selection of the monomers and optimisation of the polymer formulation and synthetic conditions using a trial and error approach. To evaluate the efficiency of the imprinting process, it is a common practice to synthesise the MIPs and a non-imprinted analogue (NIP), where the same synthetic conditions are maintained but the template is not present during the synthesis. The comparison of the two polymers in terms of rebinding abilities and

selectivity is then called imprinting factor (IF) and is used as an indication of the effectiveness of the imprinting approach.

1.6.1 MIPs in sensor technology

MIPs can be employed as recognition units in chemo sensors. Several examples have already been reported in literature, where imprinted materials were successfully used for the development of sensing devices. The most recent publications dealing with MIPs and food sample analysis are listed in the following table.

Table 1.1. Recent examples of MIPs based sensor for food sample analysis.

Analyte	**Application**	**Sensing Technique**	**Year**	**Ref**
Pyrethroids (Pesticide)	Vodka	Fluorescence	2017	[84]
2,4-dichlorophenoxyacetic acid (herbicide)	Vegetables	Fluorescence	2017	[85]
Acrylamide	Spiked water samples	Fluorescence	2018	[86]
Patulin (toxin from moulded food)	Apple juice	Phosphoresce	2017	[87]
N-nitroso-l-proline (Carcinogenic compound)	Grilled meat	Electrochemistry	2017	[88]
Sunset yellow (Synthetic Colorant)	Fruit juices and candies	Electrochemistry	2017	[89]
Methyl parathion (Pesticide)	Soil and vegetable	Electrochemistry	2018	[90]
Kanamycin (Antibiotic)	Honey and milk powder	Surface Plasmon Resonance	2018	[91]
Metolcarb (Pesticide)	Fruit and vegetables	Quartz Crystal microbalance	2017	[92]
Sulfonamides (antibiotics)	Egg White	Bragg diffraction shift	2018	[93]
2,4-dichlorophenoxyacetic acid (herbicide)	Milk	Surface-enhanced Raman scattering	2018	[94]

From the list above, it follows that MIPs have been applied in combination with a variety of detectors. Fluorescence spectroscopy and electrochemical methods are the most common, given that the instrumentations required are more frequently available to

researchers. Regarding target analytes, the focus is on organic compounds with different roles (herbicides, carcinogens, dyes) and the chemo-sensors were applied for the analysis of diverse food matrixes both solid and liquid. It can therefore be affirmed that MIPs are an effective and successful tools for the development of chemo-sensors in the analysis of food samples with a broad applicability.

1.7 Conclusion

To summarise, in this chapter the importance of food safety and quality assessment was presented, highlighting the demand for the development of novel, reliable and cost-efficient sensing devices. A wide variety of strategies can be investigated during the development of a chemo-sensor and two main categories can be defined, general and selective sensors. Both categories were studied and are presented in this thesis. Given the strong industrial perspective of the research, and a direct collaboration with the industrial sector, a strong interest was on the applicability of the chemo-sensor in the industrial environment. Therefore, given the simplicity of electrochemical sensors based on bare carbon electrodes, this strategy appealed as the most convenient during the 18 months industrial placement and the applicability of this general purpose sensor was demonstrated. Nevertheless, the development of a selective sensor revealing high selectivity for caffeine appealed as interesting, especially for an application when interference is an issue. Therefore, the applicability of MIPs for the selective caffeine recognition was also studied. However, given that the development of this type of a system requires longer time to be optimised and given the peculiar structure of the research project, there was not sufficient time to study their applicability and only preliminary results are presented. The aims and objectives of this thesis are described in more details in the following pages.

1.8 Aims and objectives

The industrial food sector is continuously seeking novel and more cost-effective alternatives to assess food safety and quality routinely. Driven by this industrial need, this thesis presents the development of sensors for the accurate evaluation of key compounds present in coffee, working in strong collaboration with an international coffee producer (illy caffè S.p.A. link). In particular, the target compound was caffeine, given its important biological aspects and its concentration being dependent on coffee variety and brewing method. The strategy to obtain a caffeine sensor was multidisciplinary and two principal approaches were pursued:

(i) Development of molecular imprinted polymers (MIPs) selective for caffeine

(ii) Use of bare carbon electrode for the development of an electrochemical sensor.

The work towards the development of MIPs is described in Chapters 2 and 3. In Chapter 2, quantum mechanical calculations were employed to investigate the behaviour of caffeine in solution in order to: (i) find if caffeine dimers and aggregates are stable in aqueous solutions and (ii) obtain a profile for the percentage of caffeine aggregates as a function of the total concentration. In Chapter 3 syntheses of MIPs are presented. The objectives were: (a) to find an appropriate functional monomer for the synthesis of MIPs in water; (b) to optimise the synthetic conditions for the polymerisation; (c) to study the rebinding abilities of the imprinted material obtained.

The second part of the thesis focusses on electrochemical methods using bare carbon electrodes as analytical tools for the development of sensors. This work was carried out at two industrial sites and the scope was to obtain a simple and cost-effective sensing device for caffeine determination in beverages. The interesting results obtained

subsequently led to application of the electrochemical procedures developed for the sensing of other key compounds present in coffee, in particular polyphenols and sucrose. This whole work is described in chapter 4.

Each chapter has a short introduction where the approach employed is presented together with the most recent literature data. Moreover, the role of caffeine, polyphenols and sucrose in relation to coffee quality is described in Chapter 4, along with the description of their biological effects.

1.9 References

1 F. Fung, H. S. Wang and S. Menon, *Biomed. J.*, 2018, **41**, 88–95.
2 F. Latronico, S. Correia, T. da S. Felicio, M. Hempen, W. Messens, A. Ortiz-Pelaez, P. Stella, E. Liebana and M. Hugas, *Curr. Opin. Food Sci.*, 2017, **18**, 50–55.
3 B. Geueke, K. Groh and J. Muncke, *J. Clean. Prod.*, 2018, **193**, 491–505.
4 M. M. Aung and Y. S. Chang, *Food Control*, 2014, **39**, 172–184.
5 E. P. Marder, P. R. Cieslak, A. B. Cronquist, J. Dunn, S. Lathrop, T. Rabatsky-Ehr, P. Ryan, K. Smith, M. Tobin-D'Angelo, D. J. Vugia, S. Zansky, K. G. Holt, B. J. Wolpert, M. Lynch, R. Tauxe and A. L. Geissler, *MMWR. Morb. Mortal. Wkly. Rep.*, 2017, **66**, 397–403.
6 M. Pereira da Costa and C. A. Conte-Junior, *Compr. Rev. Food Sci. Food Saf.*, 2015, **14**, 586–600.
7 M. P. Da Costa, B. D. S. Frasao, B. R. C. D. C. Lima, B. L. Rodrigues and C. A. C. Junior, *Talanta*, 2016, **152**, 162–170.
8 S. Summa, S. Lo Magro, A. Armentano and M. Muscarella, *Food Chem.*, 2015, **187**, 477–484.
9 F. S. Moraes, M. P. da Costa, V. L. de Melo Silva, R. V. de Barros Pinto Moreira, R. F. de Barros, E. T. Mársico, C. A. Conte-Junior and A. C. de Oliveira Silva, *Food Chem.*, 2017, **217**, 346–351.
10 X. Weng and S. Neethirajan, *Trends Food Sci. Technol.*, 2017, **65**, 10–22.
11 R. Gillibert, J. Q. Huang, Y. Zhang, W. L. Fu and M. Lamy de la Chapelle, *TrAC - Trends Anal. Chem.*, 2018, **105**, 185–190.
12 B. Socas-Rodríguez, J. González-Sálamo, J. Hernández-Borges and M. Á. Rodríguez-Delgado, *TrAC - Trends Anal. Chem.*, 2017, **96**, 172–200.
13 S. Kiani, S. Minaei and M. Ghasemi-Varnamkhasti, *J. Food Eng.*, 2016, **171**, 230–239.
14 V. Scognamiglio, F. Arduini, G. Palleschi and G. Rea, *TrAC - Trends Anal. Chem.*, 2014, **62**, 1–10.
15 X. Wang, S. Wang and Z. Cai, *TrAC - Trends Anal. Chem.*, 2013, **52**, 170–185.
16 S. Casal, T. Vieira, R. Cruz and S. C. Cunha, *Food Res. Int.*, 2014, **61**, 56–60.
17 T. B. S. Corra, *15Th Int. Sci. Colloq. Coffee*.
18 S. Gianni, F. Armando, M. Gabriella, R. Massimo, V. Sauro and A. Sergio, *Food Control*, 2007, **18**, 1267–1271.

19 M. Mesías and F. J. Morales, *J. Food Compos. Anal.*, 2016, **48**, 8–12.
20 B. Cheng, A. Furtado, H. E. Smyth and R. J. Henry, *Trends Food Sci. Technol.*, 2016, **57**, 20–30.
21 J. V. Higdon and B. Frei, *Crit. Rev. Food Sci. Nutr.*, 2006, **46**, 101–123.
22 I. A. Ludwig, M. N. Clifford, M. E. J. Jean, H. Ashihara and A. Crozier, *Food Funct.*, 2014, **5**, 1695–1717.
23 C. A. Rice-Evans, N. J. Miller and G. Paganga, *Free Radic. Biol. Med.*, 1996, **20**, 933–956.
24 L. Bravo, *Nutr. Rev.*, 2009, **56**, 317–333.
25 International Coffee Organisation, *Coffee Market Report*, 2018.
26 R. F. Smith, in *Coffee: Botany, Biochemistry and Production of Beans and Beverage*, eds. M. N. Clifford and K. C. Willson, Springer US, Boston, MA, 1985, pp. 1–12.
27 J. C. Herrera and C. Lambot, *The Coffee Tree-Genetic Diversity and Origin*, Elsevier Inc., 2017.
28 A. P. Davis, R. Govaerts, D. M. Bridson and P. Stoffelen, *Bot. J. Linn. Soc.*, 2006, **152**, 465–512.
29 C. Lambot, J. C. Herrera, B. Bertrand, S. Sadeghian, P. Benavides and A. Gaitán, *Cultivating Coffee Quality-Terroir and Agro-Ecosystem*, 2017.
30 N. Caporaso, M. B. Whitworth, S. Grebby and I. D. Fisk, *Food Res. Int.*, 2018, **106**, 193–203.
31 A. B. Rubayiza and M. Meurens, *J. Agric. Food Chem.*, 2005, **53**, 4654–4659.
32 B. Bertrand, D. Villarreal, A. Laffargue, H. Posada, P. Lashermes and S. Dussert, *J. Agric. Food Chem.*, 2008, **56**, 2273–2280.
33 R. M. Alonso-Salces, F. Serra, F. Remero and K. Heberger, *J. Agric. Food Chem.*, 2009, **57**, 4224–4235.
34 M. Gibson and P. Newsham, in *Food Science and the Culinary Arts*, ed. Elsevier Inc., 1st edn., 2018, pp. 353–372.
35 L. R. Cagliani, G. Pellegrino, G. Giugno and R. Consonni, *Talanta*, 2013, **106**, 169–173.
36 R. C. Alves, S. Casal, M. R. Alves and M. B. Oliveira, *Food Chem.*, 2009, **114**, 295–299.
37 C. Campa, J. F. Ballester, S. Doulbeau, S. Dussert, S. Hamon and M. Noirot, *Food Chem.*, 2004, **88**, 39–43.
38 F. M. DaMatta, *F. Crop. Res.*, 2004, **86**, 99–114.
39 R. G. Muschler, *Coffee Growing, Process. Sustain. Prod. A Guideb. Grow. Process. Traders, Res.*, 2008, 391–418.
40 S. Knopp, G. Bytof and D. Selmar, *Eur. Food Res. Technol.*, 2006, **223**, 195–201.
41 Y. Koshiro, M. C. Jackson, C. Nagai and H. Ashihara, *Eur. Chem. Bull.*, 2015, **4**, 378–383.
42 J. K. Moon, S. U. N. Hyui Yoo and T. Shibamoto, *J. Agric. Food Chem.*, 2009, **57**, 5365–5369.
43 R. Lang, E. F. Yagar, A. Wahl, A. Beusch, A. Dunkel, N. Dieminger, R. Eggers, G. Bytof, H. Stiebitz, I. Lantz and T. Hofmann, *J. Agric. Food Chem.*, 2013, **61**, 12123–12128.
44 A. Farah, T. De Paulis, L. C. Trugo and P. R. Martin, *J. Agric. Food Chem.*, 2005, **53**, 1505–1513.
45 A. Hulanicki, S. Glab and F. Ingman, *Pure Appl. Chem.*, 1991, **63**, 1247–1250.
46 J. M. Lim, J. H. Kim, M. Y. Ryu, C. H. Cho, T. J. Park and J. P. Park, *Anal. Chim. Acta*, 2018, **1026**, 109–116.

47 M. Del Carlo, D. Capoferri, I. Gladich, F. Guida, C. Forzato, L. Navarini, D. Compagnone, A. Laio and F. Berti, *ACS Sensors*, 2016, **1**, 279–286.

48 F. Guida, A. Battisti, I. Gladich, M. Buzzo, E. Marangon, L. Giodini, G. Toffoli, A. Laio and F. Berti, *Biosens. Bioelectron.*, 2018, **100**, 298–303.

49 X. F. Zhang, N. Li, Y. Ling, N. B. Li and H. Q. Luo, *Sensors Actuators, B Chem.*, 2018, **271**, 9–14.

50 Y. J. Lee, K. S. Eom, K. S. Shin, J. Y. Kang and S. H. Lee, *Sensors Actuators, B Chem.*, 2018, **271**, 73–81.

51 L. Guadarrama-Fernández, M. Novell, P. Blondeau and F. J. Andrade, *Food Chem.*, 2018, **265**, 64–69.

52 E. Pellizzoni, M. Tommasini, E. Marangon, F. Rizzolio, G. Saito, F. Benedetti, G. Toffoli, M. Resmini and F. Berti, *Biosens. Bioelectron.*, 2016, **86**, 913–919.

53 J. Wang, Q. Xu, W. W. Xia, Y. Shu, D. Jin, Y. Zang and X. Hu, *Sensors Actuators, B Chem.*, 2018, **271**, 215–224.

54 P. Weber, B. R. Riegger, K. Niedergall, G. E. M. Tovar, M. Bach and G. Gauglitz, *Sensors Actuators, B Chem.*, 2018, **267**, 26–33.

55 D. Grieshaber, R. MacKenzie, J. Vörös and E. Reimhult, *Sensors*, 2008, **8**, 1400–1458.

56 R. Pilolli, L. Monaci and A. Visconti, *TrAC - Trends Anal. Chem.*, 2013, **47**, 12–26.

57 S. J. Dong and B. Q. Wang, *Electroanalysis*, 2002, **14**, 7–16.

58 S. Arnaboldi, T. Benincori, R. Cirilli, W. Kutner, M. Magni, P. R. Mussini, K. Noworyta and F. Sannicolò, *Chem. Sci.*, 2015, **6**, 1706–1711.

59 T. P. Huynh, P. S. Sharma, M. Sosnowska, F. D'Souza and W. Kutner, *Prog. Polym. Sci.*, 2015, **47**, 1–25.

60 K. L. Westmacott, A. Crew, O. Doran and J. P. Hart, *Talanta*, 2018, **181**, 13–18.

61 J. K. Jadav, V. V. Umrania, K. J. Rathod and B. A. Golakiya, *LWT - Food Sci. Technol.*, 2018, **88**, 152–158.

62 G. Bolat and S. Abaci, *Sensors (Switzerland)*, , DOI:10.3390/s18030773.

63 M. Bijad, H. Karimi-Maleh, M. Farsi and S. A. Shahidi, *J. Food Meas. Charact.*, 2018, **12**, 634–640.

64 P. Balasubramanian, R. Settu, S. M. Chen, T. W. Chen and G. Sharmila, *J. Colloid Interface Sci.*, 2018, **524**, 417–426.

65 V. S. Manikandan, Z. Liu and A. Chen, *J. Electroanal. Chem.*, 2018, **819**, 524–532.

66 M. Sakthivel, M. Sivakumar, S. M. Chen and K. Pandi, *Sensors Actuators, B Chem.*, 2018, **256**, 195–203.

67 Z. Wu, F. Guo, L. Huang and L. Wang, *Food Chem.*, 2018, **259**, 213–218.

68 N. Alpar, Y. Yardım and Z. Şentürk, *Sensors Actuators, B Chem.*, 2018, **257**, 398–408.

69 K. Murtada, S. Jodeh, M. Zougagh and Á. Ríos, *Electroanalysis*, 2018, **30**, 969–974.

70 M. Amatatongchai, W. Sroysee, P. Jarujamrus, D. Nacapricha and P. A. Lieberzeit, *Talanta*, 2018, **179**, 700–709.

71 L. Redivo, M. Stredanský, E. De Angelis, L. Navarini, M. Resmini and Ľ. Švorc, *R. Soc. Open Sci.*, , DOI:10.1098/rsos.172146.

72 Ľ. Švorc, *Int. J. Electrochem. Sci.*, 2013, **8**, 5755–5773.

73 F. Canfarotta, A. Cecchini and S. Piletsky, in *Molecularly Imprinted Polymers for Analytical Chemistry Applications*, ed. W. K. and P. S. Sharma, The Royal Society of Chemistry, 2018, pp. 1–27.

74 L. Chen, S. Xu and J. Li, *Chem. Soc. Rev.*, 2011, **40**, 2922–2942.
75 M. Rutkowska, J. Płotka-Wasylka, C. Morrison, P. P. Wieczorek, J. Namieśnik and M. Marć, *TrAC - Trends Anal. Chem.*, 2018, **102**, 91–102.
76 G. Wulff, *Angew. Chemie Int. Ed. English*, 1995, **34**, 1812–1832.
77 F. Mirata and M. Resmini, in *Advances in Biochemical Engineering/Biotechnology*, 2015, pp. 107–129.
78 M. Resmini, *Analytical*, 2012, **402**, 3021–3026.
79 M. Resmini, K. Flavin and D. Carboni, *Top. Curr. Chem.*, 2012, **325**, 307–342.
80 I. Chianella, M. Lotierzo, S. A. Piletsky, I. E. Tothill, B. Chen, K. Karim and A. P. F. Turner, *Anal. Chem.*, 2002, **74**, 1288–1293.
81 I. Chianella, K. Karim, E. V. Piletska, C. Preston and S. a. Piletsky, *Anal. Chim. Acta*, 2006, **559**, 73–78.
82 I. Jelesarov and H. R. Bosshard, *J. Mol. Recognit.*, 1999, **12**, 3–18.
83 P. Thordarson, *Chem. Soc. Rev.*, 2011, **40**, 1305–1323.
84 Y. Wang, J. Wang, R. Cheng, L. Sun, X. Dai and Y. Yan, *J. Sep. Sci.*, 2018, **41**, 1880–1887.
85 M. Jia, Z. Zhang, J. Li, X. Yang and L. Chen, *Sensors Actuators, B Chem.*, 2017, **252**, 934–943.
86 Y. Liu, X. Hu, L. Bai, Y. Jiang, J. Qiu, M. Meng, Z. Liu and L. Ni, *Microchim. Acta*, 2018, **185**, 48.
87 W. Zhang, Y. Han, X. Chen, X. Luo, J. Wang, T. Yue and Z. Li, *Food Chem.*, 2017, **232**, 145–154.
88 P. Lach, P. S. Sharma, K. Golebiewska, M. Cieplak, F. D'Souza and W. Kutner, *Chem. - A Eur. J.*, 2017, **23**, 1942–1949.
89 M. Arvand, Z. Erfanifar and M. S. Ardaki, *Food Anal. Methods*, 2017, **10**, 2593–2606.
90 Y. Li, J. Liu, Y. Zhang, M. Gu, D. Wang, Y. yan Dang, B. C. Ye and Y. Li, *Biosens. Bioelectron.*, 2018, **106**, 71–77.
91 L. Zhang, C. Zhu, C. Chen, S. Zhu, J. Zhou and M. Wang, *Food Chem.*, 2018, **266**, 170–174.
92 G. Fang, Y. Yang, H. Zhu, Y. Qi, J. Liu, H. Liu and S. Wang, *Sensors Actuators, B Chem.*, 2017, **251**, 720–728.
93 Y. H. Zhang, H. H. Ren and L. P. Yu, *Anal. Methods*, 2018, **10**, 101–108.
94 M. Z. Hua, S. Feng, S. Wang and X. Lu, *Food Chem.*, 2018, **258**, 254–259.

CHAPTER 2
Computational studies on the self-association process of caffeine and paraxanthine

2.1 Introduction

The key feature of molecularly imprinted polymers (MIPs) is the presence of molecular cavities which are complementary in their size and shape (as well as position and orientation of recognising sites), to a target compound, leading to highly selective recognition. The synthetic process for obtaining MIPs was described in Chapter 1 (Section 1.6) together with several factors affecting the selectivity of the imprinted material (such as the strength of the functional monomer-template interaction, the solvent employed, concentration and percentage of different monomers). All these characteristics are commonly optimised during the development of imprinted materials, as described in more details in Chapter 3. In addition, the behaviour in solution of the template molecule, plays an important role, because self-association can decrease selectivity of the MIP. In fact, the coexistence of the monomer, dimer and higher-order aggregates during the polymer synthesis, will influence the imprinted cavities. In the Scheme 2.1 below, the effect of the template present as either a monomer or a dimer on the size of the MIP's cavities is represented schematically.

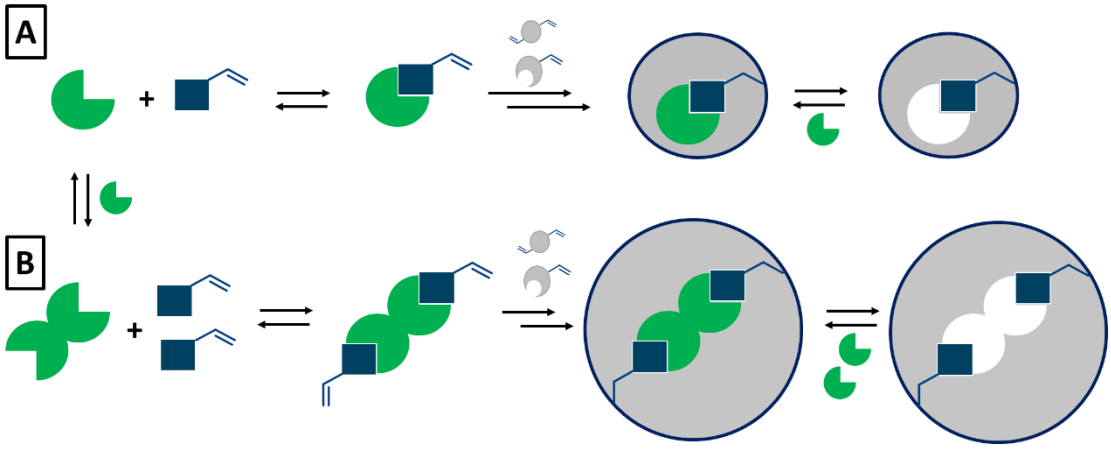

Scheme 2.1.The effect of the presence of template aggregates on the formation of molecular cavities in the MIP. (A) The case where the monomeric form of the template is present. (B): the case where the dimeric form of the template is present.

Scheme 2.1 above, is a simplified description, and it must be considered that a variety of elements including the type of functional monomer employed and the degree of cross-linking) are responsible for the selectivity of the final polymer. Nevertheless, also the size of the template during imprinting has a direct effect on the size and shape of the cavities, which ultimately influences the selectivity. The polymers depicted in Scheme 2.1 will perform differently also during rebinding, depending on the behaviour in solution of the template molecule. Using again a simplified description of the process, a graphical example is presented in Scheme 2.2 below. If in the analysed sample clusters are present, then polymers imprinted with the free template molecules cannot be employed to bind the analyte since the cavities are too small (Scheme 2.1 A). On the other hand, if in the analysed sample only monomers of the target molecule are present, polymers imprinted with the dimeric form can be still used. However, because the cavities are bigger also some interfering compounds can be hosted and, therefore, the MIP selectivity is decreased (Scheme 2.2 B).

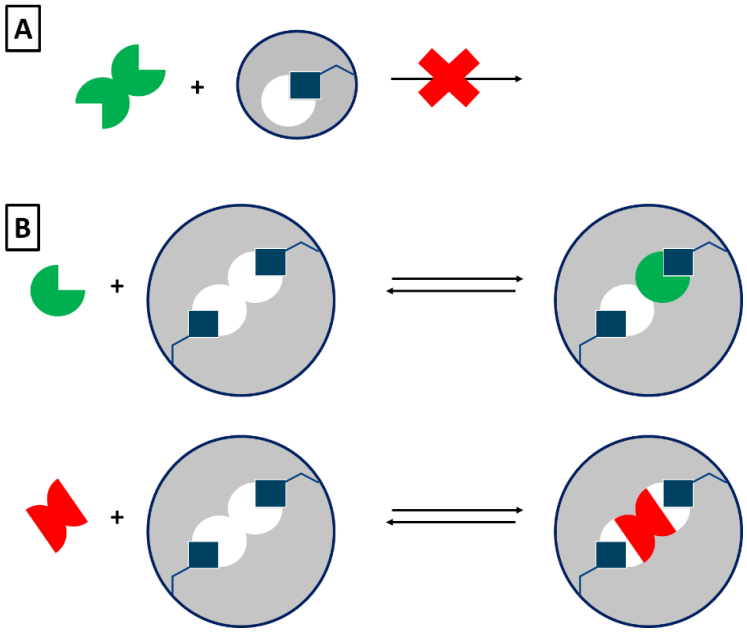

Scheme 2.2.The selectivity of MIP. (A) In the analysed sample the dimer of the template is present and the MIP selectivity to the monomer form of the target compound is not suitable. (B) In the analysed sample, the free molecule of the target is present and the MIP selectivity to the dimer can still be employed, however this MIP will be less selective and interferent compounds may bind (red form).

Scheme 2.2, although being based on a simplified model, shows the importance of the behaviour of the template molecule in solution, with regards to the recognition properties of the imprinted material.

One of the aims of the present research was to develop a new chemosensor for caffeine determination in caffeinated beverages. Given that the imprinted material must recognise caffeine in an aqueous solution, it was decided to investigate the synthesis of MIPs in water (the selection of the solvent for polymerisation will be discussed in Chapter 3). In aqueous solution, caffeine can self-associate leading to the formation of clusters which can affect the synthesis of the imprinted materials. Data on caffeine self-association are reported in the literature, obtained using a variety of techniques including nuclear magnetic resonance[1–3] and infrared spectroscopy[4], dynamic light scattering[5,6], osmometry[7], fluorescence spectroscopy[8], thermal analysis and differential scanning calorimetry[9,10]. These experimental methods rely on the use of certain self-association models, such as isodesmic, cooperative self-association, and non-cooperative self-association, to fit the experimental data and extrapolate the speciation of caffeine in solution (i.e. percentage of the monomer, dimer, trimer, etc). To support the experimental data and the fitting model employed, supporting evidence of the chemical species present in solution (monomer, and aggregates) is essential. For this purpose, computational simulation can be employed. The molecular dynamics (MD) technique is routinely used to investigate aggregation of organic molecules in solution[11,12]. Recent MD simulations of aqueous caffeine solutions conducted by Tavagnacco *et al.* have suggested extensive aggregation, with the formation of pentamer of caffeine where the molecules are: <<*stacking their flat faces against one another like coins*>>.[13–17] These simulations were, however, conducted at the limit of solubility of caffeine (about 16 mg/mL), where self-association is expected to occur, leading to aggregation. Lower concentrations

would require simulating aqueous solutions containing hundreds of millions of solvent molecules, which is at the far limit of the MD techniques. An alternative approach to determine the structure and thermodynamic stability of molecular aggregates in solution is the quantum mechanical continuum solvation approach,[18] where the solute (monomer, dimer, trimer, etc.) is treated quantum mechanically, usually at the density functional theory (DFT) level, and the solvent is described using a polarizable continuum solvation model. Senthilnithy *et al.*[19] conducted DFT calculations of caffeine dimers in water reporting a highly positive Gibbs free energy of dimerisation (+45.98 $kJ.mol^{-1}$). A similar computational work, by Bradley and Hendson, also concluded that the dimer formation is highly unfavourable in water and suggested that caffeine exists as a free monomer well below its solubility limit.[20] However, these two studies only considered a limited number of possible dimeric configurations while, weakly interacting molecular complexes, are likely to be characterised by a large number of possible dimer geometries (see Annex I). Besides, the DFT method employed in these two studies (the B3LYP functional without dispersion correction) could have affected the accuracy of the results, since the stacking interaction is not correctly evaluated by this functional.

Considering the contradictory computational results reported in the literature and given the importance of computational simulation to shed light on the molecular-details of the self-association process, a more accurate quantum mechanical approach was applied to reveal the process of self-aggregation of caffeine in aqueous solutions. The computational method is described in the following paragraph. It is an adaptation of a protocol previously employed by Di Tommaso and Watson for studying self- association of carboxylic acids[21]. To demonstrate the validity of the computational protocol employed, the same study was applied to predict the self-association process of

paraxanthine (which differ from caffeine by the replacement of one methyl group with one hydrogen atom, the structural formulae are reported in Scheme 2.3, below).

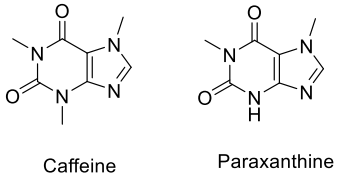

Scheme 2.3.Structural formulae of caffeine and paraxanthine

The interest in paraxanthine was generated by its very low solubility in water compared to that of caffeine (1 mg/mL and 16 mg/mL respectively), which can be linked to a different self-association behaviour. Considering the structural similarity of the two molecules and different solubility, paraxanthine was selected as the best candidate to evaluate the applicability of the computational method to caffeine analogues and further validate its accuracy when the difference in chemical structure is small.

2.2 Results and discussion

In the following section, the computational study on self-association of caffeine and paraxanthine is presented together with an experimental validation which was performed by Ms R. Anastasiadi (a colleague from the same research group where I worked). The discussion is organised into four main sections: (i) assessment of the computational procedure; (ii) computational results on self-association of caffeine; (iii) computational results on self-association of paraxanthine; (iv) experimental studies on self-association of caffeine and paraxanthine. The experimental data presented in Section 2.2.4 were acquired by Ms Anastasiadi, but are reported in this thesis to validate the computational approach and strengthen and support the conclusions of this work.

2.2.1 Assessment of the method

One of the key step to obtain reliable and accurate computational results is the selection of the appropriate computational procedure. In particular, in the case of DFT calculations, a crucial role is played by the functional. This is because it is responsible for describing the energy and the geometry of the molecules (as discussed in Annex 1). In common computational chemistry software a variety of functionals are available. Each of them has been developed and optimised for a given chemical system, for instance, organic molecules, metals, ionic interactions etc. Given the wide choice, it is essential to identify the functional that is suitable for the chemical process under investigation and, therefore, can provide accurate results. To find the optimal functional, experimental data are usually compared with computational results. To investigate the thermodynamic stability of caffeine aggregates, the computational procedure selected must be able to reproduce the chemical interactions between caffeine molecules correctly. Therefore, from X-ray diffraction data of caffeine crystals, the interaction geometries between two caffeine molecules was obtained and used as experimental reference data. Although caffeine is an achiral molecule, two non-superimposable faces of the molecule can be identified and defined as face and back (Scheme 2.4).

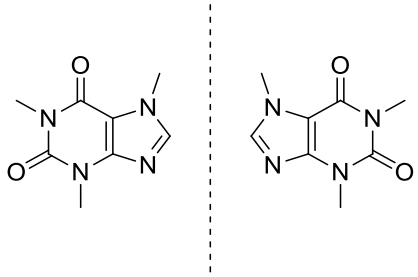

Scheme 2.4. The structural formulae of two non-superimposable faces of the caffeine molecule.

As a consequence, two major types of stacking geometries are possible: (i) the parallel one, where the face of one caffeine molecule interacts with the back of the second molecule; (ii) the anti-parallel one, where caffeine molecules interact on the same

side[22]. Previous X-ray diffraction data on caffeine crystals evidenced that both geometries exist. Therefore, the parallel[23] and anti-parallel[24] dimeric structures are reported in Scheme 2.5 and Scheme 2.6 in the next page.

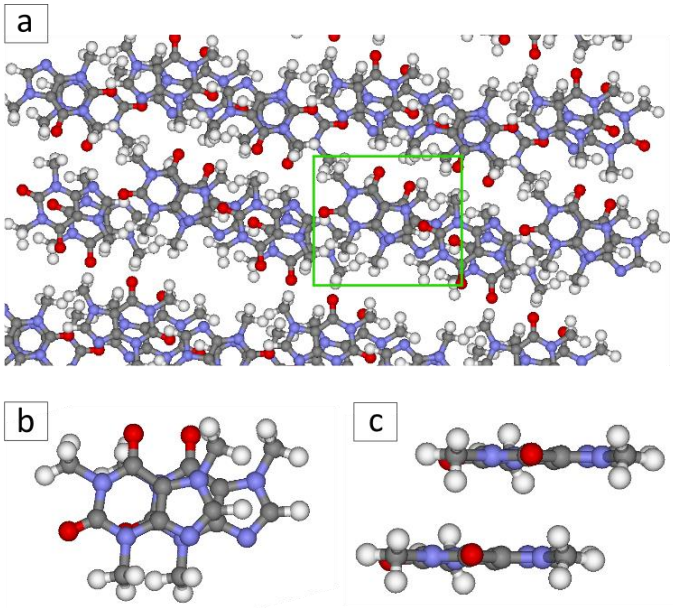

Scheme 2.5. The crystallographic structure of caffeine obtained by Sutor J.D.[23] *Panel (a) shows the crystallographic structure and highlighted in green the parallel dimer geometry taken as a model. Panel, (b) shows a top view of the structure of the dimer, which shows the overlap between the two aromatic rings. Panel (c) represents, a side view of the structure of the dimer with methyl groups oriented towards the O atoms.*

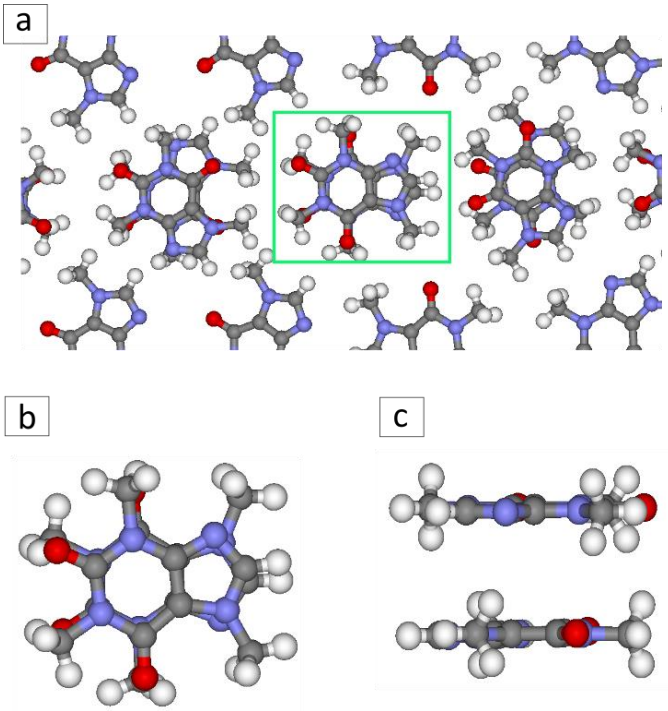

Scheme 2.6. The crystallographic structure of anhydrous caffeine obtained by Lehmann C.W. et al.[24] *Panel (a) shows the crystallographic structure and highlighted in green the anti-parallel dimer geometry taken as a model. Panel (b) shows a top view of the structure of the dimer, with the overlap of the two aromatic rings. Panel (c), illustrates a side view of the structure of the dimer with the orientation of the methyl groups towards the N and O atoms.*

In both parallel and anti-parallel dimers structures the two molecules are at a distance of 3.4 Å, which is a typical distance for π-π stacking interactions[25,26]. Interestingly, the methyl groups are rotated to allow the formation of weak $CH_3\cdots X$ (X = O and N) hydrogen (H) bonds between the two caffeine moieties (panels b and c Scheme 2.5 and Scheme 2.6). In addition, in the case of the crystallographic structure reported by Lehmann *et al.* (Scheme 2.6) two different anti-parallel synthons can be identified, one where the two molecules are rotated by 90° and the other where the two caffeine molecules are overlapped entirely (highlighted in green in Scheme 2.6). In particular, the latter is an uncommon stacking structure. In fact, aromatic compounds have an electron-rich area above and below the plane of the molecule, while at the edges there is an electron-poor region. As a consequence, the most common stacking geometry is with the two molecules off-centre (called parallel displaced) or in a T shape position, which

decrease the electrostatic repulsion of the electron-rich orbitals. Dimer structures revealing different interactions are reported in Scheme 2.7, below.

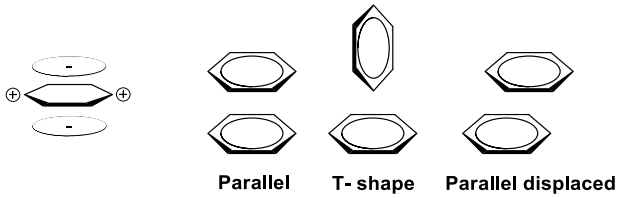

Scheme 2.7. A representation of the electron rich and poor area in an aromatic compound (in this example benzene), and three possible stacking interaction geometries: parallel, T-shape and parallel displaced.

However, when electron withdrawing moieties (such as C=O, and N) are present, the electron density of the aromatic ring is decreased and a total alignment between the two molecules is possible.[25] In addition, in the case of caffeine, the presence of methyl groups forming intermolecular hydrogen bonds favour the superimposition of the two aromatic rings. Although the electronegativity difference between the C and H atoms is small (0.35 based on the Pauling scale), the formation of weak C-H···O and C-H···N hydrogen bonds has been reported in both experimental observations,[27,28] and previous computational works.[22,29]

From the crystallographic structures reported in the literature, the following key features of the caffeine-caffeine interaction were identified: (i) two main types of interactions are possible, the parallel and anti-parallel; (ii) weak C-H···O and C-H···N hydrogen bonds between the two molecules can be formed; (iii) the two molecules can interact with a completely aligned stacking geometry. Therefore, an accurate computational method suitable to study self-association of caffeine must correctly reproduce all these features. To identify the most appropriate computational method for this study, both parallel and anti-parallel motifs found in the X-ray crystalline structure of caffeine were considered as models and the ability of various density functionals and

basis sets to reproduce these two structures was evaluated. The model structures are reported in Scheme 2.8 below.

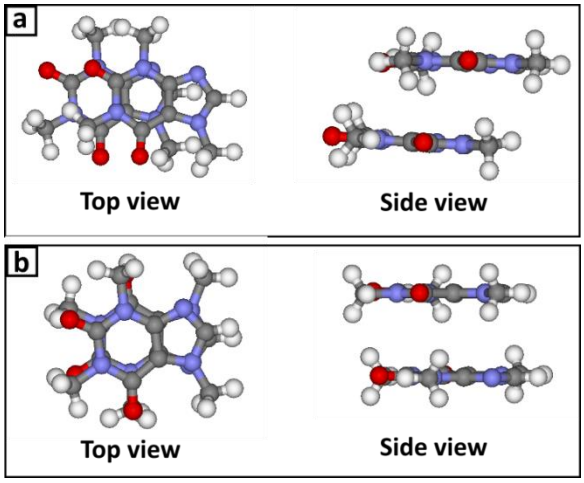

Scheme 2.8. The two dimeric motifs found in the crystal structure of caffeine the parallel (a) and anti-parallel (b)[23,24] *and employed as models to evaluate different DFT methods. The top views highlight the stacking interactions and the side views show the methyl groups forming weak H-bonds with the O and N atoms.*

In the Table 2.1, the ability of different functionals and basis sets to identify the parallel dimer geometry (Scheme 2.8a) is reported. As explained in Annex I, different DFT methods have been developed and can be categorised based on the mathematical method employed to calculate the electron-electron interaction (GGA, HDFT, HMDFT, LC-HDFT). Besides, an additional correction can be applied to compute more correctly weak interactions, such as hydrogen bonds and π-π stacking (Grimme's dispersion D and D3). It is not possible to know *a priori* if a functional will be suitable and therefore an evaluation of their applicability is necessary.

Table 2.1. Gas phase energy of formation (ΔE_{gas}) of the parallel caffeine dimer as computed by different DFT methods and ability to reproduce the interaction geometry as found in the crystallographic data.

DFT Method		Basis set	ΔE_{gas} (kJ/mol)	Ability to locate parallel crystal motif
GGA	BLYP	6-31G(d)	-24.62	×
		6-31+G(d,p)	-9.70	×
	PBE	6-31G(d)	-22.99	×
		6-31+G(d,p)	-23.45	×
GGA + Grimme's dispersion	BLYP-D3	6-31G(d)	-104.37	×
		6-31+G(d,p)	-78.25	×
	PBE-D3	6-31G(d)	-61.03	√
		6-31+G(d,p)	-48.11	√
		6-311+G(d,p)	-47.15	√
		Plane Waves	-44.64	√
	B97-D	6-31G(d)	-68.26	√
		6-31+G(d,p)	-54.34	√
		6-311+G(d,p)	-56.85	√
		6-311+G(2df,2p)	-55.01	√
	B97-D3	6-31G(d)	-65.25	√
		6-31+G(d,p)	-52.54	√
		6-311+G(d,p)	-54.84	√
HDFT	B3LYP	6-31G(d)	-27.25	×
		6-31+G(d,p)	-12.16	×
	PBE1PBE	6-31G(d)	-17.30	×
		6-31+G(d,p)	-12.04	×
HDFT + D3	B3LYP-D3	6-31G(d)	-67.13	×
		6-31+G(d,p)	-74.68	×
	PBE1PBE-D3	6-31G(d)	-83.56	×
		6-31+G(d,p)	-49.16	√
HMDFT	M06-2X	6-31G(d)	-80.55	×
		6-31+G(d,p)	-74.57	×
LC-HDFT	ωB97X-D	6-31+G(d,p)	-58.85	√
		aug-cc-pVTZ	-63.37	√

From Table 2.1, it follows that pure GGA (PBE and BLYP) and HDFT (B3LYP and PBE1PBE) functionals are not able to locate the parallel dimeric motif. In fact, all these functionals neglect dispersion interactions and therefore they are unable to accurately describe the combination of π-π and $CH_3\cdots X$ (X = O and N) interactions that characterise the parallel configuration. To accurately calculate the dispersion forces, the Grimme's

dispersion correction can be added to the calculation. Nevertheless, even with the inclusion of this correction, not all the methods were able to locate the parallel geometry found in the crystal. In fact, Grimme's-D3 corrected BLYP and B3LYP functional using methods as well as the M06-2X functional, which was specifically developed for non-covalent interactions[30] were not suitable. On the other hand, using the Grimme's-D3 corrected PBE functional (PBE-D3) and B97 (B97-D and B97-D3), the crystal dimer motif was located on the potential energy surface of the caffeine dimer, employing different basis sets. In Scheme 2.9, below, some examples of final structures of the caffeine dimer using different functionals are reported, showing the importance of the dispersion correction.

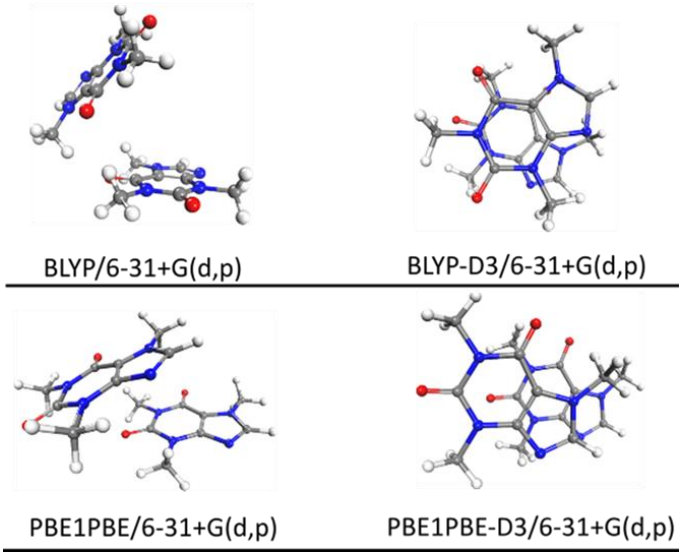

Scheme 2.9. The ability of different functionals in locating the parallel dimer geometry of caffeine as found in the crystallographic structure. On the left-hand side functionals without the Grimme's dispersion correction are reported where the two molecules are not forming a planar π-π stacking interaction. On the right-hand side the results obtained with the inclusion of the dispersion correction are reported and the resulting dimer geometries suggesting the formation of π-π stacking interactions.

With regards to the calculated binding energy (ΔE), an extensive systematic study of DFT methods by Sherrill and co-workers[31] concluded that the long-range corrected hybrid ωB97X-D functional gives an excellent description of non-covalent (hydrogen-bonded and dispersion-bound) complexes. Indeed, the geometry of the caffeine dimers

optimised using the ωB97X-D functional, together with the 6-31+G(d,p) and aug-cc-pVTZ basis sets, are consistent with the crystalline dimeric motifs. The energy obtained with this functional and augmented basis set (aug-cc-pVTZ) can be considered a reliable reference value for the estimation of the binding energy (ΔE = - 62.70 kJ/mol). However simulations with this level of theory require long time to be computed, and therefore, are not suitable for the next step where thousands of molecules have to be considered. Among the functionals able to reproduce the parallel dimer of caffeine independently of the basis set employed there are the PBE-D3, B97-D and B97-D3 functionals which are all less time demanding compared to the ωB97X-D/aug-cc-pVTZ level of theory. When PBE-D3 functional was employed, the binding energy values computed with the 6-311+G(d,p) and plane wave basis sets were approximately - 46 kJ mol^{-1}. This value is 17 kJ mol^{-1} lower than the reference value. On the other hand, the use of B97-D and B97-D3 functionals resulted in 54 kcal/mol which is closer to the reference value, thus suggesting that this two functionals can provide more accurate results.

Subsequently, a similar screening was performed using the anti-parallel geometry (Scheme 2.8 b), and the results are listed in Table 2.2, on the next page.

Table 1. Gas phase energy of formation (ΔE_{gas}) of the anti-parallel caffeine dimer, as computed by different DFT methods and ability to reproduce the interaction geometry as found in the crystallographic data.

DFT Method		Basis set	ΔE (kJ/mol)	Ability to locate the anti-parallel crystal motif
GGA	BLYP	6-31G(d)	-24.33	√
		6-31+G(d,p)	-6.35	×
	PBE	6-31G(d)	-39.67	√
		6-31+G(d,p)	-12.04	√
GGA + Grimme's dispersion	BLYP-D3	6-31G(d)	-105.13	√
		6-31+G(d,p)	-78.58	√
	PBE-D3	6-31G(d)	-88.45	√
		6-31+G(d,p)	-69.14	√
	B97-D	6-31G(d)	-91.49	√
		6-31+G(d,p)	-73.82	√
	B97-D3	6-31G(d)	-88.87	√
		6-31+G(d,p)	-70.72	√
HDFT	B3LYP	6-31G(d)	-26.79	√
		6-31+G(d,p)	-10.24	√
	PBE1PBE	6-31G(d)	-34.11	√
		6-31+G(d,p)	-22.07	√
HDFT + D3	B3LYP-D3	6-31G(d)	-95.42	√
		6-31+G(d,p)	-74.82	√
	PBE1PBE-D3	6-31G(d)	-83.56	√
		6-31+G(d,p)	-70.01	√
HMDFT	M06-2X	6-31G(d)	-83.14	√
		6-31+G(d,p)	-77.37	√
LC-HDFT	ωB97X-D	6-31+G(d,p)	-77.37	√
		aug-cc-pVDZ	-79.92	√

With the exception of the BLYP/6-31+G(d,p) level of theory, the structures optimised with all other methods correctly reproduced the anti-parallel dimer. Regarding the binding energies, the result obtained with the ωB97X-D/aug-cc-pVDZ was considered as the reference value (-79.92 kJ/mol). Application of pure GGA (BLYP and PBE) and hybrid DFT (B3LYP and PBE1PBE) functionals resulted in ΔE values for the gas-phase dimerisation lower by 41.8 to 63 $kJ.mol^{-1}$ than those computed with the ωB97D method developed specially for non-covalent interactions. This observation

confirmed that a dispersion correction must be employed to compute the association energy between caffeine molecules correctly. Moreover, in the work of Senthilnithy R. *et al.*[19] the B3LYP functional was employed without considering any dispersion correction and the final Gibbs free energy of dimerization for caffeine molecules was considerably overestimated (ΔG = + 45.98 kJ/mol), which is not in agreement with the experimental data (ΔG = - 6.27 kJ/mol)[32]. The B97-D and B97-D3 functionals performed well in reproducing the binding energy of the anti-parallel caffeine dimer, and slightly more precise data were obtained with the B97-D functional. Considering the results obtained for both the parallel and anti-parallel dimer, the B97-D functional and 6-31+G(d,p) basis set were selected as more appropriate to conduct the computational study, given also that this level of theory is less time demanding compared with studies based on the ωB97X-D/aug-cc-pVDZ, and the accuracy of the method was expected to be similar.

Subsequently, the error associated with the computational method was evaluated. As opposed to experimental work, where repetition can lead to different results and an error can be calculated, in the case of computational methodologies only the accuracy can be estimated, based on the level of theory employed. In fact, repetition of the same computational protocol will lead to exactly the same result. The change of Gibbs free energy of association of caffeine molecules in solution ($\Delta G_{\mathrm{H_2O}}$), is defined, for the dimerization process.

$$\Delta G_{\mathrm{H_2O}} = G_{\mathrm{H_2O}}(CAF_2) - 2G_{\mathrm{H_2O}}(CAF) \qquad (2.1)$$

Where $G_{\mathrm{H_2O}}$ is the Gibbs free energy in water of the caffeine dimer (CAF_2), and of caffeine monomer (CAF). The method adopted in this work to compute the free energy of association in solution ($\Delta G_{\mathrm{H_2O}}$) has an error $\varepsilon(\Delta G_{\mathrm{H_2O}})$ which is given by the sum of

the error in the evaluation of the gas phase dimerization free energy, $\varepsilon(\Delta G_{\mathrm{gas}})$, and the error in the evaluation of the solvation free energies of the reactants and products, $\varepsilon(\Delta\Delta G_{\mathrm{H_2O}})$:

$$\varepsilon(\Delta G_{\mathrm{H_2O}}) = \varepsilon(\Delta G_{\mathrm{gas}}) + \varepsilon(\Delta\Delta G_{\mathrm{H_2O}}) \qquad (2.2)$$

With regards to any error associated with the Gibbs free energy of dimerisation in vacuum ($\varepsilon(\Delta G_{\mathrm{gas}})$) this is difficult to be estimated accurately. Because there are no experimental values of the binding energy and free energy of caffeine. Therefore, the distribution of the values of ΔG_{gas} using different basis set was used to estimate the accuracy. In fact, by increasing the basis set more accurate results are obtained (more information in Annex I), and the differences between the smallest and biggest basis sets can be employed to estimate the error. As model dimer geometry, the parallel structure was employed (Scheme 2.8a). Table 2.3 reports the energetics of formation in the gas phase for the parallel dimeric structure calculated using hierarchical basis sets.

Table 2.3. Energy change of formation of caffeine parallel dimer using hierarchical basis sets. Values are reported in kJ/mol.

DFT functional	**Basis set**	ΔG_{gas}
B97-D	6-31+G(d,p)	12.33
	6-311+G(d,p)	11.75
	6-311+G(2df,2p)	8.32

The difference between the minimum and maximum value of $\Delta G^{\circ}_{\mathrm{gas}}$ is ~ 4 kJ/mol, which can be used as an estimate for error $\varepsilon(\Delta G_{\mathrm{gas}})$. With regards to the error associated with the solvation $\varepsilon(\Delta\Delta G_{H_2O})$, it is defined as the difference between the solvation free energy of the products and of the reactants. For the dimerisation $\varepsilon(\Delta\Delta G_{\mathrm{H_2O}})$ is given by:

$$\varepsilon\left(\Delta\Delta G_{\mathrm{H_2O}}\right) = \varepsilon\left[\Delta G_{\mathrm{H_2O}}(CAF_2)\right] - 2\varepsilon\left[\Delta G_{\mathrm{H_2O}}(CAF)\right] \qquad (2.3)$$

Where $\varepsilon\left[\Delta G_{H_2O}(CAF)\right]$ and $\varepsilon\left[\Delta G_{H_2O}(CAF_2)\right]$ are the errors in the computed values of the hydration free energies of caffeine monomers and dimers respectively. These energies are linked to the ability of the computational method to describe the solvation effect. Presumably, the accuracy of the computational method in describing the solvation of the monomer is equal to that of the dimer, because the same functional groups and atoms are considered. Under this approximation, therefore, equation 2.3 becomes:

$$\varepsilon\left(\Delta\Delta G_{\mathrm{H_2O}}\right) = \varepsilon\left[\Delta G_{\mathrm{H_2O}}(CAF)\right] \qquad (2.4)$$

To calculate $\varepsilon\left[\Delta G_{\mathrm{H_2O}}(CAF)\right]$ the experimental Gibbs free energy of solvation of caffeine obtained by Powder J. W. et al.[33] was compared with the solvation energies calculated herein using different DFT methods. The results are presented in Table 2.4.

Table 2.4. Gibbs free energy of hydratation of the caffeine molecule. Solvation calculations were conducted using the parallel caffeine dimer optimised at the B97-D/6-31+G(d,p) level of theory. Values in kJ/mol.

DFT functional	**Basis set**	ΔG_{H_2O}	$\varepsilon\left[\Delta G_{H_2O}\right]$
B97-D	6-31+G(d,p)	–49.16	3.68
	6-311+G(d,p)	–47.73	5.09
	6-311+G(2df,2p)	–41.59	11.24
M06-2X	6-31+G(d,p)	–53.42	–0.58
	6-311+G(d,p)	–53.78	–0.92
	6-311+G(2df,2p)	–50.53	2.30
Expt.[33]		–52.83	

At the B97-D level of theory, the effect of the basis set on the hydration free energy is significant and the error $\varepsilon\left[\Delta G_{\mathrm{H_2O}}\right]$ is in the range of 3 – 11.29 kJ/mol. On the other hand, the M06-2X is less sensitive to the nature of the basis set employed and the solvation free energy computed using the SMD/M06-2X/6-31+G(d,p) method differs by

only 0.4 kJ/mol. The M06-2X functional appeared inappropriate to describe the parallel interaction geometry (Table 2.1) and therefore, not suitable to be employed to accurately identify stable dimer geometries. Nevertheless, it was more adequate for evaluating the solvent effect, than the functional B97-D. Considering that computation time using these two functionals is similar, the M06-2X functional was employed to calculate the Gibbs free energy of caffeine dimerization in solution, once the stable caffeine dimers were identified in the gas phase with the B97-D functional. The error associated with the B97/6-31+G(d,p) method together with the SMD/M06-2X/6-31+G(d,p) solvation model is $\varepsilon(\Delta G_{\mathrm{ass}}) = \varepsilon\left(\Delta G_{\mathrm{gas}}\right) + \varepsilon\left(\Delta\Delta G_{H_2O}\right) = 4\ \mathrm{kJ/mol} + 0.4\ \mathrm{kJ/mol} = \pm 4.4\ \mathrm{J/mol}$. Errors in the range of 4 kJ/mol are usually found for DFT method because quantum mechanics results are affected by the approximations that are required to solve Schrödinger's equation (see Annex I for more information).

2.2.2 Computational results on self-association of caffeine

Following the identification of the appropriate computational method, the next step was to investigate self-aggregation of caffeine, by probing the potential energy surface (PES) of caffeine dimers and identifying the more stable dimeric structures. In fact, dimers are the first aggregates that can form during self-association. Chemical nature of intermolecular interactions in the caffeine dimer $(CAF)_2$ is expected to control its aggregation. As explained in the previous section, the caffeine : caffeine interaction is characterised not only by the π-π stacking interaction but also by weak hydrogen bonds ($CH_3\cdots O$, $CH_3\cdots N$). Therefore, several stable structures can exist, suggesting that the two structures isolated from crystallographic data do not exhaust the dimer population description. The importance of investigating all the possible dimer geometries is explained in more detail in Annex I. In the present study, a protocol previously used by Di Tommaso and Watson was applied to describe the PES accurately and identify all

possible stable dimeric structures.[21] Initially, one hundred thousand dimer structures were randomly generated using the Granada software[34]. Afterwards, a first selection based on geometrical parameters was made to eliminate improbable structures. Diffraction experiments on caffeine showed that the two molecules are at a distance of 3.4 Å. Therefore, dimeric structures where the two molecules were more distant than 4.0 Å were discarded because it was improbable that these were the most stable dimer geometries. The geometry-based selection led to 4500 possible dimeric structures. Their energy values were calculated using the NWChem software[35] and with the B97-D/6-31+G(d,p) level of theory. The obtained values were then employed to calculate the Boltzmann factor (f_i) as follow:

$$f_i = \frac{e^{-(E_i - E_0)/RT}}{\sum_{j=1}^{N} e^{-(E_j - E_0)/RT}} \qquad (2.5)$$

Where E_i is the energy of the ith dimeric structure. E_0 is the energy of the most stable dimer. *R* is the universal gas constant. *T* is the absolute temperature in kelvin. The index *j* runs over all *N* possible structures. The Boltzmann factor is computed to reduce the number of dimer geometries based on their energies. In fact, high in energy dimers will not play a role in dimerization because they are highly improbable (and the Boltzmann factor will be small). The more possible dimer structures are considered, the more accurate is the result. However, the time to complete the computation will be longer. In this study, it was decided to consider ~ 100 possible dimers for the final calculation of the Gibbs free energies. Therefore, only dimer structures with a $f_i > 0.01$ were considered for the next step. The resulting 110 dimer structures were optimized, and values of their Gibbs free energy of formation in vacuum and water were calculated. A schematic summary of the computational protocol employed is presented in Scheme 2.10 on the next page.

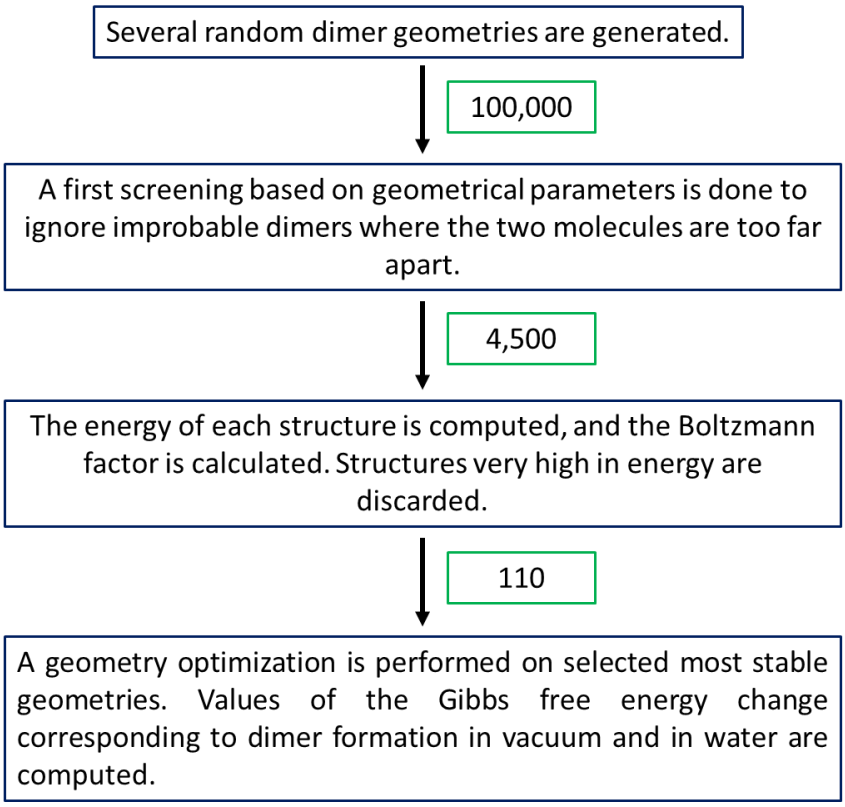

Scheme 2.10. The flow chart of the computational protocol employed in the presented study. In green boxes, the number of dimeric structures considered in each step is reported.

Once the Gibbs free energies were calculated, 40 structures with the negative dimerisation energy change were identified. Subsequently they were gathered together, based on similar interaction geometries. In fact given the initial random generation of possible structures, some copies ended up being generated. In vacuum, eight different geometries of interaction were found (I-VIII in Scheme 2.11), while in aqueous solution one geometry was stable (IX in Scheme 2.11). All the optimised structures are reported in the Scheme 2.11, and the Gibbs free energy changes due to dimerization are listed in Table 2.5.

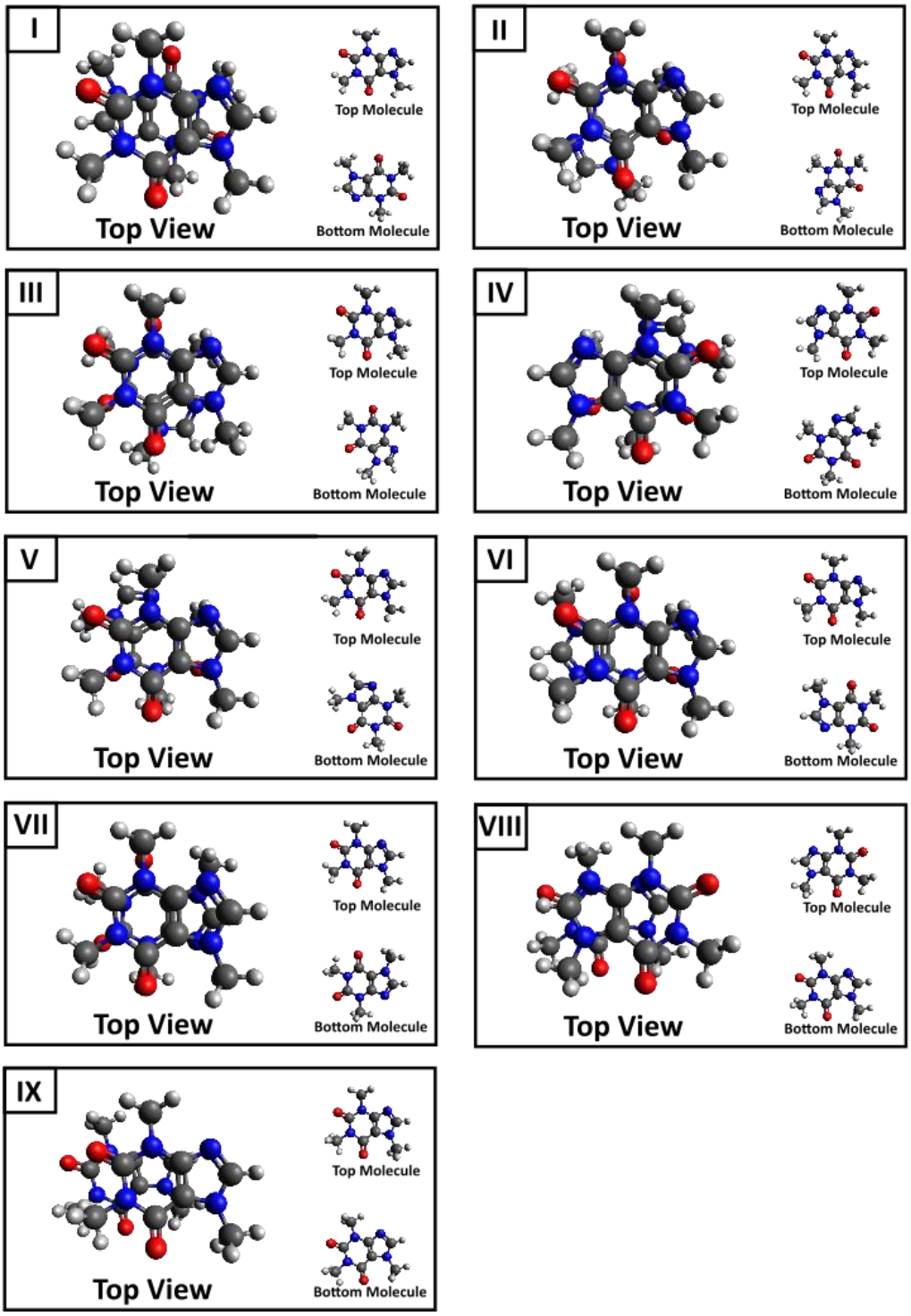

Scheme 2.11. Top view of nine low energy isomers of the caffeine dimer. To clarify the reciprocal orientation of the two caffeine molecules in the dimers, the structure of the isolated top and bottom monomers are also reported.

Table 2.5. The Gibbs free energy change accomplishing formation of the caffeine dimer, in the gas-phase (ΔG_{vac}) and aqueous solution (ΔG_{H_2O})as computed at the B97-D/6-31+G(d,p) theory level.

Dimer Geometry	ΔG_{vac}(kJ/mol)	ΔG_{H_2O}(kJ/mol)
I	-8.48	10.37
II	-8.19	10.24
III	-8.07	19.06
IV	-6.69	13.17
V	-6.35	12.37
VI	-6.35	11.70
VII	-3.30	8.99
VIII	-2.38	4.35
IX	6.81	-1.63

Interestingly, all stable structures show the formation of both π-π stacking and weak H-bond interactions. Besides, structures labelled as II and VII are very similar to the structures found by Lehmann in the caffeine crystal[24]. The configuration labelled as dimer IX correlates very well with the crystallographic motif found in the work of Sutor J. D. where caffeine was recrystallised from water[36]. Considering that dimer IX is the most stable in the aqueous phase, it can be affirmed that the aggregation of caffeine obeys the so-called "link hypothesis"[37]. According to this hypothesis the most stable interaction geometry in the water phase is found in the solid state of crystals obtained from the same solvent. The strong correlation between computational results and crystallographic data provides the key evidence of the strength of the computational protocol used herein. Previous theoretical work by Poltev *et al*. only identified five stable caffeine dimers.[22] In particular, the configurations in Poltev's study labelled as MP1, MP2, MA1, MA3, correspond, respectively, to III, I, II, VII configurations shown in Scheme 2.11. Moreover, structures I and VII agree with those considered by Senthilnithy *et al.*[19]. Structure MA2 identified by Poltev was the less stable among the five dimer configurations and, apparently, it is not a key geometry for the evaluation of the thermodynamic stability of caffeine dimers. Four new stable dimer geometries of

caffeine were identified in the present computational study (labelled as IV,V,VI,VIII in Scheme 2.11). The excellent agreement of the dimer geometries found with experimental data and previous computational results proves that the protocol employed in the presented study is reliable for predicting caffeine interaction geometries. In addition, identification of four new dimeric structures provides evidence that the current protocol is more exhaustive compared with previous studies.

Regarding the thermodynamic stability, only dimer IX was slightly stable in aqueous solution (-1.63 kJ/mol). However when the Boltzmann averaged dimerisation free energy change was calculated, a positive value was obtained (+3.84 kJ/mol) with an associated error estimated as ± 4.4 kcal/mol. The computational data suggest that although the caffeine dimer could be thermodynamically stable in aqueous solution, the monomeric form of caffeine will be predominant.

As literature reports present data on higher-order clusters of caffeine, the next step focused on using the same computational approach to evaluate the stability of these systems, containing more than two molecules of caffeine.[6,13,16,17] The configuration of the tetramer was obtained by stacking two dimers of type IX (the most stable in water) on top of each other. The configuration of the trimer was then obtained by removing one caffeine molecule from the tetramer. The optimised structures of caffeine's higher-order clusters are reported in Scheme 2.12.

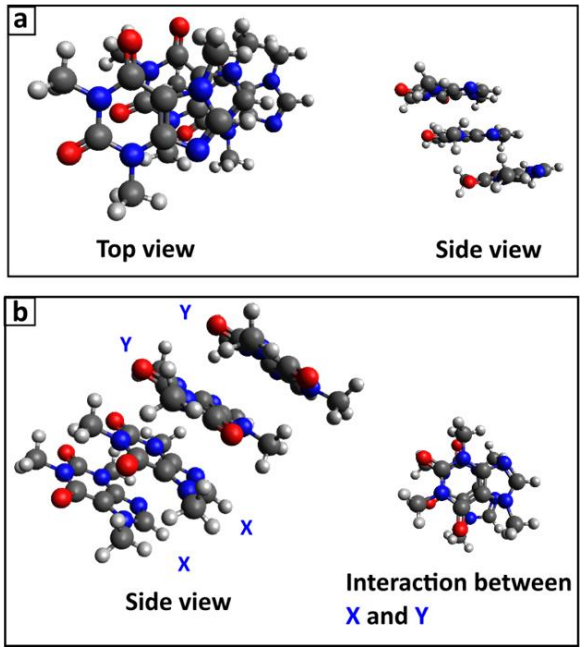

Scheme 2.12. Optimised structures of (a) the trimer and (b) the tetramer of caffeine. For the trimer, a top and a side view are reported, which show that the reciprocal orientation of the molecules is retained. In the case of the tetramer, the first two neighbouring molecules have an identical orientation while the second two caffeine molecules are rotated, leading to a final geometry of the type (XX-YY). The interaction geometry between X and Y is also reported.

Interestingly, while in the trimer the original orientation of each caffeine molecule is retained, in the tetramer the four molecules change their relative alignment, thus leading to a structure of the type (XX-YY), where the neighbouring molecules (XX) or (YY) have the same reciprocal orientation but X and Y are rotated with respect to each other (Scheme 2.12). Moreover, the arrangement of the molecules X and Y is very close to that in the dimeric configuration III (Scheme 2.11). The finding suggests that the interaction patterns found in the case of the dimer are valid also for higher-order clusters (trimer, tetramer) because the interaction geometries are similar. The thermodynamic stability of the caffeine trimer (CAF_3) was calculated using two reaction schemes: (i) the condensation of dimer IX with an additional caffeine molecule, $(CAF)_{IX} + CAF \rightarrow (CAF)_3$; (ii) the aggregation of three isolated caffeine molecules, $3CAF \rightarrow (CAF)_3$. For the tetrameter (CAF_4), the condensation of two dimers was considered, $2\ CAF_{IX} \rightarrow (CAF)_4$, as well as the association of one caffeine molecules to the trimer structure

$(CAF)_3 + CAF \rightarrow (CAF)_4$. The association of 4 caffeine molecules to form a tetramer was not considered, due to its statistical improbability. The energetics of formation of the caffeine trimer and tetramer are listed in the Table 2.6.

Table 2.6. The Gibbs free energy change associated with formation of caffeine trimer and tetramer in the gas-phase (ΔG_{vac}) and aqueous solution (ΔG_{H_2O}), as computed at the B97-D/6-31+G(d,p) theory level. Values in kJ/mol.

Specie	Reaction scheme	ΔG_{vac}	ΔG_{H_2O}
Trimer	$3\ CAF \rightarrow (CAF)_3$	20.19	8.94
	$(CAF)_{IX} + CAF \rightarrow (CAF)_3$	13.38	10.53
Tetramer	$(CAF)_{IX} + (CAF)_{IX} \rightarrow (CAF)_4$	-1.00	8.53
	$2CAF + (CAF)_{IX} \rightarrow (CAF)_4$	5.81	6.94

From Table 2.6, above, it follows that caffeine self-aggregation to form trimers and tetramers is thermodynamically unfavoured ($\Delta G_{H_2O} = +8.36\ \mathrm{kJ/mol}$) in water, even considering the error associated with the computed values (± 4.4 kJ/mol). In vacuum self-association of two dimer IX molecules is thermodynamically favoured, thus suggesting that self-aggregation and precipitation of caffeine in a super-saturated solution is likely to occur via subsequent aggregation of caffeine dimers, while trimers are more unlikely to play a role. Importantly, only one structure of caffeine trimer and one structure of caffeine tetramer were considered. Therefore, more conclusive studies on the stability of higher-order clusters must consider a wider range of interaction geometries. However the computational calculations become exponentially more time-demanding because increase of the number of atoms with the increase of the aggregate size. Therefore this more accurate study was not performed due to lack of available time,

but the trimer and tetramer geometries were obtained from the most stable dimer of caffeine.

To summarise, the results on caffeine self-association, indicate that caffeine dimers can exist in an aqueous solution, because the error associated with the measurement cannot exclude their formation ($\Delta G_{H_2O} = +3.84 \pm 4.40$ kJ/mol). However, the formation of higher-order clusters (trimers and tetramers) is thermodynamically unfavoured in aqueous solutions ($\Delta G_{H_2O} = +8.74 \pm 4.40$ kJ/mol) thus suggesting that caffeine is present in an equilibrium between the monomeric form and caffeine aggregates of type IX. However, the predominant species will be the caffeine monomer.

2.2.3 Computational results on paraxanthine self-association process

The interesting findings obtained for caffeine suggested that the method used is an efficient tool to study self-aggregation of molecules in solution. Understanding the speciation of caffeine in solution is fundamental not only for the development of molecularly imprinted polymers, but also to understand the molecular details of the interaction between caffeine and biological systems. The biological effects of caffeine are linked to its ability to bind to the adenosine A receptors leading to stimulant effects. Besides, recent publications proved that caffeine can be used as a cognitive enhancer [38], neuroprotectant [39], antiamyloidogenic and for consolidation of long-term memory in humans.[40] As the biological effects of caffeine are further investigated, it can be envisaged that there will be an interest towards caffeine analogues, as potential drugs. Understanding their self-association behaviour is an essential requirement for the evaluation of interactions with biological receptors.[41] Paraxanthine (1,7-dimethylxanthine) is the primary metabolite of caffeine, and although the two molecules are very similar in structure, the removal of one methyl group results in a significant

change of physico-chemical properties. For instance, the limit of solubility in water decreases over ten times[42]. Therefore, the thermodynamic stability of paraxanthine dimers $(PX)_2$, was investigated using the same computational protocol to provide evidence of the more general applicability of the computational method for caffeine analogues.

In analogy with the study performed on caffeine, 100,000 possible paraxanthine dimeric structures were generated initially and after a step-by-step selection process, 80 dimer configurations were considered. Then Gibbs free energy changes were calculated. Compared to the nine low-energy dimeric configurations of caffeine, the DFT study identified 20 different paraxanthine dimers stable in the gas phase or in aqueous solution (the optimised structures are reported in Scheme 2.13, next pages).

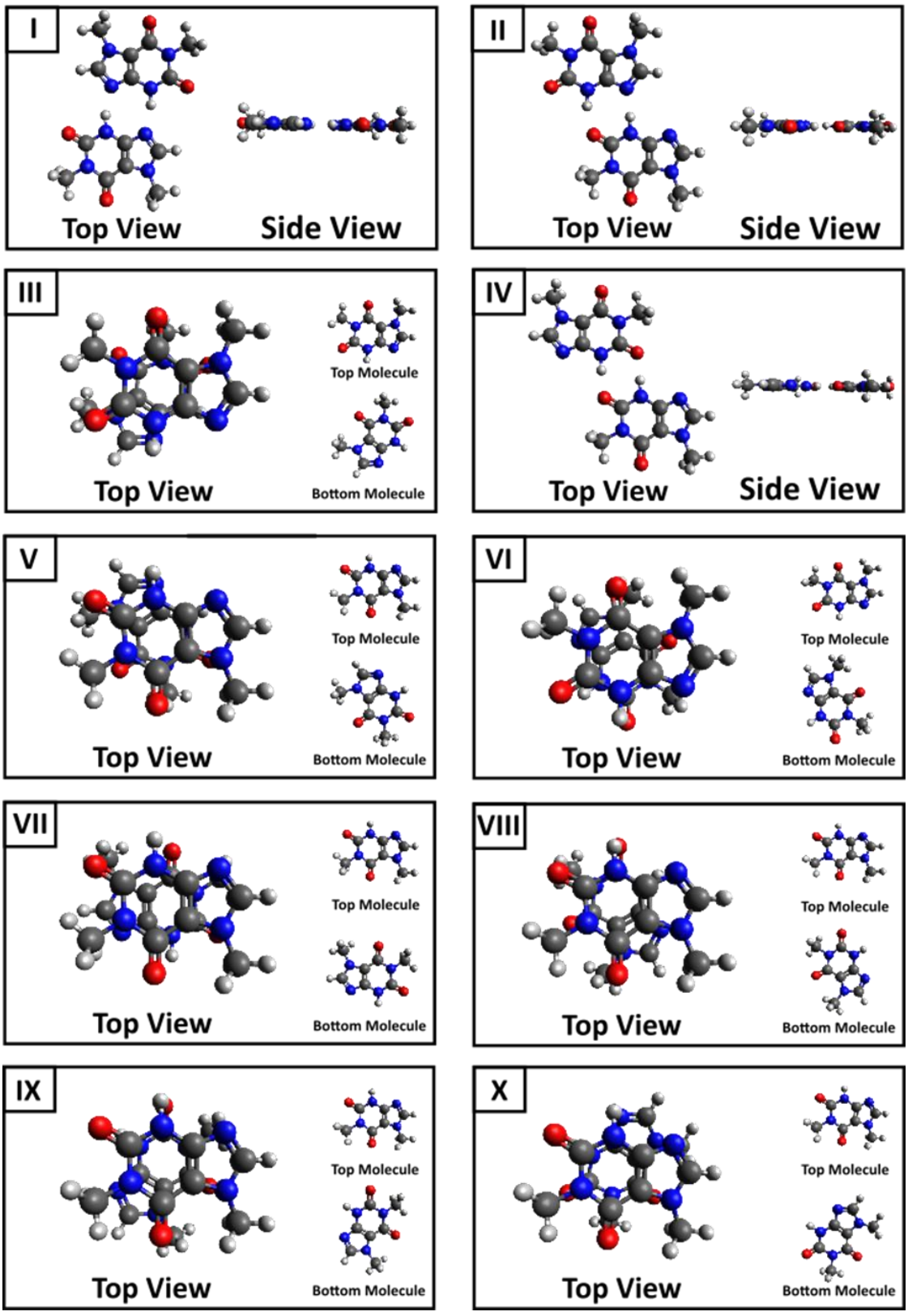
I
Top View
Side View
II
Top View
Side View
III
Top View
Top Molecule
Bottom Molecule
IV
Top View
Side View
V
Top View
Top Molecule
Bottom Molecule
VI
Top View
Top Molecule
Bottom Molecule
VII
Top View
Top Molecule
Bottom Molecule
VIII
Top View
Top Molecule
Bottom Molecule
IX
Top View
Top Molecule
Bottom Molecule
X
Top View
Top Molecule
Bottom Molecule

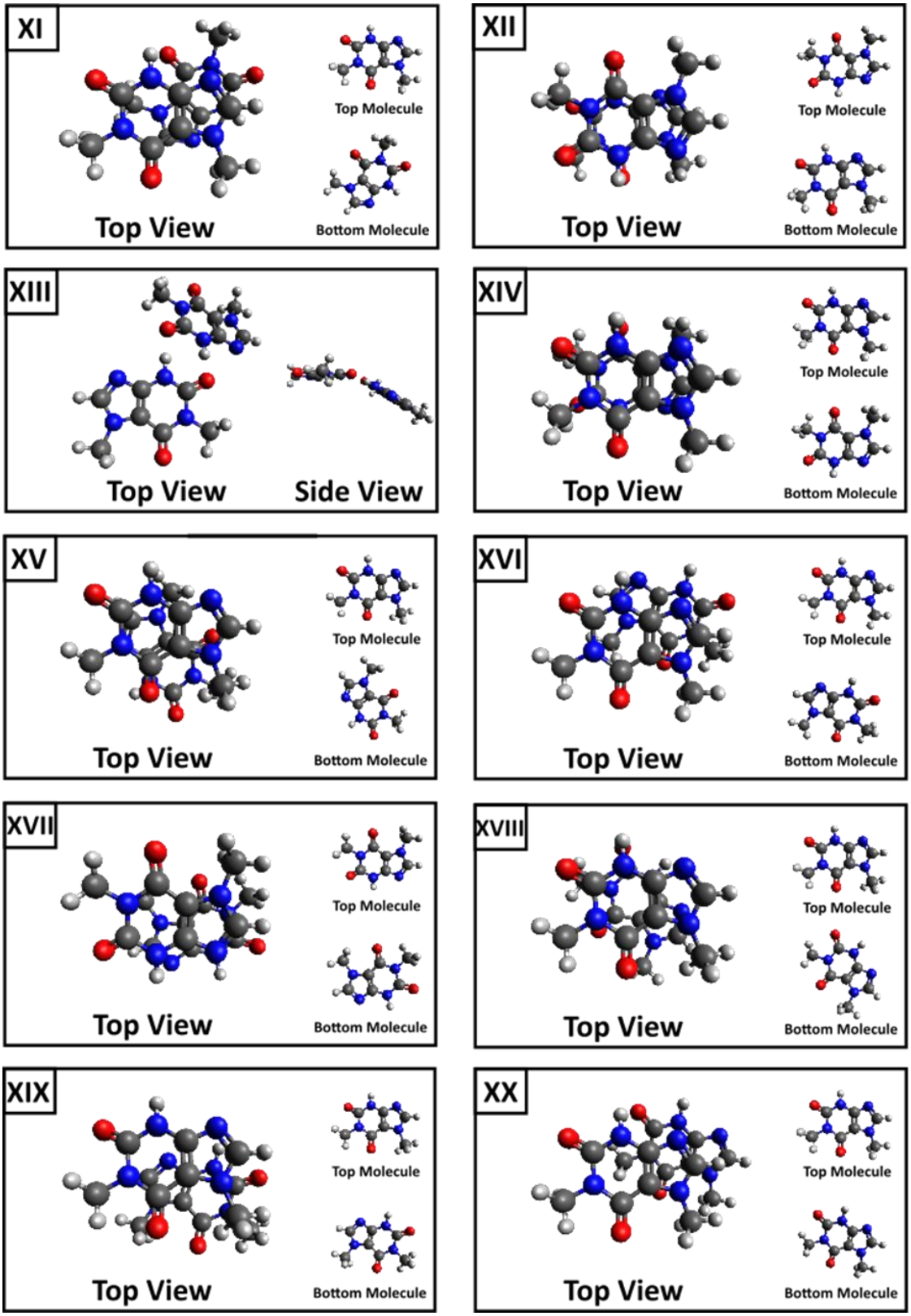

Scheme 2.13. Top view of the twenty low energy isomers of the paraxanthine dimer. To clarify the reciprocal orientation of two paraxanthine molecules in the dimers, the structure of the isolated top and bottom molecules are also reported.

The removal of one methyl group from the caffeine molecule to result in paraxanthine leads to a significant change in the interaction geometry according to the computational method. In fact, two types of structures can be identified for paraxanthine: (i) dimers I, II, IV and XIII, where the two paraxanthine units are bound by two lateral H-bonds (which was not possible in the case of caffeine); (ii) all remaining $(PX)_2$ structures, where the interaction is controlled by π-π stacking and weak $CH_3 \cdots X$ (X=O,N) hydrogen bonds. To prove that paraxanthine molecules can interact with a geometry different than that of caffeine, paraxanthine was recrystallised from methanol and an X-Ray diffraction experiment was performed in collaboration with Ms Anastasiadi, a colleague in the same research group. The crystallographic data are presented in the Scheme 2.14 in the next page.

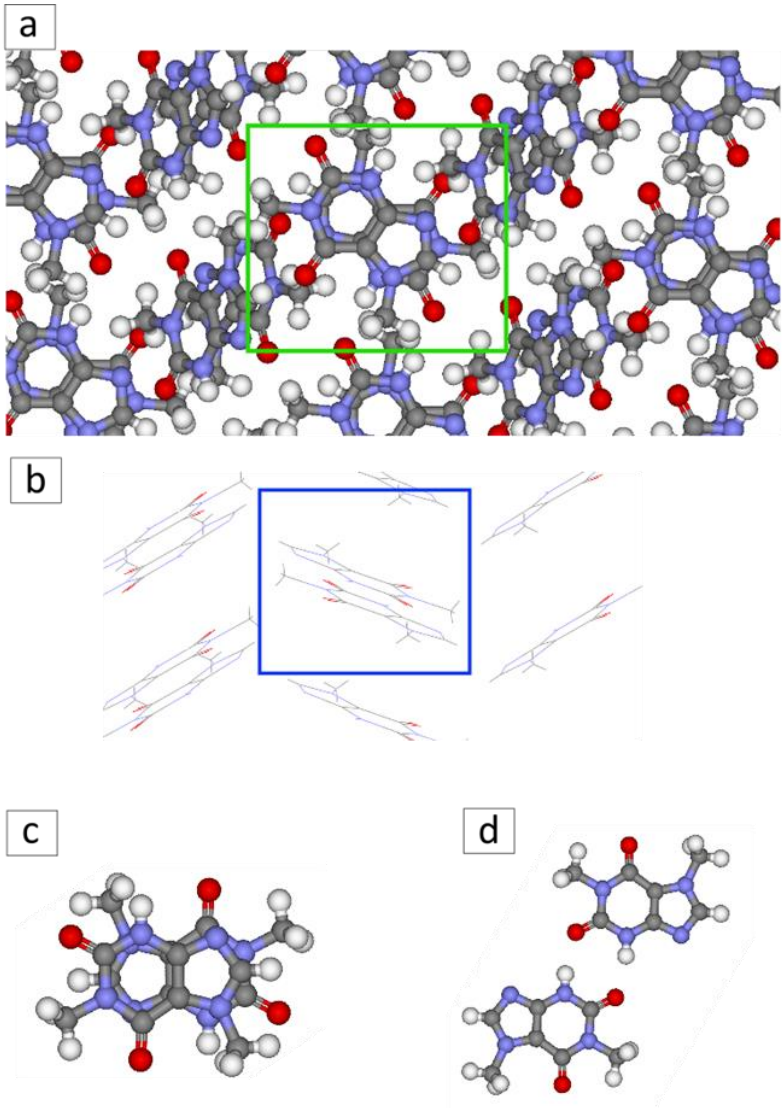

Scheme 2.14. The crystallographic structure of paraxanthine. (A): A top view showing the stacking motif highlighted in green. (B): A side view highlighting the lateral interaction (blue square). (C): A top view of the stacking interaction between two paraxanthine molecules. (D): The lateral H bond interactions between two molecules. The recrystallisation of paraxanthine step and X-ray diffraction data were collected by Ms R. Anastasiadi

From the diffraction data, two synthons were identified. That is one in which two molecules interact via π-π stacking and the other one where lateral hydrogen bonds are formed between two paraxanthine molecules. Moreover, the dimeric synthons identified in the solid state are in agreement with structures IV and VII obtained using the computational tool. The excellent agreement of the simulated structures with experimental data, also found in the case of paraxanthine, further confirmed the usefulness of the computational tool to identify possible dimeric structures.

Subsequently changes of the Gibbs free energies due to dimerisation in vacuum and water were calculated for each dimeric structure and the results are listed in table 2.6.

Table 2.6. Gibbs free energies changes due to formation of paraxanthine dimer in the gas-phase (ΔG_{vac}) and aqueous solution (ΔG_{H_2O}). Values are reported in kJ/mol.

Dimer type	ΔG_{vac}(kJ/mol)	ΔG_{H_2O}(kJ/mol)
I	-19.73	9.40
II	-15.72	8.82
III	-13.79	1.89
IV	-13.50	6.35
V	-12.96	2.80
VI	-8.82	7.82
VII	-7.86	7.86
VIII	-7.52	6.77
IX	-6.52	9.78
X	-6.23	7.40
XI	-5.81	4.39
XII	-5.31	9.61
XIII	-3.30	14.04
XIV	-3.09	7.57
XV	-2.38	0.58
XVI	-3.80	-3.84
XVII	-3.72	-2.50
XVIII	13.25	-1.84
XIX	-1.42	-1.00
XX	21.82	-0.50

In the gas phase, most of the dimers are thermodynamically stable but in aqueous solution, only the configurations forming π-π stacking interactions have a negative change of free energy of formation ($-3.76 < \Delta G_{\mathrm{H_2O}} < -0.42$ kJ/mol). The dimeric configurations showing only lateral H bonds (I, II, IV, XIII) are considerably stable in vacuum ($-19.73 < \Delta G_{vac} < -3.30$ kJ/mol) but in water dimerization is unfavourable. This behaviour is expected because water molecules will compete in the formation of H-bonds with the solute molecule and will favour stacking interaction geometries where the two molecules are overlapped and the interaction between water and the apolar aromatic ring

of paraxanthine is minimized. This finding confirmed that the solvation model employed efficiently describs both the solute-solvent interactions and solvation.

In view of a large variety of possible dimeric structures of paraxanthine dimers, a more accurate value of the Gibbs free energy of dimerisation is the Boltzmann average of different configurations. In water, the Boltzmann averaged Gibbs free energy of dimerisation was calculated to be ΔG_{H_2O} -0.46 kJ/mol. The error associated with the computational measurement was estimated to be equal to the case of caffeine (±4.4 kJ/mol). This is because similar functional groups are present in the two molecules. The error does not allow to conclude with certainty that the dimerization process for paraxanthine is favourable in water. Nevertheless, the comparison of the computed thermodynamic stability of caffeine and paraxanthine dimers shows that despite the very small structural difference between these two molecules, the free energy of formation of paraxanthine is by 5.02 kJ.mol^{-1} lower than that of caffeine, when the Boltzmann averaged values are considered. This finding suggests that the formation of more stable dimers for paraxanthine results in a higher tendency to aggregate and, therefore, to precipitate in aqueous solution, thus decreasing solubility.

2.2.4 Comparative experimental studies on caffeine and paraxanthine self-association in aqueous solutions.

The interesting computational results predicted for self-association of two very similar molecules, such as caffeine and paraxanthine, prompted a new investigation aimed at validating the computational data using an experimental approach. Therefore, isothermal titration calorimetric (ITC) experiments were conducted, by diluting highly concentrated caffeine or paraxanthine solutions in water and measuring the resulting heat. Although the experimental data were collected and analysed by Ms Anastasiadi,

the key findings are presented in this thesis to facilitate the discussion of the data related to the computational tool employed.

Dissociation experiments were performed using ITC with caffeine and paraxanthine and, for both compounds, positive heat peaks were recorded in the raw calorimetric data, thus indicating that the dissociation of both caffeine and paraxanthine in aqueous solutions is the result of an endothermic process ($\Delta H_{diss} > 0$) (Figure 2.1 and Figure 2.2).

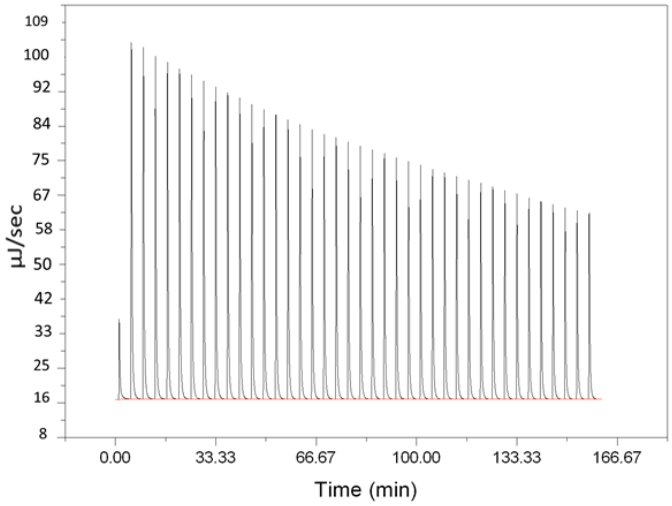

Figure 2.1. Raw calorimetric data for the dissociation experiment of caffeine. An aqueous solution of caffeine (82.4 mM) in the syringe was stepwise injected into water, at 25 °C. The data were collected by Ms. Anastasiadi.

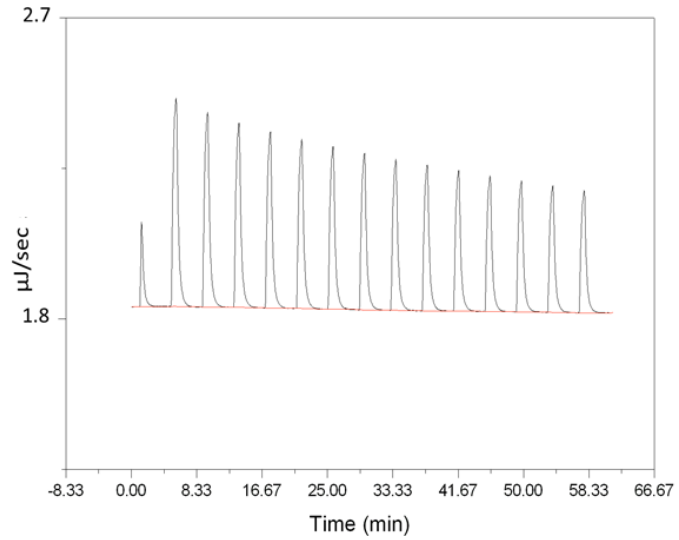

Figure 2.2. Raw ITC data for the dissociation of paraxanthine. An aqueous solution of paraxanthine (5.55 mM) in the syringe was stepwise injected in water, at 25 °C. The data were collected by Ms. Anastasiadi.

Subsequently, the integrated heat plots were constructed, and after fitting with the use of a dissociation model, the dissociation constants (K_d) and the changes in enthalpy (ΔH_{diss}) were determined together with their associated errors. The integrated plots and the fitting lines are presented in the following figures, Figures 2.3 and Figure 2.4.

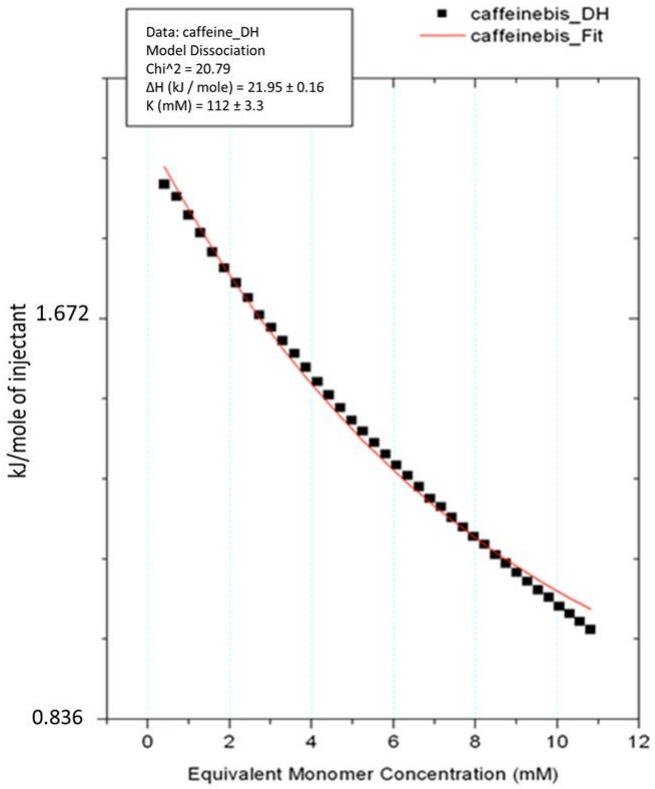

Figure 2.3. Integrated heat plots (change in enthalpy against concentration) for the dissociation of caffeine in water. The solid line corresponds to the theoretical curves with K_d = 112 ± 3.3 mM and ΔH_{diss} = 21.95 ± 0.16 kJ/mol. The data were analysed by Ms Anastasiadi.

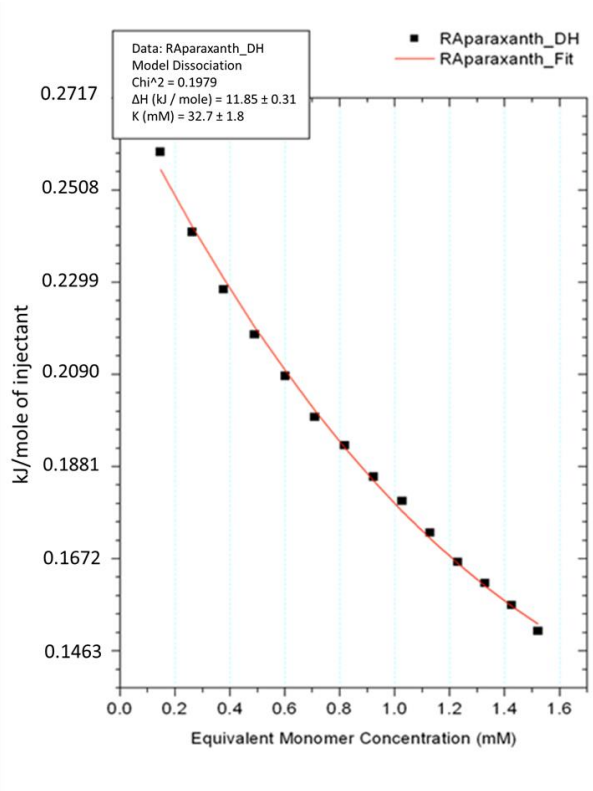

Figure 2.4. Integrated heat plots (change in enthalpy against concentration) for the dissociation of paraxanthine in water. The solid line corresponds to the theoretical curve with K_d = 32.7 ± 1.8 mM and ΔH_{diss} = 11.85 ± 0.31 kJ/mol. The data were analysed by Ms Anastasiadi.

From the dissociation heat values, the changes of enthalpy and Gibbs free energy of association were calculated according to the following mathematical relationships.

$$\Delta H_{ass} = -\Delta H_{diss} \qquad (2.6)$$

$$\Delta G_{ass} = -RTln(^{1}/_{K_{diss}}) \qquad (2.7)$$

The changes of the experimental Gibbs free energy of association and the computational results are presented and compared in Table 2.7.

Table 2.7. Changes of enthalpy and Gibbs free energy determined from the ITC dissociation experiments at 25 °C (data collected and analysed by Ms Anastasiadi.). The data are presented as association energies (kJ/mol) and the computational results are also reported for comparison.

Compound	ΔH_{ass} (ITC)	ΔG_{ass} (ITC)	ΔG_{ass} (DFT)
Caffeine	-21.94 ± 0.17	-5.43 ± 2.97	+3.84 ± 4.40
Paraxanthine	-11.83 ± 0.29	-7.90 ± 1.46	-0.46 ± 4.40

The thermodynamic values obtained herein using ITC data on caffeine self-association are in excellent agreement with those previously determined from calorimetric studies (ΔG_{ass} = –6.27 kJ.mol^{-1} at 25 °C)[32]. In the case of paraxanthine, no previous studies were conducted to study self-association. However, the good agreement found for caffeine suggests that the ITC dissociation experiments provided accurate data for paraxanthine as well. The comparison between experimental and computational data shows that, the computational method applied overestimate the Gibbs free energy changes of association for both compounds (9.28 kJ/mol for caffeine and 7.44 kJ/mol for paraxanthine). The level of agreement between the computational and experimental approaches represents a significant improvement compared to previously reported results, *e.g.* Senthilnithy R. *et al.* (ΔG_{ass} = +62.28 kJ/mol)[19], as well as the computational study done by Bradley E.S. *et al.* (ΔG_{ass} = +20.90 kJ/mol)[20] . Both these studies concluded that the caffeine dimerization process is highly unfavourable. A better agreement between experimental and computational data obtained using the presented protocol can be attributed to a more accurate searching procedure of the most stable dimeric structure, and the selection of a correct functional. This functional can describe correctly the interaction between caffeine molecules thanks to the inclusion of the dispersion correction (Grimme's dispersion correction). In addition, the difference of the change of free energies of association between caffeine and paraxanthine, ($\Delta\Delta G_{ass} = \Delta G_{ass}^{CAF} - \Delta G_{ass}^{PX}$) was 2.47 kJ.mol^{-1} and 4.30 kJ/mol as determined by ITC and calculated, respectively, showing an excellent agreement between experimental and theoretical

results, with a difference of only 1.84 kJ/mol. Although the computational method does not provide precise calculations of the change of Gibbs free energy of dimerization, it is accurate in predicting the effect of small changes in the chemical structure of caffeine with regards to the self-association process. The finding suggests that the computational approach is a useful tool for the development of caffeine analogues as potential drugs, because it predicts the effect of even small chemical changes in self-aggregation, and can therefore save time in the development of new drugs. In fact, molecules which form stable dimers are less likely to show a strong biological effect since their biological availability and activity is decreased.

Finally, a graphical comparison between the computational and experimental results is presented in Figure 2.5, where the percentage of dimers in solution with varying total concentrations of caffeine and paraxanthine are presented.

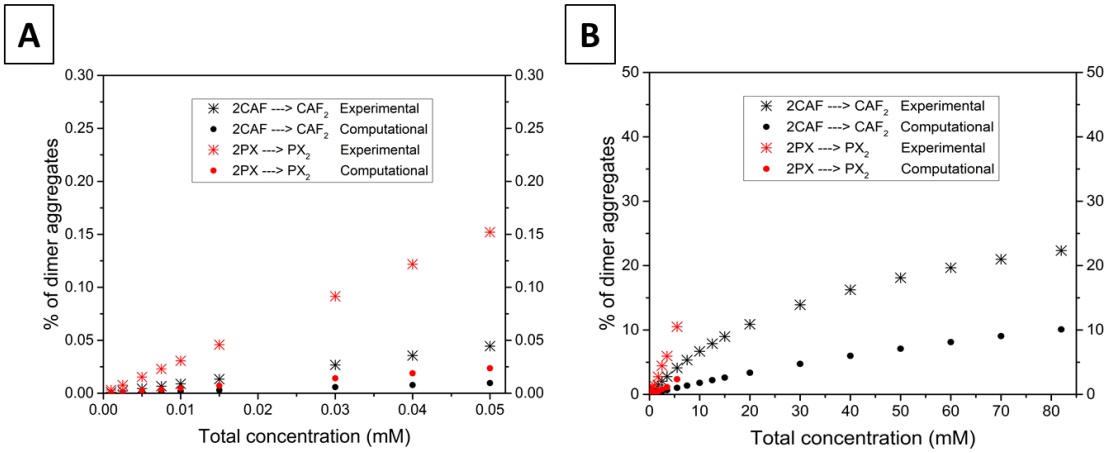

Figure 2.5. Comparison of the computational and experimental profiles of the population of dimers in solution at different total concentrations of caffeine and paraxanthine (mM). The computational points were determined using changes of the Gibbs free energy of dimerisation in water of the most stable dimers: caffeine (black circles) and paraxanthine (red circles). The experimental points were calculated using the Gibbs free energy of association determined using ITC: caffeine: (black stars) and paraxanthine (red stars). (A). A total concentration up to 0.05 mM is reported to show the diluted concentration range of biological systems. (B) The concentrations up to the solubility limits of paraxanthine (5.5 mM) and caffeine (82 mM) are depicted.

The dimer concentration in solution was determined using the monomer-dimer model, which for caffeine is given by the following equation:[43]

$$[(\mathrm{CAF})_2] = \frac{\{-1+(1+8K_\mathrm{D}[C])^{1/2}\}^2}{16K_\mathrm{D}} \qquad (2.8)$$

where, K_D is the dimerisation constant, $K_\mathrm{D} = [(\mathrm{CAF})_2]/[\mathrm{CAF}]^2$, $[C]$ is the stoichiometric molar concentration of the solute, $[C] = [\mathrm{CAF}] + 2[(\mathrm{CAF})_2]$, and [CAF] and $[(\mathrm{CAF})_2]$ are the monomer and dimer concentrations, respectively (mol L^{-1}). From Figure 2.5 it can be noticed that only at concentrations close to the limit of solubility the presence of molecular dimer is significant, but for both compounds at the concentration expected in the biological system (in the micromolar range) the concentration of both caffeine and paraxanthine dimers is negligible (< 0.2%), considering the experimental and computational data. In the case of caffeinated beverages, the concentration of caffeine can vary from 0.5 mM to 5 mM. However, even at the highest concentration expected, the presence of the caffeine dimer is negligible, based on the experimental (4% dimer present) and computational results (2% dimer present). At the concentration close to solubility limits, molecular aggregates are present as 10% for paraxanthine and 22% in the case of caffeine, when the experimental data are considered. The computational method considerably underestimates the presence of dimers at the limit of solubility. That is, in the case of paraxanthine 2% of the dimer were calculated while for caffeine a 10% of the dimer presence was computed. As previously discussed, the computational method was insufficiently precise to provide correct Gibbs free energies of dimerization (overestimation of about 8 kJ/mol), and therefore at concentrated caffeine or paraxanthine solutions the disagreement with the experimental evidence is more significant. Previous computational studies conducted by Tavagnacco L. *et al*. at the solubility limit of caffeine have shown an extensive aggregation of caffeine

molecules[6,13,16,17]. However, our computational study proved that caffeine can aggregate only as dimer and the presence of higher order clusters is improbable in aqueous solution. Besides, the dilution experiments performed with ITC have shown that even at the limit of solubility the dimer presence is considerably minor compared to caffeine monomers, thus suggesting that extensive aggregation is not occurring.

2.3 Conclusion and future work

In the present chapter, results of a DFT computational study elucidating the self-aggregation behaviour of caffeine in aqueous solutions were described given the contradictory results reported by previous computational studies, and the unclear experimental data which were not able to provide an accurate description of caffeine speciation in solution (monomer, dimer, trimer, etc.). In the presented computational study, the appropriate functional was carefully selected, and the B97-D/6-31+G(d,p) level of theory was chosen as the most appropriate for the description of the caffeine-caffeine interactions. In addition, the screening of possible caffeine structures geometries led to the identification of a stable dimer in aqueous solution ($\Delta G_{\mathrm{H_2O}} = -1.63\ kJ/mol$). However, the error associated with the measurement (±4.4 kJ/mol) was insufficiently low to state that the caffeine dimerization process is thermodynamically favoured or unfavoured. With regards to higher-order caffeine cluster, both trimers and tetramers of caffeine were found thermodynamically unfavoured ($\Delta G_{\mathrm{H_2O}} = +8.36\ kJ/mol$). Overall, the data suggest that big caffeine aggregates are not formed in solution and caffeine is present in an equilibrium between the monomer and dimer, even at the limit of solubility; in contrast with previous computational outcomes.

Considering the interest in the development of caffeine analogues as therapeutic drugs and the promising results obtained herein for caffeine, the computational tool was applied to predict the effect of small changes incurred to caffeine structure on the self-

association process. Paraxanthine was selected as a caffeine analogue because water solubility of the two compounds are very different although their structures differ only by the substitution of one methyl group with a hydrogen atom. The computational tool predicted that paraxanthine formed more stable dimers ($\Delta\Delta G_{\text{ass}} = \Delta G_{\text{ass}}^{\text{CAF}} - \Delta G_{\text{ass}}^{\text{PX}}$, = 4.30 kJ/mol) and the computational result was validated by ITC experiments performed by Ms. Anastasiadi ($\Delta\Delta G_{\text{ass}} = \Delta G_{\text{ass}}^{\text{CAF}} - \Delta G_{\text{ass}}^{\text{PX}}$, = 2.47 kJ/mol). The overall results confirmed that although non-precise changes of Gibbs free energy of dimerization are obtained, the computational tool is useful to predict how small changes in the chemical structure of caffeine affect its dimerization. Therefore, this tool can be applied in the development of caffeine analogues as potential drugs.

Future studies may focus on further evaluating the wide applicability of the computational tool, for instance by considering caffeine analogues that are reported in the literature as potential drugs[44] or considering also structural isomers of paraxanthine, like theophylline and theobromine which also show a significant different solubility in water (8.3 g/L for theophylline, and 0.5 g/L for theobromine). Structural formulae of theophylline and theobromine are shown in Scheme 2.15, below.

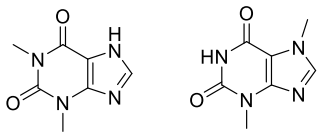

Scheme 2.15. Structural formulae of theophylline and theobromine.

To improve precision of the computational changes of Gibbs free energy of dimerisation and find a closer agreement with the experimental results, a higher theory level of the DFT method can be employed (for instance by increasing the basis set or by trying new functionals, which are continuously being developed and improved). However, the higher level of theory of the computational protocol will increase the time

required for the computational analysis to be performed. Nevertheless, considering the continuous development of faster processors and computers, in the future the application of higher level of theory and, therefore, more precise computational method will become routine.

2.4 Computational details

2.4.1 Density functional theory methods

Electronic structure calculations were carried out with the NWChem (version 6.3)[35] and Gaussian09[45] codes. Further calculations to assess the method were also performed using the plane-waves Quantum ESPRESSO[46] software suite. The B97-D2 functional[47] together with the 6-31+G(d,p) basis set were chosen to conduct geometry optimisation and compute thermal contributions to the gas-phase Gibbs free energy. The universal Solvation Model based on solute electron Density (SMD) was employed to compute the hydration free energies of the caffeine dimer, trimer and tetramer forms.[48] The SMD model together with the M06-2X/6-31+G(d,p) density functional method was used to compute changes of solvation free energy. The final Gibbs free energy was calculated according to the following equation:

$$G_{\mathrm{X}} = E_{\mathrm{e,gas}} + \delta G^{\circ}_{\mathrm{VRT,gas}} + \Delta G^{*}_{\mathrm{solv}} + RT\ln[\tilde{R}T] \quad (2.9)$$

$E_{\mathrm{e,gas}}$ is the gas-phase total electronic energy of the solute, $\delta G^{\circ}_{\mathrm{VRT,gas}}$ is the vibrational-rotational-translational contribution to the gas-phase Gibbs free energy change at T = 298 K under standard-state partial pressure of 1 atm. $\Delta G^{*}_{\mathrm{solv}}$ is the change of solvation free energy of the solute corresponding to transfer from an ideal gas at a concentration of 1 mol.L^{-1} to an ideal solution at a liquid-phase concentration of 1 mol.L^{-1}, $RT\ln[\tilde{R}T]$ is the free energy change of 1 mol of an ideal gas from 1 atm to 1 mol/L ($RT\ln[\tilde{R}T] = 7.90$ kJ/mol at $T = 298.15$ K and $\tilde{R} = 0.082052$ K^{-1}). Avogadro

software (version 1.20)[49] was employed to generate the initial structures of paraxanthine and caffeine and visualise the final dimers and aggregates.

2.4.2 Assessment of the method

To find the most appropriate computational technique, the dimeric synthons found in the crystallographic structure of caffeine were used as initial structures and structure optimisation was conducted using a variety of functionals and basis set (the complete list of methods is reported in Table 2.1 and 2.2). Gaussian 09 software was used for the geometry optimisation and afterwards, the optimised structure was visually analysed. If the initial structure was retained, the method was assessed to be able to identify correctly the caffeine-caffeine interactions. The energy change due to dimer formation was calculated as the difference of the energy of the dimer and the monomer form (Equation 2.1).

2.4.3 Probing the potential energy surface of caffeine and paraxanthine dimer

The caffeine and paraxanthine structures were obtained with Avogadro software. These structures were optimised using Gaussian 09 software at the B97-D/6-31+G(d,p) level of theory. The optimised structures were employed to generate 100,000 random dimeric structures using Granada software [34] in a box with 12 Å side. Subsequently, only dimers where molecules were at a distance < 4 Å were selected. For the obtained structures, the electronic energy was calculated using the MWChem software[35] and employing the B97-D/6-31+G(d,p) level of theory. Subsequently, the Boltzmann factor was calculated (according to Equation 2.5) and only dimeric structures with a factor > 0.01 were further considered. The resulting structures were geometry optimised and their Gibbs free energies in vacuum were calculated using the B97-D/6-31+G(d,p) method. Finally, the Gibbs free energy of solvation was calculated using the SMD/ M06-2X/6-

31+G(d,p) level of theory. Stable dimer structures were visually analysed and categorised based on similar interaction geometry.

2.4.4 Generation of caffeine trimer and tetramer

The most stable dimeric structure of caffeine was employed to generate a tetramer of caffeine by manually placing two dimers one on top of the other using the Avogadro software. The trimer was subsequently obtained from the tetramer by removing one caffeine molecule at the top. The obtained structures were optimised using Gaussian 09 at the B97-D/6-31+G(d,p) level of theory. The Gibbs free energy in gas and water phases were calculated with the same procedure as that used for the dimer.

2.5 Experimental details

All the following experiments and data analysis on paraxanthine X-ray diffraction and isothermal titration calorimetry were performed by Ms Anastasiadi and are reported in the present thesis for completeness of the arguments presented.

2.5.1 Reagents and instrumentations

Caffeine (1,3,7-trimethylxanthine), paraxanthine (1,7-dimethylxanthine) were purchased from Sigma-Aldrich as anhydrous powders. GC grade methanol (Sigma-Aldrich) was employed for recrystallisation. Aqueous solutions were prepared using deionised water. For ITC experiments, VP-ITC Microcalorimeter (MicroCal, Malvern Instruments, UK) was employed. Before analysis, the solutions were sonicated, using an ultrasonic bath (Sonorex Super BANDELIN electronic GmbH & Co. KG) for 5 min followed by degassing with ThermoVac (MicroCal, Malvern Instruments, UK).

2.5.2 X-ray crystallographic analysis of paraxanthine

Paraxanthine was recrystallised from methanol by slow solvent evaporation at room temperature. A translucent colourless block-like crystal, of approximate dimension of

0.080 × 0.150 × 0.300 mm, was used for X-ray crystallographic analysis. A total of 1088 frames were collected. The total exposure time was 3.02 hours. The frames were integrated with the Bruker SAINT software package using a narrow-frame algorithm. Crystal data at 100(2)K: $C_7H_8N_4O_2$, Mr=180.17, monoclinic crystal system. The final cell constants of *a*=7.376(7) Å, *b*=13.329(13) Å, *c*=8.193(8) Å, *β*=113.50(2)°, Volume=738.7(13) $Å^3$, space group $P2_1/n$, Z=4, $\rho_{calculated}$=1.620 g cm^{-3}, μ=0.124mm^{-1}, (R_{int}=0.0273) reflections collected within the θ range of 3°-28°. The final anisotropic full-matrix least-squares refinement on F^2, based on 7147 with I>2σ(I) and 120 variables converged at R1=0.0330 for the observed data, wR2=0.0914 for all data and Goodness of fit=1.032.

2.5.3 Dissociation experiments by isothermal titration calorimetry (ITC)

The measurements were carried out at 25°C. A solution of caffeine (82.4 mM) or paraxanthine (5.55 mM) was loaded in the syringe and step-wise injected in the cell, in degassed H_2O. The dilution effect when gradually injecting the concentrated solution of caffeine or paraxanthine in H_2O, made the aggregates to dissociate and the heat generated was measured. Reference cell was also filled with distilled H_2O. The reference power was set to 16.72 μJ/sec; initial delay 60 s; stirring rate 400 rpm; equilibration options were set to fast equilibration; feedback mode high. For both experiments, the initial injection was 5 μL and the rest aliquots were of 15 μL with 300 s spacing between each injection in order to assure signal returning to the baseline. The filter period was 2 s. The duration of the first injection was 10 s and 30 s for the following ones. The total number of injections was 30. The integrated heat changes were plotted against the concentration in the cell and all data were analysed with the Origin (version 7.0) software using a dissociation curve fitting model.

2.6 References

1 I. Horman and B. Dreux, Dimerisation of caffeine, *Helv. Chim. Acta*, 1985, **68**, 72–75.

2 D. B. Davies, D. A. Veselkov, L. N. Djimant and A. N. Veselkov, Hetero-association of caffeine and aromatic drugs and their competitive binding with a DNA oligomer, *Eur. Biophys. J.*, 2001, **30**, 354–366.

3 N. D'Amelio, L. Fontanive, F. Uggeri, F. Suggi-Liverani and L. Navarini, NMR reinvestigation of the caffeine-chlorogenate complex in aqueous solution and in coffee brews, *Food Biophys.*, 2009, **4**, 321–330.

4 M. Falk, M. Gil and N. Iza, Self-association of caffeine in aqueous solution: an FT-IR study, *Can. J. Chem.*, 1990, **68**, 1293–1299.

5 S. Banerjee, D. Bhowmik, P. K. Verma, R. K. Mitra, A. Sidhhanta, G. Basu and S. K. Pal, Ultrafast spectroscopic study on caffeine mediated dissociation of mutagenic ethidium from synthetic DNA and various cell nuclei, *J. Phys. Chem. B*, 2011, **115**, 14776–14783.

6 L. Tavagnacco, Y. Gerelli, A. Cesàro and J. W. Brady, Stacking and Branching in Self-Aggregation of Caffeine in Aqueous Solution: From the Supramolecular to Atomic Scale Clustering, *J. Phys. Chem. B*, 2016, **120**, 9987–9996.

7 E. L. Farquhar, M. Downing and S. J. Gill, The Enthalpy of Self-Association of Pyrimidine Derivatives in Water, *Biochemistry*, 1968, **7**, 1224–1225.

8 S. Banerjee, P. K. Verma, R. K. Mitra, G. Basu and S. K. Pal, Probing the interior of self-assembled caffeine dimer at various temperatures, *J. Fluoresc.*, 2012, **22**, 753–769.

9 H. Bothe and H. K. Cammenga, Calorimetric Investigation of Aqueous Caffeine Solution and Molecular Association of Caffeine, *Thermochmica Acta*, 1983, **69**, 235–252.

10 A. Cesàro and G. Starec, Thermodynamic properties of caffeine crystal forms, *J. Phys. Chem.*, 1980, **84**, 1345–1346.

11 Y. Ahn, J. K. Saha, G. C. Schatz and J. Jang, Molecular dynamics study of the formation of a self-assembled monolayer on gold, *J. Phys. Chem. C*, 2011, **115**, 10668–10674.

12 F. Mustan, A. Ivanova, G. Madjarova, S. Tcholakova and N. Denkov, Molecular Dynamics Simulation of the Aggregation Patterns in Aqueous Solutions of Bile Salts at Physiological Conditions, *J. Phys. Chem. B*, 2015, **119**, 15631–15643.

13 L. Tavagnacco, S. Di Fonzo, F. D'Amico, C. Masciovecchio, J. W. Brady and A. Cesàro, Stacking of purines in water: the role of dipolar interactions in caffeine, *Phys. Chem. Chem. Phys.*, 2016, **18**, 13478–13486.

14 L. Tavagnacco, O. Engström, U. Schnupf, M. L. Saboungi, M. Himmel, G. Widmalm, A. Cesàro and J. W. Brady, Caffeine and sugars interact in aqueous solutions: A simulation and NMR study, *J. Phys. Chem. B*, 2012, **116**, 11701–11711.

15 L. Tavagnacco, P. E. Mason, G. W. Neilson, M. Saboungi, A. Cesàro and J. W. Brady, Molecular Dynamics and Neutron Scattering Studies of Mixed Solutions of Ca ffeine and Pyridine in Water, *J. Phys. Chem. B*, 2018, **122**, 5308–5315.

16 L. Tavagnacco, U. Schnupf, P. E. Mason, M.-L. Saboungi, A. Cesàro and J. W. Brady, Molecular dynamics simulation studies of caffeine aggregation in aqueous solution., *J. Phys. Chem. B*, 2011, **115**, 10957–66.

17 L. Tavagnacco, J. W. Brady, F. Bruni, S. Callear, M. A. Ricci, M. L. Saboungi and A. Cesàro, Hydration of Caffeine at High Temperature by Neutron Scattering and Simulation Studies, *J. Phys. Chem. B*, 2015, **119**, 13294–13301.

18 R. F. Ribeiro, A. V Marenich, C. J. Cramer and D. G. Truhlar, The solvation, partitioning, hydrogen bonding, and dimerization of nucleotide bases: a multifaceted challenge for quantum chemistry, *Phys.Chem.Chem.Phys*, 2011, **13**, 10908–10922.

19 R. Senthilnithy, M. S. S. Weerasingha and D. P. Dissanayake, Interaction of caffeine dimers with water molecules, *Comput. Theor. Chem.*, 2014, **1028**, 60–64.

20 E. S. Bradley and C. H. Hendon, The impact of solvent relative permittivity on the dimerisation of organic molecules well below their solubility limits: examples from brewed coffee and beyond, *Food Funct.*, 2017, **8**, 1037–1042.

21 D. Di Tommaso and K. L. Watson, Density Functional Theory Study of the Oligomerization of Carboxylic Acids, *J. Phys. Chem. A*, 2014, **118**, 11098–11113.

22 V. I. Poltev, T. I. Grokhlina, E. González, a. Deriabina, a. Cruz, L. Gorb, J. Leszczynski, L. N. Djimant and a. N. Veselkov, The study of three-dimensional structure of caffeine associates using computational and experimental methods, *J. Mol. Struct. THEOCHEM*, 2004, **709**, 123–128.

23 J. D. Sutor, The structures of the pyrimidines and purines. VII. The crystal structure of caffeine, *Acta Cryst.*, 1958, **11**, 453–458.

24 C. W. Lehmann and F. Stowasser, The crystal structure of anhydrous beta-caffeine as determined from X-ray powder-diffraction data., *Chem. A Eur. J.*, 2007, **13**, 2908–2911.

25 C. Janiak, A critical account on π–π stacking in metal complexes with aromatic nitrogen-containing ligands †, *Dalton Trans.*, 2000, 3885–3896.

26 C. R. Martinez and B. L. Iverson, Rethinking the term ‘“ pi-stacking ”’, *Chem. Sci.*, 2012, **3**, 2191–2201.

27 J. D. Sutor, Evidence of the existence of C-H O Hydrogen Bonds in Crystals, *J. Chem. Scociety*, 1963, **0**, 1105–1110.

28 G. R. Desiraju, The C-H-O Hydrogen Bond in Crystals: What Is It ?, *Acc. Chem. Res.*, 1991, **24**, 290–296.

29 M. Karthika, L. Senthilkumar and R. Kanakaraju, Theoretical studies on hydrogen bonding in caffeine-theophylline complexes, *Comput. Theor. Chem.*, 2012, **979**, 54–63.

30 Y. Zhao and D. G. Truhlar, Exploring the Limit of Accuracy of the Global Hybrid Meta Density Functional for Main-Group Thermochemistry, Kinetics, and Noncovalent Interactions, *J. Chem. Theory Comput.*, 2008, **4**, 1849–1868.

31 L. A. Burns, Á. V.- Mayagoitia, B. G. Sumpter and C. D. Sherrill, Density-functional approaches to noncovalent interactions: A comparison of dispersion corrections (DFT-D), exchange-hole dipole moment (XDM) theory , and specialized functionals, *J. Chem. Phys.*, 2011, **134**, 084107.

32 S. J. Gill, M. Downing and G. F. Sheats, The Enthalpy of Self-Association of Purine Derivates in Water, *Biochemistry*, 1967, **6**, 272–276.

33 J. W. Ponder, C. Wu, P. Ren, V. S. Pande, J. D. Chodera, M. J. Schnieders, I. Haque, D. L. Mobley, D. S. Lambrecht, R. A. DiStasio, M. Head-Gordon, G. N. I. Clark, M. E. Johnson and T. Head-Gordon, Current Status of the AMOEBA Polarizable Force Field, *J. Phys. Chem. B*, 2010, **114**, 2549–2564.

34 L. A. Montero, A. M. Esteva, J. Molina, A. Zapardiel, L. Herna, H. Màrquez and A. Acosta, A Theoretical Approach to Analytical Properties of 2 , 4-Diamino-5-phenylthiazole in Water Solution . Tautomerism and Dependence on pH, *J. Am. Chem. Soc.*, 1998, **120**, 12023–12033.

35 M. Valiev, E. J. Bylaska, N. Govind, K. Kowalski, T. P. Straatsma, H. J. J. Van

Van Dam, D. Wang, J. Nieplocha, E. Apra, T. L. Windus and W. A. de Jong, NWChem : A comprehensive and scalable open-source solution for large scale molecular simulations, *Comput. Phys. Commun.*, 2010, **181**, 1477–1489.

36 J. D. Sutor, The Structure of the Pyrimidines and Purines. VII. The Crystal Structure of Caffeine, *Acta Crystallogr.*, 1965, **19**, 453–458.

37 R. J. Davey, G. Dent, R. K. Mughal and S. Parveen, Concerning the Relationship between Structural and Growth Synthons in Crystal Nucleation: Solution and Crystal Chemistry of Carboxylic Acids As Revealed through IR Spectroscopy, *Cryst. Growth Des.*, 2006, **6**, 1788–1796.

38 A. Nehlig, Is caffeine a cognitive enhancer?, *J. Alzheimer's Dis.*, 2010, **20**, S85–S94.

39 V. L. Batalha, D. G. Ferreira, J. E. Coelho, J. S. Valadas, R. Gomes, M. Temido-Ferreira, T. Shmidt, Y. Baqi, L. Buée, C. E. Müller, M. Hamdane, T. F. Outeiro, M. Bader, S. H. Meijsing, G. Sadri-Vakili, D. Blum and L. V. Lopes, The caffeine-binding adenosine A 2A receptor induces age-like HPA-axis dysfunction by targeting glucocorticoid receptor function, *Sci. Rep.*, 2016, **6**, 31493–3157.

40 D. Borota, E. Murray, G. Keceli, A. Chang, J. M. Watabe, M. Ly, J. P. Toscano and M. A. Yassa, Post-study caffeine administration enhances memory consolidation in humans, *Nat. Neurosci.*, 2014, **17**, 201–203.

41 M. B. Patrascu, E. Malek-Adamian, M. J. Damha and N. Moitessier, Accurately modeling the conformational preferences of nucleosides, *J. Am. Chem. Soc.*, 2017, **139**, 13620–13623.

42 S. C. B. Inc, Paraxanthine technical Information, https://www.scbt.com/scbt/product/paraxanthine-611-59-6.

43 T. Krishnan, W. C. Duer, S. Goldman and J.-L. Fortier, On the use of dilution calorimetry in the study of hydrogen-bonding self-association reactions: benzoic acid in benzene, *Can. J. Chem.*, 1979, **57**, 530–537.

44 J. W. Daly, Caffeine analogs: Biomedical impact, *Cell. Mol. Life Sci.*, 2007, **64**, 2153–2169.

45 M. J. Frisch and D. J. Trucks, G. W.; Schlegel, H. B.; Scuseria, G. E.; Robb, M. A.; Cheeseman, J. R.; Scalmani, G.; Barone, V.; Mennucci, B.; Petersson, G. A.; Nakatsuji, H.; Caricato, M.; Li, X.; Hratchian, H. P.; Izmaylov, A. F.; Bloino, J.; Zheng, G.; Sonnenberg, J. L.; Had, in *Gaussian, Inc Wallingford CT*, 2009.

46 P. Giannozzi, S. Baroni, N. Bonini, M. Calandra, R. Car, C. Cavazzoni, D. Ceresoli, G. L. Chiarotti, M. Cococcioni, I. Dabo, A. Dal Corso, S. de Gironcoli, S. Fabris, G. Fratesi, R. Gebauer, U. Gerstmann, C. Gougoussis, A. Kokalj, M. Lazzeri, L. Martin-Samos, N. Marzari, F. Mauri, R. Mazzarello, S. Paolini, A. Pasquarello, L. Paulatto, C. Sbraccia, S. Scandolo, G. Sclauzero, A. P. Seitsonen, A. Smogunov, P. Umari and R. M. Wentzcovitch, QUANTUM ESPRESSO: a modular and open-source software project for quantum simulations of materials., *J. Phys. Condens. Matter*, 2009, **21**, 395502.

47 S. Grimme, Semiempirical GGA-Type Density Functional Constructed with a Long-Range Dispersion Correction, *J. Comput. Chem.*, 2006, **27**, 1787–1799.

48 A. V Marenich, C. J. Cramer and D. G. Truhlar, Universal Solvation Model Based on Solute Electron Density and on a Continuum Model of the Solvent Defined by the Bulk Dielectric Constant and Atomic Surface Tensions, *J.Phys.Chem. B*, 2009, **113**, 6378–6396.

49 M. D. Hanwell, D. E. Curtis, D. C. Lonie, T. Vandermeersch, E. Zurek and G. R. Hutchison, Avogadro: an advanced semantic chemical editor, visualization, and analysis platform, *J. Cheminform.*, 2012, **4**, 17.

CHAPTER 3
Synthesis and characterisation of MIPs specific for caffeine

3.1 Introduction

The following chapter describes the research conducted towards the synthesis of imprinted polymers for the specific recognition of caffeine. The work was carried out over a period of 12 months based at Queen Mary University of London, as part of Professor Resmini's research group. The results and discussion section is organised in four main parts, namely: (i) selection of the functional monomer by ^{1}H- NMR titration experiments; (ii) optimisation of high-dilution radical polymerisation protocols to maximise binding interactions; (iii) characterisation of the isolated polymeric nanogels; (iv) development of a method to evaluate the rebinding properties of the polymer nanoparticles. The time available for the last part of the project was limited as a result of the compulsory secondments included in the contract. Therefore, the main focus was on the identification of an appropriate functional monomer, followed by optimisation of the polymerisation and the development of a suitable method for carrying out rebinding studies. The data on rebinding for the isolated nanogels reported in this thesis are only preliminary and would need to be further optimised and repeated in order to confirm the findings.

3.2 Results and discussion

3.2.1 Selection of the functional monomer

Molecularly imprinted polymers (MIPs) can display very selective recognition properties. However, the formation of a strong and stable pre-polymerisation complex of the template with the functional monomer(s) is a key requirement to achieve this selectivity.[1–3] As mentioned in Chapter 1 (Section 1.6), there are several approaches that can be used for imprinting, and the work within the present project was focused solely on the non-covalent approach, whereby the interactions between the functional monomer and the template involve on non-covalent interactions, such as hydrogen bonds, as well

as ionic and van der Waals interactions, etc. When the non-covalent approach is employed, it is essential to evaluate the strength of the interaction between the template and the functional monomer in the solvent, in which the polymerisation is performed. In fact, an equilibrium will be established between the free template and the template-(functional monomer) complex ([Template − FM]), as described in Scheme 3.1 below.

$$\text{TEMPLATE + FM} \underset{}{\overset{K_{ass}}{\rightleftharpoons}} \text{[Template-FM]}$$

Scheme 3.1. The chemical equilibrium of the pre-polymerisation complex formation.

$$\text{With } K_{ass} = \frac{[\text{Template}-\text{FM}]}{[\text{Template}][\text{FM}]} \qquad (3.1)$$

The negative effects of uncomplexed template molecules were explained in Chapter 1 (page 36). Ideally, the equilibrium should totally be shifted towards the complex formation, thus leading to a stoichiometric interaction, as reported by Wulff G. and Schönfeld R. in the case of amidines and carboxylic acid ($K_{ass} > 10^6$ M^{-1}).[4] In most cases, such a high affinity is not achieved, and a wide range of K_{ass} from 30 to 9000 $M^{-1}$are reported.[2,3,5] The highest affinity is usually obtained when apolar solvents are used and the interaction is based on hydrogen bonds and ionic interactions. In the present work, however, the application of hydrophobic interactions and water as a polymerisation medium were investigated and, therefore, complex stability constants in the range of 20 to 2000 M^{-1} were expected.[6] Although hydrophobic and π-π stacking interactions are weaker compared to hydrogen bond interactions, there are several advantages in using this approach which will be explained later in this section. Different techniques are available to study the non-covalent interaction between molecules, such as calorimetric experiments (e.g. isothermal titration calorimetry) as well as spectroscopic techniques based on fluorescence, UV-vis, and NMR. In particular, in the case of small organic molecules, ^{1}H NMR spectroscopy is the most convenient technique since it does not

require the two molecules to be fluorescent, or the interaction to cause a change in the UV-Vis spectroscopic properties. A typical procedure for a proton NMR spectroscopy titration experiment is to keep constant the amount of functional monomer and increase the content of the template stepwise. Due to the interaction between the template and the functional monomer, the electronic density in the complex will be different compared with that of the unbound molecules and this will result in a change of the chemical shifts of the protons. In Figure 3.1, a graphical example is depicted where a generic alcohol group forms a hydrogen bond with a ketone, leading to a shift in the O**H** proton resonance frequency (green signal in Figure 3.1B). Subsequently, it is possible to calculate the ratio between bound and unbound functional monomer directly by integration of the proton's NMR signals (Figure 3.1 A and 3.1 B).

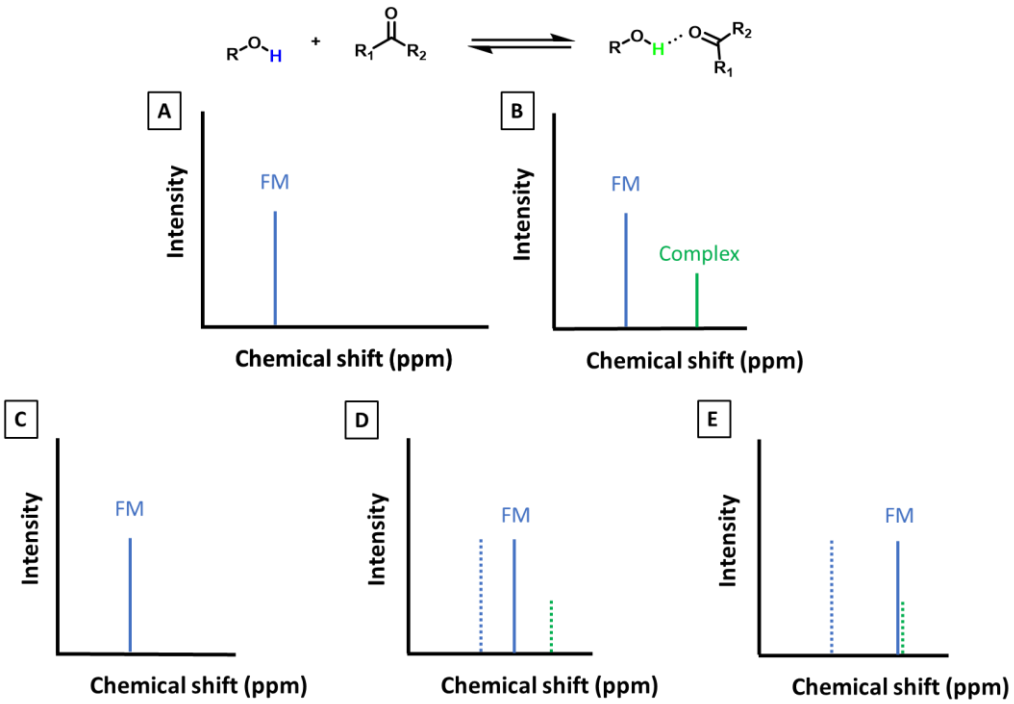

Figure 3.1. An illustrative example of a proton NMR titration experiment in the case of slow kinetics of the complex formation (case A and B) and fast kinetics of the pre-polymerisation reaction (C, D, E). The blue lines represent the chemical signals of the functional monomer uncomplexed, and the green line is the observed signal of the functional monomer complexed. In the case of fast kinetic processes, a shift of the functional monomer signal is observed by subsequent increment in the template concentration (C, D and E), and the functional monomer signal will shift from its initial position (dashed blue line D, and E) to the complex signal position (dashed green line).

However, in most cases the situation depicted in Figure 3.1 A and 3.1 B is not achieved. In fact, if the kinetics of the pre-polymerisation equilibrium are established faster or at a time similar to the time scale of recording a proton NMR experiment, then a static image of the chemical system under investigation cannot be recorded and an average between complex signal and un-complex reagents is obtained (Figure 3.1 D and 3.1 E). In particular, the observed signal (blue line) will be the result of the averaged signals of complexed and un-complexed monomer, weighted by the molar ratio, as expressed in the following equation:

$$\partial_{\mathrm{FM_{observed}}} = c_{\mathrm{FM_{UnCompl}}}\partial_{\mathrm{FM_{UnCompl}}} + c_{\mathrm{FM_{Compl}}}\partial_{\mathrm{FM_{Compl}}} \qquad (3.2)$$

Where $\partial_{\mathrm{FM_{observed}}}$ are the chemical shift of the observed signal ($\mathrm{FM_{observed}}$) (blue signal in Figure 3.1 C, D, E); the uncomplexed functional monomer ($\mathrm{FM_{UnCompl}}$, blue dashed line Figure 1 D,E) the complexed functional monomer ($\mathrm{FM_{Compl}}$ Figure 3.1 D and E dashed red line). $c_{\mathrm{FM_X}}$is the molar ratio of the un-complexed functional monomer (UnCompl) and complexed functional monomer (Compl). Therefore, by increasing the amount of complexation (for example by increasing the amount of template molecule), a proportional shift in the observed proton signals is recorded. Subsequently, a plot of the change in signal position versus template concentration provides information about the thermodynamic stability of the complex. An example of the type of graph that could be obtained is shown in Figure 3.2.

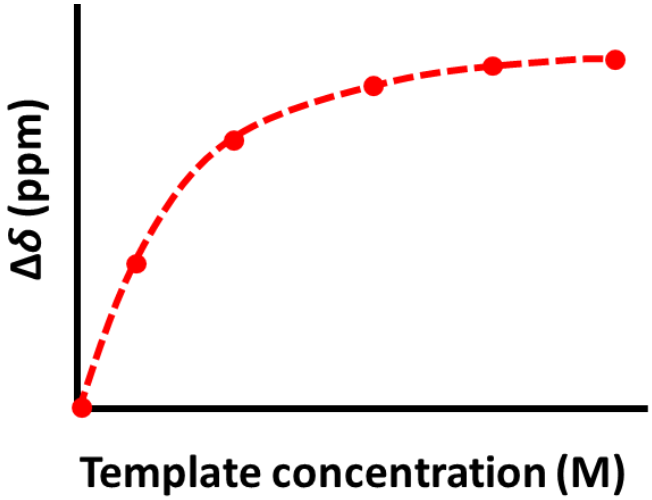

Figure 3.2. An example of the NMR spectroscopy titration curve obtained in the case of fast kinetics of the pre-polymerisation complex. A rectangular hyperbola is obtained when the shift in the proton position of the functional monomer is plotted versus the template concentration.

In the following section, the data were fitted using the one site binding model available in Origin (9.0), since its application with MIP has been previously reported in the literature.[5,7] The equation employed is reported below.

$$\Delta\partial = \frac{\Delta\partial_{\max} \times M_{\text{Template}}}{K_{\text{diss}} + M_{\text{Template}}} \qquad (3.3)$$

In equation 3.3, $\Delta\partial_{max}$ is the maximum value of shift in the proton NMR signal and K_{diss} is the dissociation constant for the complex formation. M_{Template} is the molar concentration of the template. After data fitting, the $\Delta\partial_{\max}$ and the dissociation constant are obtained. Using the following equation, the complex stability constant is calculated:

$$K_{\text{ass}} = {}^{1}/_{K_{\text{diss}}} \qquad (3.4)$$

Another advantage of proton NMR titration experiments compared to ITC measurements is that they can provide information about the interaction's geometry. In fact, the chemical groups involved in the interaction will show the largest change in the proton chemical shift.[3,5,7,8] In view of the importance of the pre-polymerisation studies and the possibility to investigate them using ^{1}H NMR spectroscopy, the next step was to select

some candidate functional monomers based on the functional groups present in caffeine. In the case of caffeine, two types of non-covalent bonds are possible: (i) hydrogen bonds with the nitrogen and oxygen of caffeine, in which case the functional monomer has to be a proton donating group (such as an acid, alcohol or amine); (ii) π-π stacking interaction in which case the functional monomer must have an aromatic ring.

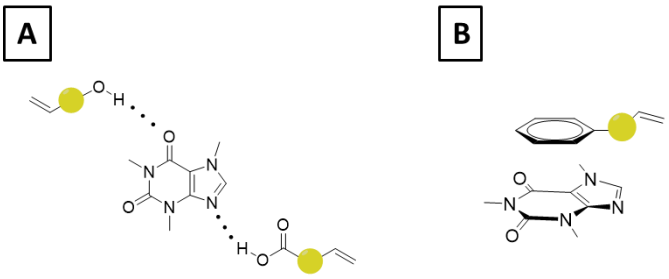

Scheme 3.2. The non-covalent interactions of caffeine. (A) hydrogen bonds between the oxygen and nitrogen atoms of caffeine and proton-donating functional monomers (as examples an alcohol and an acid). (B) the π- π stacking interaction between molecules of caffeine and a generic aromatic functional monomer.

In the case of H-bonds, to maximise the strength of the interaction, organic solvents with low polarity (such as tetrahydrofuran or chloroform) should be employed, while in the case of stacking and hydrophobic interactions the best results are expected to be achieved in aqueous solutions. From some recently published works dealing with imprinted materials and caffeine, it follows that acrylic acid and methacrylic acid are the most frequently selected as functional monomers due to their ability to form hydrogen bonds with caffeine. Low polarity solvents are used, like acetonitrile, dimethylformamide and chloroform, to favour the formation of the pre-polymerisation complex. However, the use of aqueous solutions or alcohols (methanol and ethanol) has been reported (although the formation of an H-bond complex between an acid and caffeine is unlikely to happen in these solvents). With regard to the polymerisation, the most applied is radical polymerisation in solution using a thermal initiator (such as AIBN) thanks to its simplicity in terms of the equipment required and preparation of the reaction solution. A summary of the most recent literature data is presented in Table 3.1.

Table 3.1. Most recent publications on the development of MIPs using caffeine as the template. The following acronyms were employed for the functional monomer: 3-TAA (3-thiopheneacetic acid); AA (acrylic acid); MAA (methacrylic acid); BAP (2,6-bis(acrylamido)pyridine); Am (acrylamide); 1-MA-3MI-Br (1-(a-methyl acrylate)-3-methylimidazolium bromide); TEOS (tetraethyl orthosilicate); MTES (methyltriethoxysilane); PTES (triethoxyphenylsilane). For the comonomer and crosslinker: EDOT (3,4-ethylenedioxythiophene); MBA (N,N'-methylenebis(acrylamide); EGDMA (ethylene glycol dimethacrylate); TMPTA (trimethylolpropane triacrylate); DVB (divinylbenzene); TRIM (trimethylolpropane trimethacrylate). For the solvent: DMF (dimethylformamide); ACN (acetonitrile); PBS (phosphate-buffered saline).

Functional monomer	Comonomer and crosslinker	Solvent	Polymerisation type	Year	Ref.
3-TAA	EDOT	Aqueous Solution	Electro-polymerisation	2018	[9]
AA	MBA	Aqueous Solution	GRAFT polymerisation	2017	[10]
AA or MAA or BAP	EGDMA or TMPTA	DMF	Radical polymerisation	2016	[11]
AA or MAA or BAP	EGDMA or TMPTA	DMF + Spartan 80 + heptan	Inverse-suspension polymerisation	2016	[11]
AA or MAA or BAP	EGDMA or TMPTA	ACN	Precipitation polymerisation	2016	[11]
MAA	EGDMA	DMF	Radical polymerisation	2016	[12]
AM	EGDMA	ACN	Radical polymerisation	2016	[13]
Pyrrole		PBS	Electro-polymerisation	2015	[14]
MAA	EGDMA	$CHCl_3$	Radical polymerisation	2015	[15]
MAA	DVB	MeOH	Radical polymerisation	2015	[16]
Naphtalimide and MAA	EGDMA	DMF	Electropolymerisation	2014	[17]
Pyrole	TEOS, PTEOS	Aqueous solution	Radical polymerisation	2014	[18]
MAA	EGDMA	MeOH	Radical polymerisation	2014	[19]
MAA and 1-MA-3-MI-Br	TRIM	MeOH water mixture	Radical polymerisation	2013	[20]
MAA	EGDMA	ACN	Radical polymerisation	2013	[21]
MAA	EGDMA	$CHCl_3$	RAFT Polymerisation	2013	[22]
AM	EGDMA	MeOH	Radical polymerisation	2013	[23]
TEOS and MTES and PTES		EtOH water mixture	Radical polymerisation	2013	[24]

Given the aim to develop a MIP-based chemosensor for the recognition of caffeine in an aqueous solution, hydrophobic interactions are expected to play a significant role in the binding of the target compounds, and for this reason aromatic functional monomers able to form π-π stacking interactions were selected, together with the use of water as the solvent for the polymerisation. In fact, water is advantageous because: (i) it facilitates hydrophobic interactions between the functional monomer and caffeine molecules; (ii) it avoids the use of hazardous or expensive solvents. Therefore, to evaluate the affinity between caffeine and the functional monomers, and select the most promising monomer for the synthesis of imprinted material, ^{1}H NMR spectroscopy titration experiments were performed in D_2O.

By careful inspection of the literature, it was found that 5-caffeoylquinic acid (Scheme 3.2) formed strong π-π stacking interactions with caffeine in aqueous solutions and it was therefore considered first as a functional monomer candidate.[25,26]

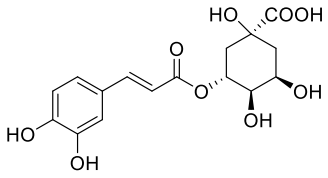

5-caffeoylquinic acid

Scheme 3.3. Structural formula of 5-caffeoylquinic acid, the most abundant chlorogenic acid in green coffee beans.

The titration was performed by adding successive amounts, ranging from 1 to 9 equivalents, of caffeine to 5-CQA solution of an initial concentration of 9 mM. As an example, in Figure 3.3, the proton NMR spectra for 0, 5 and 9 equivalents of caffeine are reported, to show the change in the protons chemical shifts.

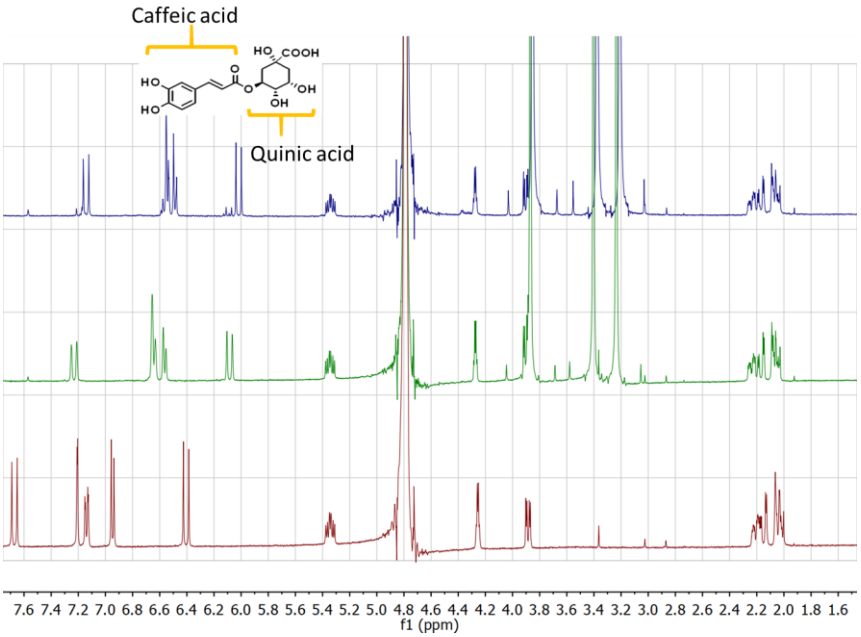

Figure 3.3. Proton NMR spectra for 5-caffeoylquinic acid titrated with caffeine in D_2O.The caffeic acid and quinic acid moieties are also specified. The red spectrum was obtained for a 9 mM caffeoylquinic acid solution. The green and blue spectra depict the proton chemical shifts after the addition of 5 and 9 equivalents of caffeine respectively.

From Figure 3.2 above, it follows that the conjugated aromatic ring protons (signals between 7.6 and 6.4 ppm) changed their chemical shifts by 0.5 ppm, while the quinic acid protons (from 5.4 to 2.0 ppm) did not show differences upon consecutive caffeine addition. This finding is in agreement with the hypothesis of a π-π stacking interaction between caffeine and the caffeoyl acid moiety of chlorogenic acid, as was previously reported by D'amelio N. *et al.*[25]. The data were fitted using a one site-specific binding model to obtain thermodynamic information on the complex stability (Figure 3.4).

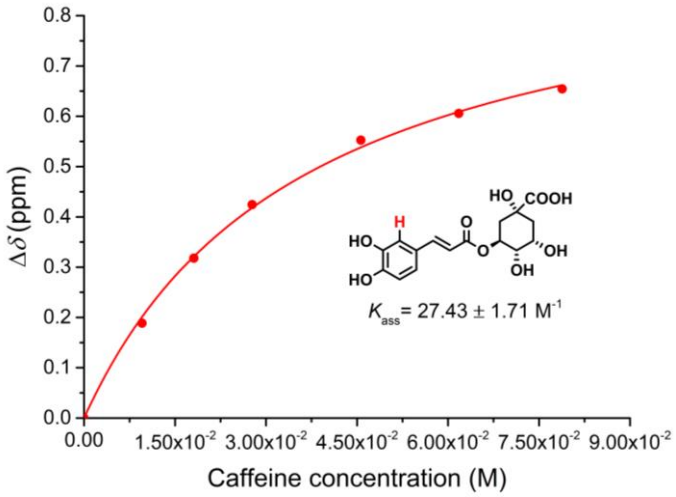

Figure 3.4. The change in the chemical shift of 5-caffeoylquinic acid upon consecutive addition of caffeine (the monitored proton is highlighted in red). One site-specific binding model was employed to fit the hyperbola and obtain the association constant.

The strong change in chemical shift observed ($\Delta\delta$ = 0.65 ppm after addition of 9 equivalents of caffeine) and the saturation trend line upon subsequent caffeine additions allowed the calculation of the complex stability constant, K_{ass} = 27.43 ± 1.42 M^{-1}, which is in excellent agreement with that found by D'Amelio N. *et al.* (30 ± 4 M^{-1}).[25] This agreement confirmed that a non-covalent interaction between caffeine and caffeoylquinic acid occurred in an aqueous solution. However, considering that the non-aromatic moiety of 5-CQA was not responsible for the interaction and given that the ester bond is relatively unstable in aqueous solutions, especially at non-neutral pH, caffeic acid (structural formula reported below, Scheme 3.4) was identified as a more convenient choice. In fact, the aromatic functionality is still present, but the ester bond has been replaced with the carboxyl group and, therefore, it is expected to be chemically more inert.

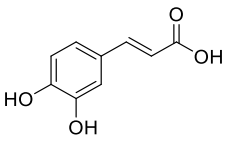

Caffeic acid

Scheme 3.4. The structural formula of caffeic acid.

One concern was given by the reactivity towards radical polymerisation of the α,β-unsaturated double bond of caffeic acid (see reaction Scheme 3.5, below) that would change the overall geometry of the molecule.

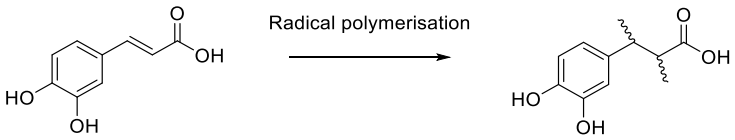

Scheme 3.5. The reactivity of the α,β-unsaturated double bond during radical polymerisation.

The change in geometry can affect binding interactions. Therefore, a titration experiment using 3,4-dihydroxyhydrocinnamic acid was initially performed. The chemical structure of 3,4-dihydroxyhydrocinnamicacid is reported in Scheme 3.6 below, followed by the ^{1}H NMR titration data presented in Figure 3.4.

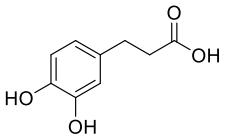

3,4-dihydroxyhydrocinnamic acid

Scheme 3.6. The structural formula of 3,4-dihydroxyhydrocinnamic acid.

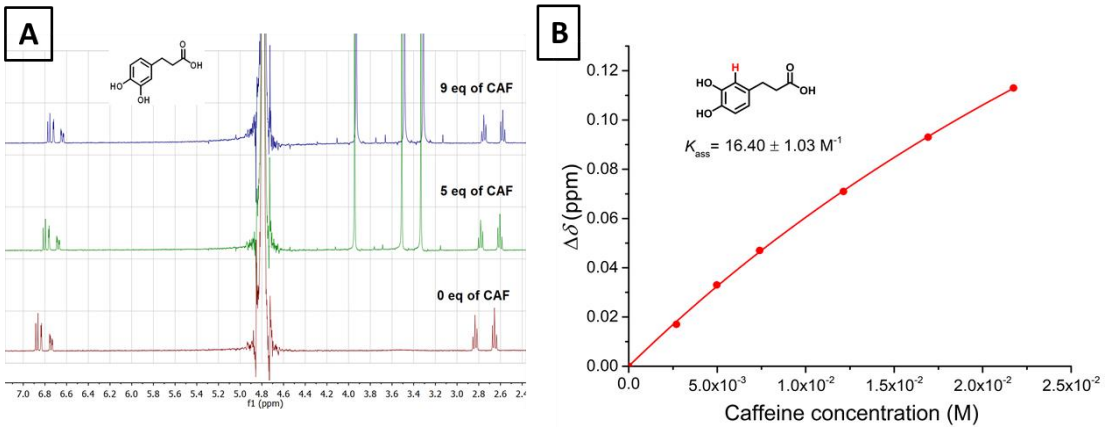

Figure 3.5. Proton NMR titration of 3,4-dihydroxyhydrocinnamic acid with caffeine in D_2O. (A) The red spectrum was obtained using a 3 mM 3,4-dihydroxyhydrocinnamic acid solution in D_2O. The green and blue spectra depict the proton spectra after the addition of 5 and 9 equivalents of caffeine, respectively. (B) The plot of the chemical shift of 3,4-dihydroxyhydrocinnamic acid upon increasing caffeine concentration. The investigated proton is coloured in red. A one site-specific binding model was employed to fit the hyperbola and calculate the dissociation constant.

From Figure 3.5, it follows that the shift of the aromatic protons (6.9-6.7 ppm) is less significant compared with that recorded for caffeoylquinic acid. Hence, a lower complex stability constant was calculated for the complex of caffeine with 3,4-dihydroxyhydrocinnamic acid (16.40 M^{-1}). This finding suggests that the planarity of the conjugated aromatic system of chlorogenic acid plays a fundamental role in the interaction with caffeine and hydrogenated analogues are not equally strong binders, even though an aromatic phenolic ring is still present. As a result, neither 5-CQA nor caffeic acid were considered appropriate functional monomers. That was because of the loss of the α,β-unsaturated bond led to a lower affinity for caffeine. This means that the molecular recognition properties in the final polymer will be not as effective as expected based on the pre-polymerisation studies.

The next step was to evaluate a number of alternative compounds, shown in Scheme 3.7, as functional monomers, all characterised by an aromatic moiety expected to form π-π stacking and hydrophobic interactions with caffeine. In the first instance, also molecules without the polymerisable moiety where evaluated by studying their ability to interact with caffeine via ^{1}H-NMR spectroscopy.

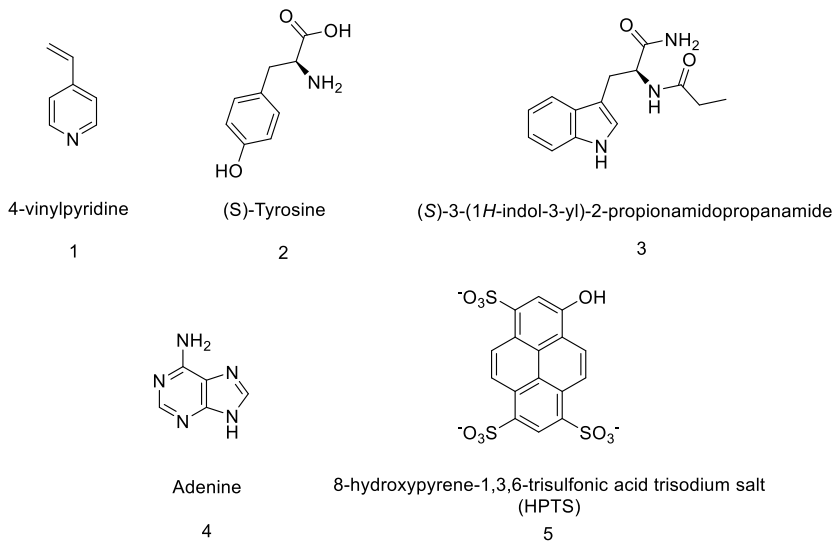

Scheme 3.7. Structural formulae of the aromatic compounds evaluated as potential functional monomers for the development of MIPs selective to caffeine.

Molecules 1 to 4 were previously employed during the functional monomer selection,[7,27] while HPTS (molecule 5) was reported to form a strong 1:1 complex with caffeine by Rochat M. *et al*.[28] The titration experiment was performed using D_2O as the solvent and by adding increasing amounts of caffeine, from 0 to 9 equivalents. The change in the chemical shift was then used to estimate the stability constant of the complex of caffeine with the functional monomer. The ^1H NMR spectra and titration curves for molecules 1-4 are reported in Figure 3.6, on the next page.

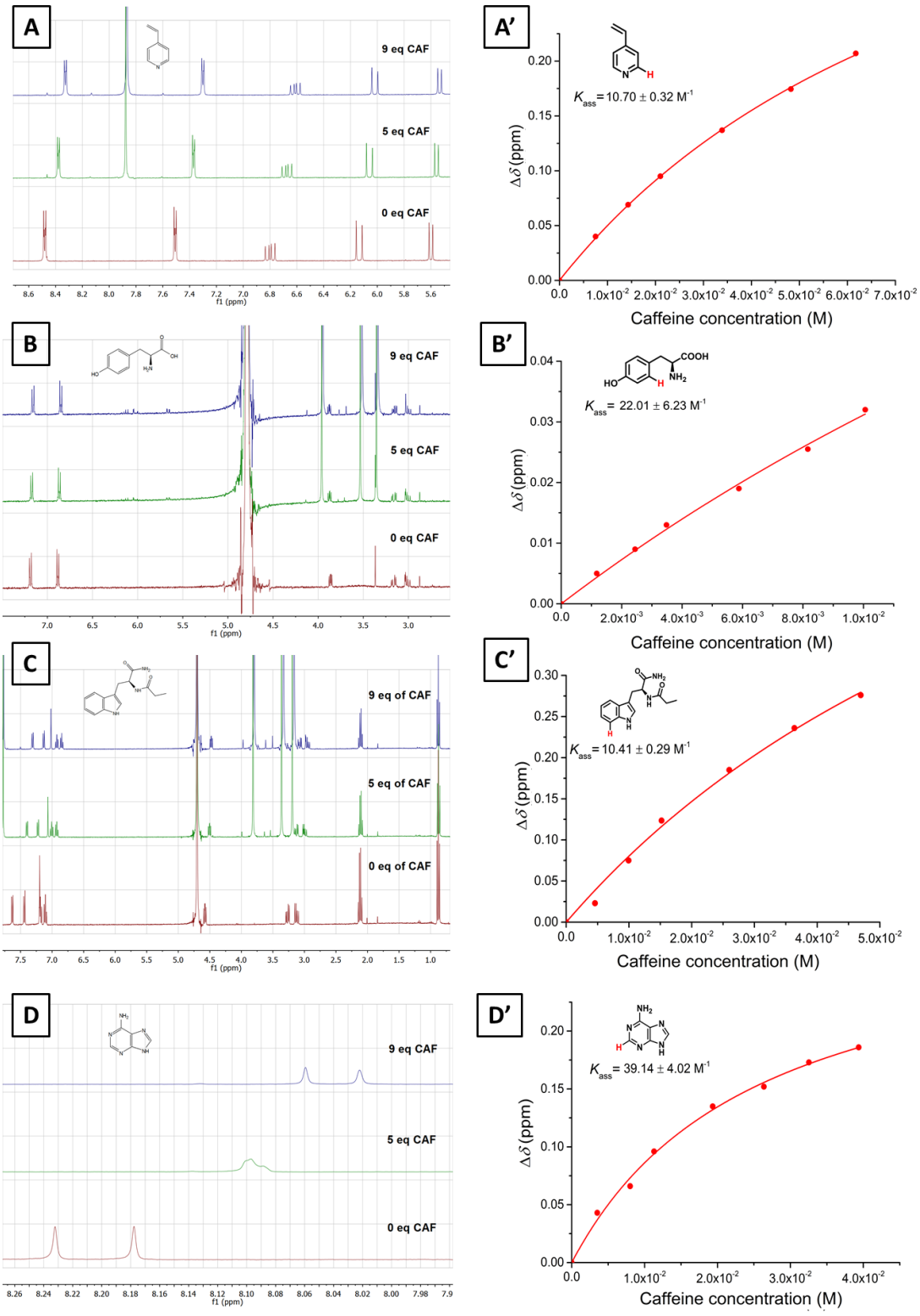

Figure 3.6. Proton NMR spectroscopic titration experiments using different possible functional monomers (molecules 1 to 4 Scheme 3.7), for devising MIPs selective for caffeine. Increasing amounts of caffeine (from 0 to 9 equivalents) were subsequently added during each titration experiments and the change in the chemical shift of the functional monomer was plotted against the caffeine concentration in order to determine the complex stability constant (A'-D').All titrations were performed using D_2O,as the solvent.

In the case of HPTS the proton NMR spectra at different equivalents of caffeine and the titration curve obtained for determination of the complex stability constant are reported in Figure 3.7.

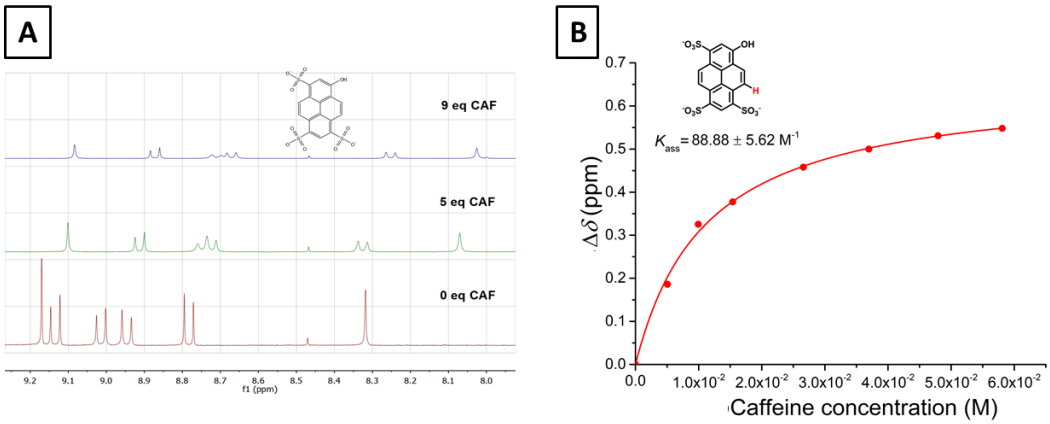

Figure 3.7. (A) Proton NMR spectroscopy titration of HPTS (8-hydroxypyrene-1,3,6-trisulfonic acid trisodium salt) with caffeine in D_2O. The red spectrum was obtained using a 6 mM HPTS. The green and blue spectra depict the proton spectra after the addition of 5 and 9 equivalents of caffeine, respectively. (B) the plot of the chemical shift of HPTS upon increasing caffeine concentration. The investigated proton is coloured in red and a one site-specific binding model was employed to fit the hyperbola and calculate the dissociation constant.

Among the different molecules evaluated, HPTS most strongly complexed caffeine in pure D_2O, as evidenced by a significant chemical shift change (0.52 ppm after addition of 9 caffeine equivalents) and the plateau in the trend line obtained, which are linked to the formation of a strong intermolecular complex. The complex stability constant determined in the case of HPTS was K_{ass} = 89 M^{-1}. The value is over twice that for adenine (K_{ass} = 39.14 M^{-1}), which was the second most promising molecule among the seven candidates screened. In addition, the complex stability constant of 89 M^{-1} is a valuable achievement in view of hydrophobic interaction between caffeine and aromatic moiety of HPTS, considering previous reported data where the constant values ranged from 30 to 60 M^{-1}.[25,29] Therefore, HPTS was selected as the most promising functional monomer and the next step focused on the synthesis of its polymerisable derivative. The

esterification of the phenolic oxygen atom with acryl chloride was anticipated to be the most convenient approach and the retrosynthesis is reported in Scheme 3.8.

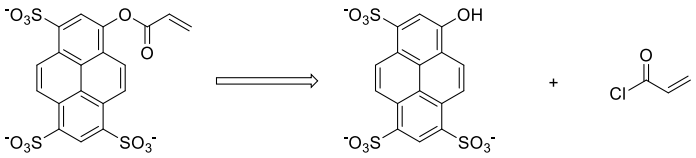

Scheme 1.8. Retrosynthetic scheme for the synthesis of a polymerisable derivative of HPTS.

The choice of the acryloyl unit was determined by the desire to have the same functional group to maintain a similar reactivity during radical polymerisation (a more detailed discussion on the choice of co-monomer and crosslinker for the polymer synthesis is presented later in this chapter). In literature, a variety of protocols for the esterification of phenolic groups have been published, involving both the use of anhydrous conditions and organic solvents, as well as aqueous solutions. In particular, the latter ones are more interesting since no hazardous or expensive solvents are necessary. Moreover, the procedure is simpler, because it does not require using anhydrous conditions. Furthermore, HPTS shows a higher solubility in water while in organic solvents this solubility is limited because of highly charged character of HPTS. The first synthetic procedure was based on the work of Chanthamath S. *et al.* who used an acetone:water mixture of volume ratio of (4:1) and K_2CO_3 as the base.[30] Considering the low solubility of HPTS in acetone-water mixtures, the reaction was performed using water with the addition of different inorganic bases, including K_2CO_3, $NaHCO_3$ and NaOH, and acryloyl chloride ranging from 1 to 4 equivalents. The general reaction scheme is presented in Scheme 3.9, on the next page.

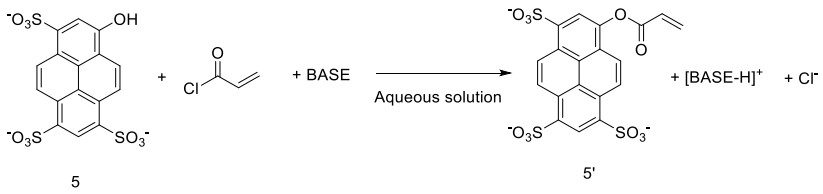

Scheme 3.9.General reaction procedure for the synthesis of a polymerisable derivative of HPTS in aqueous solution using acryloyl chloride.

Despite numerous attempts, the desired product 5' in Scheme 3.9 could not be isolated and, instead, unreacted HPTS, was consistently recovered as evidenced by NMR shown in Figure 3.8. This possibly suggests that the acryloyl chloride may be preferentially reacting with water instead of the HPTS hydroxyl group.

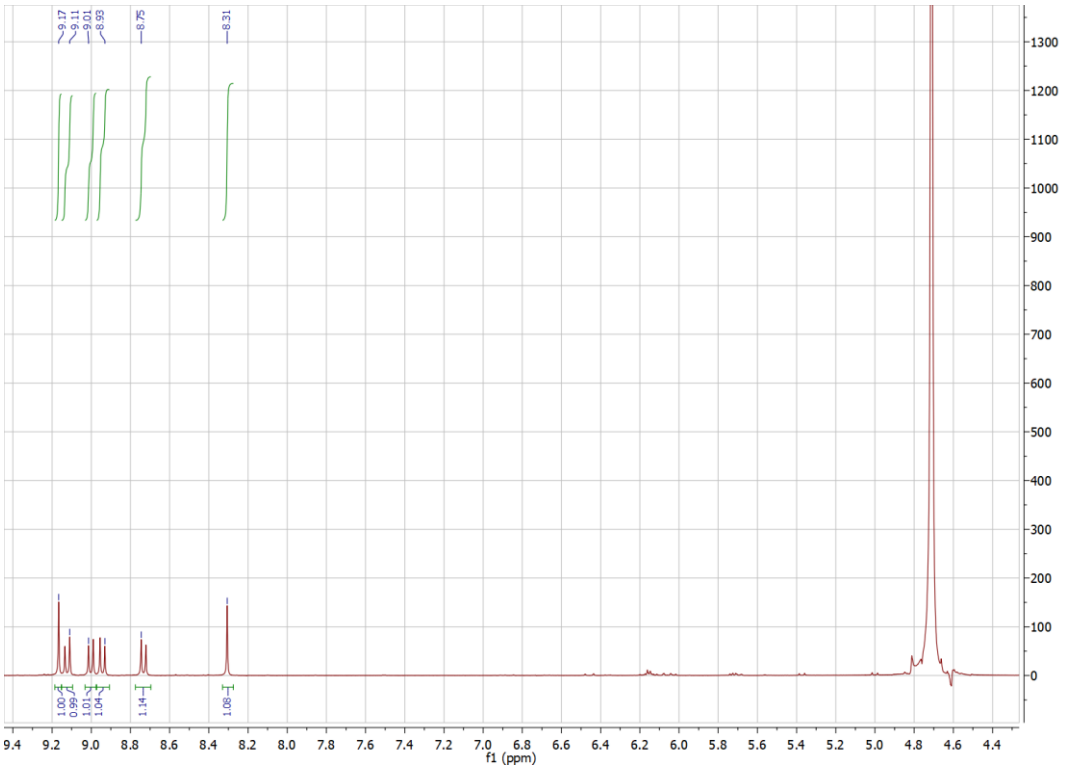

Figure 3.8. Proton NMR spectrum of the isolated product from the aqueous phase after workup of the reaction of HPTS with 4 equivalents of acryloyl chloride in water using NaOH as the base. The spectrum shows that HPTS did not react and the acrylic acid ester was not formed.

Therefore, the system was changed completely, and an attempt was made to conduct the reaction under anhydrous conditions using an organic solvent, such as DMSO, that could sufficiently solubilise HPTS. The protocol used was based on a reported procedure by Barteselli A. *et al*. where propionyl chloride was successfully employed for acylation of

an oxime in anhydrous DMSO using NaH as the base.[31] Unfortunately, the desired product was not obtained herein and unreacted HPTS was again recovered, as confirmed by the TLC analysis and ^{1}H NMR spectra. Given the difficulties encountered, it was decided to change the polymerisable unit and vinyl benzyl chloride was selected instead. The reaction procedure was adopted from Srivatsan S. G. *et al.* and the reaction procedure is presented in the Scheme 3.10, below.[32]

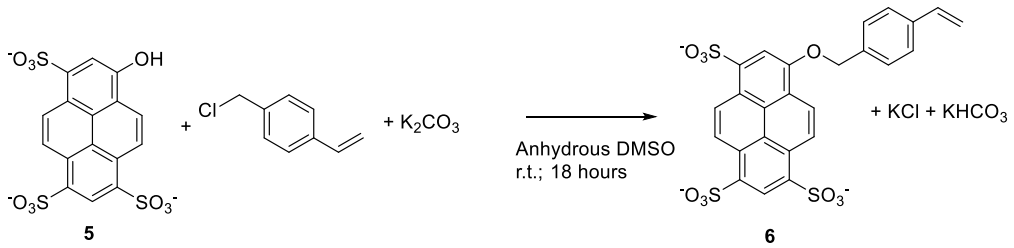

Scheme 3.10. Reaction procedure for the synthesis of a polymerisable derivative off HPTS using 4-vinyl benzyl chloride. The reaction conditions were based on the published work of Srivatsan S. G. et al..[32]

Initially, the reaction was tested using one equivalent of chloride with a reaction time of 18 hours. The TLC analysis of the solution indicated the presence of unreacted HPTS and a new compound. The ^{1}H-NMR spectroscopy analysis of the crude product confirmed the presence of these compounds (Figure 3.9 on the next page).

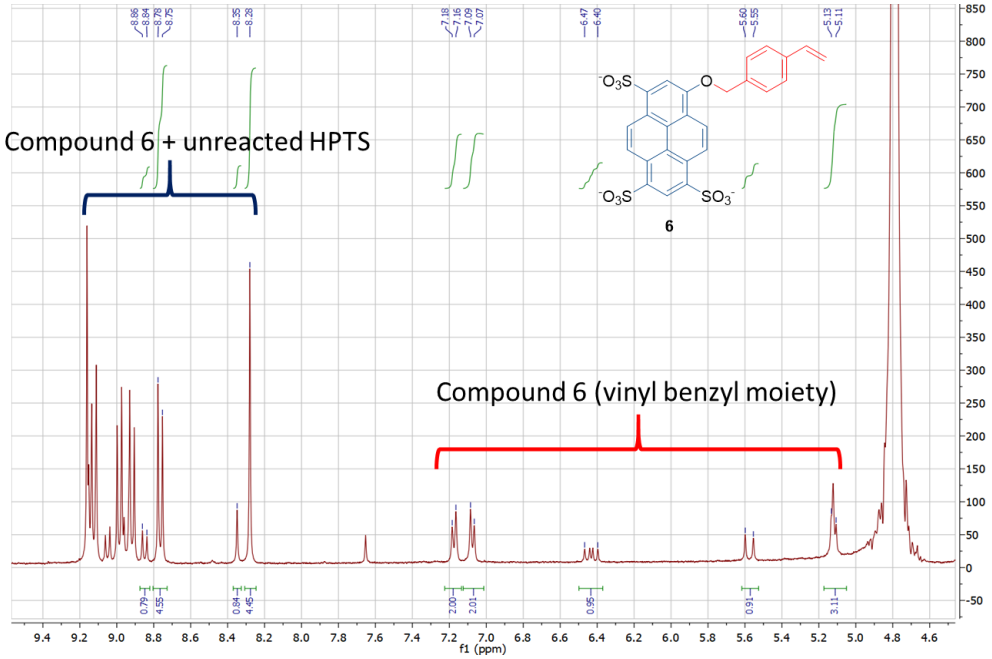

*Figure 3.9. Proton NMR spectrum of the isolated product from the aqueous phase after workup of the reaction of HPTS with 1 equivalent of 4-vinyl benzyl chloride in anhydrous DMSO and using K_2CO_3 as the base. The spectrum confirms the presence of both unreacted HPTS and the desired polymerisable derivative (compound **6**) in the ratio of 5:1, based on proton integration.*

The signals of the benzylvinyl moiety are present in the range of 7.2 to 5.11 ppm and the signals of HPTS are all duplicated, evidencing the presence of both unreacted HPTS and its polymerisable derivative. By integration of the proton signal the ratio of 1:5 was calculated (compound **6** : unreacted HPTS). Given that the TLC analysis of the reaction solution did not show evidence of any unreacted chloride, the hypothesis was that benzyl chloride was being consumed. The subsequent step was to increase the equivalents of benzyl chloride to improve the chemical yield. Reactions were carried out using 5, 10 and 20 equivalents of chloride. After 18 hours, the reaction performed with 10 and 20 equivalents appeared to be completed according to the TLC analysis and the ^{1}H NMR spectrum of the product obtained did not show any signal of unreacted HPTS. Compound **6** was isolated with high purity based on the proton NMR spectrum. As an example the ^{1}H NMR spectrum using 10 equivalents is reported in Figure 3.10.

*Figure 3.10. The proton NMR spectrum of the isolated product from the aqueous phase after workup of the reaction of HPTS with 10 equivalents of 4-vinyl benzyl chloride in anhydrous DMSO with the use of K_2CO_3 as the base. The spectrum shows only the signal of the desired product (compound **6**).*

The need to use 10 equivalents of chloride in order to completely convert HPTS to the desired polymerisable analogue was not investigated further, together with the unexpected different reactivity of HPTS with acryloyl and benzyl chloride (acryloyl chloride was expected be more electrophilic and reactive). Although these findings were interesting, the priority was given to the synthesis of MIPs containing HPTS as the functional monomer. Therefore, the subsequent step was to evaluate the affinity of product **6** for caffeine by performing an ^{1}H NMR spectroscopy titration as accomplished previously.

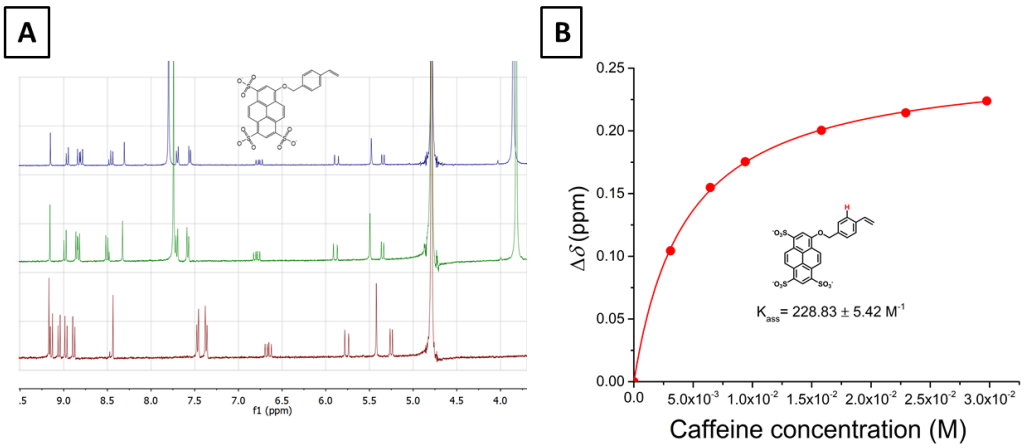

*Figure 3.11. The proton NMR spectroscopy titration of compound **6** with caffeine in D_2O. (A) The red spectrum was obtained using a **6** mM concentration of compound **6**. The green and blue spectra depict the proton spectra after the addition of 5 and 9 equivalents of caffeine respectively. (B) The plot of the chemical shift of compound **6** dependence on increasing caffeine concentration. The investigated proton signal is coloured in red and a one site-specific binding model was employed to fit the hyperbola and calculate the dissociation constant.*

The titration experiment evidenced a π-π stacking interaction between caffeine and compound **6**, with the complex stability constant of 229 M^{-1}. This value is three times higher compared to that for HPTS. Interestingly, the protons showing the strongest interaction are on the phenyl ring of the polymerisable moiety (7.5 ppm). However, a stable interaction was also identified using the proton of HPTS (from 9.2 to 8.5 ppm) which suggested that both aromatic rings are involved in the formation of the pre-polymerisation complex. The chemical shift of the HPTS protons was moved to higher fields, while signals of the phenyl protons were displaced to lower fields. Presumably, this difference results from the geometry of interactions and the consequent shielding and deshielding effect. Although this finding was interesting, accurate studies on the geometry of interaction would have required further experimental data (such as the X-ray or NOESY NMR experiments). Considering that the precise geometry of interaction was not an essential requirement and the time available was limited, this was not investigated further because the MIP devising was the primary aim of this work.

3.2.2 Optimisation of the polymerisation conditions

Solvent

A strong interaction between the template and the functional monomer favours the recognition properties in the polymer. However, a number of other experimental factors, including the choice of solvent and the type of cross-linker as well as the polymerisation methods can play a role. In particular, the solvent choice is crucial in allowing the formation of pores in the polymers, controlling the solubility of the monomers and polymer, and affecting the template-functional monomer interaction. Aqueous solutions are rarely employed for the synthesis of MIPs. This choice can be justified because in numerous cases interactions between the functional monomer and the template is based on hydrogen bonds which are easily disrupted in aqueous media. In contrast, the interaction between caffeine and compound **6** is based on π-π stacking interactions, which are favoured by aqueous environments.[33–35] To investigate the effect of the organic solvent presence on the pre-polymerisation complex properties, the system was studied using mixed solvent solutions of water : acetonitrile (9:1 v:v), water : THF (7:3 and 9:1 v:v). The proton NMR titration spectra and the corresponding thermodynamic values are reported in the Figure 3.12.

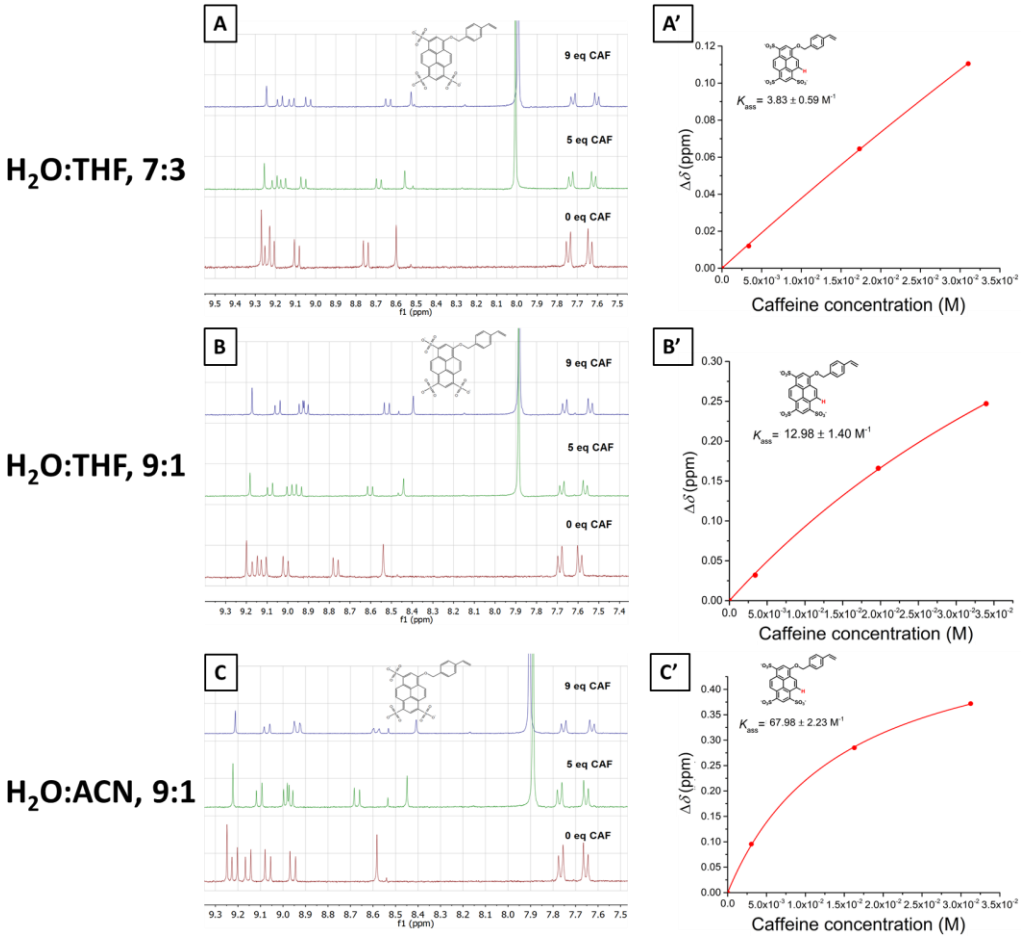

*Figure 3.12. The proton NMR spectroscopy titration of compound **6** with (A) caffeine in D_2O:THF(d8) 7:3, (B) D_2O:THF(d8) 9:1 and (C) D_2O:ACN (d3). The red spectrum was obtained using a 6 mM of compound **6**. The green and blue spectra depict the proton spectra after the addition of 5 and 9 equivalents of caffeine, respectively. (A'), (B') and (C'): Plots of the chemical shift of compound **6** dependence on increasing caffeine concentration. The investigated proton signal is coloured in red and a one site-specific binding model was employed to fit the hyperbola and calculate the dissociation constant.*

From Figure 3.12 above, it follows that the addition of organic solvents significantly affects the interaction of compound **6** with caffeine, with a significant concomitant decrease in the K_{ass}. The best result was obtained using 10% ACN, which resulted in K_{ass} of 67.98 M^{-1}. This value is almost a third lower compared to that of 228.30 M^{-1} determined for titration using pure D_2O. The difference between the two organic solvents on the pre-polymerisation complex stability, arises from probably the higher electric permittivity of acetonitrile (37.9) than that of tetrahydrofuran (7.59). In view of the

critical role of the pre-polymerisation complex in reaching high selectivity of the final imprinted material, it was decided to pursue the MIP synthesis using water as the solvent.

Initiator

The optimisation of the polymerisation conditions was continued with the evaluation of the effect of varying the amount of initiator. Previous experience in the research group of Professor M. Resmini is in the synthesis of nanogels using high-dilution radical polymerisation, which allows the isolation of nano-sized particles that are able to form a stable colloid in water, of a high active surface area. Usually the polymerisation is thermally triggered by a radical initiator activated at 70°C under nitrogen atmosphere. When radical polymerisation is carried out, it is important to asses if the template molecule acts as a radical scavenger or is chemically unstable in the presence of radicals. In fact, if stable radicals of caffeine are formed then they can react with the monomers thus leading to a covalent incorporation of caffeine in the polymer matrix. This incorporation will block the availability of binding sites. On the other hand, if caffeine is rapidly degraded to smaller products, it cannot be used as the template. In the particular case of caffeine and methylxanthines, previous works reported in literature have evidenced that caffeine is a radical scavenger in the presence of ˙OH.[36,37] Therefore, before starting studies on the polymerisation, the stability of caffeine under the reaction conditions, employed for the MIP synthesis, was investigated. A model polymer formulation which was 5% in HPTS polymerizable (compound **6**), 75% in N,N'-methylebis(acrylamide) (MBA) and 20% in Am was considered with a total monomer concentration (Cm) of 0.25% and the ratio of functional monomer:caffeine equal to 1 (the formulation of the polymer will be discussed in the next section). To evaluate the reactivity of caffeine with radicals, a mock polymerisation experiment was performed, where caffeine and the radical initiator only were allowed reacting. The caffeine

concentration was determined at time zero and after 24 h (typical polymerisation reaction time). The following percentage of the radical initiator (ammonium persulfate) were considered, 0, 1, 5 and 10% (based on the total amount of polymerisable double bonds). The reaction was performed both at 70 °C and at room temperature using TEMED [1,2-bis(dimethylamino)ethane] as the catalyst. The results are listed in table 3.2 below.

Table 3.2. The amount of caffeine degraded under radical polymerisation conditions using water as the solvent and ammonium persulfate as the initiator at either 70 °C or room temperature using TEMED [1,2-bis(dimethylamino)ethane] as the catalyst.

% of radical initiator	% of caffeine degraded	
	Reaction at 70 °C	Reaction at room temperature with the addition of TEMED
0	0	0
1	11	0.4
5	37	1.4
10	84	3.7

From Table 3.2, it is evident that when the reaction is performed at 70 °C, a high percentage of caffeine is lost after 24 hours because of its antioxidant properties and reactivity to radical species. In contrast, the reactivity of caffeine toward radicals is much lower when the reaction is performed at room temperature; even when using 10% of initiator, less than 4% of caffeine is degraded after 24 hours. The conclusion from this was that caffeine is stable under polymerisation conditions at room temperature. Therefore, it was decided to synthesise all polymers at room temperature using TEMED as the catalyst.

The next step focused on the optimisation of the amount of initiator used, to ensure a monomer conversion close to 100%. For this purpose, the polymerisation was conducted in deuterated solvents and the proton NMR spectra were recorded both before starting the polymerisation and after 24 hours of polymerisation. The amount of double bonds

was assessed by signal integration, and then compared with an internal standard (dimethyl sulfone). Initially, 1% of the initiator was considered and the experiment was performed for both the MIP and the NIP to further evaluate if caffeine interferes with the polymerisation reaction. After 24 hours, the polymerisation conversion was 40% in the case of the MIP and 61% in the case of the NIP. The difference between the MIP and NIP synthesis efficiency can be linked to the effect of caffeine as a radical quencher. On the overall the data indicate that 1% of initiator was insufficient to complete the polymerisation in 24 hours. Therefore, the amount of initiator was increased to 5%.

Table 3.3.Conversion of the polymerisation reaction using different amounts of the ammonium persulfate initiator (1 and 5%). The polymerisation was performed using D_2O as the solvent and the amount of unreacted monomers was assessed using proton NMR spectroscopy.

Initiator	Conversion MIP	Conversion NIP
1%	40%	61 %
5%	98 %	99 %

When 5% of the initiator was used, both in the case of the MIP and NIP, the conversion of monomers was exceeded 98% after 24 hours. The proton NMR spectra are reported in Figure 3.13. After 24 hours, a clear decrease in the integrations of the double bonds present (area from 6.4 to 5.7 ppm) can be observed. Moreover, caffeine signals (3 singlets from 3.9 to 3.0 ppm) retained the same integration size compared to that of internal standard, thus suggesting that caffeine is stable under the reaction conditions employed, in agreement with the previous findings (Table 3.2). To summarise, these findings evidences that by using 5% of the ammonium persulfate initiator at room temperature, the conversion is complete and caffeine is stable.

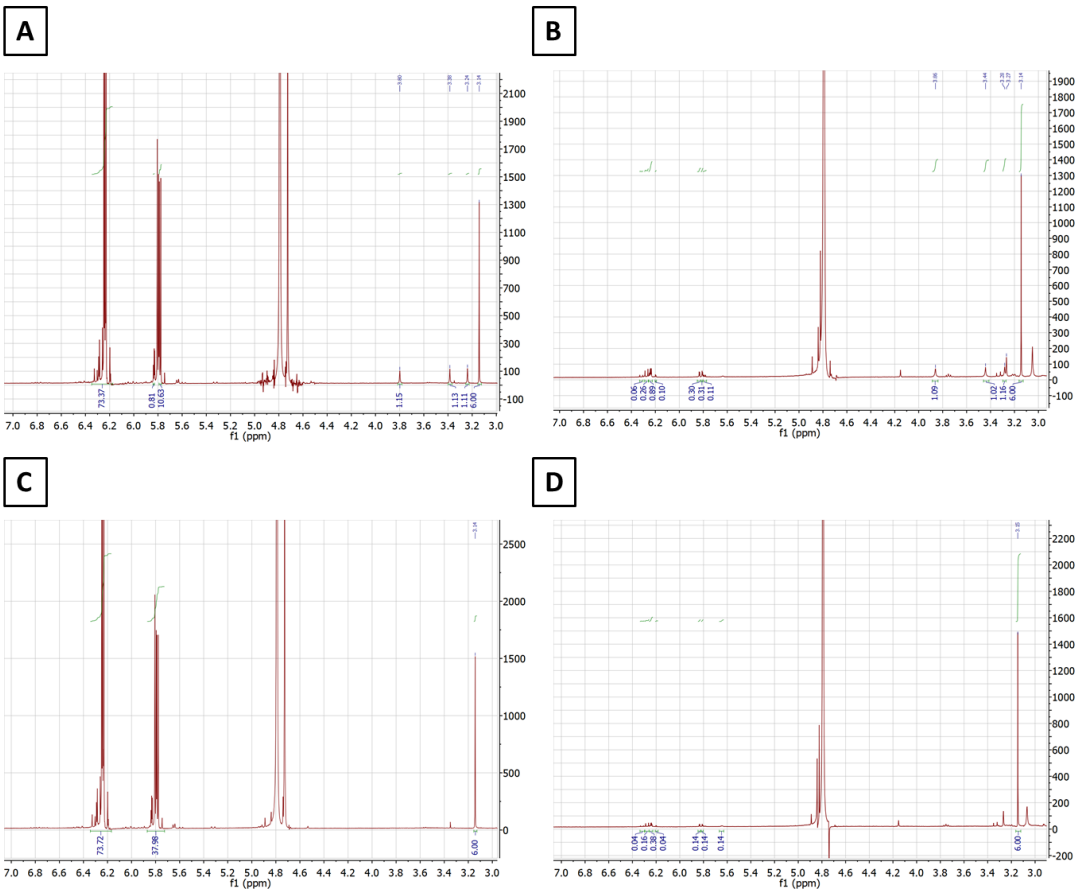

Figure 3.13. Studies on the polymer conversion after 24 hours using 5% of initiator. (A) and (B): The proton NMR spectra for the MIP at time 0 and after 24 hours, respectively. (C) and (D): The proton NMR spectra of the NIP at time 0 and after 24 hours. In both cases negligible amount of unreacted monomers were present after 24 hours.

Polymer formulation and synthesis

The subsequent step focussed on synthesis of both the MIP and NIP. The formulation of the polymer comprised 5% of functional monomer, 75% of the crosslinker and 20% of the comonomer (percentage based on moles). The 5% content of the functional monomer was kept low because compound **6** has three negative charges but also a very hydrophobic structure. Therefore there was a concern about the degree of changes in the polymer structure that a higher functional monomer percentage would bring. MBA was selected as the crosslinker because the MBA and the obtained polymers are chemically more inert than ester crosslinkers (such as EGDMA). This is because the latter can

hydrolyse in aqueous solutions. The structural formulae of MBA and EGDMA are reported in Scheme 3.11.

Scheme 3.11.Structural formulae of N,N'-methylenebis(acrylamide) (MBA) and ethylene glycol dimethacrylate (EGDMA).

A relatively high amount of crosslinker was employed (75%) with the aim of obtaining a rigid 3-D structure with cavities that would ensure a high selectivity in analyte rebinding. As the comonomer, Am was employed, based on reported data where a combination of Am and MBA led to nanogels able to form a stable colloidal system in aqueous solutions.[7] Moreover, both MBA and Am are commercially available and are not expensive. The chemical structures and the percentage of the monomers employed for the synthesis of MIP and NIP are reported below.

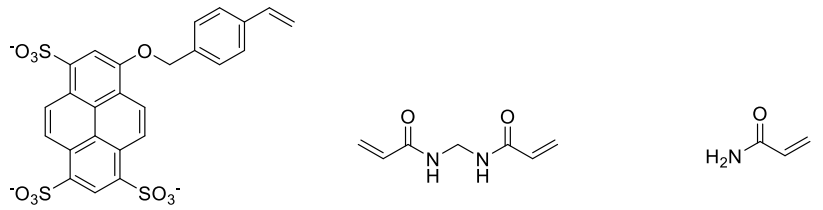

Scheme 3.12. Structural formulae of the monomers employed for synthesis of the MIP and NIP. The percentage (in moles) used is also reported.

The first polymerisation attempt was conducted using the same conditions as those for the synthesis accomplished using deuterated solvent because the use of that conditions led to almost 100% polymer conversion. The purification involved dialysis against distilled water and freeze-drying. Surprisingly, the final yield of the polymer was 10% in the case of the MIP and 40% in the case of the NIP. In view of the NMR data indicating that all monomers were expected to react completely, the low chemical yield was

attributed to the high dilution conditions. Under these conditions, a mixture of polymers containing a large proportion of low molecular weight short chains is formed. These short chain polymers are lost during purification via dialysis. The difference in the chemical yield between the MIP and NIP was hypothesised to be due to different nanoparticle sizes, with the NIP nanoparticles being bigger. However, considering the small amount of polymer recovered, no further characterisation was done to prove the hypothesis and the focus was moved towards increasing the total monomer concentration, using concentrations (Cm) of 0.5% and 1%. The obtained yields after the polymerisation and dialysis are reported in Table 3.4.

Table 3.4. Polymerisation yields after dialysis and freeze-drying using different total monomer concentrations (Cm)

Cm	MIP Yield	NIP Yield
0.25%	10%	40%
0.5%	80%	86%
1%	93%	90%

When the total monomer concentration was increased from 0.25 to 1%, the polymerisation yield became higher, going from 10% to 93% for the MIP and from 40% to 90% for the NIP. This yield increase supports the hypothesis that when Cm 0.25% was employed, although all monomers reacted, the low total monomer concentration led to a large proportion of short-chain polymers that were lost during the dialysis. Both sets of polymers obtained with a Cm of 0.5% and 1% were considered equally suitable as candidate materials to be studied further, given the high polymerisation yields and the incorporation of HPTS. This incorporation was expected to provide selectivity towards caffeine. However, because of the limited time to evaluate the analyte rebinding characteristics, only polymers synthesised at Cm 1% were considered further. The polymer formulations were: 5% of functional monomer (polymerisable HPTS), 75% of MBA as the crosslinker, 20% of Am and a total monomer concentration of 1%.

Characterisation of the polymers

The characterisation of the nanogel polymers involved analysis of the particle size using dynamic light scattering (DLS) and measurement of the zeta potential. During DLS analysis, a polymer dispersion in a solvent (usually water) is irradiated with light and the scattering of this light, due to the presence of nanoparticles in the colloidal system, is recorded. The change over time of the scattered image is then monitored. With the known viscosity of the system and the temperature, the instrument calculates the size of the nanoparticles present by approximating them to spheres. The DLS principle is that bigger particles move slower. Therefore, over-time the scattered image is changed less, compared to that for smaller particles. The original output from the software is the size distribution of the particles based on the intensity of light scattered. Figure 3.14 the data obtained for the MIP and NIP polymers synthesised with Cm 1% are presented.

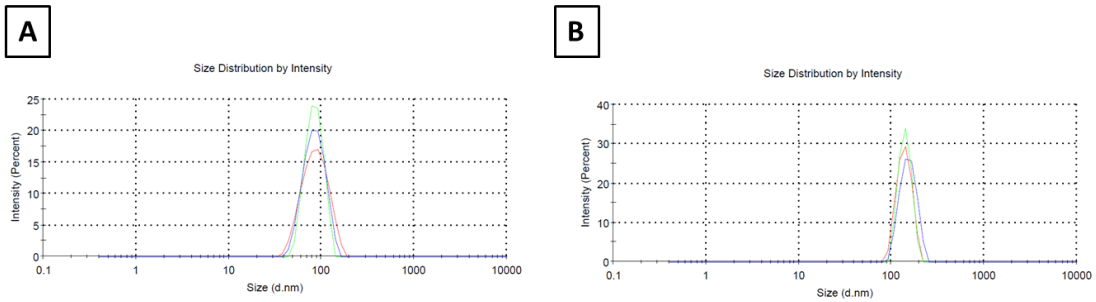

Figure 3.14. Size distribution by intensity obtained using dynamic light scattering for the (A) MIP and (B) NIP using a 0.5 mg/mL polymer dispersion.

The measurement was done in triplicate to ensure data repeatability, and the particle size distributions for all the measurements are reported in Table 3.5, below.

Table 3.5. Size distribution and the polydispersity index of the polymers synthesised, as measured using dynamic light scattering of dispersions of MIP and NIP in water (0.5 mg/mL).

Measurement No.	MIP		NIP	
	Size (nm)	Polydispersity index	Size (nm)	Polydispersity index
1.	88.59 ± 29.85	0.325	138.5 ± 24.73	0.584
2.	84.56 ± 17.89	0.213	140.7 ± 20.90	0.358
3.	85.50 ± 22.11	0.270	153.0 ± 29.80	0.370

It can be observed from both Table 3.5 and Figure 3.14 that MIP nanoparticles (average size 86.22 nm) were smaller compared to those of NIP (average size 144.07 nm). The observed difference may be linked to the presence of caffeine during the MIP synthesis, and caffeine radical quenching properties, which do not allow the MIP chain to grow as much as the NIP chain. However, to support this hypothesis, the synthesis of the polymer should be repeated to verify its reproducibility, and a comparative study using another template molecule (which does not behave as a radical quencher) should be performed to understand if the difference in size is generally observed for all MIP and NIP preparations. This however was not considered a priority in the project and, therefore, was not carried out because of lack of time.

After the DLS intensity data are obtained, the software transforms the data using a mathematical algorithm to provide information on size based on the number and the volume of the particles.[38] These two distributions are useful because bigger particles scatter more light than the smaller ones, resulting in an overestimation of the size (when intensity is employed).[38] The particle's dimensions based on the number and volume are provided in Figure 3.15.

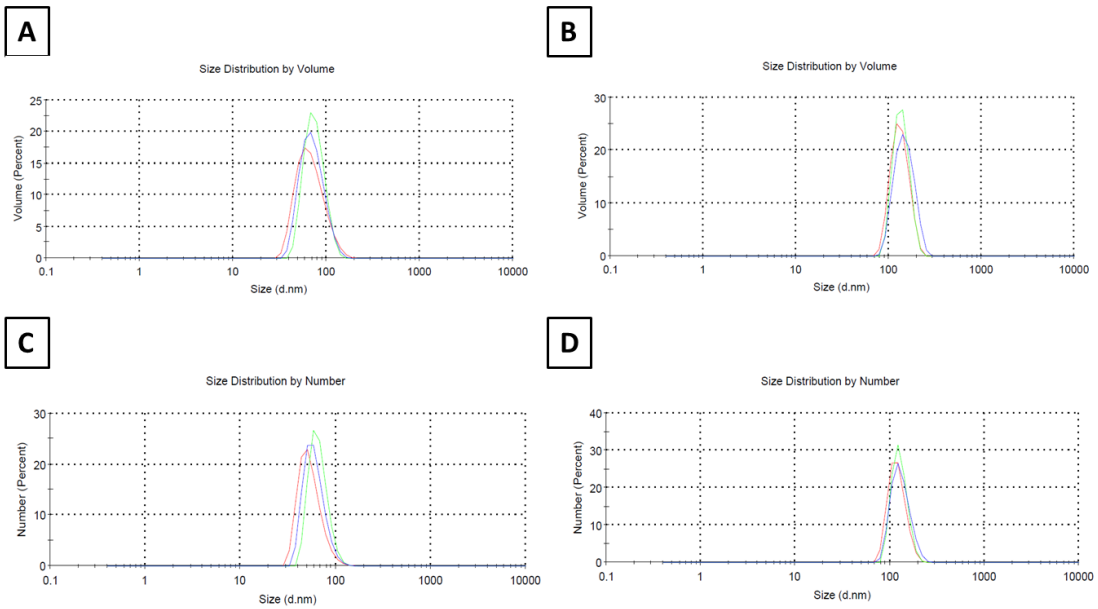

Figure 3.15. Size distribution by volume (A and B) and number (C and D) obtained using dynamic light scattering for the MIP (A and C) and NIP (B and D) using a 0.5 mg/mL dispersion of a polymer in solution.

Table 3.6. Size distribution (nm) of the polymer prepared as measured using dynamic light scattering of a dispersion of MIP and NIP in water (0.5 mg/mL). The data are presented considering the distribution by volume and number.

Measurement No.	Distribution by volume		Distribution by Number	
	MIP	NIP	MIP	NIP
1.	75.66 ± 18.66	137.7 ± 26.67	66.57 ± 16.54	127.9 ± 23.79
2.	72.41 ± 21.12	149.2 ± 34.96	60.42 ± 15.57	131.8 ± 29.98
3.	69.87 ± 24.29	133.8 ± 29.16	54.68 ± 15.54	120.8 ± 25.41

The sizes obtained using volume and number distributions were slightly lower compared with the intensity, as expected, since intensity can overestimate the particle size. However, considering the error associated with the measurements, no significant differences between the three methods were found and the values obtained using intensity distribution were considered valid. Subsequently, the zeta potential of the particles in aqueous solution was measured and the graphs with the data obtained are reported in Figure 3.16.

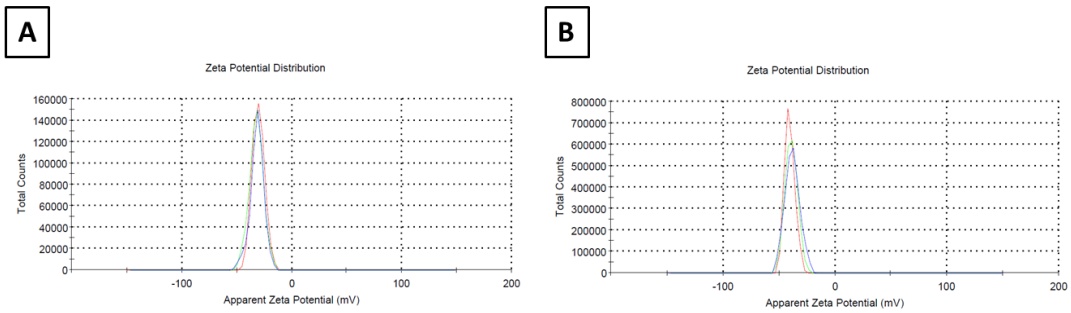

Figure 3.16. Zeta potential distribution for the MIP (A) and NIP (B) particles, measured in a dispersion of polymer in water with concentration 0.5 mg/mL.

Table 3.7. Zeta potential values for the MIP and NIP measured in a dispersion of polymers in water with concentration 0.5 mg/mL. The measurement was repeated in triplicate.

Measurements	MIP	NIP
1	-30.5 ± 6.56	-40.5 ± 6.25
2	-32.3 ± 5.67	-39.1 ± 4.57
3	-31.6 ± 6.45	-38.1 ± 5.59

From Figure 3.16 and Table 3.7 above, it follows that the zeta potential of both MIP and NIP nanoparticles is negative, which is expected since the functional monomer employed has a triple negative charge. The slight difference between MIP and NIP may suggest that in the case of the MIP the functional monomer was incorporated inside the polymer matrix in the course of imprinting, or different amounts of HPTS were incorporated in MIP and NIP. However in view of the experimental error found, further experimental evidence is required to support this hypothesis.

3.2.3 Studies of the analyte binding properties of the nanogels

Having synthesised and characterised the nanogels imprinted with caffeine, the subsequent step focused on the study of the analyte binding abilities of both imprinted and non imprinted polymers, by HPLC. During the analyte binding, an equilibrium is established between caffeine bound to the polymer and caffeine free in solution. By increasing the amount of caffeine (while polymer concentration is fixed) an increment

in the amount of caffeine bound to the polymer is expected, up to saturation of all possible binding sites.

The analyte binding experiment protocol can be summarised into the following steps: (i) add caffeine to a stable dispersion of nanogels in water at fixed concentration and stir overnight at room temperature; (ii) separate the polymer with the bound caffeine from the solution and asses the remaining amount of caffeine not bound present in the supernatant solution. The experiment is graphically depicted in Scheme 3.13 below.

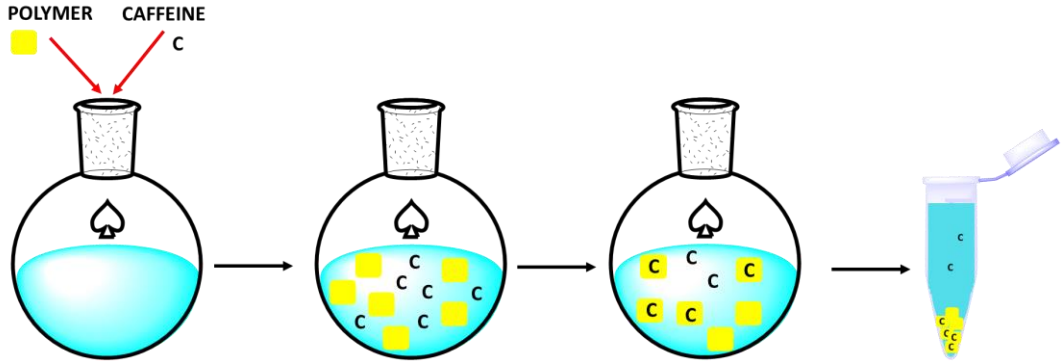

Scheme 3.13. General procedure of the analyte binding experiment to assess the amount of caffeine bound to the polymer.

The critical steps for this experiment are: (i) ensure that sufficient time is allowed to reach equilibrium; (ii) find an appropriate procedure to separate the polymer nanoparticles with bound caffeine from the remaining solution (with unbound caffeine). With regard to the time required to reach the equilibrium, it was decided to initially work at a fixed time and give priority to the development of a protocol to separate the bound caffeine from the unbound. Two techniques were evaluated: (i) precipitation by centrifugation; (ii) separation using centrifugal filters.

Precipitation by centrifugation was investigated given its simplicity compared to the use of centrifugal filters. However, the amount of precipitate depends on the total amount of the polymer initially dispersed and, therefore the applicability of this method at low

polymer concentration presented some challenges. To estimate the amount of polymer still present in solution after centrifugation, a UV-vis calibration curve was constructed and the obtained spectra for polymers of different concentrations are reported in Figure 3.17.

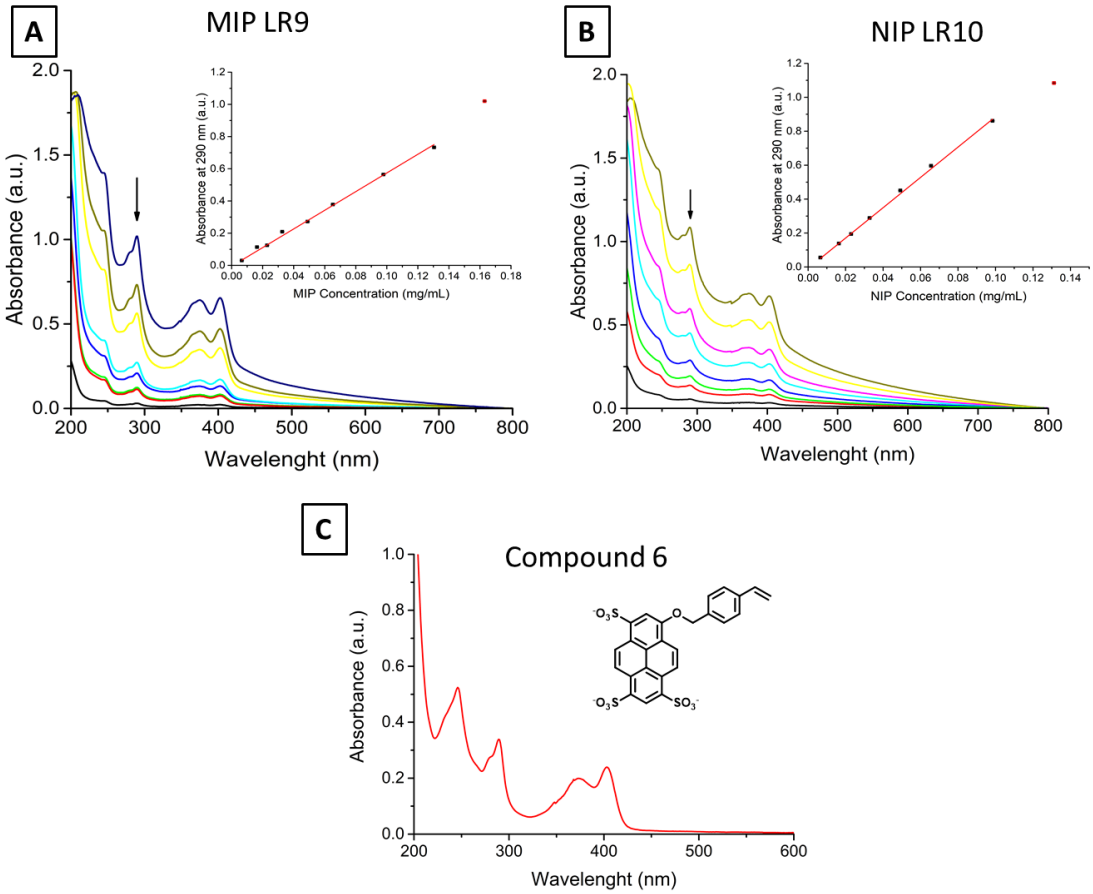

Figure 3.17. UV-vis spectra (A) for the MIP at different concentrations (0.09 to 0.17 mg/mL) and (B) NIP. In all cases, the polymer was dispersed in deionised water. In the inset, the constructed calibration curve is depicted. (C) The UV-vis spectrum of the synthesised functional monomer.

The recorded UV-vis spectra of the polymers (Figure 3.17 A and 3.17 B) confirmed that the synthesised functional monomer was incorporated in both the NIP and MIP matrixes. In fact, absorption bands between 270 and 400 nm are ascribed to the functional monomer (HPTS) moiety because the crosslinker and the other monomer employed (MBA and Am) do not absorb at these wavelengths. To plot a calibration curve, the absorbance at 290 nm was selected because a sharp and distinct peak was recorded for both polymers. The obtained fitting equations are reported below.

$$Abs\ (290\ nm) = 5.72\ (\pm 0.08) \times MIPconcentration\ (mg/ml) \quad (3.5)$$

$$Abs\ (290\ nm) = 8.82\ (\pm 0.01) \times NIPconcentration\ (mg/ml) \quad (3.6)$$

Interestingly, the slopes of lines drawn using the two equations were significantly different, which can arise from a difference between MIP and NIP regarding: (i) size of the particles; (ii) amount of functional monomer (HPTS polymerisable) incorporated; (iii) location of the functional monomer. The particle size, can affect the absorption because of light scattering; bigger particles will scatter more light and, therefore, show a higher absorbance. However, considering that the dynamic light scattering data showed the MIP and NIP being 88 nm and 144 nm respectively, the observed difference in absorbance cannot be solely linked to the difference in the particle diameter. Similarly, the location of the functional monomer (inside or on the surface of the polymer) cannot explain completely the absorbance difference. On the other hand, a difference in the incorporation of HPTS in the polymer matrix can be used to explain the UV spectra obtained. In fact, the theoretical formulation of the polymer (where 5% of the functional monomer is present) can differ from the real one. In addition, given the very small amount of the functional monomer used, small changes in incorporation can result in significant size differences. Under this hypothesis, the ratio of the obtained slopes can be used to correct the amount of the functional monomer present with a more realistic value.

As mentioned previously, centrifugation was investigated initially as a method to separate the polymer from aqueous solutions. After centrifugation, the initial yellow colloidal mixture (Figure 3.18 A) led to the formation of some precipitate while the supernatant solution displayed a loss of colour. (Figure 3.18 B).

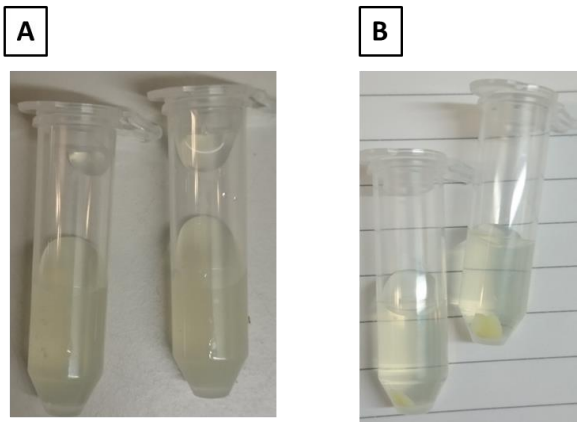

Figure 3.18.The dispersion of MIP and NIP in water (3 mg/mL) (A) before and (B) after centrifugation step.

To quantify the amount of polymer still present in the colloidal system, the UV-vis spectra were recorded (Figure 3.19).

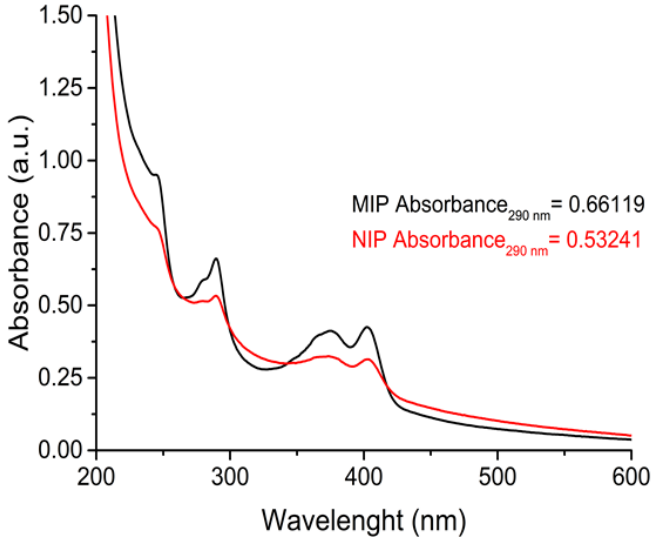

Figure 3.19. UV-vis spectra of the supernatant phase after centrifugation of a dispersion of the polymer in water (3 mg/mL).

Based on the absorbance value recorded, it was estimated that 26% of MIP and 10% of NIP did not precipitate. Given that the centrifugation procedure did not allow for satisfactory precipitation of the polymer from the solution and proved to be heavily dependent on the initial polymer concentration, it was deemed to be insufficiently accurate. Therefore, the use of centrifugal filters was investigated, given its higher potential for wider applicability because this method does not rely on the initial polymer concentration. Two different filter materials were examined namely, PTFE and

regenerated cellulose, both with a cut off of 3 kDa, which is smaller than the cut-off of the dialysis membrane employed during purification of the polymer (3.5 kDa cut-off). In view of the lower cut-off of the filters, no significant amount of the polymer was expected to pass through. To confirm this hypothesis, the UV-vis spectra of the filtered solutions were recorded and are shown in Figure 3.18, below.

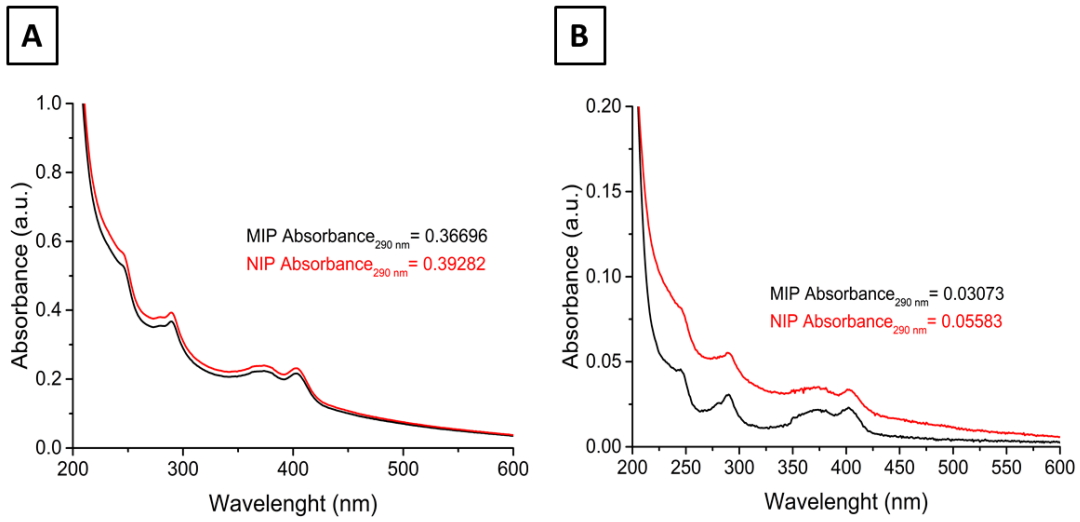

Figure 3.18. UV-vis spectra of the filtered solution after centrifugation of the polymer dispersion in water (3 mg/mL), using (A) the PTFE and (B) regenerated cellulose centrifugal filters. The black and red curves depict the spectra of the MIP and NIP, respectively. The absorbance at 290 nm is also reported in the graph.

Surprisingly, in the case of the PTFE filters (Figure 3.18 A) the amount of the polymer which passed through, was higher than that passing through the regenerated cellulose filters, in which less than 2% of the initial polymer was found in the filtered solution. Although both filters have the same cut-off, they showed different separation properties, which is probably linked to a lower affinity between the polymer and regenerated cellulose, compared with the polymer and PTFE. In view of better results achieved with regenerated cellulose filters, these filters were considered as the most appropriate to separate the polymer with bound caffeine from the free caffeine solution.

The full analyte rebinding experimental details are reported in the Material and Methods section at the end of this chapter. Briefly, the MIP and NIP polymers were dispersed in

water with different amounts of caffeine (0.05 to 1.71 mg/mL). The mixture was stirred overnight. After subsequent centrifugation through the filters, the amount of free caffeine in the filtered solution was determined by HPLC analysis. A graphical description of the experiment is depicted in Scheme 3.14, below.

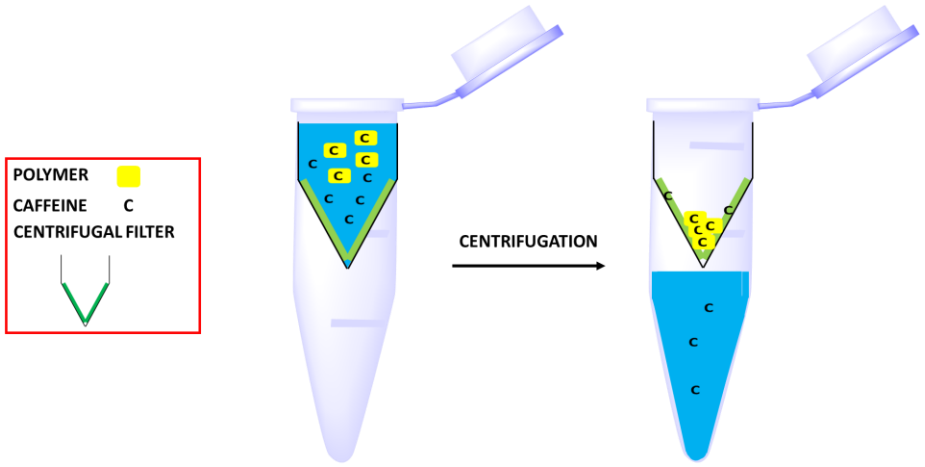

Scheme 3.14. Graphical representation of the analyte binding experiment using the centrifugal filters. In particular, the issue of the amount of caffeine bound to the filters after centrifugation is depicted.

The filters allowed separation of the polymer from the solution. However, some caffeine was possibly retained by the filter itself, thus leading to overestimation of the caffeine bound to the polymer. In order to correct for this effect, a control experiment was performed, in the polymer absence, under the same conditions. The raw data for the bound caffeine are listed below.

Table 3.8.The amount of caffeine bound to the MIP, NIP and the centrifugal filters (Control) at different initial caffeine concentrations. The concentration of MIP and NIP was kept constant at 3 mg/mL.

Initial caffeine concentration (mg/mL)	Caffeine bound (mg)		
	MIP (LR9)	NIP (LR10)	Control (no polymer)
0.05	0.0183	0.0312	0.005
0.16	0.0488	0.0461	0.009
0.27	0.0715	0.0637	0.014
0.55	0.1480	0.1521	0.029
1.12	0.3201	0.2952	0.034
1.71	0.4177	0.3463	0.071

A key parameter required to determine if the analyte binding protocol can provide accurate results is its repeatability. Therefore, to evaluate the error associated with the procedure developed, a triplicate experiment at 0.55 mg/mL of caffeine was conducted and the data are presented in Table 3.9, below.

Table 3.9. Repeatability studies using an initial concentration of caffeine of 0.55 mg/ml. The mean value, standard deviation and relative standard deviation for the experiment performed in triplicate are reported for the MIP, NIP and the control experiment without the polymer.

	Mean value caffeine bound (mg)	Standard deviation (mg)	Relative standard deviation (RSD)
MIP	0.14546	0.00523	4 %
NIP	0.1556	0.00338	2 %
Control	0.02882	0.00281	10 %

In the case of the polymers, a very low relative standard deviation was found (> 5%), while in the case of the control, a higher RSD (10%) was calculated. Most probably, this higher value was obtained because the amount of caffeine is five times lower and, therefore, the accuracy is limited. Nevertheless, the obtained data evidenced that the protocol is reproducible and can provide sufficiently precise values of caffeine bound to the polymer. Subsequently, the amount of caffeine bound to the polymer was corrected to eliminate the amount of caffeine adsorbed onto the filter's membrane (by subtraction of the control experiment from the MIP and NIP). Moreover, considering the different number of binding sites in the two polymers, a correction based on the UV-vis spectroscopy data was also applied. The equation employed for correcting the values are reported in the Material and Methods section. In the histography in Figure 3.19, the amount of caffeine bound to the MIP and NIP, at different initial caffeine concentrations, is shown.

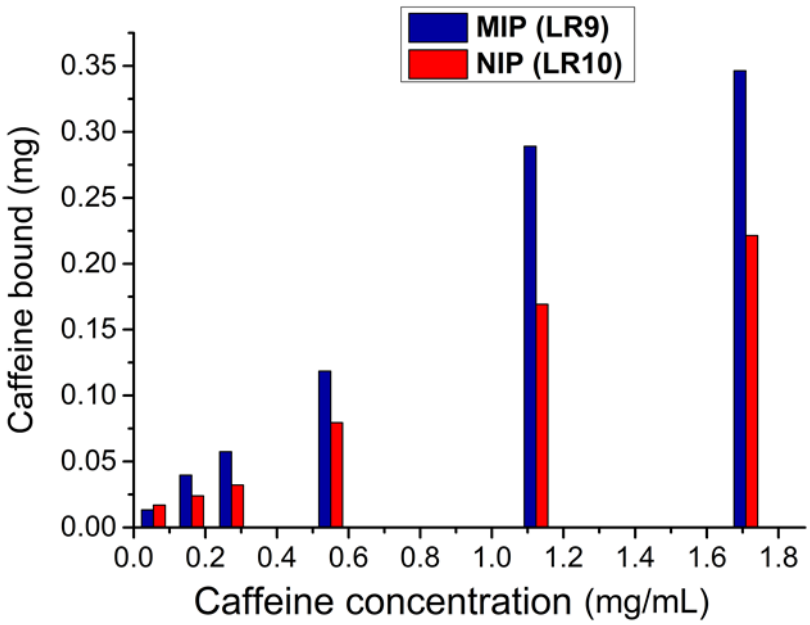

Figure 3.19. The amount of caffeine bound to the polymer versus initial concentration of caffeine for the MIP (blue) and NIP (red). The experiment was performed using a fixed polymer concentration of 3 mg/mL at 25 °C.

From this histogram, it follows that the MIP bound more caffeine than the NIP, with the exception of the first point (0.05 mg/mL) where results for the two materials were similar. However, at this low concentration, the measurement error could have affected the result. Using the ratio between the amount of caffeine bound for the MIP and NIP, a mean imprinting factor of 1.64 was calculated. When compared with previously reported MIP for caffeine, the obtained imprinting factor is low. However, it must be considered that higher imprinting factors are usually achieved only after a meticulous optimisation of the polymer formulation. In fact, the ratio of the functional monomer to the crosslinker can have a considerable effect on the analyte binding properties of the resulting polymer matrix.[1] The caffeine immobilisation in and on the polymers can result from the polymer network binding (due to clustering of caffeine on the polymer surface) and cavity binding thanks to the presence of cavities. The latter can only occur in the MIP, thanks to the templating effect. Therefore, the NIP can be employed as an indication of the amount of caffeine bound non-specifically only. Therefore, by subtracting the NIP from the MIP binding, cavity binding can be evaluated (Figure 3.20).

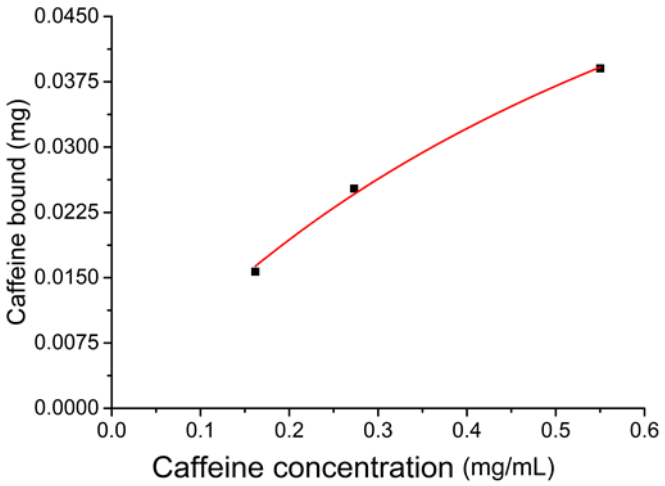

Figure 3.20. The amount of caffeine bound to the MIP cavities, at different caffeine concentrations in solution. The amount of caffeine bound was calculated using the difference from the MIP and NIP. The fitting was done using equation 3.1, in Section 3.1 of this thesis.

From Figure 3.20, above, a saturation trendline can be observed, which provides evidence for the existence of binding sites in the MIP matrix thanks to the caffeine templating effect during the polymer synthesis. Among the six points that were presented in Figure 3.19, the first point at 0.05mg/mL was not considered, given the error associated with the measurement of very low quantities. The points at high caffeine concentrations (1.12 and 1.71 mg/mL) were also omitted, given that very high concentrations led to oversaturation and predominance of network binding events, which altered the results. Overall, the preliminary results obtained provided evidence that the selected functional monomer (HPTS polymerisable) can be employed for the synthesis of MIPs selective for caffeine. Because of the tight schedule of the project, there was insufficient time to further investigate the analyte binding process and provide more robust data on the amount of caffeine bound, the kinetics of the rebinding process, and the selectivity of the polymers. Besides, the polymer formulation is another important factor to be optimised in order to find the best ratio of the functional monomer to the crosslinker and maximise the recognition properties.

3.3 Conclusion and future work

To summarise, this chapter presents data related to the synthesis of imprinted polymers selective for caffeine, starting with the identification of an appropriate functional monomer to bind caffeine in aqueous solutions (polymerisable HPTS, K_{ass} = 229 M^{-1}), followed by the optimisation of the synthetic conditions (aqueous solutions as media, 5% of initiator, room temperature, 24 hours). The polymer formulation was initially set to 75% of MBA as crosslinker, 5% of HPTS polymerisable and 20% of Am as the comonomer. The synthesised polymers (MIP and NIP) were then characterised using dynamic light scattering, which evidenced similar sizes for the MIP and NIP (88 nm and 144 nm, respectively) and a negative zeta potential (-30 and -40 mV for MIP and NIP, respectively). Subsequently, a method to perform the analyte binding experiment was identified and among different options, the use of regenerated cellulose centrifugal filters was found as most convenient. The preliminary results on the caffeine analyte binding from aqueous solutions showed that both the MIP and NIP could bind caffeine and an imprinting factor of 1.64 was determined, thus suggesting that the imprinting can increase the affinity towards caffeine. As stated at the end of the previous section, more experiments must be performed to validate the promising initial results and different polymer formulations need to be considered for a more complete study.

3.4 Materials and Methods

3.4.1 Reagents

Caffeine (ReagentPlus grade > 99%), *N,N′*-methylenebis(acrylamide) (MBA) (grade 99%), Am (grade ≥ 99%), ammonium persufate (ACS reagent grade≥ 98%), *N,N,N′,N′*-tetramethylethylenediamine (ReagentPlus, grade> 90%) (TEMED), 8-hydroxypyrene-1,3,6-trisulfonic acid trisodium salt (HPTS) (grade 97%), potassium carbonate (ACS reagent grade 99%), sodium hydroxide (ACS reagent grade 97%), sodium bicarbonate

(ACS reagent grade 99.7%), acryloyl chloride (grade 97%), 4-vinylbenzyl chloride (grade 90%), sodium hydride (60% dispersed in mineral oil) and dimethyl sulfone (grade 98%) were all purchased from Sigma-Aldrich Inc. Tetrahydrofuran (THF), acetonitrile (ACN), methanol (MeOH), water (for HPLC analysis), chloroform, diethyl ether (Et_2O) and dichloromethane, were purchased as HPLC grade; anhydrous DMSO (water content <0.0005%) were purchased from Sigma-Aldrich Inc. D_2O, THF (d8) and ACN (d3) for NMR spectroscopy were purchased from Cambridge Isotopes laboratories Inc with grade > 99.95%. Oxygen-free nitrogen gas was purchased from BOC gases Ltd.

3.4.2 Apparatus

Reagentplus pipettes (various volumes) were purchased from Gilson Inc. and employed for the addition of accurate solution volumes < 10 mL. Microliter Hamilton syringes (0.5 mL) from Hamilton company was also employed for the analyte binding experiment. Otherwise, volumetric cylinders were employed for measuring the volume of liquids. For the dialysis purification step, cellulose Visking dialysis membranes with the 3.5-kDa cut off were purchased from Medicell membranes Ltd. Aluminum oxide matrix on polyester thin-layer chromatography (TLC) plates were employed for TLC analysis. These were purchased from Sigma-Aldrich. Acrodisc® syringe filters GHP membranes (diameter 25 mm, pore size 0.45 μm) were employed for filtration. The USC100TH ultrasonic bath (VWR) was employed for sonication. Proton NMR spectra were recorded using a Bruker 400 MHz Avance III spectrometer. The proton spectra were analysed using MestReNova 11 software (Mestrelab Research S.L.R.). Peak multiplicity was determined by visual analysis of the spectra and the following abbreviations were employed: singlet (s), doublet (d), doublet of doublet (dd), triplet (t), quartet (q), multiplet (m). The chemical shift (δ) is reported as part per million (ppm). Solvent's

proton resonance frequency was set based on the values reported by Gottlieb H. E. *et al.*[39] Coupling constants (*J*) are reported in Hz.

Dynamic light scattering (DLS) data and ζ-potential measurements were performed using a Zetasizer Nano ZS from Malvern equipped with a 4-mV He-Ne laser (λ =633 nm) and a detector at a 173º angle. For DLS measurements, disposable cuvettes DTS0012 were employed while in the case of ζ-potential measurements, disposable cuvettes DTS1060 from Malvern were used. The data were handled using Zetasizer software 7.11 (Malvern Instruments Ltd.).

Water purifier Purelab Option (ELGA) was employed for experiments requiring deionised water. Resistivity above 18 MΩcm.

Evaporation processes were performed using a Buchi Rotavapor R-200 and Heidolph G1.

Sample freeze-drying was performed on a Lyotrap from LTE scientific LTD (UK).

High-performance liquid chromatography (HPLC) experiments were performed on Infinity II series 1260 equipped with a Quaternery pump, multisampler, multicolumn thermostat and UV-vis diode arrays detector purchase from Agilent Ltd. A C18 HPLC column H1-5C18-250A from Hichrom was employed.

Cary 100 UV-vis spectrophotometer (Agilent Technologies) equipped with thermostat unit and Fisherbrand™ quartz cuvette (light path 10 mm) from Fisher Scientific were employed for UV-vis spectra recording. All spectra were recorded at 25 °C with background correcting by previously recording the UV-vis spectra of the solvents employed.

The Eppendorf 5418 R refrigerated centrifuge, with Rotor FA-45-18-11 was employed for the centrifugation step. The 0.5 mL PTFE (Polytetrafluoroethylene) centrifugal filters 3 kDa cut-off were purchased from VWR Scientific. Amicon® Ultra-0.5 Centrifugal

Filters 3 kDa cut-off from Merck Millipore were employed. Before using the centrifugal filters, these were washed using 0.5 mL of deionised water and centrifuged at 14,000 rpm for 25 minutes. For data analysis, plotting and fitting of the data, Origin 9.1 software (OriginLab Corporation) was employed setting a confidence level interval at 95%.

3.4.3 General procedures

Anhydrous reactions

All reactions requiring anhydrous solvents were performed using previously dried glassware, by placing them in an oven at 70 °C for 24 hours. During the synthesis, after the solid reagents were added, the reaction flask was closed with silicon Suba-Seal septa and the solvent was added using a syringe. Vacuum nitrogen steps (five times) were applied to fill the reaction flask with inert gas atmosphere. Each vacuum and nitrogen step was 20 seconds long. Subsequently, a balloon filled with anhydrous nitrogen was connected to the reaction flask to ensure the presence of inert gas atmosphere.

HPLC analysis and caffeine concentration determination

The HPLC procedure was previously developed in the Professor Resmini group. The procedure involved the use of a mixture of methanol : water, 40 : 60 v : v with a flow rate of 0.7 mL/min. The temperature of the column and injection chamber were set at 25 °C. An injection volume of 10 µL with a draw speed and injection speed of 200 µL/min were set. Caffeine retention time was 6.9 min. The concentration of caffeine was determined by monitoring the absorbance at 273 nm, and by comparison with a previously obtained calibration curve (Figure 3.20).

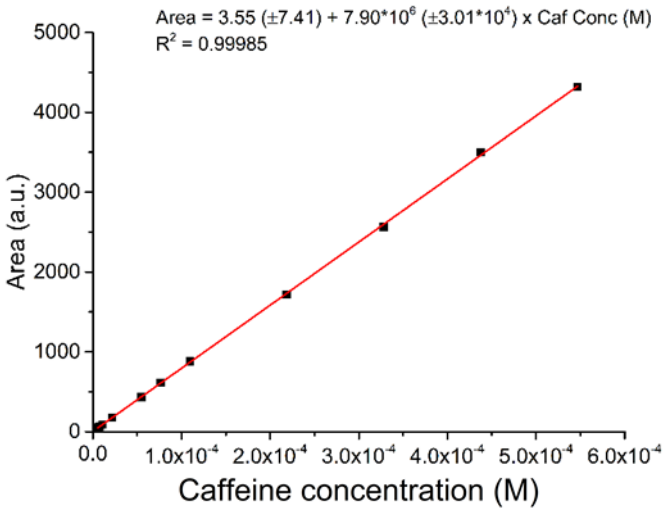

Figure 3.20. The calibration curve for the HPLC determination of caffeine.

NMR titration experiment

A known amount of a possible functional monomer was dissolved in 1 mL of deuterated water. A 16-scan proton NMR spectrum was recorded and, subsequently, one chemical equivalent of caffeine was added by dissolving it in the initial solution, and then the ^{1}H NMR spectrum was recorded. This latest step was repeated by adding 2, 3, 5, 7 and 9 equivalents of caffeine. For the experiments using the D_2O : THF (d8) or D_2O : ACN (d3) mixture, the same procedure was applied but only 0, 1, 5 and 9 equivalents of caffeine were evaluated. The chemical shift was determined considering the peak centre and the variation in the chemical shift ($\Delta\partial$) was calculated following Equation 3.2 (Section 3.2.1)

Subsequently, variation in the chemical shift was plotted against the molar concentration of caffeine and the data were fitted using a one-site specific binding model leading to the determination of the dissociation constant (K_{diss}) and subsequently the association constant as explained in the Results and discussion section.

3.4.4 Proton NMR peak assignation

The assignment of the proton NMR peaks for the molecules evaluated as the caffeine binder is reported below.

(1S,3R,4R,5R)-3-{[(2E)-3-(3,4-Dihydroxyphenyl)-2-propenoyl]oxy}-1,4,5-trihydroxycyclohexanecarboxylic acid. (Caffeoylquinic acid)

^{1}H NMR (400 MHz, D_2O): δ 7.67 (d, *J*= 15.96 Hz, 1H, -HC=CH-COO-), 7.21 (d, *J*= 1.89 Hz, 1H, Ar), 7.14 (dd, *J*= 1.93Hz, *J*= 8.30Hz, 1H, Ar), 6.95 (d, *J*= 8.23, 1H, Ar), 6.41 (d, *J*= 15.96 Hz,1H, -HC=CH-COO-), 5.35 (dt, *J*=11.07, *J*=4.76, 1H,-OCH-CH_2-),4.27-4.24 (m,1H,-O-CH-CH(OH)-CH-(OH)-), 3.88 (dd, *J*=9.91, *J*=3.28, 1H, -CH(OH)-CH-(OH)-), 2.23-2.13 (m, 2H, CH_2-C(OH)-COOH)), 2.06-2.00(m, 2H, CH_2-C(OH)-COOH)).

3-(3,4-Dihydroxyphenyl)propanoic acid

^{1}H NMR (400 MHz, D_2O): δ 6.87 (d, *J*= 8.11 Hz, 1H, Ar), 6.83 (d, *J*= 2.10 Hz, 1H, Ar), 6.74 (dd, *J*= 8.09 Hz, *J*= 2.10, 1H, Ar), 2.83 (t, *J*= 7.31 Hz, 2H, Ar-CH_2-CH_2-COOH), 2.65 (t, *J*= 7.21 Hz, 2H, Ar-CH_2-CH_2-COOH).

4-Vinylpyridine

^{1}H NMR (400 MHz, D_2O): δ 8.48 (m, 2H, Ar), 7.51 (m, 2H, Ar), 6.80 (dd, *J*= 10.95 *J*= 17.68, 1H, Ar-CH=CH_2), 6.13 (d, *J*= 17.68, 1H, Ar-CH=CH_2), 5.60 (d, *J*= 10.95, 1H, Ar-CH=CH_2).

(S)-2-Amino-3-(4-hydroxyphenyl)propanoic acid

^{1}H NMR (400 MHz, D_2O): δ 7.19 (d, *J*= 8.53, 2H, Ar), 6.88 (d, *J*= 8.55, 2H, Ar), 3.86 (dd, *J*= 5.12 *J*= 7.73, 1H,CH_2-CH(NH_2)-COOH), 3.16 (dd, *J*= 4.90 *J*= 14.50, 1H,CH_2-CH(NH_2)-COOH), 3.05 - 2.95 (m, 1H,CH_2-CH(NH_2)-COOH).

(S)-3-(1H-indol-3-yl)-2-propionamidopropanamide

^{1}H NMR (400 MHz, D_2O): δ 7.63 (d, *J*= 7.91, 1H, Ar), 7.44 (d, *J*= 8.10, 1H, Ar), 7.20-7.17 (m, 2H, Ar), 7.11 (dt, *J*= 1.10 *J*= 7.48, Ar), 3.27 (dd, *J*= 8.13 *J*= 14.46, 1H,CH_2-CH(NH-)-COOH), 3.12 (dd, *J*= 8.20 *J*= 14.48, 1H,CH_2-CH(NH-)-COOH), 2.12 (q, *J*= 7.65, 2H, NHOC-CH_2-CH_3), 0.88 (t, *J*= 7.64, 3H, NHOC-CH_2-CH_3).

9H-purin-6-amine. (Adenine)

^{1}H NMR (400 MHz, D_2O): δ 8.23 (s, 1H, Ar), 8.18 (s, 1H, Ar).

8-Hydroxypyrene-1,3,6-trisulfonic acid trisodium salt

^{1}H NMR (400 MHz, D_2O): δ 9.17 (s, 1H, Ar), 9.13 (d, *J*= 9.77, 1H, Ar), 9.01 (d, *J*= 9.61, 1H, Ar) 8.95 (d, *J*= 9.78, 1H, Ar), 8.78 (d, *J*= 9.62, 1H, Ar), 8.32 (s, 1H, Ar).

8-((4-Vinylbenzyl)oxy)pyrene-1,3,6-trisulfonate (Compound 6)

^{1}H NMR (400 MHz, D_2O): δ 9.17 (s, 1H, Ar), 9.14 (d, *J*= 9.84, 1H, Ar), 9.05 (d, *J*= 9.61, 1H, Ar) 8.97 (d, *J*= 9.83, 1H, Ar), 8.88 (d, *J*= 9.62, 1H, Ar), 8.43 (s, 1H, Ar), 7.47 (d, *J*= 8.14, 2H, Ar), 7.37 (d, *J*= 8.13, 2H, Ar), 6.66 (dd, *J*= 11.02 *J*= 17.50, 1H, Ar-C<u>H</u>=CH_2), 5.76 (d, *J*= 17.42, 1H, Ar-CH=C<u>H_2</u>), 5.42 (s, 2H, Ar-O-C<u>H_2</u>-Ar), 5.25 (d, *J*= 11.15, 1H, Ar-CH=C<u>H_2</u>).

3.4.5 Synthesis of a polymerizable analogue of HPTS

Synthesis of compound 5' in aqueous solutions

In a one-neck round-bottom flask, 20 mg of HPTS (38 µmoles) were dissolved in 5 mL of deionised water, a green solution was obtained. Next, 1.52 mg of $NaHCO_3$ (0.30 mmoles) were added, and then the reaction mixture was cooled using an ice bath and, subsequently, 4.65 µL (38 µmoles) of acryloyl chloride were added. The solution was then left under stirring at room temperature overnight. The reaction progress was monitored using thin-layer-chromatography (TLC) (eluent: water : THF : MeOH 5 : 4 : 1 v : v : v). Subsequently, the green aqueous phase was acidified to pH = 3 (using 1 M HCl) and then extracted using Et_2O (10 mL for three times). The aqueous phase was subsequently freeze-dried. The yellow solid obtained was analysed using proton NMR spectroscopy. Only unreacted HPTS was recovered (yield 90%). The same procedure was applied using different bases (K_2CO_3 and NaOH) and acryloyl chloride (from 1 to 4 equivalents) leading to the same results.

Synthesis of compound 5' in anhydrous conditions

20 mg of HPTS (38 µmoles) were dissolved in 16 mL of anhydrous DMSO. A colourless solution was obtained. Next, 7.36 mg of NaH were added (0.15 mmoles), and then the reaction mixture was purged with nitrogen, forming a green solution. Subsequently, to 13 µL of acryloyl chloride were added (0.15 mmoles) the solution under stirring and then the reaction was let at room temperature for 18 hours. Afterwards, 10 mL of $CHCl_3$ and 10 mL of deionised water were added. The two phases were separated using a separating funnel, and then the green aqueous phase was washed twice with 10 mL of $CHCl_3$. The water phase was evaporated using a rotavapor and 17.40 mg of a yellow solid were obtained, and then the proton NMR spectra were recorded using D_2O. Only unreacted HPTS was isolated (yield 90 %).

Synthesis of compound 6

A sample of 200 mg of HPTS (0.38 mmoles), 138.21 mg of K_2CO_3 (38 mmoles) and 120 mL of anhydrous DMSO were placed in a one-neck round-bottom flask. The obtained yellow mixture was stirred using a magnetic stirrer under nitrogen atmosphere. To ensure the inert gas atmosphere, a balloon of nitrogen was connected to the reaction flask. Subsequently, benzyl chloride (540 µL, 3.8 mmoles) was added and then the reaction mixture was left stirred at room temperature for 18 hours. The reaction progress was monitored using TLC (eluent: water : THF : MeOH 5 : 4 : 1 v : v : v). Once the reaction was completed, based on the TLC analysis, the mixture was filtered using paper filters to eliminate the undissolved K_2CO_3. After the solvent was then evaporated, the obtained yellow oil was triturated with 10 mL of chloroform to yield a yellow solid. Then, the mixture was filtered with Buckner filter and filtering paper. The solid was washed three times with 5 mL of chloroform. 220.50 mg of yellow solid were obtained

(yield 88%). Proton NMR chemical shifts of the isolated compound was given in Section 3.4.4

3.4.6 General procedure of polymer synthesis and composition calculations

The amounts of the functional monomer, template, crosslinker and comonomer were calculated using the following step-by-step procedure. Initially, the amount of the functional monomer to be used was decided. The amount of the crosslinker and the comonomer required were calculated according to the following equations, and taking into consideration the polymer formulation:

$$mg_{Crosslinker} = mmoles_{FM} \times \frac{\%_{Crosslinker}}{\%_{Functional\ monomer}} r.m.m._{Crosslinker} \quad (3.8)$$

$$mg_{Comonomer} = mmoles_{FM} \times \frac{\%_{Comonomer}}{\%_{Functional\ monomer}} r.m.m._{Comonomer} \quad (3.9)$$

The amount of the initiator was calculated according to the moles of polymerizable double bonds present in the reaction, using the following equation:

$$mg\ initiator = (mmoles_{FM} + 2mmoles_{Crosslinker} + mmoles_{Comonomer}) \times initiator\ \% \times r.m.m._{Initiator} \quad (3.10)$$

Where $initiator\ \%$ was decided before starting the synthesis.

When the polymerisation reaction was performed at room temperature, the amount of the catalyst (TEMED) was kept proportional to the initiator amount according to the equation below:

$$1\ \mu L\ of\ TEMED : 2\ mg\ ammonium\ persulfate \quad (3.11)$$

Finally, the amount of solvent required was calculated based on the total monomer concentration (C_m):

$$Volume\ solvent\ (L) = (mg_{Comonomer} + mg_{Crosslinker} + mg_{FM}) \times \frac{C_m}{100} \times \frac{1}{Solvent\ density} \quad (3.12)$$

A typical synthesis procedure is described below:

Caffeine and all of the monomers were placed into a Wheaton glass bottle and then they were dissolved in the calculated amount of solvent to reach the desired C_m. Once all reagents were dissolved, the calculated amount of the initiator was added, followed by TEMED addition if the polymerisation was performed at room temperature. The Wheaton bottle was then sealed using PTFE-faced rubber septa. 3 nitrogen/vacuum steps were applied in order to eliminate oxygen from the reaction mixture, each nitrogen or vacuum step was approximately 10 seconds long. If the reaction was performed at 70 °C the Wheaton bottle was placed inside an oven and the temperature was set at 70 °C. When the polymerisation was performed at room temperature, the reaction bottle was placed on the laboratory bench. After 24 hours, an equal volume of methanol was added, and then the solution was stirred for 24 hours at room temperature in a round-bottom flask using a magnetic stirrer. Subsequently, the solution was put in dialysis against 5 L of deionised water for three days (three changes per day). The dialysed solution was frozen using liquid nitrogen and freeze-dried. A fluffy solid was obtained and weighted to calculate the yield.

3.4.7 Reactivity of caffeine during radical polymerisation

A stock solution of caffeine was prepared by dissolving 14.90 mg in 10 mL of deionised water in a volumetric flask. Similarly, aqueous stock solution of ammonium persulfate and TEMED were prepared using 31.23 mg and 17 µL, respectively, in 10 mL of deionised water. In Wheaton glass bottles, the following amounts of the stock solutions were placed (Table 3.10).

*Table 3.10. Amounts of stock solutions for the experiment of reactivity of caffeine during radical polymerisation. A typical polymerisation formulation containing 75% of MBA, 5% of compound **6**, and 20% of Am was considered to calculate the amount of the initiator required for the reaction.*

Solution	Caffeine (mL)	Ammonium persulfate (mL)	TEMED (mL)	Deionised water	Initiator %
1a	1	0	0	9	0
1b	1	0	0	9	0
2a	1	0.2	0	8.8	1
2b	1	0.2	0.2	8.6	1
3a	1	1	0	8	5
3b	1	1	1	7	5
4a	1	2	0	7	10
4b	1	2	2	5	10

The Wheaton bottles were subsequently sealed, and then the nitrogen/vacuum steps were applied to generate an inert gas atmosphere and simulate the conditions employed during the polymer synthesis. An aliquot of solution was taken and analysed with HPLC to determine the content of caffeine at time 0. Subsequently, the solutions named *a* were placed in the oven at 70 °C, while the solutions named *b* were placed in an laboratory bench. After 24 hours, another aliquot of the reaction solution was taken and the content of caffeine present was determined with HPLC.

3.4.8 Optimisation of initiator concentration

For the optimisation of the amount of the initiator, the reaction was performed using D_2O and monitored using proton NMR spectroscopy. The following stock solutions were prepared using D_2O and 5-mL glass vials:

*Table 3.11. Stock solutions for polymerisation in D_2O. A typical polymerisation formulation containing 75% of MBA, 5% of compound **6**, and 20% of Am was considered.*

	Monomer **6**	Caffeine	MBA	AM	APS	TEMED	Dimethyl sulfone
mg	5.35	4.99	30.11	9.75	50	100 µL	21.78
mL	1	1	2	3	1	1	5
mg/mL	5.35	4.99	15.05	3.25	50	100	4.356

The following polymer preparations were done by adding the following amounts of stock solutions into a Wheaton bottle.

Table 3.12. Amounts of stock solutions employed for the polymerisation in D_2O. In all cases Cm of 0.25% was employed and the reaction was performed under nitrogen atmosphere for 24 h at room temperature.

	Monomer 6	Caffeine	MBA	AM	APS	TEMED	D_2O
LR 1	181 µL	30 µL	238 µL	136 µL	1.73 µL	0.90 µL	1.40 mL
LR 2	181 µL		238 µL	136 µL	1.73 µL	0.90 µL	1.40 mL
LR 3	181 µL	30 µL	238 µL	136 µL	8.68 µL	4.34 µL	1.40 mL
LR 4	181 µL		238 µL	136 µL	8.68 µL	4.34 µL	1.40 mL

Before the initiator addition, 0.6 mL of the reaction solution were taken and, then 10 µL of the internal standard stock solution were added. The proton NMR spectrum was recorded. Similarly, after 24 hours from the initiator addition and the catalyst, 0.6 mL of the reaction solution were taken, 10 µL of internal standard stock solution were added and subsequently the proton NMR spectrum was recorded. By integration of the vinyl proton peaks and comparison against the integration for the internal standard protons, the polymerisation conversion was determined.

3.4.9 Polymer synthesis LR5, 6, 7, 8, 9, 10

The general procedure described in Section 3.4.6 was employed. In the following Table 3.13, the amount of reagents employed and the final polymerisation yields are reported.

Table 3.13. Polymer reagent amounts and the polymerisation yield. In all cases 5% of the initiator was employed and the reaction was performed using deionized water at room temperature with the addition of TEMED.

Polymer	Cm %	Compound 6 (mg)	Caffeine (mg)	MBA (mg)	Am (mg)	Yield (%)
LR 5	0.25	4.80	0.80	17.13	1.90	10
LR 6	0.25	4.82		17.24	1.92	40
LR 7	0.5	4.60	0.81	17.79	2.10	80
LR 8	0.5	4.62		17.78	2.10	86
LR 9	1	4.79	0.82	17.66	2.20	93
LR 10	1	4.77		17.41	2.30	90

After 24 hours, the polymers were freeze-dried and isolated, the removal of caffeine from the MIP was assed by dispersing 1 mg of the polymer in 1 mL of MeOH, and then sonicating the solution for 15 minutes before subsequent analysis using the HPLC. In all cases, no caffeine was detected, providing evidence that it was removed during the dialysis step.

3.4.10 Sample preparation for DLS and ζ-potential measurements

Approximately 1 mg of the polymer was dispersed in 2 mL of deionised water, and then the colloidal system obtained was sonicated for 15 minutes. The dispersed sample solution was subsequently filtered through 0.45-μm filters and poured into cuvettes for DLS and ζ-potential measurements.

3.4.11 UV-vis calibration curve of MIP and NIP

A sample of 3 mg of polymer (MIP or NIP) was dispersed in deionised water in a 10-mL volumetric flask. Then, the colloidal system obtained was sonicated for 5 minutes. The following diluted systems were then prepared:

Table 3.14. Polymer concentrations employed for preparation of the UV-vis calibration curve of the polymer

Polymer Concentration mg/mL
0.006
0.016
0.023
0.032
0.049
0.065
0.098
0.13
0.16

The UV-vis spectrum was recorded in triplicate and the average value was calculated.

Based on the slopes of the calibration curve, the binding site correction factor was calculated, as follows:

$$Binding\ site\ correction = \frac{Slope_{MIP}}{Slope_{NIP}} \quad (3.13)$$

3.4.12 Precipitation of polymer using centrifugation

3 mg of the polymer were dispersed in 1 mL of deionised water. The colloidal system was sonicated for 5 minutes. The sample was then centrifuged at 14,000 rpm at 25 °C for 30 minutes. UV-vis spectra were recorded to determine the amount of polymer still present in the supernatant.

3.4.13 Separation of polymer from dispersion using centrifugal filters

Similarly to the previous experiment, a dispersion of polymer (3 mg/mL) was sonicated for 5 minutes, and then 0.5 mL of the mixture were poured into the centrifugal filters (PTFE and regenerated cellulose filters). The samples were subsequently centrifuged at 14,000 rpm at 25 °C for 25 minutes. The amount of polymer present in the filtered solution was determined by recording the UV-vis spectrum, and then comparing the absorbance with the previously obtained calibration curve.

3.4.14 Analyte rebinding experiment procedure

10 mg of a polymer were dispersed in 3 mL of deionised water, and then sonicated for 5 minutes. 0.5 mL of this solution were poured into 6 different glass vials. A stock solution of caffeine was prepared by dissolving 9 mg of caffeine in deionised water in a 10-mL volumetric flask. From the caffeine stock solution, the following diluted solutions were made the prepared (Table 3.15)

Table 3.15. Caffeine solutions in deionised water prepared at different concentrations.

Solution number	Caffeine concentration (mg/mL)
1	0.30
2	0.91
3	1.52
4	3.04
5	6.09
6	1.37

150 µL of each solution were added to the six different vials containing 0.5 mL of the polymer dispersed in deionised water. The solutions were left under gentle stirring overnight using a magnetic stirrer, at 25 °C (temperature was monitored using an oil bath). 0.5 mL of the solutions were subsequently transferred into a regenerated cellulose filter and centrifuged at 14,000 rpm for 30 minutes at 25 °C. The volume of the filtered solution was determined using a 0.5 mL Hamilton syringe. The recovered volumes are listed in Table 3.16.

Table 3.16. Recovered volumes after centrifugation during the analyte rebinding experiment for the MIP LR9, NIP LR10 and the control experiment. The initial loaded value was 0.5 mL in all cases.

Caffeine concentration (mg/mL)	Recovered volumes filtered solution (mL)		
0.05	MIP	NIP	Control
0.16	0.46	0.46	0.48
0.27	0.46	0.46	0.46
0.55	0.47	0.46	0.48
0.55	0.46	0.46	0.47
0.55	0.47	0.46	0.47
1.12	0.47	0.46	0.48
1.71	0.46	0.46	0.48

The concentration of caffeine in the filtered solutions was assessed by HPLC and the amount of caffeine was subsequently calculated. Finally, the amount of caffeine bound to the polymer was determined by difference from the initial amount of the caffeine

present. This procedure was applied for the MIP, NIP and a control experiment in the polymer absence. The control experiment was conducted to evaluate the amount of caffeine adsorbed to the regenerated cellulose filters, which caused an overestimation of the caffeine bound to the polymer. Therefore, the amount of caffeine adsorbed to the filter was subtracted from both the MIP and NIP raw data, as shown below.

$$Caffeine\ bound_{corrected_{MIP}} = Caffeine\ bound_{MIP} - Caffeine\ adsorbed \quad (3.14)$$

$$Caffeine\ bound_{corrected_{NIP}} = (Caffeine\ bound_{NIP} - Caffeine\ adsorbed) \times Binding\ site\ correction \quad (3.15)$$

In addition, to normalise the values for the amount of the functional monomer present in the MIP and NIP, the ratio of the UV-vis calibration slopes (page 129) was determined.

3.5 References

1 B. Sellergren, F. L. Dickert, O. Hayden, S. Mcniven, I. Karube, G. M. Murray, M. Manuel Uy, D. Kriz, R. J. Ansell, M. Kempe, L. Schweitz, S. Nilsson, F. Lanza, L. I. Andersson, J. Matsui, T. Takeuchi, A. G. Mayes, N. Perez, C. Alexander, E. N. Vulfson, P. K. Dhal, M. G. Kulkarni, R. A. Mashelkar, K. Tsukagoshi, M. Murata, M. Maeda, D. Y. Sasaki, M. J. Whitcombe, E. N. Vulfson, G. Wulff, A. Biffis, I. A. Nicholls, H. S. Andersson and A. J. Hall, *Techniques and Instrumentation in Analytical Chemistry*, 2001, vol. Volume 23.

2 J. Svenson, N. Zheng, U. Föhrman, I. A. Nicholls, J. Svenson, N. Zheng, U. Föhrman and I. A. N. The, *Anal. Lett.*, 2005, **38**, 57–69.

3 A. J. Hall, P. Manesiotis, M. Emgenbroich, M. Quaglia, E. De Lorenzi and B. Sellergren, *J. Org. Chem.*, 2005, **70**, 1732–1736.

4 G. Wulff and R. Schönfeld, *Adv. Mater.*, 1998, **10**, 957–959.

5 U. Athikomrattanakul, M. Katterle, N. Gajovic-Eichelmann and F. W. Scheller, *Biosens. Bioelectron.*, 2009, **25**, 82–87.

6 C. R. Martinez and B. L. Iverson, *Chem. Sci.*, 2012, **3**, 2191–2201.

7 E. Pellizzoni, M. Tommasini, E. Marangon, F. Rizzolio, G. Saito, F. Benedetti, G. Toffoli, M. Resmini and F. Berti, *Biosens. Bioelectron.*, 2016, **86**, 913–919.

8 Kuriyan, Konforti and Wemmer, *Mol. Life*, 2009, 1–58.

9 S. Kong, J. C. Yang and J. Y. Park, *Sens. Actuators, B Chem.*, 2018, **260**, 587–592.

10 D.-T. Tian, Y.-C. Zhou, L. Xiong and F.-T. Lu, *Adv. Polym. Technol.*, 2017, **36**, 68–76.

11 D. Oliveira, A. Freitas, P. Kadhirvel, R. C. S. Dias and M. R. P. F. N. Costa, *Biochem. Eng. J.*, 2016, **111**, 87–99.

12 J. Y. Park, *Analyst*, 2016, **141**, 5709–5713.

13 Y. Dong, L. F. He, X. H. Zhang and X. R. Jiang, *Dig. J. Nanomater. Biostructures*, 2016, **11**, 1319–1326.
14 V. Ratautaite, D. Plausinaitis, I. Baleviciute, L. Mikoliunaite, A. Ramanaviciene and A. Ramanavicius, *Sens. Actuators, B Chem.*, 2015, **212**, 63–71.
15 A. L. Latorre, M. C. Cela Pérez, S. F. Fernández, J. M. L. Vilariño and M. V. G. Rodríguez, *React. Funct. Polym.*, 2015, **91**–**92**, 51–61.
16 F. S. Mehamod, K. KuBulat, N. F. Yusof and N. A. Othman, *Int. J. Technol.*, 2015, **6**, 546–554.
17 S. Rouhani and F. Nahavandifard, *Sens. Actuators, B Chem.*, 2014, **197**, 185–192.
18 B. Rezaei, M. Khalili Boroujeni and A. a. Ensafi, *Biosens. Bioelectron.*, 2014, **60**, 77–83.
19 Q. Zhu, C. Ma, H. Chen, Y. Wu and J. Huang, *Microchim. Acta*, 2014, **181**, 303–311.
20 X. Luo, R. Dong, S. Luo, Y. Zhan, X. Tu and L. Yang, *J. Appl. Polym. Sci.*, 2013, **127**, 2884–2890.
21 N. Phutthawong and M. Pattarawarapan, *Polym. Bull.*, 2013, **70**, 691–705.
22 P. Cormack and F. Mehamod, *Sains Malaysiana*, 2013, **42**, 529–535.
23 X. Liu, N. Sun, Q. Zhu, M. Wu, Y. Ye and H. Chen, *J. Chromatogr. A*, 2013, **1304**, 10–17.
24 M. J. Shin, Y. J. Shin and J. S. Shin, *J. Org. Polym. Mater.*, 2013, **3**, 1–5.
25 N. D'Amelio, L. Fontanive, F. Uggeri, F. Suggi-Liverani and L. Navarini, *Food Biophys.*, 2009, **4**, 321–330.
26 A. Belay, H. K. Kim and Y.-H. Hwang, *Luminescence*, 2016, **31**, 565–572.
27 H. J. Spijker, F. L. Van Delft and J. C. M. Van Hest, *Macromolecules*, 2007, 12–18.
28 S. Rochat, S. N. Steinmann, C. Corminboeuf and K. Severin, *Chem. Commun.*, 2011, **47**, 10584–10586.
29 W. Xu, T.-H. Kim, D. Zhai, J. C. Er, L. Zhang, A. A. Kale, B. K. Agrawalla, Y.-K. Cho and Y.-T. Chang, *Sci. Rep.*, 2013, **3**, 2255–2262.
30 S. Chanthamath, S. Takaki, K. Shibatomi and S. Iwasa, *Angew. Chemie - Int. Ed.*, 2013, **52**, 5818–5821.
31 A. Barteselli, S. Parapini, N. Basilico, D. Mommo and A. Sparatore, *Bioorganic Med. Chem.*, 2014, **22**, 5757–5765.
32 S. G. Srivatsan, M. Parvez and S. Verma, *Chem. - A Eur. J.*, 2002, **8**, 5184–5191.
33 Y. Hoshino, T. Kodama, Y. Okahata and K. J. Shea, *J. Am. Chem. Soc*, 2008, **130**, 15242–15243.
34 Y. Hoshino, H. Koide, T. Urakami, H. Kanazawa, T. Kodama, N. Oku and K. J. Shea, *J.Am.Chem.Soc*, 2010, 1–5.
35 M. Daoud Attieh, Y. Zhao, A. Elkak, A. Falcimaigne-Cordin and K. Haupt, *Angew. Chemie - Int. Ed.*, 2017, **56**, 3339–3343.
36 M. M. Sunil Paul, U. K. Aravind, G. Pramod, A. Saha and C. T. Aravindakumar, *Org. Biomol. Chem.*, 2014, **12**, 5611–5620.
37 J. R. León-Carmona and A. Galano, *J. Phys. Chem. B*, 2011, **115**, 4538–4546.
38 Malvern Ltd., *Zeta potential theory*, 2013.
39 H. E. Gottlieb, V. Kotlyar and A. Nudelman, *J. Org. Chem.*, 1997, **62**, 7512–7515

CHAPTER 4
Electrochemical sensor for coffee analysis

4.1 Bare glassy carbon electrode as sensing platform for caffeine determination

4.1.1 Introduction

Caffeine (Scheme 4.1) is the best known phytochemical compound present in coffee, a valuable commodity with a worldwide production totalling over 9 millions tons per year.[1]

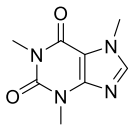

Scheme 4.1. Structural formula of caffeine.

Among the different chemical species present in coffee beans, caffeine content is not primarily linked to the taste of the final brew, but to the well-known biological activities. In our body, caffeine mainly acts as adenosine A-receptor antagonist, with a significant effect on processes like sleep, arousal, cognition, learning and memory,[2] but it also shows antioxidant activity.[3] When the intake of caffeine is moderate (less than 400 mg per day), positive effects can be experienced, such as higher concentration and decreased tiredness,[4] and in such doses its use has also been documented for the treatment of respiratory diseases.[5] However, a higher dosage of caffeine may cause cardiovascular and calcium balance problems [6] and there is still a debate on what can be considered a safe amount of caffeine intake, especially for children and young adults.[7] The concentration of caffeine in coffee beverages is often influenced by numerous factors, including the type of bean used and the brewing stage. Caffeine can also be found in other drinks in different concentrations, such as energy drinks (ca. 0.30 g/L), soft drinks (0.1 g/L) or in drugs as active ingredient (usually 200 mg/tablet) or excipient (65 mg/tablet). Given the widespread presence and use of caffeine, one of the most important issues in terms of quality control relates to the ability of monitoring caffeine content accurately.

Numerous analytical techniques and protocols have been previously developed and reported for the detection and quantification of caffeine. An overview of the most recent analytical methods for the determination of caffeine is presented in Table 4.1, below, together with the limit of detection reported for each case.

Table 4.1. Comparison of different analytical techniques for caffeine determination, based on recently reported works.

Analytical Method	Limit of Detection	Application	Reference
Liquid chromatography	Usually in the order of 10^{-7} M but can be as low as 10^{-9} M	Different matrices from beverages to biological samples (blood, urine, saliva)	[8–10]
Capillary electrophoresis	$5 \cdot 10^{-5}$ M	Serum samples	[11]
Nuclear Magnetic Resonance	$7 \cdot 10^{-7}$ M	Salivary samples	[12]
Surface-Enhanced Raman Scattering	$2 \cdot 10^{-6}$ M	Tertiary solid mixtures of paraxanthine theobromine and caffeine	[13]

Liquid chromatographic methods are the technique most employed for caffeine detection, thanks to the excellent analytical performance (i.e., high sensitivity, wide linear dynamic concentration range, selectivity, and robustness) and the possibility to be applied with a variety of matrices. Other analytical techniques have been investigated and found suitable for caffeine detection, like capillary electrophoresis, nuclear magnetic resonance and surface-enhanced Raman scattering. All these techniques, however, require expensive analytical instrumentation, highly trained personnel, and elevated maintenance costs which limit the routine determination of caffeine in an industrial environment. Moreover, given the high concentration of caffeine in caffeinated products, highly sensitive methods are not necessarily required for the development of a caffeine sensor. In fact, for routine analysis of caffeine-containing beverages in an industrial environment, the main key requirements for a sensor are: (i) minimal number of pre-

treatment steps of the sample; (ii) fast analysis times; (iii) use of solvents that are not expensive or toxic; (iv) low cost and high stability over time. Despite interesting advances in recent years, these problems remain a significant challenge in the coffee industry.[14,15] Among the most promising approaches currently being investigated, electrochemistry has one of the highest potential, having been shown to satisfy most of the requirements.[16–19] In particular, the development of modified electrodes starting from bare carbon material (glassy carbon, boron doped diamond, graphene, and screen printed carbon electrodes) has led to remarkable results and interesting applications.[20–23] The surface modification is crucial in obtaining excellent performance regarding sensitivity and selectivity, although the significant additional costs, both in terms of added labour and final price of the device, represent a limiting factor. Moreover, the short-term stability and the reproducibility of the preparation of modified electrodes has been highlighted recently as an important issue, which discourages further applications especially in industry.[24–26] Bare electrodes, without functionalization, represent an interesting alternative, in particular when high sensitivity is not required. This approach makes use of a simpler system, resulting in low costs for both production and use and a demonstrated long-term stability.[27]

In view of the important biological effects, a broad consumption of caffeinated beverages and the lack of simple, cost-effective and long-time stable caffeine sensors, a project was developed in collaboration with Biorealis Ltd and illy caffè S.p.A investigating the applicability of bare carbon electrodes as sensing platform to quantify caffeine in coffee brews. Among the different electrode materials, bare glassy carbon electrode (GCE) was selected as the most interesting one for the devising of the sensing platform, thanks to its long-term stability, wide anodic potential range and a relatively low cost.[28,29] The work

described in the rest of this chapter was carried out while being seconded to Biorealis Ltd (9 months) and illy Caffè (9 months).

4.1.2 Results and discussion

In this chapter the research into the applicability of using GCE as a caffeine sensor is presented and the work and the results are organised into three main sections: i) optimization of the conditions (i.e., supporting electrolyte, and instrumental settings for Differential Pulse Voltammetry (DPV) and Square Wave Voltammetry (SWV)); ii) analytical performance (i.e., calibration curve and selectivity studies); iii) real samples analysis.

4.1.2.1 Optimization of the conditions

Previous works[20,27,30] reported that the electrochemical oxidation of caffeine on bare and modified electrodes is highly irreversible, as evidenced by the absence of a reduction signal in the reverse cathodic scan when a cyclic voltammetry (CV) experiment is performed. The oxidation involves the transfer of 4 electrons and 4 protons, leading to the formation of a trimethyl uric acid derivative.[31,32] The initial oxidation, which is the rate limiting step, involves the oxidation of the five-membered ring of caffeine in a two-electrons, two-protons reaction. The product is a derivative of uric acid, which is then rapidly oxidised to the diol analogue in two-electrons, two-protons reactions, as shown in Scheme 4.2.

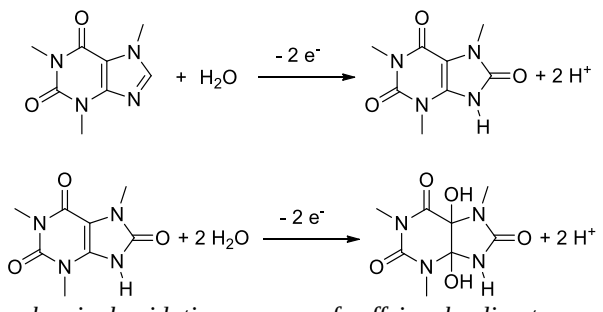

Scheme 4.2. The electrochemical oxidation process of caffeine, leading to a uric acid derivative.

Previous literature data indicate that the electrochemical sensing of caffeine provides better results when it takes place in acid solutions (for instance 0.4 M $HClO_4$[27] or 0.1 M H_2SO_4[30]) or acidic buffer with pH < 2[22]. Recently Chalupczok *et al.* [33] reported that the ionic strength of the supporting electrolyte is a key parameter to be tuned together with electrolyte concentration and pH when platinum group oxide electrodes are employed. Although this work focused on different electrode material, it was decided to investigate if the ionic strength had a similar effect on glassy carbon. A careful consideration of previous literature and on the basis of past experience of the research group involved in this project, three strong acids were identified as potential supporting electrolytes both monoprotic (HNO_3, $HClO_4$) and diprotic (H_2SO_4). A range of concentrations from 0.01 M up to 0.5 M was investigated, chosen in order to have a sufficient concentration of supporting electrolyte while avoiding highly concentrated acid solutions which can lead to oxidation of the glassy carbon electrode.[34,35] In Figure 4.1 the results of a cyclic voltammetry evaluation of caffeine solutions (0.5mM) using different supporting electrolytes in different concentrations are presented.

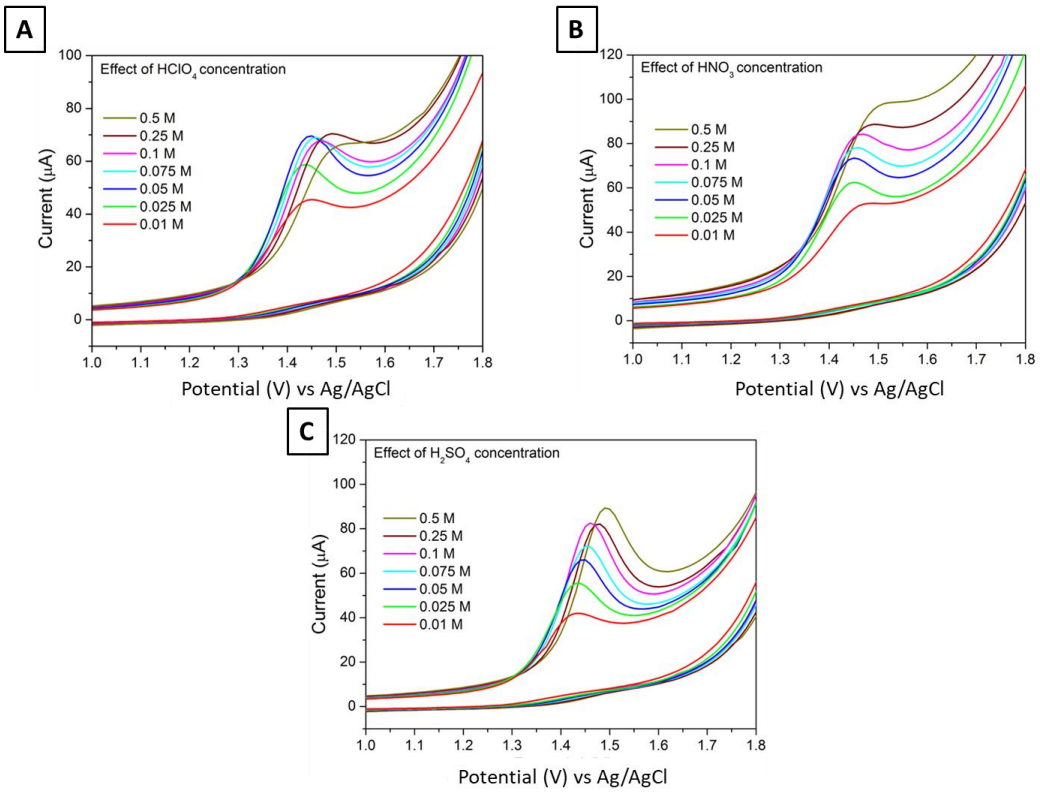

Figure 4.1. The effect of different perchloric, nitric and sulphuric acid aqueous solutions, on electrochemical oxidation of 0.546·mM caffeine solution on GCE using CV (scan rate of 100 mV/s).

From Figure 4.1 above, it can be observed that independently from the electrolyte being used, caffeine was oxidised at ~ 1.40 V, and an increase in the concentration of the supporting electrolyte resulted in a slight peak potential shift towards higher potentials. This result is consistent with the oxidation process reported in Scheme 4.2, in which protons are produced during the reaction. Therefore, the following equation for the oxidation potential can be written:

$$E = E_0 + \frac{RT}{ZF}\ln\left(\frac{(a_{\mathrm{CAFox}})(a_{\mathrm{H}^+})^n}{(a_{\mathrm{CAF}})}\right) \qquad (4.1)$$

Where E is the oxidation potential recorded, E_0 is the standard oxidation potential, R is the universal gas constant, T is the absolute temperature, Z is the number of electrons involved in the process, F is the Faraday constant, a is the activity of the chemical species, and n is the number of protons involved in the process.[27] According to equation

4.1, the higher the acid concentration, the higher is oxidation potential, as a result of the lower pH. In addition from Figure 4.1 above it can be noticed that overall, by the increase of the concentration of the supporting electrolyte was accompanied by an enhancement in the peak current and, moreover, background current was observed. Among the three acids, sulfuric acid led to a sharper and narrower peak suggesting that higher sensitivity can be achieved using this supporting electrolyte. To confirm that sulphuric acid could allow achieving higher sensitivity, the signal to noise ratio at different concentrations of the three supporting electrolytes were calculated and the data listed in Table 4.2, below.

Table 4.2. The HNO_3, $HClO_4$ and H_2SO_4 concentration effect on the S/N ratio of caffeine oxidation. Cyclic voltammetry was employed using a scan rate of 100 mV/s, three consecutive voltammograms were recorded, and the mean value was used for the signal and noise level evaluation. Caffeine concentration was 0.546 mM.

Concentration (M)	*S/N*		
	HNO_3	$HClO_4$	H_2SO_4
0.01	2.66	2.12	2.84
0.025	2.92	2.15	3.10
0.05	3.18	2.25	3.34
0.075	2.74	2.04	3.54
0.1	2.74	2.01	3.67
0.25	2.51	1.70	3.31
0.5	2.21	1.46	3.11

From Table 4.2 above, it follows that sulphuric acid shows a higher *S/N* ratio at all concentrations employed and the highest ratio is achieved at 0.1 M H_2SO_4. The highest performance achieved with sulphuric acid can also be appreciated in Figure 4.2 where the three supporting electrolytes are compared at the concentration where the highest S/N ratio was observed. Application of 0.1 M H_2SO_4 leads to higher peak current, lower background current and narrower peak. These data provided strong evidence that, among the three acids, H_2SO_4 was the most appropriate supporting electrolyte for caffeine determination.

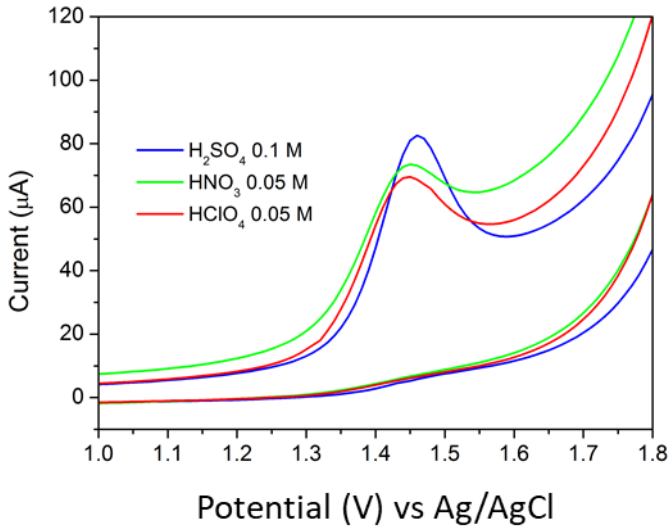

Figure 4.2. Comparison of CVs voltammograms of optimal concentrations of perchloric, nitric and sulphuric acid for electrochemical oxidation of 0.546·mM caffeine solution on GCE (scan rate of 100 mV/s).

A concern on the use of sulphuric acid was raised based on previous data reported in the literature[35–37] reporting that a change in morphology of glassy carbon can be observed when sulfuric acid is employed and long electrochemical pre-treatments are applied. Therefore the cyclic voltammograms recorded for solution containing only H_2SO_4 from 0.01 M up to 1 M were recorded and are presented in Figure 4.3, below.

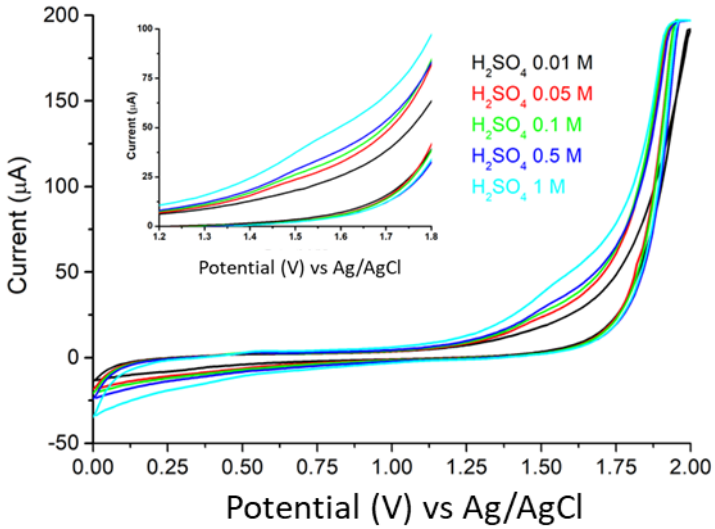

Figure 4.3. Cyclic voltammograms for different concentrations of H_2SO_4 solutions: all voltammograms were recorded with a scan rate of 100 mV/s. Black line 0.01 M H_2SO_4, red line 0.05 M H_2SO_4, green line 0.1 M H_2SO_4, navy-blue line 0.5 M H_2SO_4 , light blue line 1 M H_2SO_4 .

Only at high concentrations (i.e. 1 M and 0.5 M) a broad signal was recorded in the direct scan at 1.55 V suggesting the oxidation of carbon atoms from the GCE surface in highly acidic conditions, which can decrease the reproducibility and long-term stability of the sensor. Therefore sulfuric acid concentrations exceeding 0.1 M were not considered appropriate for the application of the sensor in an industrial environment.

When voltammograms for the three acids at the same concentration were compared (Figure 4.4) it was observed that the use of monoprotic acids (HNO_3 and $HClO_4$) resulted in a broad oxidation signal with higher background current. Instead, diprotic acid (H_2SO_4) rendered a better developed signal in terms of width, sharpness, and lower background currents. The findings support the results of Chalupczok and coworkers who suggested that the ionic strength of the solution does influence the oxidation signals even when concentrations and pH values of the solutions are the same.[33]

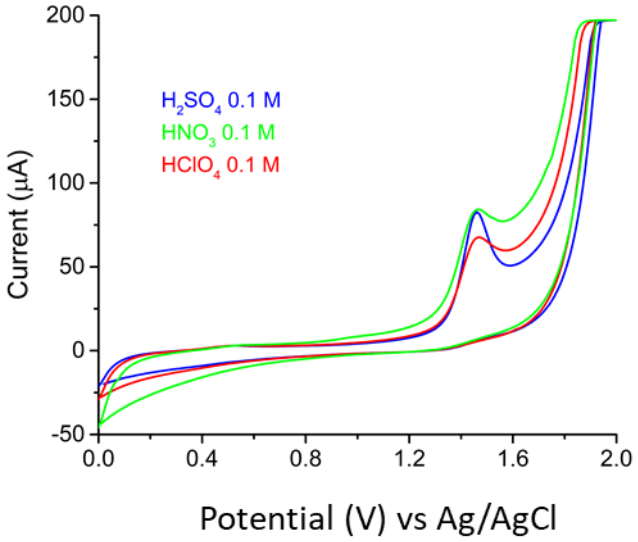

Figure 4.4. Comparison of CV voltammograms for monoprotic (HNO_3 and $HClO_4$) and diprotic (H_2SO_4) acids, at the same concentration (0.1 M), as supporting electrolyte. CV voltammograms were recorded at 100 mV/s at the caffeine concentration of 0.546·mM.

Subsequently, some electrochemical pre-treatment steps were done to understand their effects on the caffeine oxidation current. In fact, previous literature data have shown that electrochemical pre-treated carbon electrodes showed a higher sensitivity towards

caffeine.[38,39] Therefore, five consecutive cyclic voltammograms were recorded for 0.5-mM caffeine solution in 0.1 M H_2SO_4 and both positive and negative potentials (-2.00, +1.00, +1.75, +2.00 V) were tested for different cycle times (up to 60 seconds); the effects on the voltammograms are depicted in Figure 4.5, below.

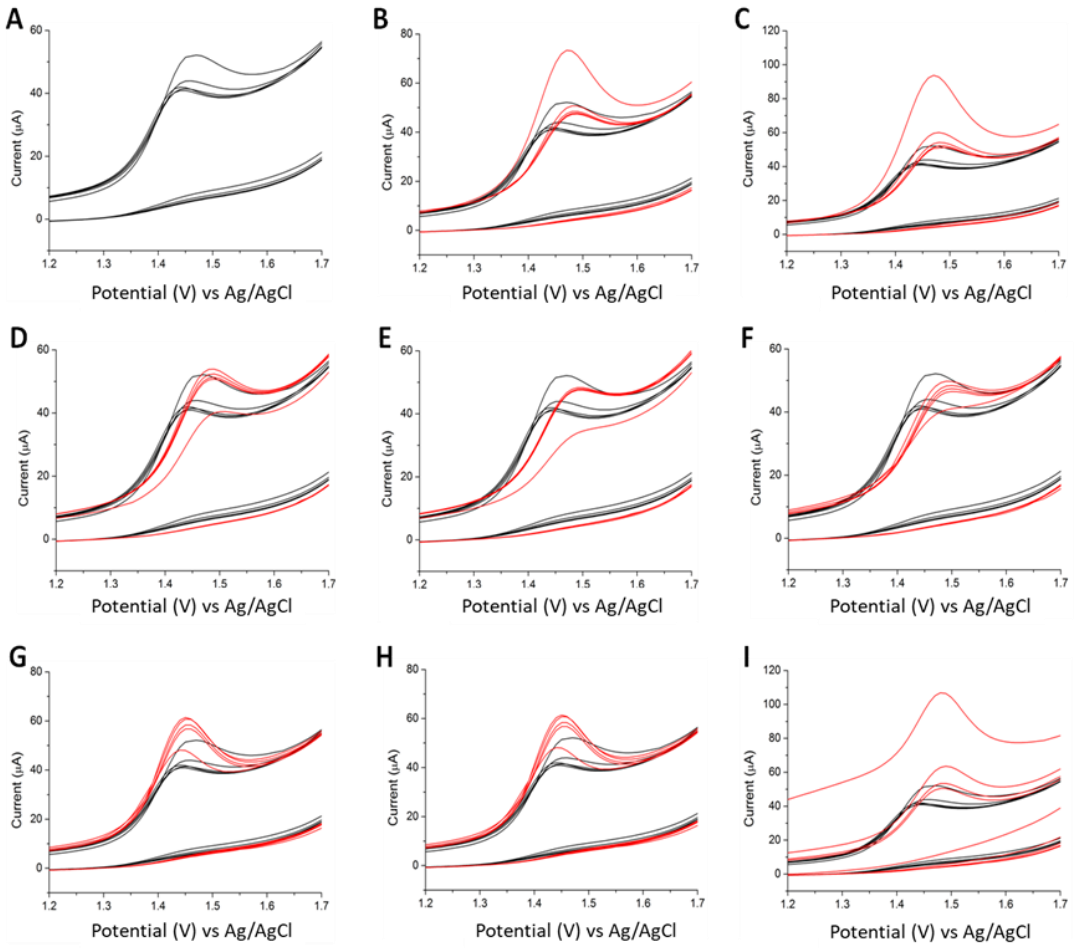

Figure 4.5. Electrochemical pretreatment effects on cyclic voltammograms, of 0.546 mM caffeine in 0.1 M H_2SO_4, using GCE. A scan rate set to 100 mV/s. (A) In black lines, five consecutive cyclic voltammograms without any pre-treatment. In red, five consecutive cyclic voltammograms using the following electrochemical pretreatments: (B): + 1.0 V for 30 s. (C): +1.0 V for 60 s. (D): +1.75 V for 30 s. (E): +1.75 V for 60 s. (F): +2.0 V for 15 s. (G): +2.0 V for 30 s. (H): +2.0 V for 60 s. (I): -2.0 V for 30 s.

When no electrochemical pre-treatments were applied, the first signal recorded was followed by less intense, but repeatable peaks (Figure 4.5A). When +1.0 V was applied for 30 s (B) or 60 s (C) the difference between the first scan and the following ones increased, and an enhancement in the peak intensity was observed. Interestingly,

application of higher conditioning potentials led to an opposite trend. That is the first scan recorded a signal lower in intensity. In particular, when +1.75 V was applied (D, E) there was still a significant difference between the first and subsequent voltammograms, while when +2.0 V was used (F, G, H) the gap was considerably decreased. When a negative potential of -2V the voltammogram repeatability was low (Figure 4.5 I). Among the different conditioning potentials applied, +2.0 V for 30 s provided the highest mean peak intensity (30% higher compared with that recorded with no pre-treatment). When the same potential was applied for shorter time (15 s) the mean peak intensity was comparable to the no pre-treatment situation, while when the potential of + 2.0 V was applied for 60 s, the effects on caffeine oxidation signal were similar to those when the potential of +2.0 V for 30 s was applied proving that 30 s was a sufficient pre-treatment time. Previous studies on anodically pre-treated GCE reported a higher sensitivity with an enhancement in the signal intensity more significant compared with the results reported in Figure 4.5. The higher performance is however achieved by employing long pre-treatment times (from 5 to 25 min) and in some cases highly acidic or basic conditions (H_2SO_4 1M, NaOH 1M)[40] which lead to an increase in the porosity of the electrode and the oxidation of its surface.[38–41] However, the reproducibility of the surface modification and the long-term stability of the sensor are not usually investigated and may be an issue, as described above in this chapter. Therefore, in this study only short pre-treatment steps were considered, in order to limit the electrode surface modification, knowing that the enhancement in the sensitivity of the instrument would not have been as significant as in the case of the application of long pre-treatment steps.

The next step focused on the evaluation of the reproducibility of the method. This was achieved by applying the pre-treatment step (+2.0 V, 30 s) and measuring five consecutive CV curves for a caffeine solution (1.25 mM in 0.1 M H_2SO_4). The relative

standard deviation of caffeine peak current was 4.5%, which confirmed that GCE provides a precise measurement tool for caffeine sensing under the conditions optimised. The voltammograms are presented in Figure 4.6 below.

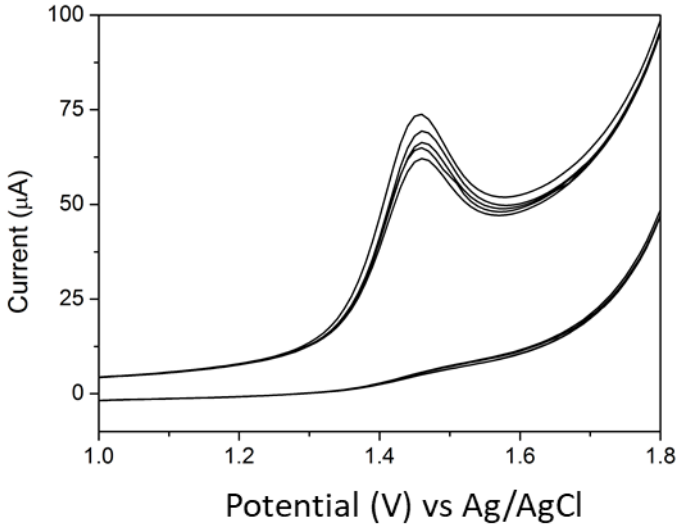

Figure 4.6. Repeatability study using cyclic voltammetry. 5 consecutive determinations of 1.25 mM caffeine in 0.1 H_2SO_4; pre-treatment +2.0 V, 30 s; scan rate 100 mV/s.

GCE is well known for adsorbing molecules on its active surface during the electrochemical measurement, thus usually leading to a decline of the peak of the particular analyte due to the surface inactivation by the analyte and/or products of its electrode reaction. In order to evaluate the role of either adsorption or diffusion on GCE in controlling the electrode reaction of caffeine, the effect of changing the scan rate was monitored. A wide scan rate range was examined, i.e. from 10 up to 500 mV/s, and the recorded voltammograms are presented in Figure 4.7, below.

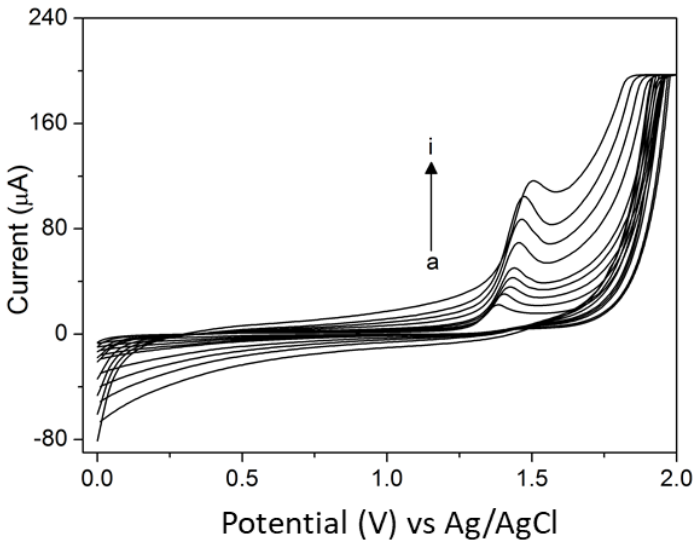

Figure 4.7. CV curves for 1.25 mM caffeine at different scan rates: (a) 10, (b) 25, (c) 50, (d) 75, (e) 100, (f) 200, (g) 300, (h) 400 and (i) 500 mV/s in 0.1 M H_2SO_4 on GCE, eletrode pre-treatment: +2 V, 30 s.

By increasing the scan rate, the oxidation peak shifted towards higher potentials, which is observed when the kinetics for electron-transfer between the electrode and the molecule are considerably slower than the mass transport. Therefore, a shift of the electrochemical signal is observed under static conditions.[42] A similar behaviour was reported also by Svorc L. *et al.* who employed boron doped diamond electrode for caffeine sensing.[27] The analysis of the relationship between the current peak of caffeine (in μA) and scan rate (mV/s) is reported in Figure 4.8. This analysis shows that there is a slightly more linear trend between current and square root of scan rate. In addition, the plot of the logarithm of the peak current vs. the logarithm of the scan rate (Figure 4.8 C) appeared to be linear, with the slope of 0.41, consistent with the theoretical value (0.50) for a diffusion-controlled process.[43] The low intercept value (5.82 mV/s) and high linearity (R^2=0.98) with the square root of the rate, together with the slope of the logarithmic plot (close to 0.5) indicate that the redox process of caffeine on GCE is predominantly driven by diffusion, and the effect of adsorption in electrochemical caffeine sensing may be considered as minor, even when using GCE as the working electrode.

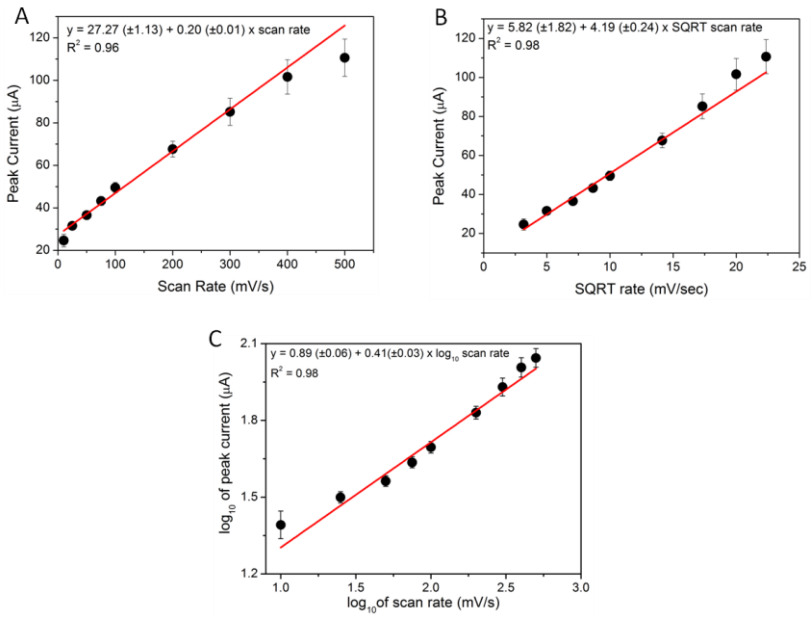

Figure 4.8. The potential scan rate effect study. (A) The relationship between peak current and the scan rate. (B) The relationship between peak current and the square root of the scan rate. (C) The relationship between the log_{10} of peak current and log_{10} of the scan rate. The linear regression equations for each fitting are reported at the top of each graph.

Cyclic voltammetry is a useful technique to study the electrochemical properties of an analyte and evaluate the effects of changing the supporting electrolyte on the redox properties of a target compound. However, more precise analytical experiments are usually obtained using differential pulse (DP) and square wave (SW) voltammetry. These low-potential amplitude techniques use a non-linear increment of the potential over time to eliminate the background noise and, therefore, enhance the *S*/*N* ratio. In fact, in the case of CV, the potential is linearly increased until a preset value, at which the scan is reversed back to the initial potential and the cycle is closed (Figure 4.9 A). However, by using a linear potential change and monitoring continuously the current, both faradaic and capacitative contributions are recorded. Faradaic current arises from the electrode reaction under study, while the capacitative contribution is electrode charging caused by the movement of ions in proximity to the electrode when a potential is applied. This non-faradaic process increases the noise level and in order to decrease it, pulsed techniques can be utilised. In the case of DPV (Figure 4.9 B) the potential

applied is the combination of a staircase ramp and pulses, and the current recorded (I) is the difference between the current measure immediately before applying (I_1) and stopping (I_2) the potential pulse; in this way the non-faradaic current is subtracted. In the case of SWV (Figure 4.9 C) the potential applied is the sum of a stairway ramp and a square wave, and the measured current is again the difference between that measured just before and at the end of the potential pulse.

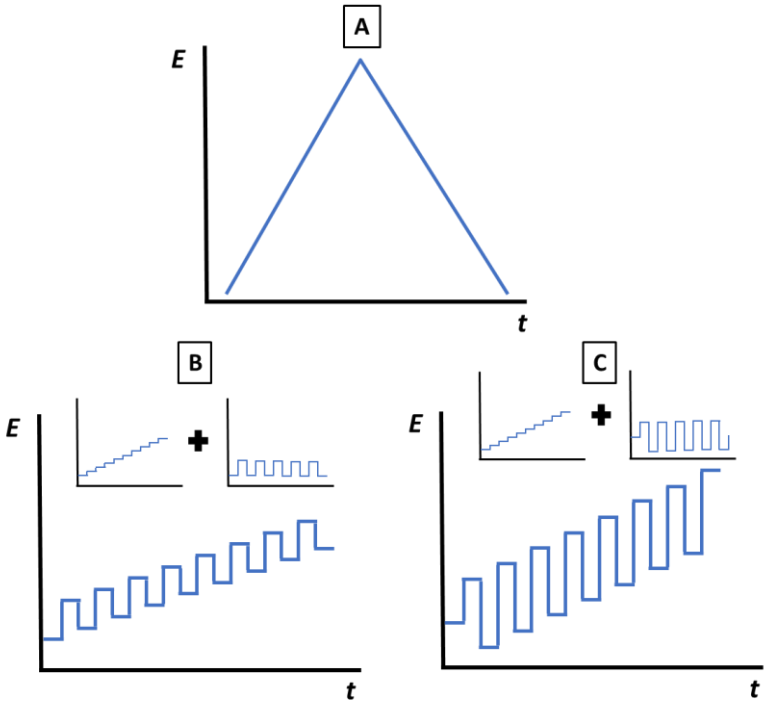

Figure 4.9. The applied potential (E) versus time (t) in the case (A) of cyclic voltammetry, (B) differential pulse voltammetry and (C) square wave voltammetry.

The enhancement in sensitivity of pulsed techniques compared with cyclic voltammetry is achieved only after having found the appropriate pulse to be applied. Common potentiostats allow for variation of the pulse potential and time in the case of DPV and pulse amplitude and pulse frequency in the case of SWV. The change of these instrumental settings affect the voltammogram recorded in terms of signal intensity, noise level and width of the peak. The appropriate pulse parameters have to be identified experimentally on a trial and error basis and found every time a sensor is devised. In fact, the effects of changing the instrumental settings on the electrochemical signal are closely

dependent upon the nature of the analyte, electrode material and supporting electrolyte. In addition, the optimisation process is not much time-consuming. It is a common practice to subsequently tune the pulse amplitude and time in the case of DPV and pulse amplitude and frequency in the case of SWV. Starting from the instrument default settings one can reach the optimal condition in terms of peak intensity and noise level by adjusting pulse parameters. In Figure 4.10 the effect of changing the pulse potential on the DP voltammogram of a 0.44 mM caffeine solution is shown.

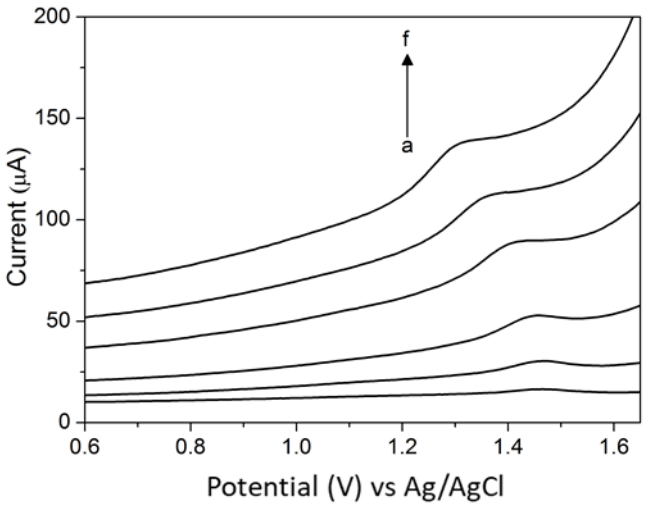

Figure 4.10. DPV curves for 0.44 mM caffeine in 0.1 M H_2SO_4 on GCE for different pulse potentials: (a) 10, (b) 25, (c) 50, (d) 100, (e) 150 and (f) 200 mV. Pulse time was set to 10 ms and the scan rate was 100 mV/s.

A range of pulse amplitudes of 10 to 200 mV was evaluated and a direct growth and widening of the caffeine oxidation peak were observed together with a sharp enhancement in the background current. To balance the DPV peak current, the peak width and noise level, the most appropriate pulse amplitude was 50 mV and, therefore, no further pulse amplitude were considered. Subsequently, the effect of the pulse duration was studied (Figure 4.11), exploring a range of 5 to 150 ms. When the pulse duration was increased from 5 to 100 ms, there was a proportional decrease in the background current, while when 150 ms was set, the background current rose again. In

terms of peak current the highest value was obtained using 10 ms, which was therefore selected as the optimal pulse duration.

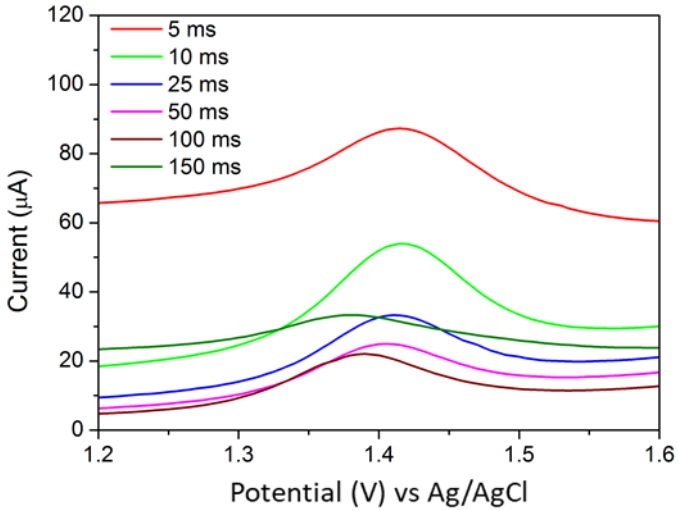

Figure 4.11. DPV curves for 0.44 mM caffeine in 0.1 M H_2SO_4 on GCE for different pulse time duration: 5 (red), 10 (light green), 25 (blue), 50 (pink), 100 (wine) and 150 ms (olive green). The pulse amplitude was set at 50 mV, and the scan rate was 100 mV/s.

The peak current and width are also affected by the scan rate and the signal is usually improved when the scan rate is decreased. On the other hand, the time to perform the analysis is longer, and in order to reach high sensitivity without compromising the speed of the sensing platform, 30 mV/s was selected as the optimal scan rate. This was because sharper and higher peaks were obtained and the time needed to record the voltammogram was ~ 1 minute (Figure 4.12).

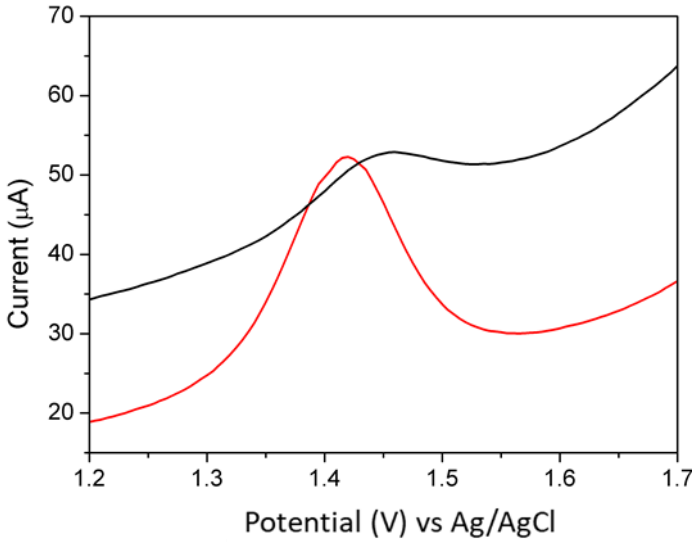

Figure 4.12. DPV curves for 0.44 mM caffeine in 0.1 M H_2SO_4 on GCE for two different scan rates, 100 mV/s (black line) and 30 mV/s (red line). Pulse amplitude was set at 50 mV while pulse duration at 10 ms.

After optimisation of the instrumental parameters for the DPV analysis, the focus was on optimising the SWV determinations. For that a similar trial-and-error approach was used and the pulse amplitude and pulse frequency were tuned. When the pulse amplitude was increased (from 10 to 150 mV) an enhancement in caffeine SWV peak current and background current was observed up to 100 mV. However, when a pulse amplitude of 150 mV was applied a negative voltammogram was recorded (Figure 4.13). The peak width increased with the pulse amplitude increase. Therefore, 50 mV was selected as an optimal pulse amplitude to limit the peak widening and the noise level increase.

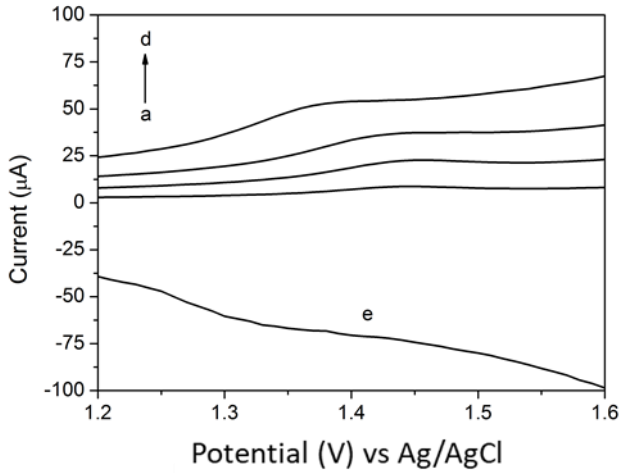

Figure 4.13. Pulse amplitude optimisation for SWV analysis, of 0.44 mM caffeine in 0.1 M H_2SO_4. Frequency was set at 50 Hz, while pulse amplitude was (a) 10, (b) 25, (c) 50, (d) 100, (e) 150 mV.

The subsequent step was to optimise the pulse frequency. For that, a range of 1 to 50 Hz was investigated (the results are reported in Figure 4.14, below). A proportional enhancement in the caffeine SWV peak current and background current with the increase of pulse frequency was noticed, but a more defined peak was obtained at low pulse frequency. However, low frequencies lead also to low scan rate and the time to perform the analysis is higher. As a consequence, as it was previously done for DPV, to balance analysis time and of the peak current, 5 Hz was set as an optimal pulse frequency.

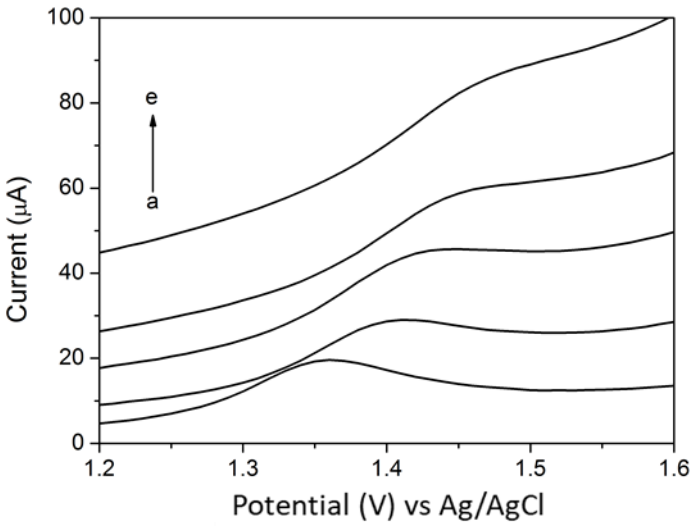

Figure 4.14. Optimisation of pulse frequency for the SWV analysis using a 0.44 mM caffeine in 0.1 M H_2SO_4. Pulse amplitude was set to 50 mV while frequency was set at: (a) 1, (b) 5, (c) 10, (d) 25, (e) 50 Hz.

A summary of the optimal instrumental settings for DPV and SWV analysis is listed in Table 4.3.

Table 4.3. The optimised instrumental parameters for the DPV and SWV determination of caffeine in 0.1 M H_2SO_4 using bare GCE, an electrochemical pre-treatment step of 2.0 V for 30 s was applied before recording the voltammograms.

DPV			SWV	
Pulse Potential	Pulse Time	Scan Rate	Pulse Amplitude	Pulse Frequency
50 mV	10 ms	30 mV/s	50 mV	5 Hz

4.1.2.2 Analytical performance

After having optimised the supporting electrolyte and the instrumental parameters of DPV and SWV, the calibration curve for caffeine was derived to evaluate the sensitivity and linear dynamic concentration range of the two pulse techniques. A caffeine concentration range of 3 up to 2725 µM was investigated. For that, three consecutive voltammograms were recorded and the mean peak current was considered. In the following Figures 4.15 and 4.16 the voltammograms and calibration curves are presented, starting with DPV (Figure 4.15).

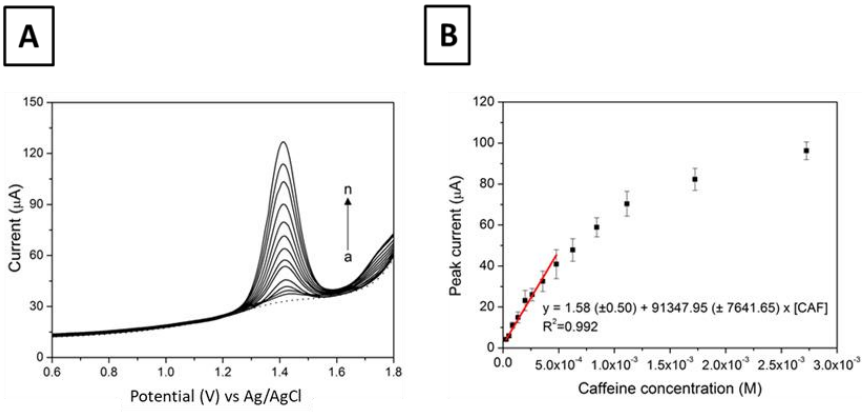

Figure 4.15. (A): DPV curves for various caffeine concentrations: (a) 0; (b) 28; (c) 53; (d) 86; (e) 135; (f) 199; (g) 263; (h) 356; (i) 479; (j) 627; (k) 841; (l) 1112, (m) 1724 and (n) 2725 µM in 0.1 M H_2SO_4 on GCE. DPV parameters: pulse amplitude of 50 mV, pulse time of 10 ms and scan rate of 30 mV/s. An electrochemical pre-treatment step of 2.0 V for 30 s was applied before analysis. (B): Calibration curve for caffeine determination using DPV taking into consideration the peak current (µA). The red line is the linear dynamic concentration range found with its linear regression equation reported at the bottom of the graph.

The limits of detection (LOD) and quantification (LOQ) were estimated from the calibration curve using the formulae shown below.

$$\boldsymbol{LOD = 3 \times \frac{error_{y\ intercept}}{sensitivity}} \qquad (\mathbf{4.2})$$

$$\boldsymbol{LOQ = 10 \times \frac{error_{y\ intercept}}{sensitivity}} \qquad (\mathbf{4.3})$$

With regards to DPV, a measurable current signal was recorded when the concentration of caffeine was higher than 28 µM and a significant linear relationship of the caffeine peak current against concentration was observed from 28 to 479 µM (R^2 =0.992) and the LOD and LOQ were 16.4 and 54.7 µM, respectively. The SW voltammograms at different caffeine concentration and the relative calibration curves are reported in Figure 4.16 below.

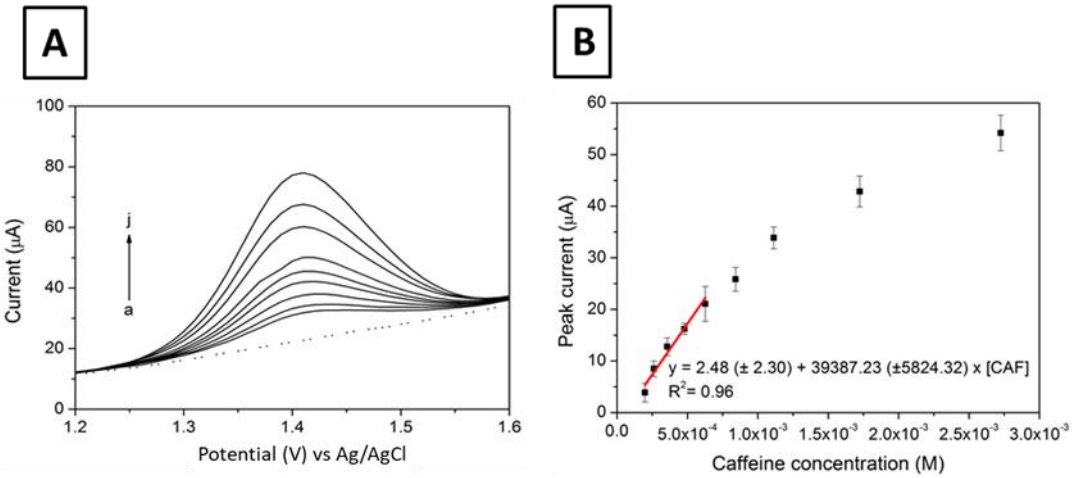

Figure 4.16. (A): SWV curves for various caffeine concentrations: (a) 0; (b) 199 (c) 263; (d) 356; (e) 479; (f) 627; (g) 841; (h) 1112; (i) 1724 (j) 2725 µM in 0.1 M H_2SO_4 on GCE. SWV parameters: pulse amplitude 50 mV, pulse frequency 5 Hz. An electrochemical pre-treatment step of 2.0 V for 30 s was applied before the determination. (B): Calibration curve for caffeine using the SWV taking into consideration the peak current (µA). The red line is the linear dynamic concentration range found with its equation reported at the bottom of the graph.

Using the optimised settings for SWV, a lower sensitivity for caffeine determination was achieved, and a distinct signal was recorded for concentrations higher than 199 µM with the linear dynamic concentration range of 199 to 627 µM and the LOD of 175.52 µM. A comparison of analytical parameters of the DPV and SWV determination is presented in the Table 4.4.

Table 4.4. Summary of analytical performance of DPV and SWV at GCE as the caffeine sensor using 0.1 M H_2SO_4 as supporting electrolyte.

Low amplitude Technique	Sensitivity (μA/M)	LOD (μM)	Linear range (μM)	R^2
DPV	9.13×10^4	16.42	28 - 479	0.99
SWV	3.94×10^4	175.52	199 - 627	0.96

DPV appeared superior to SWV with the sensitivity level twice as high, ten times lower LOD and wider linear dynamic concentration range, thus suggesting that the sensor can be applied to a broader range of caffeine concentrations and for very dilute caffeinated beverages. Therefore, DPV was selected as the most appropriate electroanalytical technique for the determination of caffeine in 0.1 M H_2SO_4 using bare GCE.

Common caffeinated beverages, such as coffee and different soft drinks, contain other chemical species, which may interfere with the signal of caffeine, thus significantly affecting the reliability of the method. Therefore, the next step focused on the evaluation of the efficiency of the analytical method in the presence of interferences. The effect of glucose and sucrose was investigated, as these sugars are commonly present in various beverages, and at high concentration in the case of soft drinks. Although these compounds are not oxidised on bare carbon electrodes, they may be adsorbed onto the working electrode surface, thus considerably affecting the analyte signal. The structural formulae of glucose and sucrose are shown in Scheme 4.3.

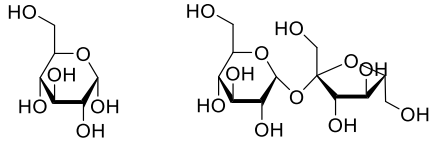

Scheme 4.3. Structural formulae of D-(+)-glucose and sucrose.

The effects of adding 1, 10 and 100 equivalents of sugars (compared to caffeine) on the DPV voltammograms is reported in Figure 4.17 and 4.18.

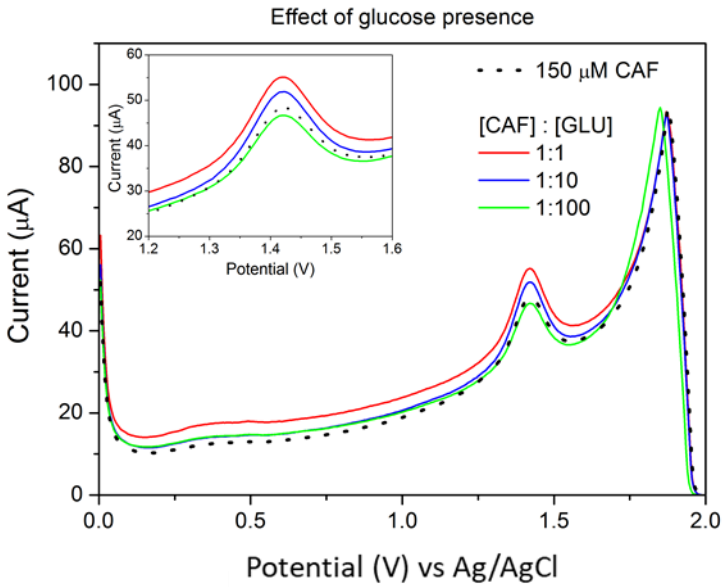

Figure 4.17. DPV voltammograms demonstrating the effect of the presence of glucose (GLU) on the current peaks of 150 µM caffeine in 0.1 M H_2SO_4 on GCE. The concentration ratios between caffeine and glucose are stated in the figure display. DPV parameters: pulse amplitude 50 mV, pulse time 10 ms and scan rate 30 mV/s. An electrochemical pre-treatment step of 2.0 V for 30 s was applied before the determination. The inset presents the magnified caffeine signal.

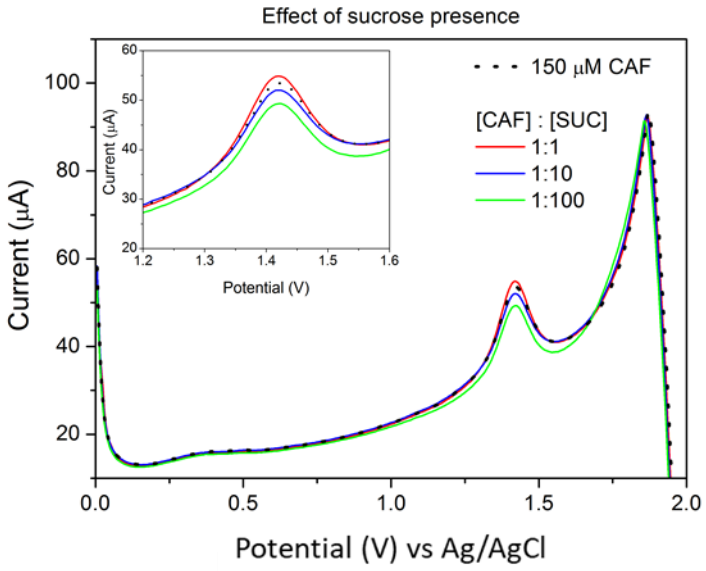

Figure 4.18. DPV voltammograms demonstrating the effect of the presence of sucrose (SUC) on current response of 150 µM caffeine in 0.1 M H_2SO_4 on GCE. The concentration ratios between caffeine and sucrose are stated in the legend of the figure. DPV parameters: pulse amplitude 50 mV, pulse duration 10 ms and a scan rate 30 mV/s. An electrochemical pre-treatment step of 2.0 V for 30 s was applied before the determination. In the inset an enlargement of caffeine signal.

The results revealed that, as expected, no new signals appeared in the voltammograms in the range of 0 to 2.0 V. Besides, the caffeine peak potential and shape are not much

influenced by the presence of these sugars up to 100 times higher concentration (inset to Figures 4.17 and 4.18). However, a moderate change in the background current was recorded, especially in the case of glucose, which is probably due to its adsorption on the surface of the working electrode. Nevertheless, this behaviour was not expected to significantly influence caffeine determination in real samples when standard addition method is employed. Subsequently, selectivity studies aiming at evaluation of the detection selectivity towards structurally related compounds, such as theophylline, theobromine and paraxanthine, were also performed. The structural formulae of the compounds considered are reported in Scheme 4.4, below.

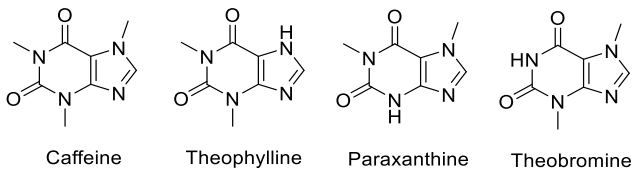

Scheme 4.4. Structural formulae of caffeine and the dimethylxanthines employed for the selectivity study.

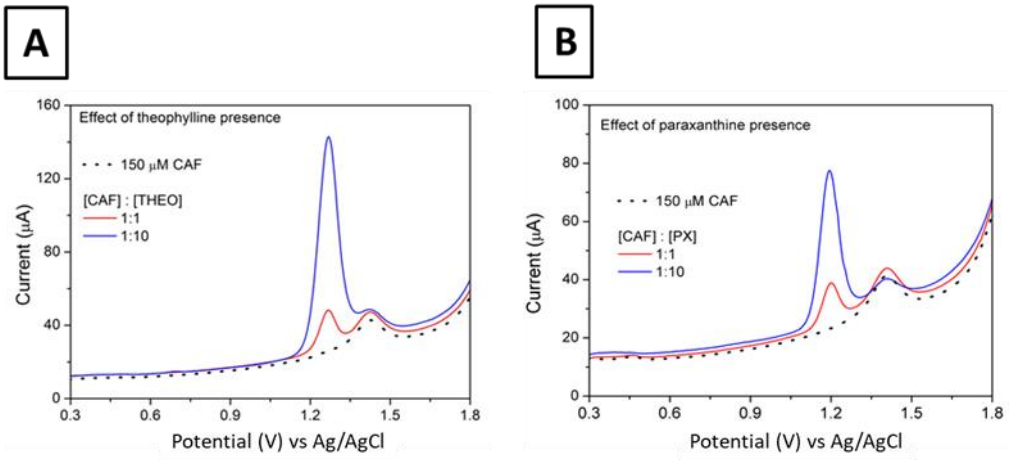

Figure 4.19. DPV voltammograms demonstrating the effect of the presence of (A) theophylline and (B) paraxanthine on the current response of 150 µM caffeine in 0.1 M H_2SO_4 on GCE. The concentration ratios between caffeine and theophylline are stated in the figure legend. DPV parameters: pulse potential 50 mV, pulse duration 10 ms and scan rate 30 mV/s. An electrochemical pre-treatment step of 2 V for 30s was applied prior analysis.

Figure 4.19 above, displays the effect of the presence of theophylline and paraxanthine (both at the 1:1 to 1:10 concentration ratio), respectively. These dimethyl xanthines were oxidised at a potential lower compared that of caffeine (+1.26 and +1.22 V for

theophylline and paraxanthine, respectively). This peak-to-peak separation (towards caffeine) led to no differences in the shape and position of the caffeine peak. On the other hand, the peak current of caffeine decreased by approximately 10% when an equimolar concentration ratio of caffeine and theophylline was present. In the case of paraxanthine, the oxidation peak of caffeine increased negligibly (2%). The selectivity observed so far is promising and provides important preliminary data for the potential use of GCE for the simultaneous detection and quantification of caffeine and paraxanthine and/or theophylline, when they are present at similar concentrations.

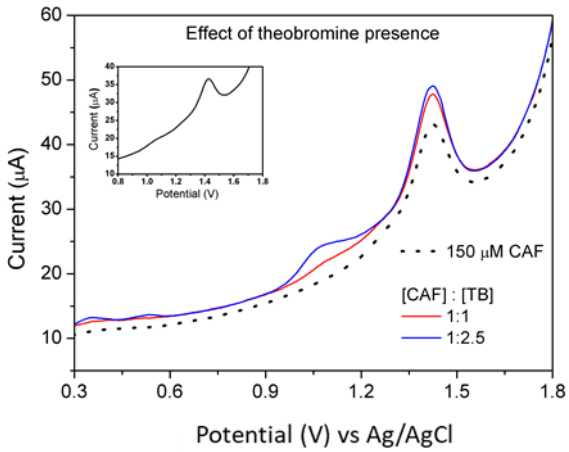

Figure 4.20. DPV voltammograms demonstrating the effect of the presence of theobromine (TB) on the current response of 150 μM caffeine in 0.1 M H_2SO_4 on GCE. The concentration ratios of caffeine and theobromine are stated in the figure legend. DPV parameters: pulse amplitude 50 mV, pulse duration 10 ms and a scan rate 30 mV/s. An electrochemical pre-treatment step of 2.0 V for 30 s was applied before determination. In the inset the DPV voltammogram of 333 μM TB in 0.1 M H_2SO_4 is shown.

In the case of theobromine, an increase of 15% in caffeine signal was observed when an equimolar ratio was present (Figure 4.20). The DPV curve for 333.3 μM theobromine (in the inset of Figure 4.20) revealed that under the experimental conditions used, theobromine rendered two oxidation peaks at +1.10 and +1.42 V, the second one overlapping with the caffeine peak. Overall, when the concentration ratio of the interfering xanthines to caffeine was high (up to 10:1), a partial overlapping of the signals was observed for theophylline and, in the case of paraxanthine, a decrease of

50% in the caffeine peak current was observed. However, this limitation was not expected to affect the reliable determination of caffeine in caffeinated beverages (coffee, soft drinks) where the concentration of theophylline, theobromine and paraxanthine is negligible.[44,45]On the other hand, in the case of coffee samples, polyphenols are usually present in similar amounts as caffeine (2.14 g/L in the final brew). [46] Although these compounds are electrochemically active, their oxidation peak potential (around 0 to 600 mV) is different from caffeine; besides, their oxidation is suppressed in acidic solutions.[47] As a consequence, no significant voltammetric peaks attributing to polyphenols and affecting the caffeine peak were observed during the analysis of coffee samples, as shown in Figure 4.21 below, where a typical voltammogram of a coffee espresso in 0.1 M H_2SO_4 is reported.

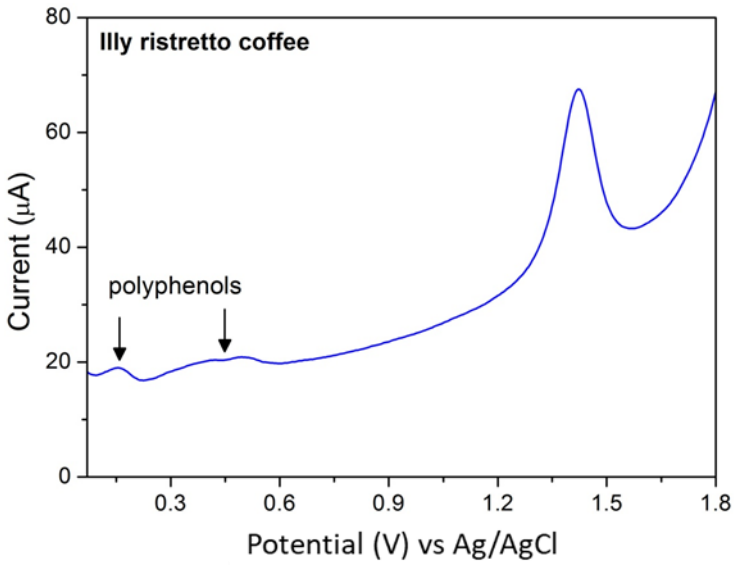

Figure 4.21. DPV voltammogram for a coffee sample (ristretto espresso coffee) manifesting the presence of polyphenols in 0.1 M H_2SO_4 on GCE. DPV parameters: pulse amplitude 50 mV, pulse duration of 10 ms and a scan rate 30 mV/s. An electrochemical pre-treatment step of 2.0 V for 30 s was applied before the analysis.

Considering the LOD achieved (16 μM), the repeatability of the measurements (relative standard deviation of 4.5%) and high selectivity, the developed method is a promising

analytical tool for caffeine determination. The final assessment of the sensing platform was done by determining the content of caffeine in real samples.

4.1.2.3 Real Samples analysis

Three different espresso brews (regular, *lungo* and *ristretto*), and four different commercially available caffeinated beverages (3 soft drinks and 1 energy drink) were analysed using the optimised DPV method. A sample aliquot was diluted in 0.1 M H_2SO_4 to have an adequate signal that could be integrated and in the figure below the DPV voltammograms for each sample are reported (the dilutions made are described in the Materials and Methods section).

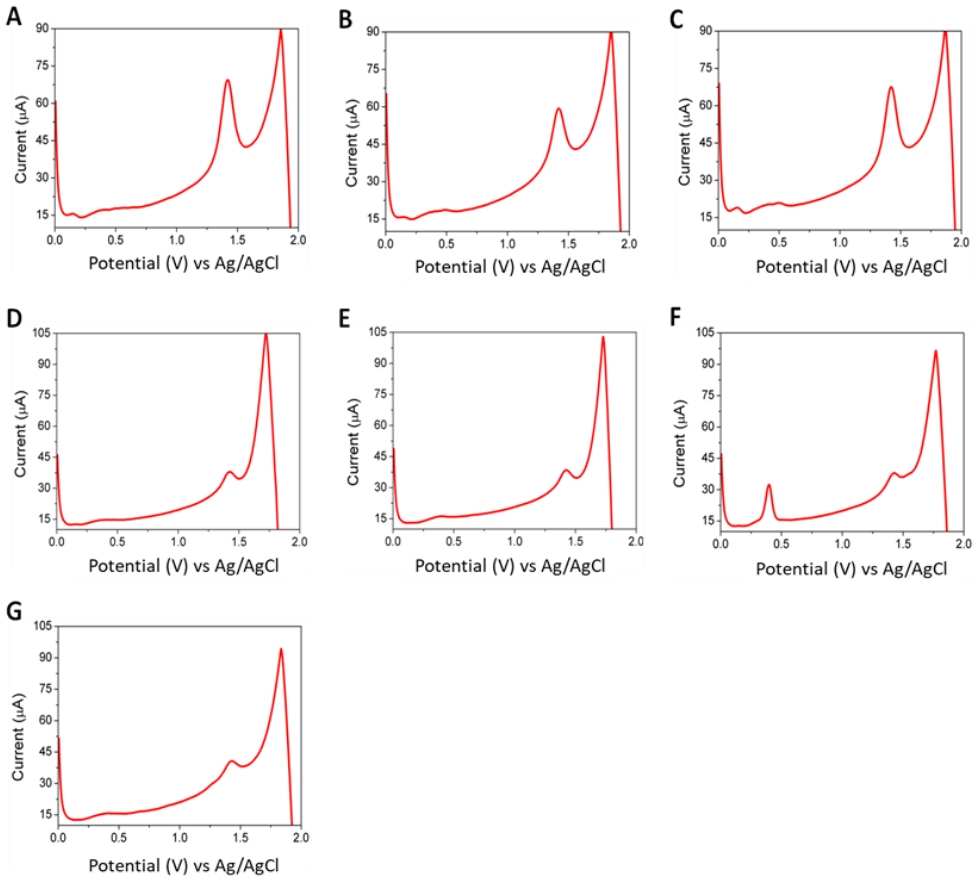

Figure 4.22. The DPV voltammograms of seven caffeinated beverages. (A) Coffee regular espresso; (B) Coffee espresso lungo; (C) coffee espresso ristretto; (D) Coca-Cola; (E) Pepsi Cola; (F) Kofola; (G) Red Bull. All samples were adequately diluted in 20 mL of 0.1 M H_2SO_4. DPV parameters: pulse amplitude 50 mV, pulse time 10 ms and a scan rate 30 mV/s. An electrochemical pre-treatment step of 2.0 V for 30 s was applied before the analysis.

From the graphs reported above it is clear that for most of the beverages the voltammogram recorded a signal for caffeine (at ~1.40 V) without any additional distinctive peaks, but in the case of Kofola (Figure 4.22 F) a well-defined peak at ~0.40 V was recorded. No further investigation was done to identify the unknown analyte, because a large peak-to-peak separation (compared to that of caffeine) allowed caffeine determination without interference issues. In the case of the coffee brews, some undefined peaks at 0.2-0.5 V were observed, possibly due to the presence of polyphenols, which are present at high concentration in coffee. However, in acidic solutions their oxidation is significantly hindered (see interference study paragraph, Section 4.1.2.2). When caffeine was determined using the calibration curve previously constructed, the values were underestimated compared to the labelled data. The disagreement between the calibration curve and the real sample is typical for complex matrixes (i.e. food, biological samples, etc.), and is referred as the matrix effect. In fact, the co-presence of plenty of compounds in real samples affects the response of the sensor to caffeine, leading to a mismatch between the signal measured on the sample and the calibration curve derived for a pure solvent solution. To overcome this issue, a calibration curve is obtained with the sample itself, employing the standard addition method. This method is based on the addition of a known amount of the sample in the supporting electrolyte solution followed by the addition of equal volumes of a standard solution of the analyte. The different signal values are then plotted against the amount of the analyte added with the standard, and the sample concentration is extrapolated as the absolute value of the abscissa-intercept;[48] an example is reported in Figure 4.23, below, for clarity.

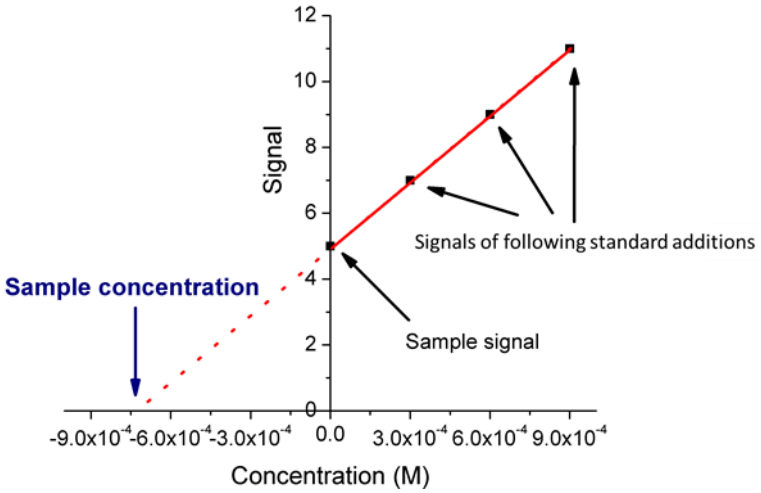

Figure 4.23. An illustrative example of the standard addition method analysis to extrapolate the concentration of an analyte in the sample.

Therefore, the standard addition method was employed for accurate determination of caffeine content in beverages. For that, five consecutive DPV curves were recorded after each standard solution addition and the mean peak current was considered in order limit the error associated with the measurement. In Figure 4.24 an example is presented of standard addition method analysis of a Coca-Cola sample using the developed assay.

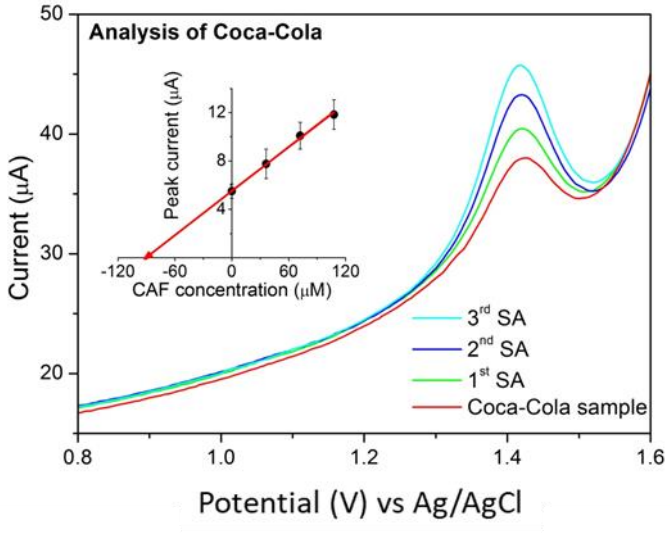

Figure 4.24. DPV curves for caffeine determination in a Coca-Cola sample using the standard addition method and 0.1 M H_2SO_4 on GCE after addition of 4 mL of the sample and after spiking of 80, 160 and 240 µL of 10 mM caffeine solution. DPV parameters: pulse amplitude 50 mV, pulse duration 10 ms and a scan rate 30 mV/s. An electrochemical pre-treatment step of 2.0 V for 30 s was applied before the analysis. The determination by standard addition method is depicted in the inset.

The extrapolated caffeine concentrations for the seven analysed beverages are listed in Table 4.5 below, using the proposed electrochemical technique and employing a reference UHPLC technique. The experimental conditions for the chromatographic technique are reported in the Materials and Methods section.

Table4.5. Real samples analysis of seven different caffeinated beverages (n = 5). Two independent techniques were used, namely the proposed electrochemical technique and the UHPLC technique.

Commercial caffeinated beverage	**Determined Caffeine content (g/L)***	
	Proposed DPV	**Reference**
Regular espresso coffee	3.047 ± 0.142	3.170 ± 0.195
Lungo espresso coffee	1.709 ± 0.178	1.672 ± 0.153
Ristretto espresso coffee	4.843 ± 0.291	5.326 ± 0.139
Coca-cola	0.098 ± 0.010	0.095 ± 0.008
Pepsi-cola	0.100 ± 0.006	0.110 ± 0.010
Kofola	0.070 ± 0.010	0.063 ± 0.005
Red Bull	0.361 ± 0.097	0.311 ± 0.028

*95% confidence interval calculated according [mean ± $t_{n-1,\alpha}$ SD/sqrt(n)]; $t_{4;\,0.05}$ = 2.13

As can be noticed from the Table 4.5 above, the caffeine concentration is very different in the analysed beverages, with soft drinks containing the lowest amount (from 0.070 to 0.100 mg/mL). The energy drink contains over three times more caffeine compared to that of the soft drinks and the highest concentration is present in espresso coffee. Regarding the espresso brews, it was observed that there was a significant variability in caffeine concentration based on the brewing methods, with *ristretto* coffee of 3 times higher caffeine concentration than that of *lungo* espresso. However, the volume of *ristretto* espresso is around 15-20 mL while a *lungo* brewed espresso is around 40-50 mL, therefore, the amount of caffeine present in weight is similar. To prove the reliability and accuracy of the measurements acquired using GCE, the same samples were analysed using a comparative UHPLC technique that is routinely employed at illy caffè S.p.A. for

determination of caffeine in beverages. The results obtained using both analytical techniques are presented in Table 4.5 and indicate that the caffeine concentrations determined by the new technique (DPV) are in good agreement with the one obtained by the chromatographic technique (standard deviation below 10%). In addition, it is common practice to use the paired *t*-test, when two different sets of data are compared, in order to check if the difference in values between the two analytical approaches is statistically significant or not.[27,48] According to this test at a 95% confidence level, no statistically significant differences were noticed between the values found by these techniques since the calculated *t* value (1.04) was lower than that tabulated (2.45 for α = 0.05 and number of measurements n = 5). Therefore, the developed DPV procedure provided high accuracy of caffeine determination in caffeinated beverages, without any interference problems.

4.1.3 Conclusion and future work

To summarise this part of the work, bare GCE was successfully employed for the development of a simple and efficient analytical assay for the quantification of caffeine in various beverages (coffee, soft drinks and energy drinks). The experimental conditions for the analysis were optimized, in terms of the supporting electrolyte (0.1 M H_2SO_4), electrochemical pre-treatment (+2.0 V for 30 s) and instrumental setting for the DPV (pulse amplitude 50 mV, pulse duration 10 ms, scan rate 30 mV/s) and SWV (pulse amplitude 50 mV, frequency 5 Hz) analysis. DPV was more sensitive to caffeine and was therefore employed for quantification experiments. The effect of possible interfering agents was also examined. The results showed that the presence of sugars (glucose and sucrose) and structurally related xanthines, such as theophylline, theobromine and paraxanthine do not compromise caffeine determination in caffeinated beverages. Seven commercially available caffeinated drinks were analysed to assess the wider

applicability of the developed analytical assay. The results were in good agreement with those obtained by UHPLC. The proposed procedure is simple and convenient, because it does not involve any pre-treatment of the samples. In addition, this analytical assay using GCE is rapid and useful for caffeine quantification. Therefore, it can be used as an innovative alternative to conventional analytical methods in routine quality assessment and assurance. This work was accepted in a peer-reviewed journal and is now published in RS open science as a full paper.

As part of my scheduled secondments plan, during my last part of PhD and after having developed the described caffeine sensor, I had the opportunity to work at illy Caffé S.p.A. for 9 months, and given the good results obtained using GCE, illy Caffè showed a strong interest in evaluating the applicability of electrochemistry as the analytical tool to be applied for coffee analysis. In particular, besides caffeine, polyphenols are another important class of biologically active compounds present in coffee. Therefore, the work continued with the development of a simple and cost-effective electrochemical sensor for simultaneous determination of polyphenols and caffeine in samples of different coffees (green and roasted coffee beans extract and coffee brews). The work is presented and discussed in Section 4.2, below.

4.2 Screen-printed carbon paste electrode for simultaneous determination of polyphenols and caffeine in coffee brews

4.2.1 Introduction

Caffeine is probably the most known compound present in coffee. However, the beneficial effects of this beverage are not limited to caffeine because coffee beans are rich in several other bioactive compounds.[49] Among them, polyphenols are a very interesting class of such compounds. In the last decade, an increasing number of scientific studies have proved that polyphenols are responsible for antioxidant activity, anti-inflammatory effects[50,51], metabolism and glucose level regulation with prevention of type II diabetes[52–54] and prostate cancer prevention[55]. The polyphenols term includes different chemical compounds and two main classes are distinguished, namely,: i) flavonoids and ii) non-flavonoids.

The flavonoids are compounds containing phenolic OH functional groups and two aromatic rings linked via a three-carbon bridge; these compounds are widely diffused in the plant kingdom and some examples of the most common ones are reported in Scheme 4.5.

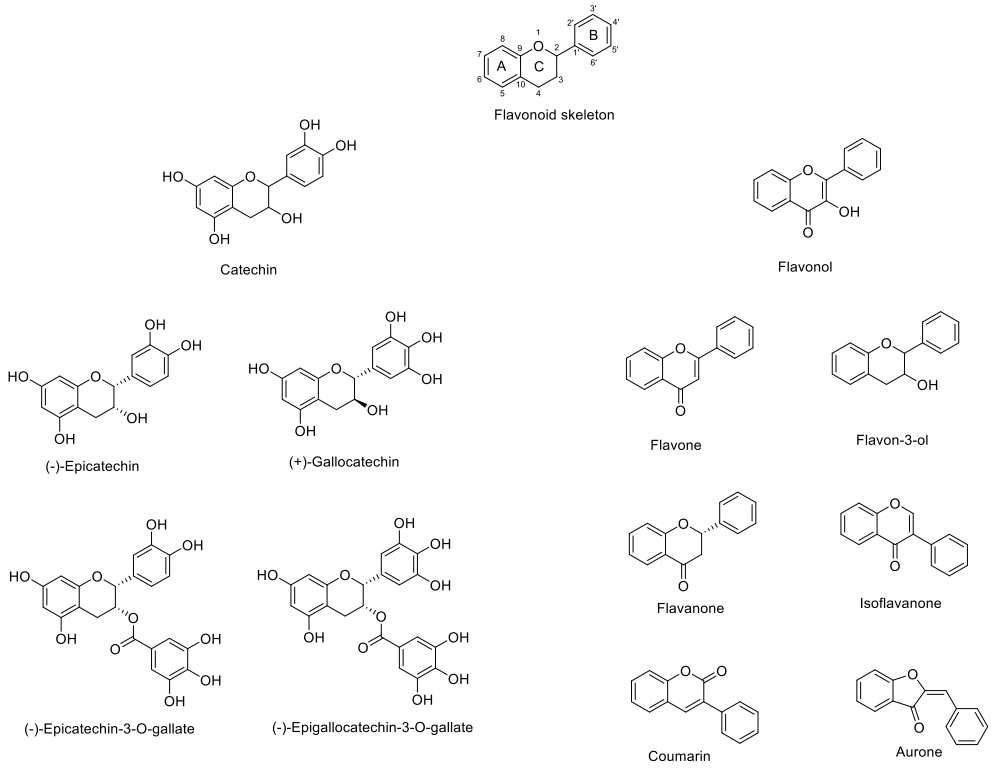

Scheme 4.5.Structural formulae of a flavonoid general skeleton and some examples of the most common flavonoid molecules.[56]

The two major sub-groups of flavonoids are catechin and flavonol sub-groups but there are derivatives which can be their simple stereoisomers or more complex analogues.[56] The non-flavonoid class is also varied, and the compounds can be organised into three main categories: (i) derivatives of gallic acid, which is the precursor of tannins; (ii) derivatives of hydroxycinnamic acid (mainly caffeic acid, p-coumaric acid and ferulic acid) which are present as mono- and diesters of quinic acid; (iii) resveratrol isomers and glycosylated derivatives. The structural formulae of some compounds are given in the Scheme 4.6.

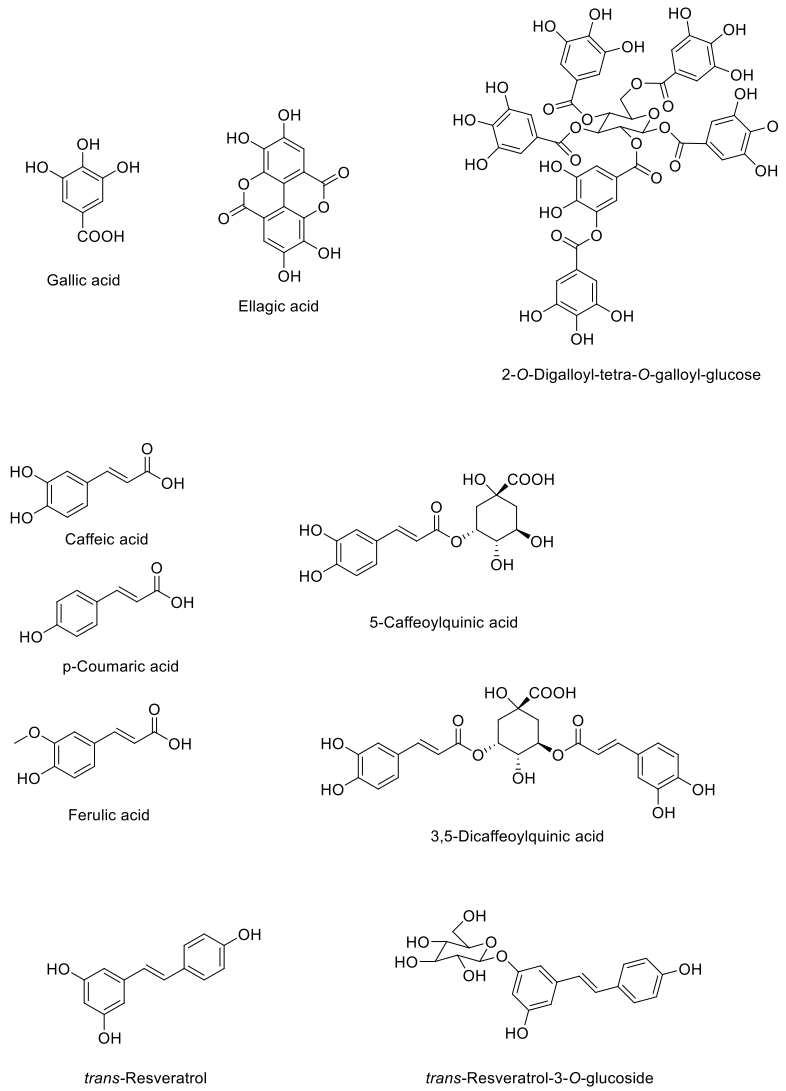

Scheme 4.6.Structural formulae of some non-flavonoid polyphenols.

The daily intake of polyphenols is approximately 1g for an adult but significant variations are observed with different dietary styles. Besides, recent studies suggested that a higher intake of polyphenols is associated with a longer life time expectation.[57–59] Fortunately, polyphenols are widely found in the vegetable kingdom and in coffee and tea in particular.

In coffee beans, there are non-flavonoid polyphenols and, especially, mono- and diesters of hydroxycinnamic acid and quinic acid, which are called chlorogenic acids (CGAs). Their general structural formula is presented in Scheme 4.7, below.

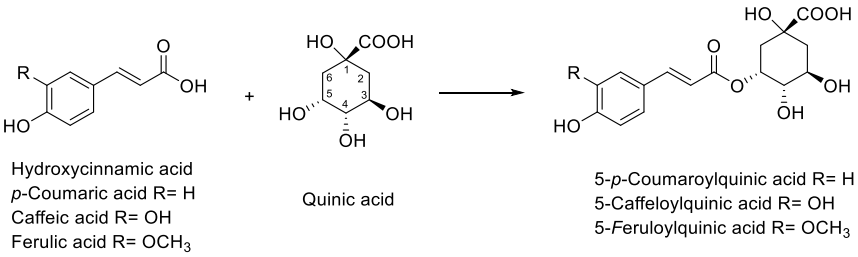

Figure 4.7. Structural formulae of hydroxycinnamic acid and quinic acid which form chlorogenic acids. As an example, the ester in position 5 is reported.

In green coffee beans, 5-caffeoylquinic acid (5-CQA) is the predominant species accounting for over than 50% of the total polyphenolic content, followed by its 3, and 4 regioisomers and feruloylquinic and dicaffeoylquinic acids, also with the corresponding regioisomers (their structural formulae are reported in Scheme 4.8, below).

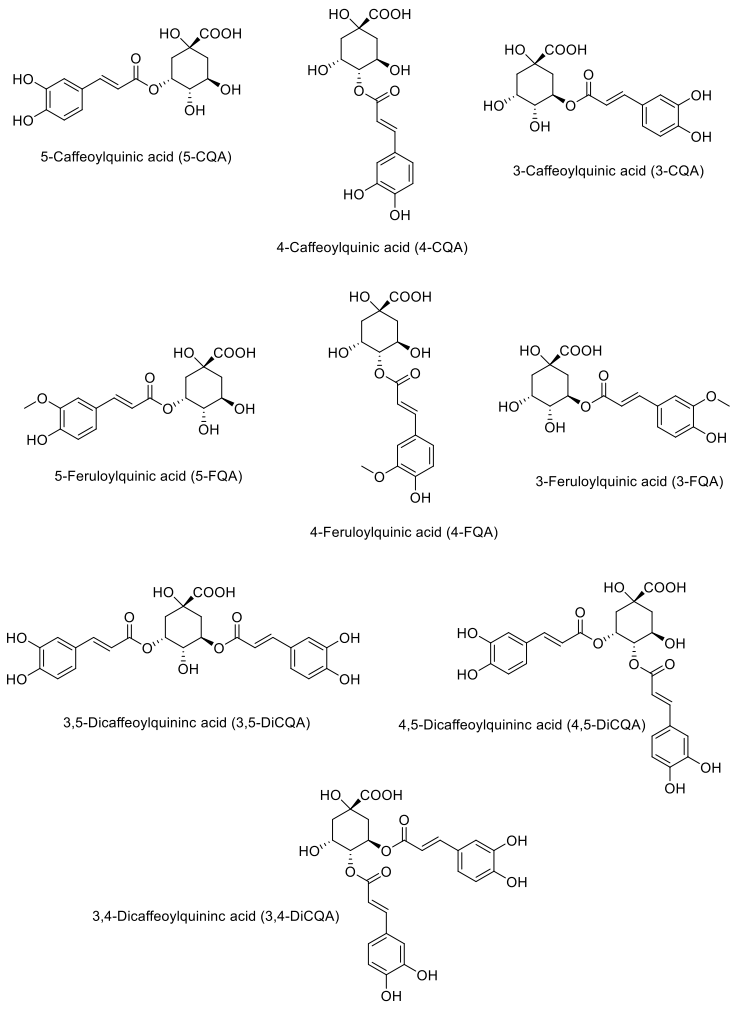

Scheme 4.8. Structural formulae of major polyphenolic compounds present in green coffee beans.

The total concentration and relative distribution of chlorogenic acids differs, depending upon factors, such as coffee species, origin and roasting process.[60] In *Coffea Arabica,* the content of chlorogenic acid is between 4 and 8% (w/w dry basis) while in *Coffea Canephora* the content is higher 6-11%.[56] During the roasting process, a significant change happens because of the high temperature employed (180-220 °C) and the pressure created inside the beans (about 5 atm) which lead to a significant variation in the total polyphenols content.[61–63] At the beginning of the roasting process, acyl migration reaction occurs, together with the hydrolysis reaction. Later, in the roasting stage epimerisation of quinic acid, decarboxylation of caffeic acid, polymerisation of the derivatives and lactonisation of CGAs also takes place. Besides, the Maillard reaction with amino groups of aminoacids proceeds.[64] In Scheme 4.9 below, the reactions arising from the roasting step are summarised, considering 5-CQA as a model.

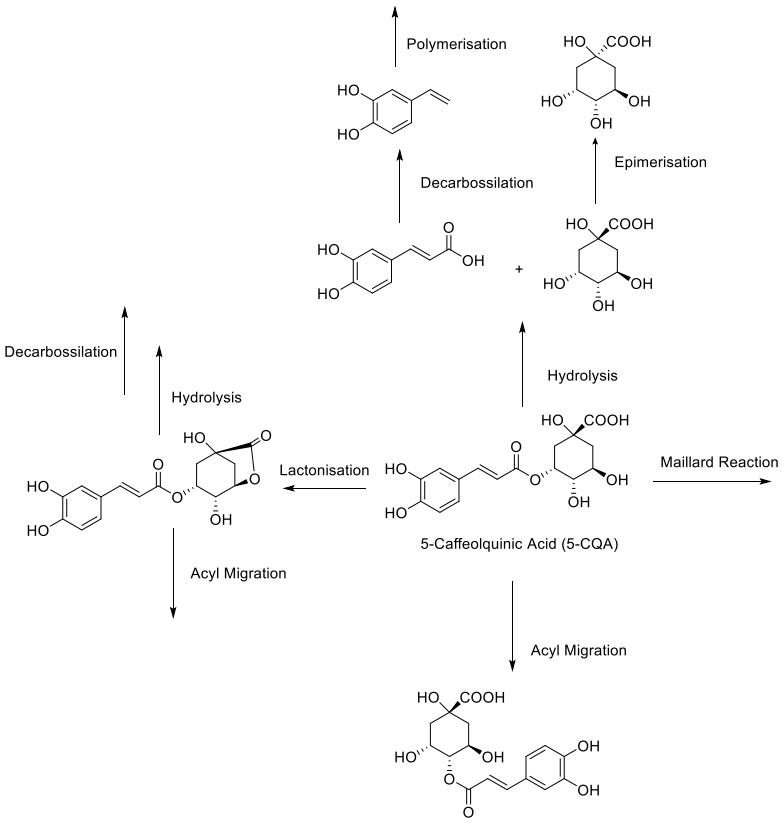

Scheme 4.9. Possible reactions occurring during roasting of green coffee beans. As a model molecule, 5-CQA was considered but the same chemical processes can occur with all polyphenols present in coffee beans.

Roasting is an art and the roasting process applied (such as time, temperature ramp, final temperature) has an enormous impact on the amount of chlorogenic acids reacting; excessively long roasting time leads to degradation of 95% of the initial content.[64] However it must be considered that the lowering in the chlorogenic acids content does not correspond to a proportional decrease in the total polyphenols concentration. This is because most of the phenolic groups are still present but as a plethora of derivatives of chlorogenic acids, which have not yet been identified completely.

Considering the widespread and interesting biological effects of polyphenols, the development of sensing platforms able to detect and quantify these compounds is of great economical and scientific interest. However, because of variety of chemical structures included and complexity of food matrices, accurate quantification of the total polyphenols content is still a challenge.[65] Most of the published polyphenol determination methods are based on chromatographic techniques, such as LC[65,66], HPLC[49,67,68], UHPLC[69,70], and GC[71], with both UV and mass detectors. The main advantage of chromatographic techniques is the possibility to separate and quantify each different compound present in the mixture. In fact, when the chromatographic step is avoided, a signal arising from the sum of all polyphenol present in the sample is obtained. Although this signal is merged, the total concentration of polyphenols is still a valuable information for studying the effect of different diets on human health. Many non-chromatographic protocols are reported in literature based on different methods, including FT-Raman[72], UV [73] and NMR spectroscopy[74] as well as electrochemical methods. In particular, electrochemistry is an interesting technique because it measures directly the redox properties of a compound which can be related to its anti-oxidant activity. In Table 4.6 below, the most recent examples of electrochemistry-based methods for the determination of polyphenols are presented.

Table 4.6.Recently published studies on the use of electrochemical techniques for quantification of polyphenols in different matrices. The following acronyms were used: BDD (Boron Doped Diamond), TiO (Titanium oxide); CPE (Carbon paste electrode); GCE (Glassy carbon electrode); PGE (Pencil graphite electrode), SPCPE (Screen-printed carbon paste electrode) Au (Gold electrode).For modifiers, the followings acronyms are reported: N/A (Not applicable); AuNPs (Gold Nano Particles); BMIM-PF6 (1-butyl-3-methylimidazol-3-ium hexafluorophosphate), PEDOT (poly(3,4-ethylenedioxy thiophene); PSS (poly(4-styreneslfonic acid); MWCNT (Multi-walled carbon nanotubes); GO (Graphene oxide); MIS (molecularly imprinted siloxane). Regarding the techniques employed, the following acronyms were used: SWAdSV (Square wave adsorption stripping voltammetry); CV (cyclic voltammetry); Amp (amperometry); CP (Chronopotentiometry); SWV (Square wave voltammetry); DPV (Differential pulse voltammetry); AdSV (adsorptive stripping voltammetry).

Electrode	Modifier	Technique	Application	LOD (µM)	Linear range (µM)	Year	Ref.
BDD	N/A	SWAdSV	Beverages	0.4	2.8-170	2018	[75]
TiO	AuNPs:PEDOT:PSS	CV	N/A	2	2-10000	2017	[76]
CPE	BMIM-PF_6	SWV	Herbal extract	0.01	0.02-2.5	2017	[77]
GCE	MWCNT:GO:tyrosinase	Amp	Fruit juice	0.3	0.3-300	2017	[78]
GCE	N/A	CP	Coffee	0.57	5-100	2017	[79]
PGE	N/A	DPV	Green Coffee	0.07	0.1-500	2016	[80]
GCE	PEDOT	CV	Coffee and tea			2016	[81]
GCE	N/A	DPV	Coffee	1.2		2016	[82]
SPCPE	MWCNT	DPV	Coffee beans	0.3	0.5-445	2016	[83]
SPCPE	GO and Nafion	Amp	Coffee	2.67	2.67-26.50	2015	[84]
GCE	Poly-(aminosulfonic acid)	CV	Pharmaceutical products	0.04	0.4-12	2014	[85]
Au	MIS	DPV	N/A	0.15	0.5-14	2013	[86]
BDD	N/A	AdSV	Coffee, energy drinks	1.26	5-145	2013	[87]
GCE	MWCNT	DPV	Coffee	0.69	1-1000	2013	[88]

From Table 4.6 it can be noticed that, in most cases, modified electrodes were developed using carbon-based materials. As explained in Section 4.1.1 above, modified electrodes have the advantage of increasing the sensitivity, but the reproducibility of the electrode preparation and the long-term stability of the material are in many cases not satisfactory for industrial applications. According to literature data, all electrochemical methods reported so far are insufficiently selective to differentiate between different polyphenols present in real samples. This is because redox properties of these compounds are very similar. As a consequence, one single oxidation peak is observed and the results are expressed as the polyphenol concentration.

In view of valuable results obtained with respect to caffeine determination and on increased interest in determination of polyphenols, this task seemed feasible because of a pronounced difference in oxidation potential between caffeine and polyphenols. It was decided to develop a simple and cost-effective electrochemical sensor for simultaneous determination of polyphenols and caffeine in coffee samples (espresso brews, green beans and roasted beans extract). To perform electrochemical experiments, a small and portable potentiostat was acquired by illy Caffè (μStat 400 from Methrohm Italy) and the applicability of screen-printed carbon paste electrodes for this purpose was investigated.

4.2.2 Results and discussion

On the followings pages, the development of an electrochemical method for the simultaneous determination of caffeine and the total polyphenols content in caffeinated beverages is presented. In similarity with the work on glassy carbon electrode, the discussion is divided into three main sections involving: (i) optimization of the determination conditions; (ii) analytical performance and (iii) real sample analysis. Screen-printed carbon paste Electrode (SPCE) were employed to develop the assay. The

interest in this type of electrodes is due to the simplicity of use, low cost and the possibility to perform the analysis using micro volumes of the electrolyte solution as shown in Figure 4.25, below.

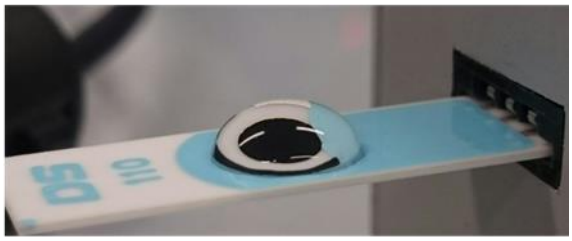

Figure 4.25. An example of the single drop of supporting electrolyte (100 µL) dispensed over the screen-printed carbon paste electrode.

4.2.2.1 Optimization of the conditions

The initial step was focused on finding a suitable supporting electrolyte for simultaneous determination of polyphenols and caffeine. It is reported in the literature that acidic conditions are the most favourable for the determination of caffeine because of a sharp and well-defined CV oxidation peak is recorded. On the other hand, it has also been reported that the oxidation of polyphenols in acidic conditions is suppressed.[82,84] In the previous work on caffeine determination using a bare GCE in the real sample analysis no additional peaks, besides those of caffeine oxidation, were recorded in the voltammograms of coffee samples in 0.1 M H_2SO_4 (see discussion on interference studies in Section 4.1.2.3 above). Therefore, acetate buffer of pH = 5 was initially tested as the supporting electrolyte solution, in order to avoid highly acidic solutions. In the Figure 4.26, below, the cyclic voltammograms of 0.5 M acetate buffer (pH = 5) in the absence (dash line) and presence (full line) of an equimolar solution of 5-CQA and caffeine are presented. 5-CQA was selected as the model compound for studying the electrochemical properties of chlorogenic acids, because it is the most abundant compound out of all different polyphenols present in coffee beans.

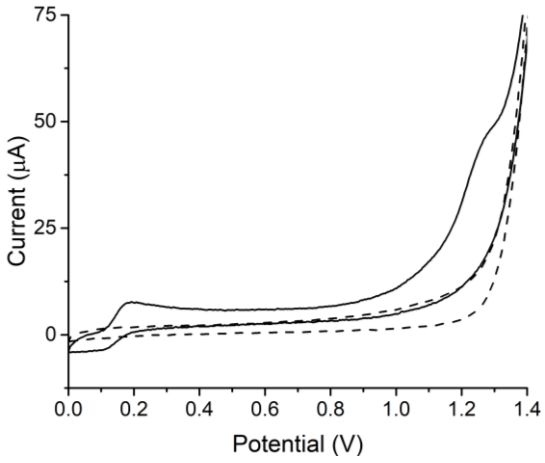

Figure 4.26. Cyclic voltammograms for the supporting electrolyte solution (0.5 M acetate buffer, pH 5) (dash line), and of an equimolar mixture of 5-CQA and caffeine ($4.02 \times 10^{-4} M$) in the same supporting electrolyte (solid line). The scan rate was 100 mV/s.

Two oxidation peaks were identified, i.e. one at 0.19 V for 5-CQA and the other at 1.19 V for caffeine. During the negative potential scan, a cathodic peak corresponding to reduction of the oxidised polyphenols was recorded at 0.15 V. The electrochemical behaviour of both analytes is well described in the literature, and in the case of caffeine it is reported in Section 4.1.2.1, above, at the beginning of this chapter. In contrast to caffeine, the oxidation of polyphenols is reversible. It is described by the general scheme shown below.

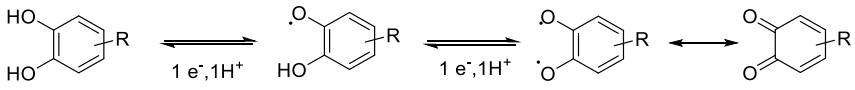

Scheme 4.9. Electrochemical oxidation and reduction of a general catechol molecule to the corresponding quinone analogue via the lost of two electrons and two protons.

The reaction involves oxidation of the catechol unit to the quinone analogue. The process starts with the loss of one electron and the formation of a radical which is stabilised through the H bond of the vicinal OH group. The stabilised radical subsequently loses a second electron and proton, which leads to a quinone derivative. The obtained quinone can be reduced back to the catechol analogue following the same chemical path.[89,90] When 0.5 M acetate buffer (pH = 5) was employed (Figure 4.26,) both signals of 5-CQA

and caffeine were recorded, thus suggesting that simultaneous determination of the two molecules is feasible under these solution conditions. To evaluate the effect of changes in the supporting electrolyte concentration on electrochemical behaviour of the two analytes, a series of solutions with concentrations ranging from 0.01 M to 1 M was examined, while maintaining an equimolar ratio of the two target analytes. In Figure 4.27 below, the recorded cyclic voltammograms are reported.

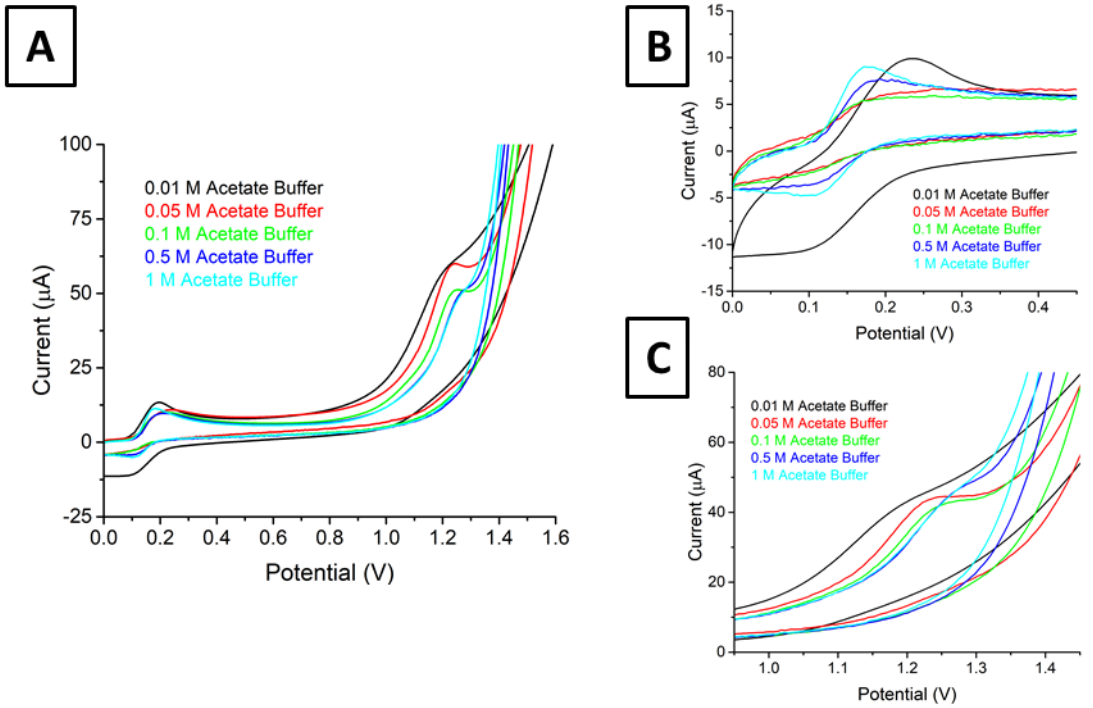

Figure 4.27. CV screening of solutions of different acetate buffer concentrations (pH = 5), with an equimolar solution of 5-CQA and caffeine (4.02×10^{-4}M). The different concentrations evaluated were, as follows: 0.01 M (black line); 0.05 M (red line); 0.1 M (green line); 0.5 M (blue line); and 1 M (light blue line). (A) Complete cyclic voltammograms. (B) and (C) CV curves magnification of the oxidation potential of 5-CQA and caffeine, respectively. The scan rate was 100 mV/s.

The signal-to-noise ratio (*S*/*N*) at different acetic buffer concentrations are listed in Table 4.7 below, for 5-CQA and caffeine.

Table 4.7. Signal, noise and S/N ratios for 5-CQA and caffeine oxidations using acetate buffers (pH = 5) of different concentrations. A $4.02 \times 10^{-4} M$ *equimolar solution of the two analytes was employed. As signal and noise mean values of three consecutive cyclic voltammograms were considered.*

Acetate buffer concentration (M)	5-CQA			Caffeine		
	Signal (μA)	Noise (μA)	S/N	Signal (μA)	Noise (μA)	S/N
0.01	9.89	1.48	6.68	35.97	27.83	1.29
0.05	6.67	3.67	1.82	27.29	15.75	1.73
0.1	5.83	2.13	2.74	23.83	11.17	2.13
0.5	7.17	1.92	3.73	22.17	9.46	2.34
1	9.00	1.63	5.54	22.50	8.63	2.61

In the case of the 5-CQA signal, the highest *S*/*N* was achieved at the lowest (0.01 M) and highest (1.0 M) concentration of the buffer supporting electrolyte. In the case of caffeine, the noise is considerably decreased by the increase of concentration of the supporting electrolyte and the optimal *S*/*N* ratio is obtained at 1.0 M acetate buffer (pH = 5). Subsequently, to further investigate the role of the supporting electrolyte on the 5-CQA and caffeine oxidation, a second organic acid (citric acid) was evaluated by exploring a concentration range from 0.01 M to 1.0 M. The cyclic voltammograms are depicted in Figure 4.28, and the *S*/*N* ratios are listed in Table 4.8, below.

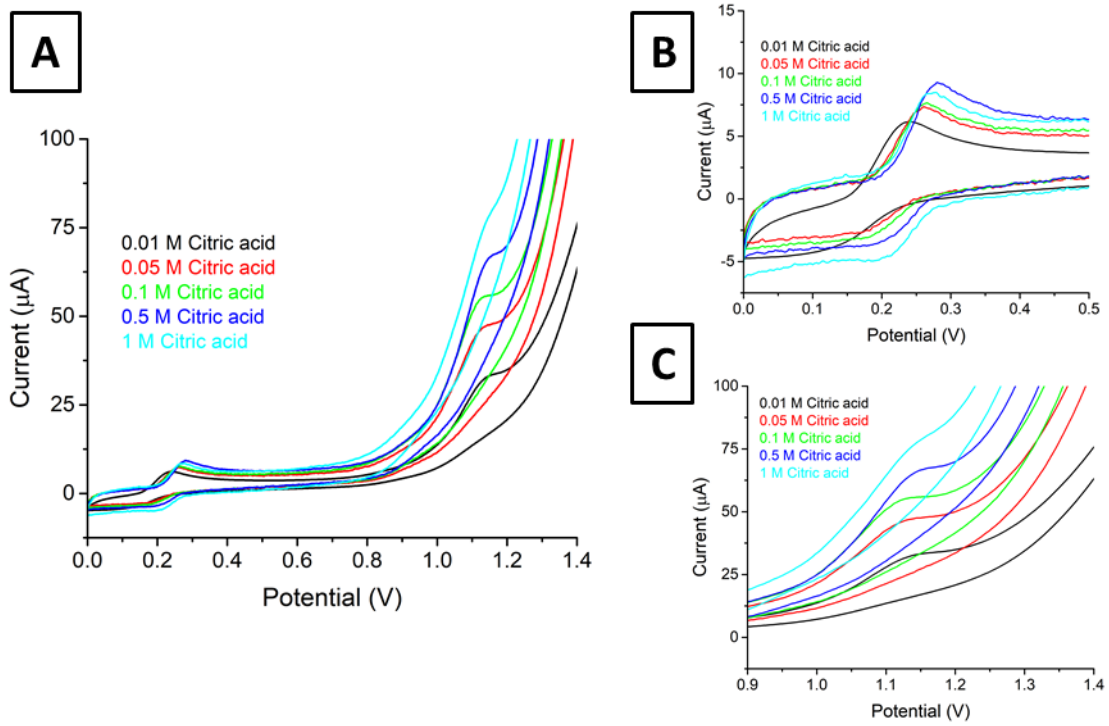

Figure 4.28. Cyclic voltammograms for different citric acid concentrations with an equimolar solution of 5-CQA and caffeine ($4.02 \times 10^{-4} M$). The different acid concentrations were, as follows: 0.01 M (black line); 0.05 M (red line); 0.1 M (green line); 0.5 M (navy blue line); and 1.0 M (light blue line). (a) The complete cyclic voltammograms. (B) and (C) the CV curve magnified at the oxidation potential of 5-CQA and caffeine, respectively. The scan rate was 100 mV/s.

Table 4.8. S/N ratios of 5-CQA and caffeine oxidation signals using citric acid of different concentrations. A $4.02 \times 10^{-4} M$ equimolar solution of the two analytes was employed. As signal and noise mean values of three consecutive cyclic voltammograms were used.

Citric acid concentration (M)	5-CQA			Caffeine		
	Signal (µA)	Noise (µA)	S/N	Signal (µA)	Noise (µA)	S/N
0.01	6.15	1.32	4.65	33.23	15.94	2.09
0.05	7.33	1.83	4.01	47.54	26.17	1.82
0.1	7.67	2.08	3.68	55.83	32.50	1.72
0.5	9.29	2.13	4.37	66.58	32.00	2.08
1	8.42	2.42	3.48	78.58	45.29	1.74

From the data summarised in Table 4.8, above, it can be observed that at higher citric acid concentrations, signals and the noise, both at the potential of polyphenols and caffeine oxidation are enhanced. Consequently, the *S/N* ratio is insignificantly affected by the change in concentration of citric acid. Interestingly, the 5-CQA signal is higher in

more concentrated citric acid solutions and is comparable with those obtained at pH = 5 (Table 4.7). This result suggests that the oxidation signal of 5-CQA is not affected by the increase of the citric acid concentration and thus lowering the pH of the supporting electrolyte when SPCE are employed. To further investigate if acidic conditions are suitable for simultaneous determination of 5-CQA and caffeine, two strong inorganic acids were employed as supporting electrolytes (H_2SO_4 and H_3PO_4). In both cases, the concentration range 0.01 M to 1.0 M was employed. The voltammograms recorded are reported in Figure 4.29 below together with Table 4.9 of *S*/*N* ratios, starting with sulphuric acid.

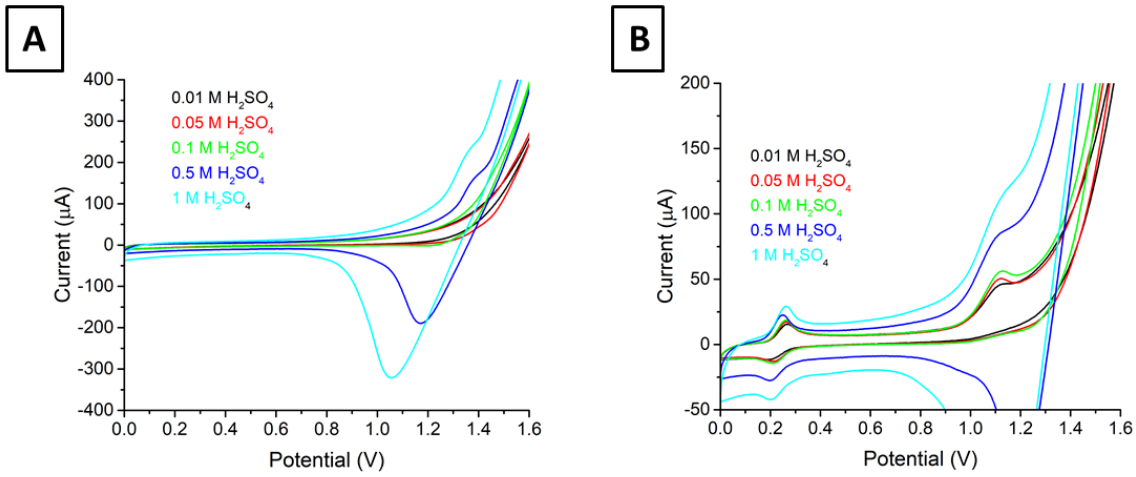

Figure 4.29. Cyclic voltammograms at different sulfuric acid concentrations of: (A) only the supporting electrolyte and (B) an equimolar mixture of 5-CQA and caffeine solution ($4.02 \times 10^{-4} M$). The different acid concentrations are as follows: 0.01 M (black line), 0.05 M (red line), 0.1 M (green line), 0.5 M (blue line), 1.0 M (light blue line). The scan rate was 100 mV/s.

In Figure 4.29 the cyclic voltammograms at different H_2SO_4 concentrations (Figure 4.29 A) and with an equimolar mixture of 5-CQA and caffeine (Figure 4.29 B) are presented. At concentrated sulfuric acid solutions (i.e. 0.5 M and 1.0 M) an oxidation peak at 1.35 V during the direct anodic scan and a reduction peak on the reversed cathodic scan between 1.0 and 1.2 V were recorded. The signals can arise either from some contaminants present in the purchased H_2SO_4 or may be caused by the oxidation of the working and counter electrode in a highly acidic medium, which however does not

interfere with caffeine and 5-CQA oxidation because two distinct peaks were recorded for these two analytes. An enlargement of the CV curves at the potential of 5-CQA (Figure 4.30 A) and caffeine (Figure 4.30 B) oxidation is presented below.

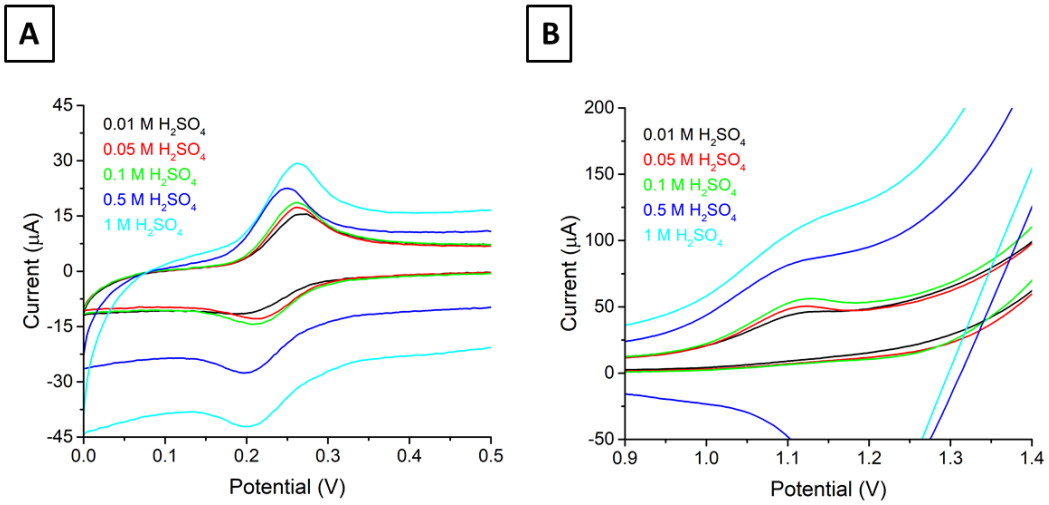

Figure 4.301. Screening of different sulfuric acid concentrations with an equimolar solution of 5-CQA and caffeine ($4.02 \times 10^{-4}M$). The different acid concentrations were as follows: 0.01 M (black line); 0.05 M (red line); 0.1 M (green line); 0.5 M (blue line); and 1.0 M (light blue line). (A) an enlargement of the CV curves at the oxidation potential of polyphenols. (B) an enlargement of the CV curve at the oxidation potential of caffeine. The scan rate was 100 mV/s.

Interestingly, 5-CQA rendered one oxidation and one reduction peak in all of the concentrations of sulfuric acid used. Moreover, the peaks are higher and narrower compared to those previously recorded using organic acid. The peak currents and signal-to-noise ratios are listed in Table 4.9, below.

Table 4.9. S/N ratios of 5-CQA and caffeine oxidation peak current at different concentrations of sulfuric acid. A $4.02 \times 10^{-4}M$ equimolar solution of the two analytes was employed. As the signal and noise, the mean values of three consecutive cyclic voltammograms were used.

H_2SO_4 concentration (M)	5-CQA			Caffeine		
	Signal (µA)	Noise (µA)	*S/N*	Signal (µA)	Noise (µA)	*S/N*
0.01	15.46	3.13	4.95	46.62	26.71	1.75
0.05	17.33	3.21	5.40	40.71	26.38	1.54
0.1	18.63	3.25	5.73	54.87	27.96	1.96
0.5	22.46	3.83	5.86	88.42	40.37	2.19
1	29.25	7.13	4.11	119.75	68.21	1.76

From Table 4.9 it follows that use of higher acid concentration leads to progressive enhancement in the signal and noise with the *S/N* ratios insignificantly affected by the acid change concentration. However, the signals for both analytes were found to be higher, as compared to those in the case of the previously employed supporting electrolyte. Apparently, even in acidic solution of high concentration the simultaneous determination of 5-CQA and caffeine is feasible when SPCE is used. To further explore the applicability of inorganic acids as supporting electrolytes, orthophosphoric acid was employed. The data on the effect of H_3PO_4 concentration on cyclic voltammograms of 5-CQA and caffeine are presented in Figures 4.31 here below.

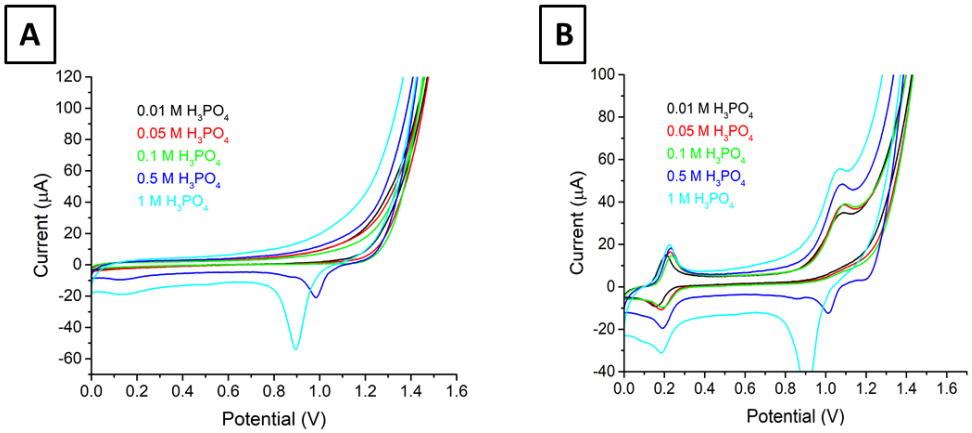

Figure 4.31. Cyclic voltammograms for orthophosphoric acid at different concentrations of: (A) only the supporting electrolyte. (B) An equimolar mixture of 5-CQA and caffeine solution (4.02×10^{-4} *M). The different acid concentrations are as follows: 0.01 M (black line), 0.05 M (red line), 0.1 M (green line), 0.5 M (blue line), 1.0 M (light blue line). The scan rate was 100 mV/s.*

Similarly as for sulfuric acid, for 0.5 and 1.0 M orthophosphoric acid two new current peaks were recorded during the reverse cathodic scan, when only the supporting electrolyte was present (Figure 4.31 A), a broad peak at 0.15 V and a sharper one between 0.9 and 1 V. This result further suggests that the electrodes are not stable in highly acidic solutions as was discussed above for the study involving GCE (Section 4.1.2.1). However, also in the case of H_3PO_4 no interference with the signals of the two analytes

was observed in the direct anodic scan as it can be seen in the enlargements of CV curves in Figure 4.32, below.

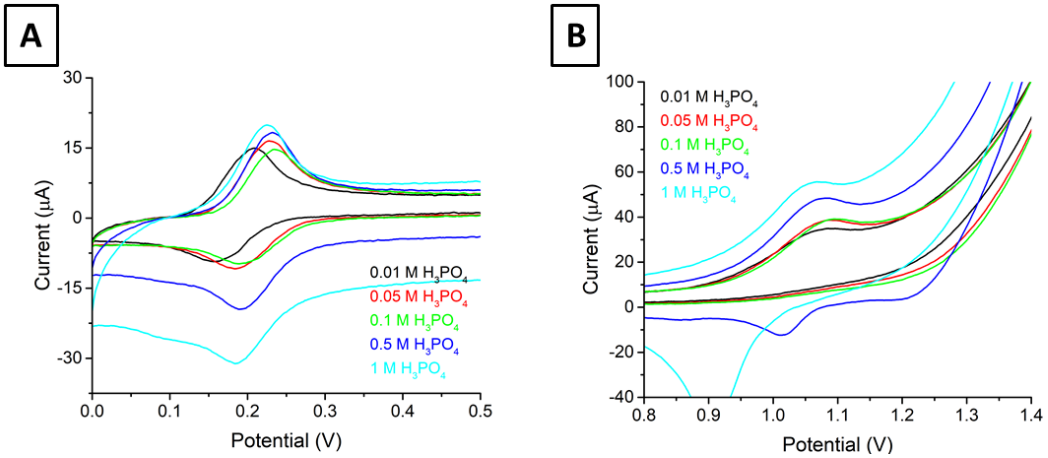

Figure 4.32. Screening of different citric acid concentrations of an equimolar solution of 5-CQA and caffeine ($4.02 \times 10^{-4} M$). The different acid concentrations were as follows: 0.01 M (black line); 0.05 M (red line); 0.1 M (green line); 0.5 M (blue line); and 1.0 M (light blue line). (A) An enlargement of the CV curve at the oxidation potential of polyphenols. (B) An enlargement of the CV curve in the oxidation potential of caffeine. The scan rate was 100 mV/s.

In Table 4.10, below, the signals, noise levels and *S*/*N* ratios for both analytes at different H_3PO_4 concentrations are listed.

Table 4.10. The S/N ratio of the 5-CQA and caffeine oxidation signals at different concentrations of phosphoric acid. A $4.02 \times 10^{-4} M$ equimolar solution of the two analytes was employed. As the signal and noise, the mean values of three consecutive cyclic voltammograms were used.

H_3PO_4 concentration (M)	5-CQA			Caffeine		
	Signal (µA)	Noise (µA)	*S*/*N*	Signal (µA)	Noise (µA)	*S*/*N*
0.01	14.96	2.00	7.48	37.92	22.04	1.72
0.05	16.50	2.04	8.09	38.71	13.33	2.90
0.1	14.71	1.67	8.81	37.79	12.71	2.97
0.5	18.29	2.25	8.13	46.08	22.00	2.09
1	19.87	3.42	5.81	58.08	36.21	1.60

The peak currents were higher at 0.5 M and 1.0 M H_3PO_4 for both analytes. However, in terms of the *S*/*N* ratios, the highest value was obtained at 0.1 M H_3PO_4.

To summarise and discuss the results of the different supporting electrolyte employed, Table 4.11 listing signals, the noise level and *S*/*N* ratios is presented below considering

only the optimal concentration of each of the supporting electrolyte. The corresponding voltammograms are present in Figure 4.33, below.

Table 4.11. Comparison of the four different supporting electrolytes tested. For each supporting electrolyte the concentration at which the highest S/N ratio was selected.

Supporting electrolyte	5-CQA			Caffeine		
	Signal (µA)	Noise (µA)	*S/N*	Signal (µA)	Noise (µA)	*S/N*
Acetate Buffer pH 5 (1 M)	9.00	1.63	5.54	22.50	8.63	2.61
Citric acid (0.01 M)	6.15	1.32	4.66	33.23	15.94	2.09
H_2SO_4 (0.5 M)	22.46	3.83	5.86	88.42	40.37	2.19
H_3PO_4 (0.1 M)	14.71	1.67	8.81	37.79	12.71	2.97

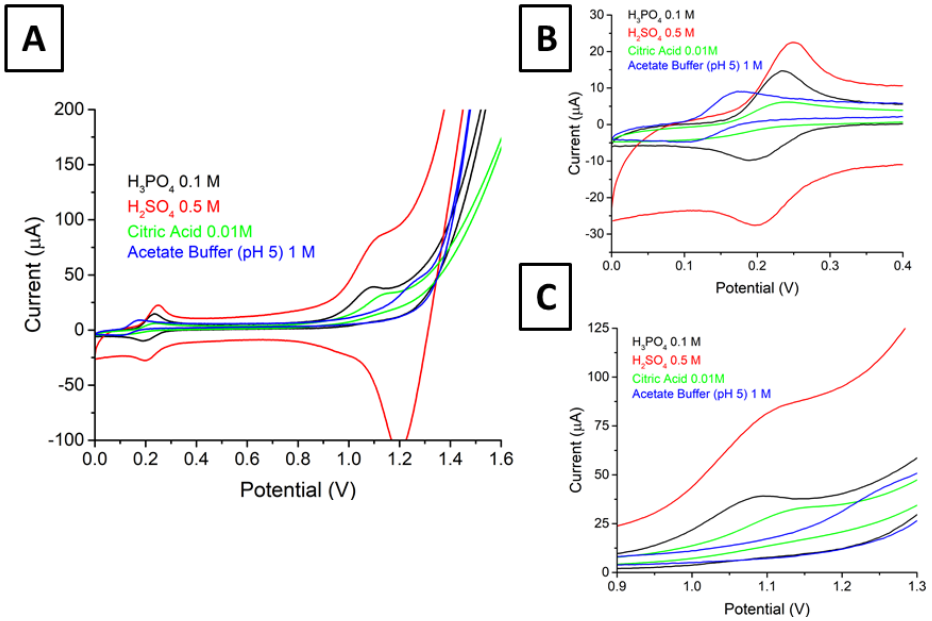

Figure 4.33. Comparison of CV curves for optimal concentrations of different supporting electrolytes. The cyclic voltammograms were recorded in all cases using a scan rate of 100 mV/s and an equimolar solution ($4.02 \times 10^{-4} M$) of 5-CQA and caffeine in 0.1 M orthophosphoric acid (black line), 0.5 M sulfuric acid (red line), 0.01 M citric acid (green line) and 1.0 M acetate buffer (pH 5) (blue line).

From the Table 4.11 and Figure 4.33, above, it can be seen that, higher signals in terms of the peak current and width are recorded and for 5-CQA in particular when strong inorganic acids (i.e. sulfuric and orthophosphoric) were employed. This result suggests that strong inorganic acids are more convenient as the supporting electrolyte for simultaneous determination of 5-CQA and caffeine when SPCE are employed. Between

the two strong acids evaluated, sulfuric acid led to a higher peak current and higher noise level, while in the case of 0.1 M H_3PO_4, the three times lower noise level measured, led to a higher *S*/*N* ratio. In 0.5 M H_2SO_4 electrode surface oxidation was observed (peak on the reverse, cathodic, scan at 1.20 V) which can affect the properties of the material and lead to low reproducibility of the measurement, if not controlled. Therefore, considering the higher S/N ratio and the absence of electrochemical signals due to the oxidation of the electrode surface, 0.1 M H_3PO_4 was selected as the optimal supporting electrolyte for all further experiments.

Once a suitable supporting electrolyte was selected, the next step was to identify the optimal instrumental parameters for the DPV and SWV analysis, because these low amplitude techniques are more sensitive than cyclic voltammetry. In all the following experiments, an equimolar mixture of 5-CQA and caffeine was employed (0.23 mM). As was previously done with the GCE sensor, three parameters were optimised in the case of DPV, namely the pulse amplitude, pulse duration and scan rate. The pulse amplitude range investigated was 25 to 250 mV and its effect on the DPV voltammograms is depicted in Figure 4.34. The optimisation was done using a trial-and-error approach starting from the default instrumental settings. In fact, it is difficult to predict the most appropriate pulse settings because these are dependent on several factors including the working electrode material, the supporting electrolyte and nature physicochemical properties of the analytes.

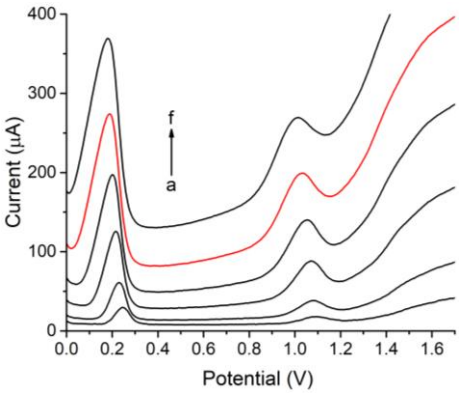

Figure 4.34. Optimisation of the pulse amplitude for the DPV analysis. Scan rate was set at 40 mV/s and pulse time at 10 ms. The different pulse amplitudes tested were: (a) 25, (b) 50, (c) 100, (d) 150, (e) 200 and (f) 250 mV. A 2.34×10^{-4} *M equimolar mixture of the two analytes in 0.1 M* H_3PO_4 *was prepared.*

When the pulse amplitude was increased, a direct enhancement in the peak currents, widths and background currents for both analytes was observed. In particular, in the case of 5-CQA at 250 mV pulse amplitude (curve f Figure 4.34) the peak started at 0 V and finished at 0.25 V, while the caffeine signal started at 0.85 V and finished at 1.20 V. Wide peaks can lead to overlapping with those of possible interfering agents, thus decreasing applicability of the sensor. Therefore, to balance peak currents and peak widths, a pulse amplitude of 200 mV was chosen as the optimal instrumental setting. The subsequent optimisation step focused on the pulse duration; a range of 2.5 to 50 ms was investigated, and the effect of this duration on the voltammogram is depicted in Figure 4.35, below.

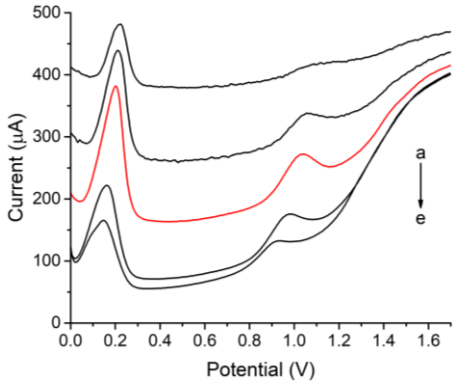

Figure 4.35. Optimisation of pulse duration for the DPV analysis. A scan rate was set at 40 mV/s and pulse amplitude at 200 mV. The different pulse durations tested were: (a) 2.5, (b) 5, (c) 10, (d) 25, (e) 50 ms. A 2.34×10^{-4} *M equimolar mixture of the two analytes in 0.1 M* H_3PO_4 *was prepared.*

With the increase of pulse duration the background decreases proportionally while the peak current reached maximum at the intermediate pulse duration (10 ms) for both analytes. To obtain the highest peak currents, a pulse duration of 10 ms was selected as optimal. Once the pulse amplitude and duration were optimised the effect of scan rate was investigated. For that, the potential was linearly scanned from 5 to 40 mV/s, and the results are depicted in Figure 4.36, below.

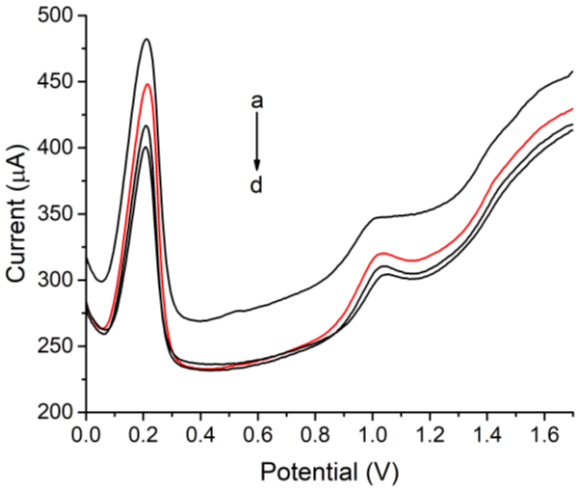

Figure 4.36. Optimisation of the scan rate for the DPV analysis. The different scan rates tested were: (a) 5, (b) 10, (c) 20 and (d) 40 mV/s. The pulse amplitude was set at 200mV and pulse duration at 10 ms. A 2.34×10^{-4} *M equimolar mixture of the two analytes in 0.1 M* H_3PO_4 *was prepared.*

From Figure 4.36, above, it follows that the background current significantly decreased when the scan rate was doubled from 5 to 10 mV/s. However, further increase in the scan rate led to lower signals for both analytes, without significantly affecting the noise level. Therefore, 10 mV/s was selected as the optimal scan rate to ensure low background current and high peak current.

The second low amplitude potential technique applied was SWV. In this case, two instrumental parameters were optimised namely, pulse amplitude and pulse frequency. Initially, the effect of pulse amplitude on simultaneous determination of 5-CQA and caffeine was investigated, studying a pulse amplitude range of 10 to 150 mV. Figure 4.37 shows the results.

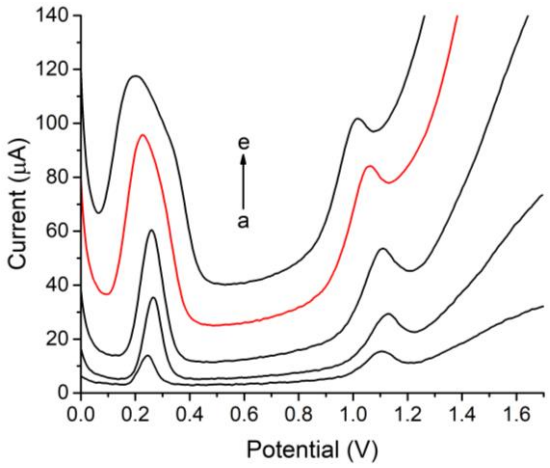

Figure 4.37. Optimisation of pulse amplitude for the SWV analysis. Pulse frequency was set at 10 Hz. The different pulse amplitudes tested were: (a) 10, (b) 25, (c) 50, (d) 100, (e) 150 mV. An 2.34×10^{-4} *M equimolar mixture of the two analytes in 0.1 M* H_3PO_4 *was prepared.*

As already noticed during the optimisation for DPV analysis, as the pulse amplitude increased the background current, peak currents, and peak widths were enhanced. The optimum balance between peak currents and peak widths was at 100 mV amplitude. That was because the higher pulse amplitude led to a significant widening of the peak, in particular for 5-CQA.

Once the pulse amplitude was optimised, the pulse frequency was optimised studying a range of 5 to 75 Hz and the effect of this frequency on the square wave voltammograms is depicted in Figure 4.38, below.

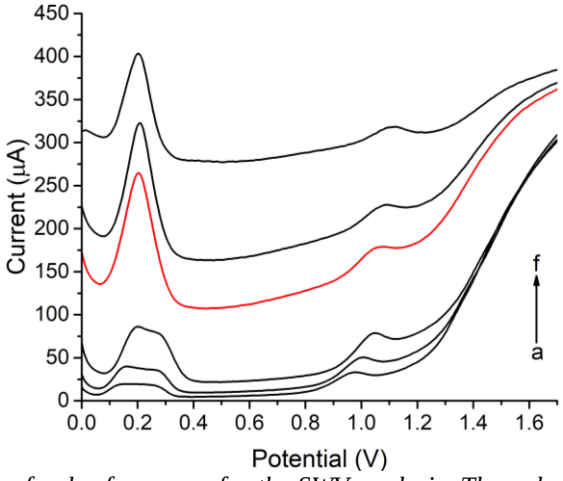

Figure 4.38. Optimisation of pulse frequency for the SWV analysis. The pulse amplitude was set at 100 mV. The different pulse frequencies tested were: (a) 5, (b) 10, (c) 25, (d) 35, (e) 50 and (f) 75 Hz. A 2.34×10^{-4} *M equimolar mixture of the two analytes in 0.1 M* H_3PO_4 *was prepared.*

From Figure 4.38, it follows that with the increase of the pulse frequency the background current increased proportionally, while the peak intensity reached the highest value at 35 Hz both for 5-CQA and caffeine. In particular for the 5-CQA, a broad peak was recorded at low frequency (up to 25 Hz), at elevated frequencies the peak was sharp, thus indicating possibility of higher sensitivity. The optimal value of pulse frequency was 35 Hz, because this value allowed obtaining high peak signals and short analysis time. In Table 4.12 below, a summary of the optimal instrumental settings for DPV and SWV are listed.

Table 4.12. Optimised of the instrumental settings for the DPV and SWV analysis. 0.1 M H_3PO_4 was employed as the supporting electrolyte and an equimolar concentration of the two analytes was used (2.34×10^{-4} M).

	DPV			SWV	
	Pulse amplitude (mV)	Pulse duration (ms)	Scan rate (mV/s)	Pulse amplitude (mV)	Pulse frequency (Hz)
Studied range	25 – 250	2.5 – 50	5 – 40	10 – 150	5 – 75
Optimal value	200	10	10	100	35

The peak currents under optimised instrumental settings for both analytes are listed in Table 4.13, below.

Table 4.13. DPV and SWV peak currents for 5-CQA and caffeine with the optimised instrumental settings (Table 4.12). In both cases 0.1 M H_3PO_4 was employed as the supporting electrolyte and an equimolar concentration of the two analytes (2.34×10^{-4} M) was used.

Analyte	Peak current (μA)	
	DPV	SWV
5-CQA	203.10	31.48
Caffeine	146.48	18.24

As evident from Table 4.13, DPV peaks were higher for both analytes, thus suggesting that higher sensitivity can be achieved with this technique. On the other hand, in view of the optimised instrumental settings, the SWV determinations were faster because the whole voltammograms (from 0 to 1.70 V) were recorded in less than one minute, while in the case of DPV three minutes were required. Considering that sensitivity was not expected to be an issue for coffee sample analysis (given the high concentration of both caffeine and polyphenols), the priority was given to the analysis time and SWV was selected as the most appropriate technique.

4.2.2.2 Analytical performance

In order to determine the SPCE sensitivity for detection of 5-CQA and caffeine, a calibration curve was constructed using SWV and a concentration range 5.79×10^{-7}M to 8.85×10^{-4} M was investigated. Initially, an equimolar ratio of the two analytes was chosen and the average of 3 consecutive square wave voltammograms was considered as peak intensity current. In the case of 5-CQA the signal was recorded for concentrations higher than 3.24×10^{-6} M and the SWV voltammograms are reported in Figure 4.39A. This figure shows into more detail the concentration range in which the sensor response was linear.

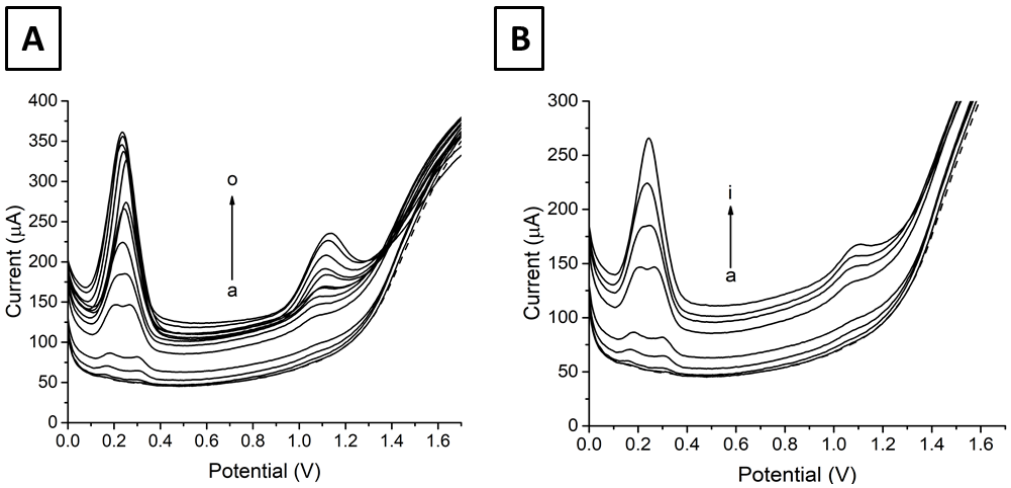

Figure 4.39. Square wave voltammograms at different equimolar concentrations of 5-CQA and caffeine in 0.1 M H_3PO_4 with the following instrumental settings: pulse amplitude 100 mV, pulse frequency 35 Hz. (A) The entire concentration range investigated. (B) The concentration range at which the signal was linearly dependent on concentration. The concentrations were, as follows: (a) 0 M (b) $3.24 \times 10^{-6} M$ *(c)* $4.69 \times 10^{-6} M$ *(d)* $7.36 \times 10^{-6} M$ *(e)* $9.21 \times 10^{-6} M$ *(f)* $3.24 \times 10^{-5} M$ *(g)* $4.69 \times 10^{-5} M$ *(h)* $6.66 \times 10^{-5} M$ *(i)* $8.85 \times 10^{-5} M$ *(j)* $1.28 \times 10^{-4} M$ *(k)* $2.34 \times 10^{-4} M$ *(l)* $3.24 \times 10^{-4} M$ *(m)* $4.69 \times 10^{-4} M$ *(n)* $6.66 \times 10^{-4} M$ *and (o)* $8.85 \times 10^{-4} M$.

As was previously done in the case of the GCE sensor (Section 4.2.2 of this chapter), the calibration curves were obtained by plotting the peak current versus the analyte concentration (Figure 4.40A and 4.40 B). In addition, considering that in the case of 5-CQA a broad peak was recorded at low concentrations (from 3.24 to 9.21 μM), the peak area (i.e. peak charge) was employed to obtain a calibration curve and check if linearity was wider and higher.

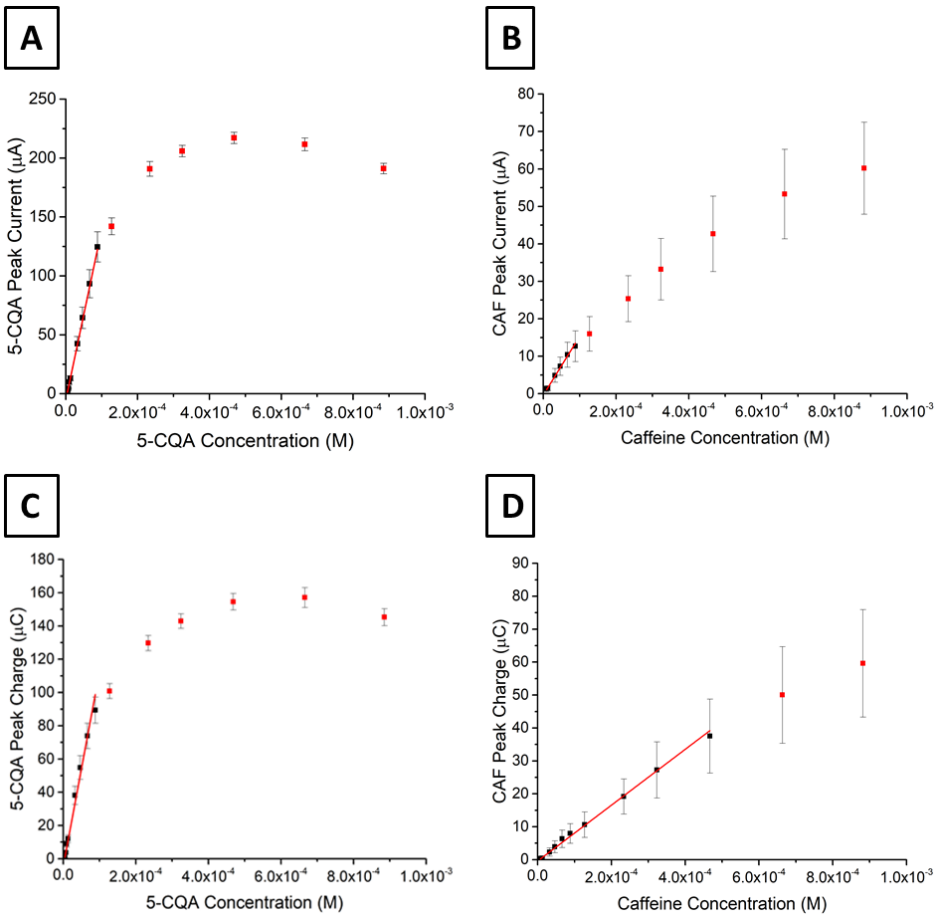

Figure 4.40. (A and C) Calibration curves for 5-CQA and (B and D) caffeine in 0.1 M H_3PO_4 using SWV and the following instrumental settings: pulse amplitude 100 mV and pulse frequency 35 Hz. (A) and (B) show the relationship between the analyte peak current (µA) and concentration (M). Figure (C) and (D) depict the relationship between the peak charge (µC) and the analyte concentration (M). 3 consecutive SWV voltammograms were recorded and the mean values were employed together with the standard deviation determined.

In the case of 5-CQA (Figure 4.40 A and 4.40 C), there were no significant differences when either peak current or peak charge were employed. In fact, a linear range of 3.24×10^{-6} to 8.85×10^{-5} M was observed in both cases. On the other hand, in the case of caffeine (Figure 4.40 B and 4.40 D) a wider linearity range was observed when the peak charge was employed (up to 4.68×10^{-4} M). The latter effect, may be explained considering the broadness of the caffeine peak, which allowed a more precise calculation of the peak area (charge) compared to its current. Surprisingly, this effect was not observed in the case of 5-CQA, which also showed broad oxidation peaks at low concentrations. A summary of the analytical performance in terms of the sensitivity, limit

of detection and linearity is presented in Table 4.14, below, for 5-CQA and caffeine using both peak currents and peak charges.

Table 4.14. Analytical performance of the screen-printed carbon paste electrode for simultaneous determination of 5-CQA and caffeine in 0.1 M H_3PO_4, using SWV (pulse amplitude 100 mV, pulse frequency 35 Hz). Both the peak current and peak area were evaluated for both analytes. Five consecutive SWV voltammograms were recorded as well as mean values and standard deviations were employed to draw calibration curves.

	5-CQA		Caffeine	
	Peak current	Peak charge	Peak current	Peak charge
Sensitivity	$1.45 \times 10^6 (\mu A/M)$	1.17×10^6 $(\mu C/M)$	$1.57 \times 10^5 (\mu A/M)$	$8.48 \times 10^4 (\mu C/M)$
LOD	7.64×10^{-7} M	1.15×10^{-6} M	3.51×10^{-6} M	1.10×10^{-6} M
Linear range	From 3.24×10^{-6} to 8.85×10^{-5} M	From 3.24×10^{-6} to 8.85×10^{-5} M	From 7.36×10^{-6} to 8.85×10^{-5} M	From 7.36×10^{-6} to 4.68×10^{-4} M
R^2	0.989	0.982	0.985	0.980

Table 4.14, above, shows that, the sensitivity of the sensor is ten times higher towards 5-CQA than caffeine, using both peak currents and charges. The higher sensitivity can be explained considering that polyphenol oxidation occurs at lower potentials and therefore, the background current is lower and the signal-to-noise ratio higher compared to that for caffeine (as also shown in Table 4.11). In addition, the working electrode is made of a carbon paste, which is a porous material known to adsorb molecules on its surface.[91,92] As a result, affinity and adsorption of polyphenols were higher than that of caffeine leading to a higher concentration of 5-CQA in the electrode proximity. This hypothesis needs further experimental evidence to be confirmed. However, the priority of this work was given to the applicability of the sensor for coffee products analysis. Therefore, no further experiments were performed to investigate the above difference in sensitivity. To summarise, both the peak current and charge were employed to obtain the calibration curves for 5-CQA and caffeine. The only significant difference was observed for the linear range of caffeine, which was wider when the peak charge was used, thus suggesting that the sensor could be applied to a broader range of caffeine concentrations.

As a consequence, in all further experiments the peak charge was employed for analytical purposes.

When two analytes are simultaneously quantified, it is important to investigate whether the presence of one analyte influences the electrochemical signal of the other. Therefore, two further calibration curves were obtained but, in this case, only the concentration of one analyte was increased while that of the other analyte was always kept at the initial concentration. In Figure 4.41, below, the SWV voltammograms of different concentrations of 5-CQA at constant caffeine concentration (3.05×10^{-5} M) are presented, together with the calibration curve for 5-CQA.

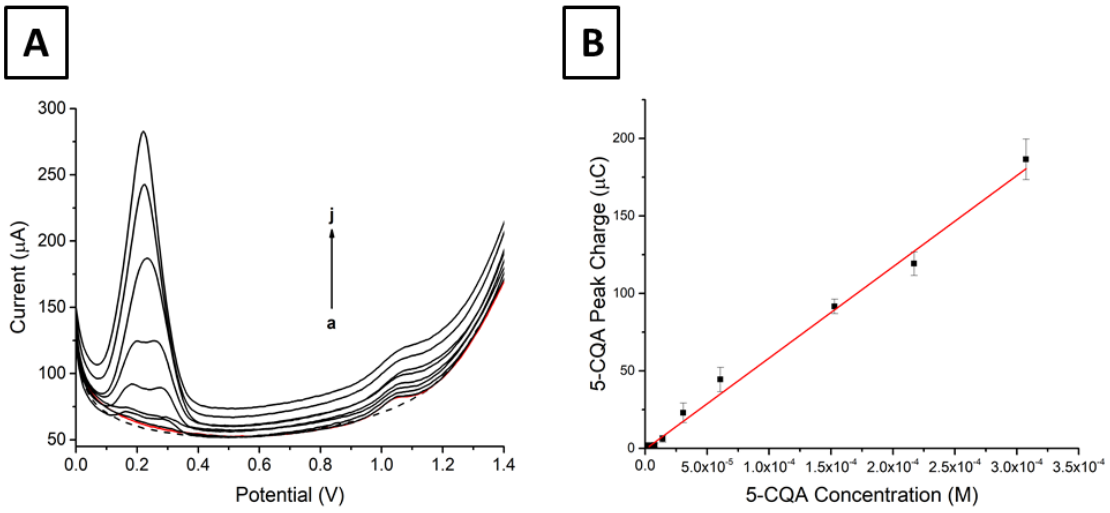

Figure 4.41.The response of the sensor when 5-CQA concentration is changed while that of caffeine is fixed at 3.05×10^{-5} *M. (A) Different SWV voltammograms for both analytes in 0.1 M* H_3PO_4*; pulse amplitude 100 mV and pulse frequency 35 Hz. (a) The supporting electrolyte only. (b) Only* 3.05×10^{-5}*M caffeine and: (c) 5-CQA* 3.07×10^{-6} *M. (d) 5-CQA* 7.65×10^{-6} *M. (e) 5-CQA* 1.42×10^{-5} *M. (f) 5-CQA* 3.07×10^{-5} *M. (g) 5-CQA* 6.07×10^{-5} *M. (h) 5-CQA* 1.53×10^{-5} *M. (i) 5-CQA* 2.17×10^{-4}*M. (j) 5-CQA* 3.07×10^{-4}*M. (B) The calibration curve for 5-CQA; 5 consecutive voltammograms were recorded and the mean values and the standard deviations were employed to plot the graph.*

From Figure 4.41, above, it follows that upon consecutive addition of 5-CQA, a linear signal enhancement together with an increment in the background current were observed.

With regards to caffeine, the peak charge was maintained constant from the absence of 5-CQA to the presence of 10 equivalents of 5-CQA and a relative standard deviation of 4% was calculated. The values are listed in Table 4.15, below.

Table 4.15. The caffeine peak charge in the presence of different equivalents of 5-CQA. Caffeine concentration was kept fixed at $3.05 \times 10^{-5}\ M$*. 5 consecutive SWV voltammograms were recorded and the mean value is presented in the table.*

Number of 5-CQA equivalents	Caffeine peak charge (μC)
0	1.35
0.1	1.41
0.25	1.41
0.5	1.40
1	1.36
2.5	1.45
5	1.29
7	1.30
10	1.45

Subsequently, a similar experiment was performed by keeping the concentration of 5-CQA fixed (3.05×10^{-5}M) while the caffeine concentration was varied from 0 up to 10 equivalents. The resulting voltammograms and the calibration curve constructed are reported in Figure 4.42 on the next page.

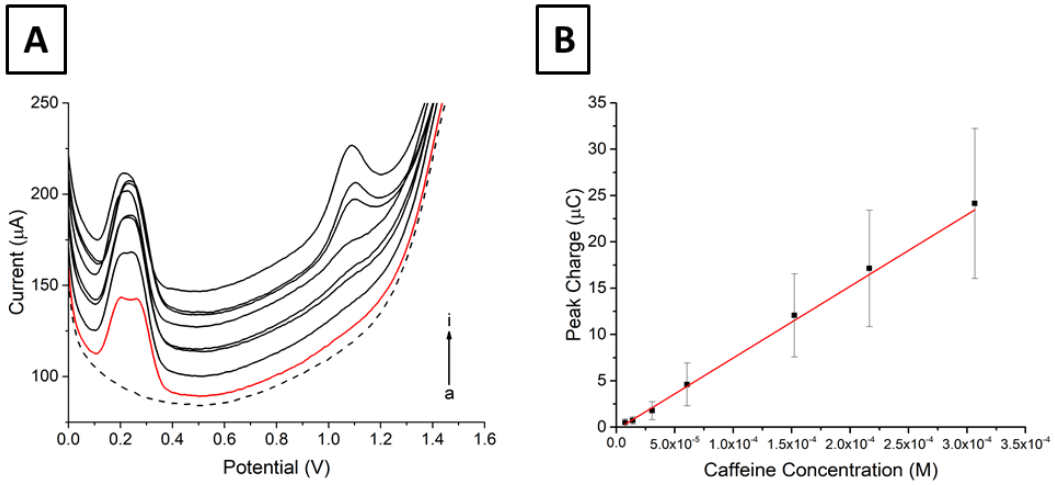

Figure 4.42. The SWV response of the sensor when caffeine concentration is changed while 5-CQA content is fixed at 3.05×10^{-5} *M. Figure A shows the different SW voltammograms recorded in* H_3PO_4 *0.1 M, with pulse amplitude of 100 mV and pulse frequency of 35 Hz. (a) The supporting electrolyte only. (b)* 3.05×10^{-5} *M 5-CQA, (c)* 7.63×10^{-6} *M caffeine (d)* 1.41×10^{-5} *M caffeine (e)* 3.06×10^{-5} *M caffeine (f)* 6.04×10^{-5} *M caffeine, (g)* 1.52×10^{-5} *M caffeine, (h)* 2.16×10^{-4} *M caffeine, (i)*3.06×10^{-4} *M caffeine. (B) The relationship between the caffeine peak charge and its concentration; five consecutive voltammograms were recorded and the mean value as well as the standard deviation were employed to plot the graph.*

From this experiment it follows that the caffeine peak charge varied linearly with the caffeine concentration from 7.63×10^{-6} M to 3.06×10^{-4} M, while the peak current of 5-CQA was insignificantly affected and a relative standard deviation of 7% was calculated.

Table 4.16. The 5-CQA peak charge in the presence of different equivalents of CAF. Caffeine concentration was kept constant at 3.05×10^{-5} *M. 5 consecutive SWV voltammograms were recorded and the mean value is presented in the table.*

Number of caffeine equivalents	5-CQA peak charge (μC)
0	38.79
0.10	44.99
0.25	47.09
0.5	44.84
1	44.48
2.5	44.10
5	42.87
7	40.45
10	37.86

Overall, the SPCE response was linear when the concentration of only one analyte was changed. Besides, thanks to the large peak-to-peak separation (1.0 V), there was no interference between the two signals, even when one analyte was ten times more concentrated. Therefore, these latest experiments provided a strong evidence that the proposed SWV method is appropriate for simultaneous determination of 5-CQA and caffeine, even in solution where one analyte is present in excess, given that no interference was observed.

Subsequently, after having studied the sensitivity of the sensing SPCE platform, the repeatability of the measurements was investigated running consecutive SWV experiments and also using different electrodes of the same batch. A solution containing an equimolar concentration of 5-CQA and caffeine (30.6 µM) was analysed with the same electrode and 23 consecutive SWV voltammograms were recorded. The results are depicted in Figure 4.43, below.

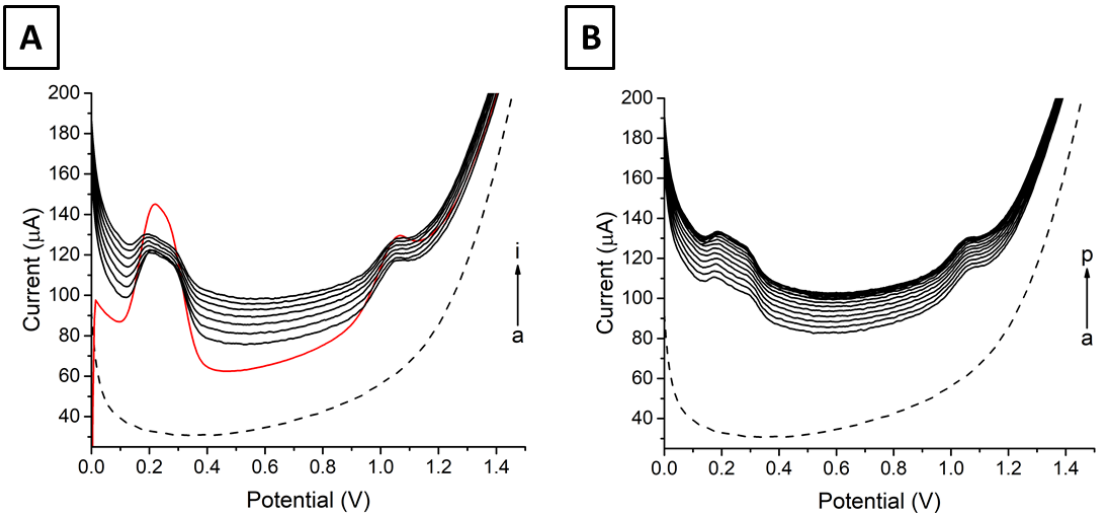

Figure 4.43. Repeatability study. A 30.6 µM equimolar solution of 5-CQA and caffeine was analysed by recording 23 consecutive SWV voltammograms using the optimised instrumental parameters (pulse amplitude 100 mV, pulse frequency 35 Hz). (A) The first eight voltammograms, in red the first voltammogram is indicated. (B) The subsequent 15 voltammograms. The dashed curve is the voltammogram of the pure supporting electrolyte (0.1 M H_3PO_4).

During consecutive voltammograms recording, it was observed that the background current increased from the first voltammograms onwards. On the other hand, the peak currents for both 5-CQA and caffeine decreased significantly between the first scan and those subsequent until a stable value was reached after eight scans. In Figure 4.44, below the decrease in the peak charge with the increase of the number of voltammograms recorded for 5-CQA and caffeine is reported.

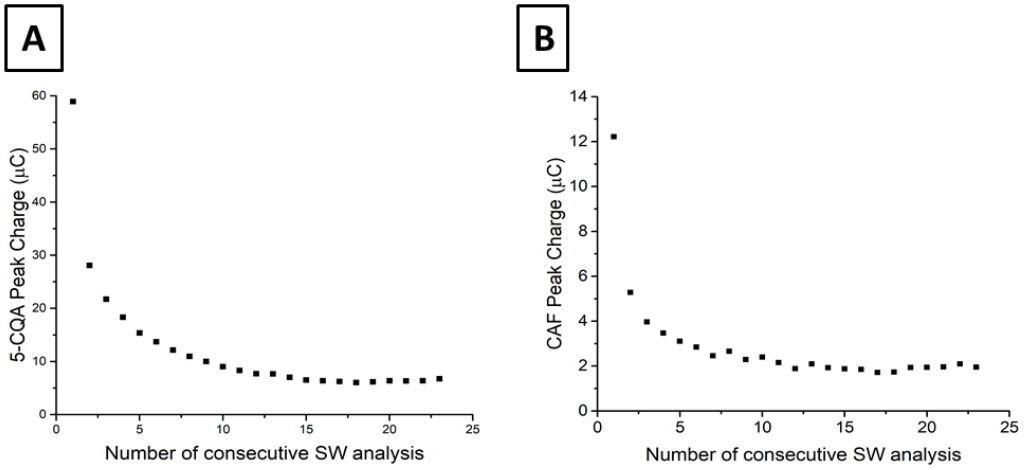

Figure 4.44. (A) The decrease in the peak charge after 23 consecutive SWV scans, for 5-CQA and (B) caffeine. A 30.5 µM equimolar solution of the two analytes was analysed; the instrumental parameters were, as follows (pulse amplitude 100 mV, pulse frequency 35 Hz), 0.1 M H_3PO_4 supporting electrolyte.

A peak current decrease in consecutive scans is usually observed for carbon paste electrodes because of high absorption properties of this material, which lead to a progressive decrease of the analyte concentration in the electrode proximity.[92,93] As a consequence, only the last 15 voltammograms were considered for evaluation of the repeatability since the concentration of analytes is constant. Relative standard deviations of the signal charge of 7% and 6% were calculated for 5-CQA and caffeine, respectively.

Afterwards, the electrode to electrode repeatability was studied, because the previous experience of the research group, where the work was carried out, showed that the electrode-to-electrode repeatability can be an issue with screen-printed electrodes.

Therefore, three electrodes were used and five consecutive SWV voltammograms were recorded for an equimolar solution of 5-CQA and caffeine. In Figure 4.45, below, the third voltammogram for each electrode is reported.

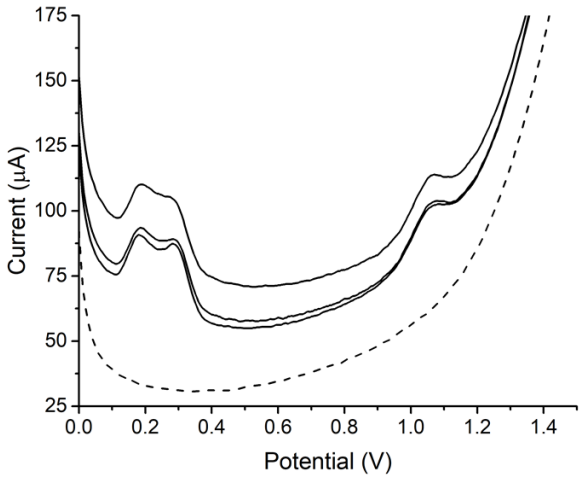

Figure 4.45. The electrode-to-electrode repeatability. An equimolar solution (30.5 µM) of 5-CQA and caffeine in 0.1 M H_3PO_4 was used and five consecutive voltammograms recorded. For all three electrodes, only the third voltammogram recorded is shown. The instrumental settings for the SWV analysis were as follows: pulse amplitude 100 mV, pulse frequency 35 Hz.

From Figure 4.45 above, it follows that the background current changed between different electrodes thus indicating that there was a variation in the properties of the electrode material, possibly linked to the screen printing manufacturing process and different conductivity properties of the final material. Nevertheless, when the peak areas of both 5-CQA and caffeine were calculated, similar values were determined, Table 4.17, below.

Table 4.17. The electrode-to-electrode repeatability. The peak charge for 5 -CQA and caffeine are reported as mean values of 5 consecutive voltammograms of an equimolar solution (30.5 µM) of 5-CQA and caffeine in 0.1 M H_3PO_4. The instrumental settings for the SWV analysis were as follows: pulse amplitude 100 mV, pulse frequency 35 Hz.

	Peak charge of 5-CQA (µC)	Peak charge of caffeine (µC)
Electrode 1	19.88	4.93
Electrode 2	20.03	4.67
Electrode 3	21.69	4.38

Among the three different electrodes employed the relative standard deviation of the signals was 5% for 5-CQA and 6% for caffeine. The above experiment provided evidence that, the measured peak charge for both 5-CQA and caffeine were repeatable, although some electrode-to-electrode variations were observed. Therefore screen-printed electrodes can be employed for accurate determination of both analytes. If the peak charge is used, no differences are expected on the quantification experiments.

To summarise the analytical performance study, the electrode was more sensitive towards the determination of 5-CQA. However, the detection limits for both analytes were found suitable for the determination of caffeine and polyphenols in coffee extract. Besides, the sensor is accurate also for solutions where a non-equimolar concentration of the two target compounds is present. Regarding the electrode-to-electrode repeatability, good results were obtained, with a relative standard deviation of 5-CQA and caffeine signals lower than 10% when three different electrodes were employed. Lastly, in term of repeatability among consecutive measurements, satisfactory results were obtained with a relative standard deviation below 10% for fifteen consecutive measurements.

4.2.2.3 Real samples

The above experiments were performed in solutions containing only the two analytes and suggested that SPCE is a suitable material for simultaneous determination of polyphenols and caffeine in 0.1 M H_3PO_4. However, to evaluate the applicability of the sensing platform, the analysis of a real sample is the crucial step. Therefore, an extensive analysis of different coffee extracts (using both green and roasted beans) and coffee espresso preparations was made. Standard addition method was applied for accurate quantification of both analytes, and the results were compared with those obtained using

an appropriate chromatographic method, performed by a trained employee of illy Caffè S.p.A.

For a coffee producer, it is mandatory to accurately assess the amount of caffeine present in their selling products. In particular, an ISO accredited method is regularly employed for analysis of coffee beans at illy Caffè ensuring high reliability of the results (ISO protocol 20481:2008). According to this protocol, after the sample preparation, the concentration of caffeine is assessed using an HPLC method. Considering that the proposed sensor is faster, simpler and economically more convenient than a chromatographic method, it was decided to compare the two determination methods and evaluate the reliability of the proposed SWV platform. For that purpose, three different blends of coffee were analysed: (i) the idillyum, which is a mixture of coffee beans with a natural lower content in caffeine; (ii) the regular 100% Arabica blend of illy Caffè; (iii) the LVU blend, which is a mixture of beans with a final higher content in caffeine compared to the regular blend. All blends were analysed in duplicate and the sample preparation was performed by a trained employee of illy Caffè to ensure that the ISO protocol was correctly followed. Once the samples were prepared, the content of caffeine was determined using the conventional HPLC method and by the SWV based sensor. The complete experimental details of the electrochemical analysis are reported in the experimental section. The results obtained using the two analytical methods are reported in the Table 4.18.

Table 4.18. Real samples analysis; comparison of the proposed SWV method with the accredited HPLC method for caffeine determination. In the case of the SWV method, the caffeine concentrations are reported as the mean of 5 consecutive measurements and are reported, as follows [mean ± $i_{n-1,\alpha}$ SD/sqrt(n)]; t_4; 0.05 = 2.13. The deviation is reported as percentage ($\frac{SWV\ value - HPLC\ value}{HPLC\ value} \times 100$).

Coffee blend type	Caffeine concentration (mg/L)		Deviation (%)
	SWV method	Accredited HPLC method	
Idillyum	35.42 ± 1.08	29.90	18
	34.70 ± 0.70	29.85	17
Regular	59.48 ± 1.99	59.47	0
	66.08 ± 1.32	57.80	14
LVU	123.89 ± 1.63	114.54	8
	109.77 ± 0.34	102.08	8

From Table 4.18 it can be noticed that the three coffee blends contained a significantly different amount of caffeine, and the proposed SWV method always overestimated the content of caffeine in solution with a deviation between the proposed sensor and the accredited HPLC method below 20%. Nevertheless, the simple and fast electrochemical method precisely discriminated among the three types of coffee blends. Therefore, it can be employed for the caffeine determination with adequate accuracy (deviation < 20%). Interestingly, in all the analysed samples the SWV voltammograms recorded only one signal at 1.10 V for caffeine oxidation and no signals arising from the oxidation of polyphenols were recorded (Figure 4.46). Moreover, a comparative UHPLC analysis confirmed the absence of polyphenols in all six samples. No further studies were done to elucidate why polyphenols were not present. However, the long pre-treatment of the sample in boiling water with MgO may lead to the degradation of 5-CQA and other polyphenols. The square wave voltammograms for each blend type are reported in Figure 4.46.

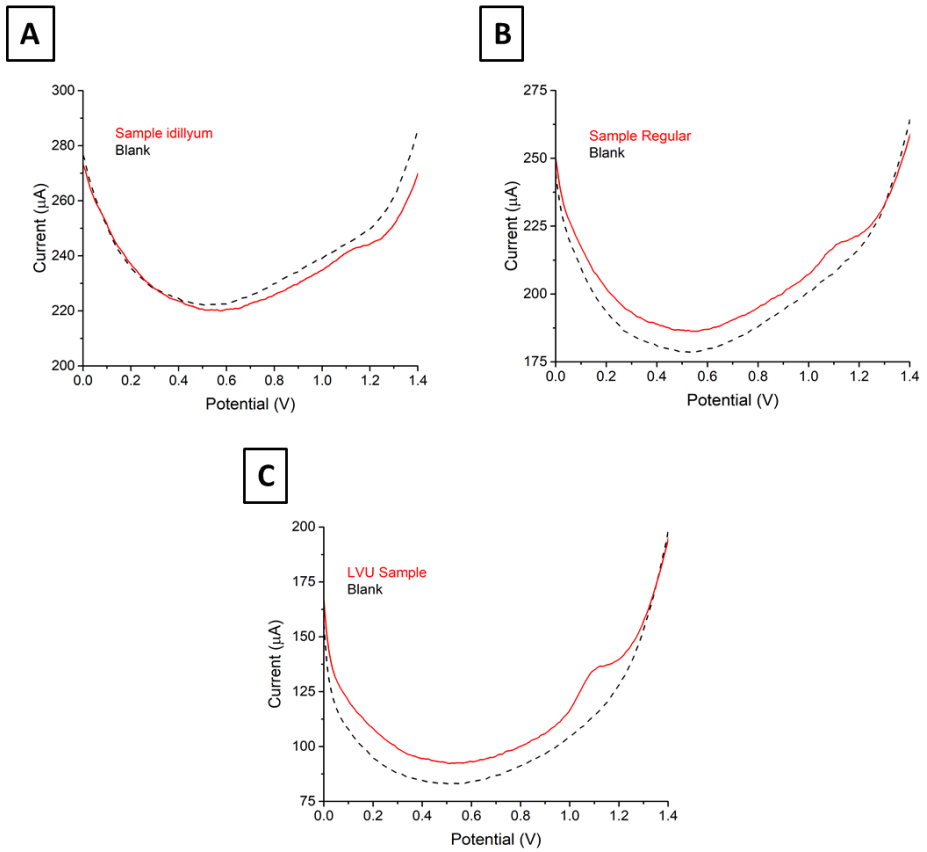

Figure 4.46. Real sample analysis. All analysis were performed using 0.1 M H_3PO_4 as the supporting electrolyte under the optimised conditions (pulse amplitude 100 mV, pulse frequency 35 Hz);, and the voltammogram for the pure supporting electrolyte is shown as a black dashed curve. (A) The SWV voltammogram for the idyllium sample. (B) The SWV voltammogram for a regular sample. (C) The SWV voltammogram for the LVU sample.

From the voltammograms shown in Figure 4.46, above, it can be observed that the measured currents were different in the case of the three samples since three different SPCE electrodes were employed, and this observation agrees with the electrode-to-electrode repeatability studies (Figure 4.45). Nevertheless, a clear peak at 1.1 V was clearly identified in all cases and by using the standard addition method the different electrode-to-electrode performance did not affect the accurate quantification of caffeine.

Subsequently, it was decided to assess the ability of the electrochemical sensor to determine the content of polyphenols and caffeine in espresso brews. Two different blends of coffee were employed, the illy espresso and the illy idillyum espresso and for both blends the regular espresso and the espresso *lungo* were prepared according to the

procedure reported by Ferrari M. *et al.* [94]. In the case of the espresso coffee both the signal of polyphenols and caffeine oxidation were recorded, and no further peaks were observed in the potential range scanned (from 0 to 1.4 V). The SW voltammograms are reported in the figure below.

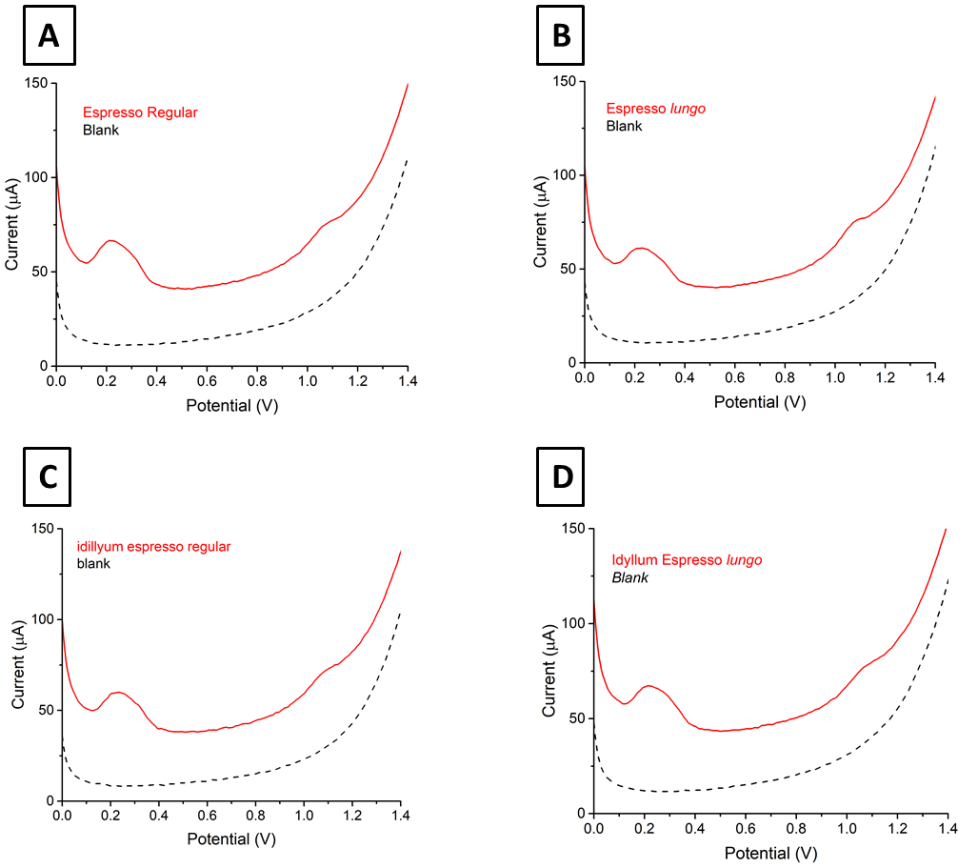

Figure 4.47. Real sample analysis. All analysis were performed using 0.1 M H_3PO_4 as the supporting electrolyte using the optimised conditions (pulse amplitude 100 mV, pulse frequency 35 Hz). The voltammogram of the pure supporting electrolyte is shown in black dashed curve. All samples were diluted 10 times with distilled water before being analysed. (A) The SWV voltammogram for regular espresso. (B) The SWV voltammogram for the lungo espresso. (C) The SWV voltammogram for idillyum regular espresso. (D) The SWV voltammogram of idillyum lungo espresso.

Using the standard addition method, the total content of polyphenols and the concentration of caffeine was assessed, and the results obtained are listed in table 4.19. As comparative method a UHPLC based protocol regularly employed at illy caffè for coffee espresso analysis was used.

Table 4.19.Real sample analysis, coffee espresso brews. The total content of polyphenol is reported as grams equivalent of 5-CQA both for the SWV and UHPLC method. The content values are reported as mean of 5 consecutive measurements according and are reported as follows [mean ± tn-1,α SD/sqrt(n)]; $t_{4;\,0.05}$ = 2.13. The deviation is reported as percentage($\frac{SWV\ value - HPLC\ value}{HPLC\ value} \times 100$).

Sample	Polyphenols ($g_{5\text{-CQA eq}}$/L)		Deviation (%)	Caffeine (g/L)		Deviation (%)
	SWV method	UHPLC method		SWV method	UHPLC method	
Espresso regular	3.63 ± 0.07	2.69	35	3.02 ± 0.01	3.11	-3
Espresso *lungo*	2.92 ± 0.06	2.23	31	2.40 ± 0.01	2.62	-10
Idillyum Espresso regular	3.21 ± 0.05	2.95	9	1.52 ± 0.09	1.54	-2
Idillyum espresso *lungo*	2.75 ± 0.07	2.72	1	1.38 ±0.10	1.42	-3

Regarding the determination of caffeine content, excellent results were achieved for all the four brews and a good agreement between the UHPLC and the proposed SWV methods was observed (deviation < 10%). The analysis of the total content of the polyphenols showed an over-estimation in all cases, especially for the illy regular blend. This overestimation may be linked to an intrinsic difference between the two samples as well as to a low accuracy of the electrochemical sensor in the determination of polyphenols. As explained in the introduction, roasted coffee beans contains a plethora of polyphenolic compounds which can contribute to the electrochemical signal. On the other hand, the comparative method employed was optimised to quantify only the isomers of caffeoyl-, feruloyl- and dicaffeoyl-quinic acids, and some minor polyphenols are not detected. As a consequence, the chromatographic method provides a more detailed picture of the total polyphenol content in the case of green beans, where the degradation due to the roasting process has not occurred. Therefore, to assess if either the disagreement between the chromatographic and electrochemical methods was linked to the wide variety of polyphenolic compound present in roasted coffee or to the low

accuracy of the sensor, the analysis of green coffee beans was performed. Both Arabica and Robusta green beans were analysed as described in the material and method section, and the results are listed in the Table 4.20 below.

Table 4.20. Real sample analysis, green coffee beans extract. The concentrations are reported as mg of analyte per g of green coffee beans. The content of polyphenol is presented as milligrams equivalent of 5-CQA both for the SWV and UHPLC method. The deviation is reported as percentage($\frac{SWV\ value - HPLC\ value}{HPLC\ value} \times 100$*).*

Sample	Polyphenols concentration (mg/g)		Deviation (%)	Caffeine concentration (mg/g)		Deviation (%)
	SWV method	UHPLC method		SWV method	UHPLC method	
Arabica 1	58.26 ± 2.24	60.07	-3	6.84 ± 0.10	10.42	-44
Arabica 2	50.60 ± 3.10	57.06	-11	6.00 ± 0.36	9.74	-48
Robusta	73.85 ± 1.62	78.42	-6	8.79 ± 0.58	18.01	-51

The analysis of three green coffee extracts showed a higher agreement between the electrochemical and chromatographic method with regards to the quantification of the total polyphenols content. In fact, in green beans the majority of polyphenols present are chlorogenic acids and both analytical methods were developed for the quantification of this class of compounds. The finding proved the reliability of the sensor for accurate quantification of the total polyphenols content in green beans and supports the hypothesis that the disagreement found in the case of espresso brews is linked to the complexity and varieties of polyphenolic compound present. With regards to the quantification of caffeine, the electrochemical method was found to underestimate the caffeine content in comparison with UHPLC analysis. Previously published work also showed that the content of caffeine in green arabica beans should be about 1% (w/w) and for Robusta beans should be 2% (w/w), as found with the chromatographic method. However,

although non-accurate analysis on caffeine content were obtained a clear difference between Arabica and Robusta was still observed with the electrochemical sensor. In the Figure 4.48, the voltammograms of the three samples analysed are reported.

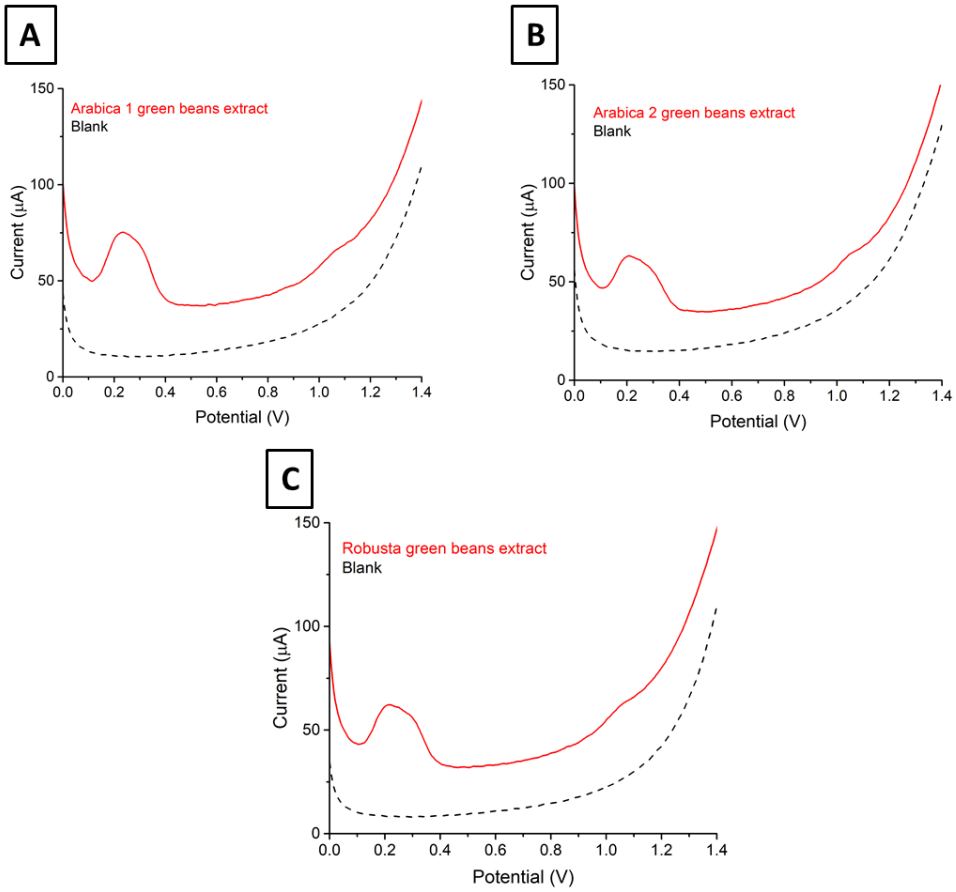

Figure 4.48. Real Sample analysis, green coffee extract. All analysis were performed using 0.1 M H_3PO_4 as the supporting electrolyte under the optimised conditions (pulse amplitude 100 mV, pulse frequency 35 Hz), and the voltammogram of the pure supporting electrolyte is shown in black dash line. (A) The SWV voltammogram of Arabica coffee beans extract. (B) The SWV voltammogram of a second Arabica coffee bean extract. (C) The SWV voltammogram of a Robusta coffee extract.

To summarise the real samples analysis, three types of samples were analysed: (i) 6 samples of roasted beans prepared according to the accredited method for caffeine determination; (ii) 4 different espresso brews; (iii) 3 green bean coffee extracts. The analysis following the accredited method and the analysis of coffee brews, showed that the proposed electrochemical sensor provides accurate analysis of caffeine content and therefore is a valid, simple and cost-effective alternative to chromatographic method for

the analysis of roasted beans and espresso brews. In the case of green coffee extract, imprecise values on caffeine concentration were obtained, probably due to the low concentration in the sample. With regards to the evaluation of the total polyphenols content excellent results were obtained with the green coffee beans and espresso brew, although in this case an adequate comparative method was not found.

4.2.3 Conclusion and future work

An accurate, cost-effective and straightforward electrochemical sensor based on bare screen-printed carbon electrode (SPCE) was developed for the simultaneous determination of the total polyphenols content and caffeine concentration. Different supporting electrolytes were evaluated and the best results were achieved using 0.1 M H_3PO_4. The instrumental setting for both DPV and SWV methods were optimised and SWV was selected as more appropriate analytical method for fast analysis. The calibration curves were constructed and the sensor was found to be more sensitive towards the determination of 5-CQA however for both analytes the calibration curve showed good linearity, linear range and LOD in the µM range for both molecules. In addition, SPCE provides precise analysis (relative standard deviation < 10%) and the electrode-to-electrode repeatability was found satisfactory. The applicability of the sensor was established by analysing 13 samples of green and roasted beans extract and espresso brews; the electrochemical sensor provided accurate analysis of the total polyphenols content in all the samples analysed, and precise caffeine concentration for roasted beans and espresso samples; while an underestimation was found in the case of green beans extract. The overall excellent results achieved demonstrate that the developed SPCE sensor is a simple and cost-effective alternative to chromatographic method for accurate determination of caffeine and total polyphenols content. In order to further evaluate the reliability of the sensor for polyphenols analysis in espresso brews,

a different comparative method should be employed for example the Folin-Ciocalteau colourimetric assay[95,96]. In fact this latest method, like the electrochemical sensor developed, is designed for the total polyphenols content determination. Given the complexity and variety of polyphenolic compounds present in the roasted beans, an exhaustive analysis of the total polyphenol content is not easy to be achieved with only chromatographic methods, and different analytical assays should be compared. However, during my placement at illy Caffè, the Folin-Ciocalteau was not investigated, but the scientific interest was turned to sucrose, and the applicability of an amperometric biosensor for the analysis of sucrose content in green coffee beans was studied, and is reported in the following section.

4.3 Sucrose in green coffee beans

4.3.1 Introduction

The characteristic aroma and appealing flavour of a coffee cup arise from the combination of more than 1000 volatile compounds which are formed during the roasting process, from more complex starting reagents, which are called aroma precursors and among them sucrose plays a crucial role.[97]

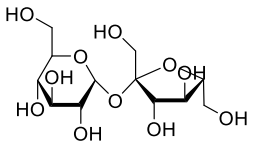

Scheme 4.10. Structural formula of sucrose, one of the main flavour precursor in coffee.

Sucrose represents more than 90% of the total content of free sugars present in green coffee beans and during roasting is completely consumed through two main reactions, caramelisation and the Maillard reaction. The products obtained are a plethora of furans, ketones, aldehydes and phenols which are responsible for the flavour, aroma and colour of the final coffee brew. The amount of sugars present in coffee beans is affected by

many factors such plant species, ripening state, local climate and soil composition. A wide difference in sucrose content between Robusta and Arabica was observed with the latter containing a concentration two times higher.[98–100] When non-commercially available coffee species are considered the spectra of sucrose content can vary from 4 to 10 % (w/w based), as accurately studied by Campa C. *et al*[101]. Two recent publications have also demonstrated that the concentration of sucrose in the beans is directly related to the ripening of coffee cherries with more mature fruits leading to higher sucrose content beans.[102,103] In addition, local climate, soil composition and storage conditions may affect the concentration of sugars. However, definitive and conclusive studies have not yet been performed.[104] Interestingly, sucrose content in green beans has been identified as a direct marker of the bean quality since the higher content of sucrose leads to a final cup of coffee richer in flavour and aroma.[100,102] Considering that several factors can affect the quality of coffee beans and sucrose content, coffee roasters must assess the quality of beans thanks to the judgement of professional tasters before buying the product. Nevertheless, the development of simple and cost-effective analytical instruments to scientifically evaluate coffee bean quality is highly desirable since they can provide an objective result and reduce the subjective human error. A recent collaboration between illy Caffè and Biorealis has brought about the development of a fast and straightforward amperometric biosensor for sucrose monitoring in green coffee bean.[105] The study proved that the biosensor is a simpler, faster and more cost-effective alternative to the HPLC method for accurate and precise measurement of sucrose content in green coffee beans. The applicability of the biosensor was already proved for Arabica, Robusta and Liberica coffee beans, however illy caffè showed a keen interest in further exploring the applicability of the sensor and determine the concentration of sugars in commercially non-available coffee species. In addition a blind test was done to assess

whether the biosensor can be applied to discriminate between Arabica and Robusta. Finally, the effect on sucrose level of different drying methods was investigated, and all these results are presented hereafter as a merged result and discussion section.

4.3.2 Results and discussion

To explore the wide variability of sucrose in different coffee species and investigate the applicability of the biosensor for non commercially available coffee varieties, nine different coffee samples were analysed, including the two most traded (Arabica and Robusta) and seven wild coffee species. One coffee sample for each species was analysed in triplicate and the mean value and standard deviation are presented in the graph below.

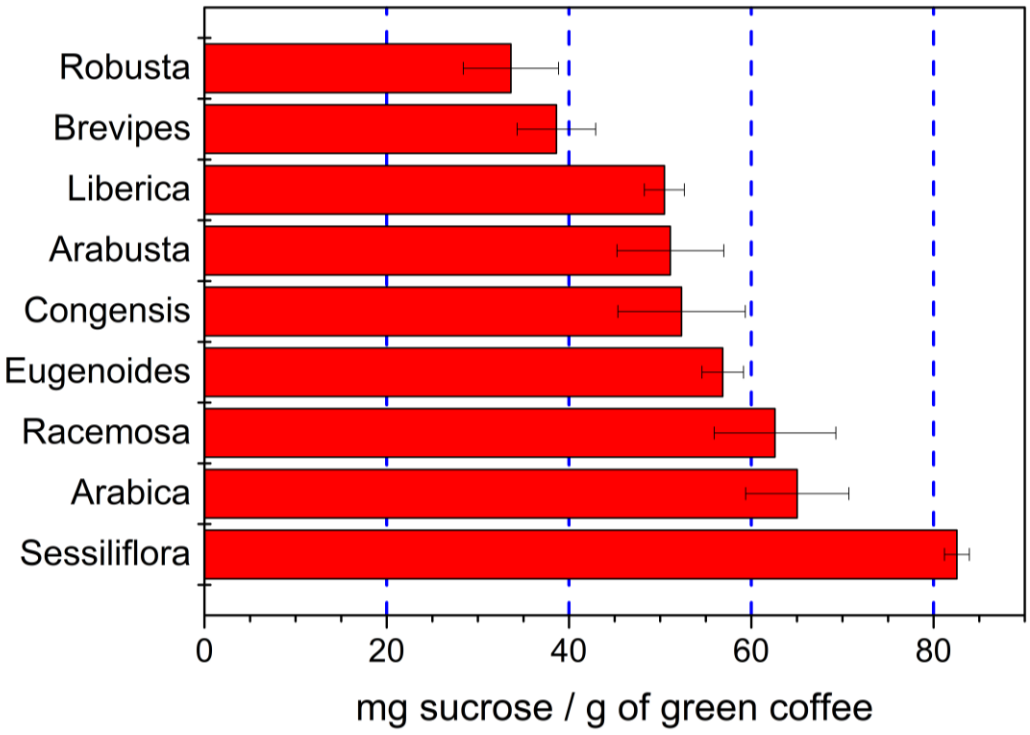

Figure 4.49. Bar diagram of the sucrose content in different coffee species. One sample of each species was analysed in triplicate and the mean values with the standard deviation (error bar) are reported.

The content of sucrose in the green beans analysed was found to vary significantly among different species, with Robusta containing the lowest amount (3.5% w/w) and

Coffea Sessiliflora having more the double the content (8.2% w/w). To investigate the interspecies variability accurately, different samples from several trees of the same species should be considered, moreover the origin, cultivation method and post-harvesting procedures should also be as similar as possible to limit the factors affecting sucrose concentration. However, the results reported in Figure 4.49 are in good agreement with a previous study of Campa C. *et al.* who reported the data corrected for the beans moisture level and therefore slightly higher percentage of sucrose were obtained[101]. Nevertheless, the results in Figure 4.49 suggested that the small and portable amperometric biosensor has wide applicability and can also be applied for non-commercially available coffee beans.

Subsequently, given the significant difference in sucrose content between Arabica and Robusta, a blind test employing 14 grounded coffee beans from different origin was done and based on the sucrose content a discrimination between the two species was done (data reported in the Figure 4.50, below).

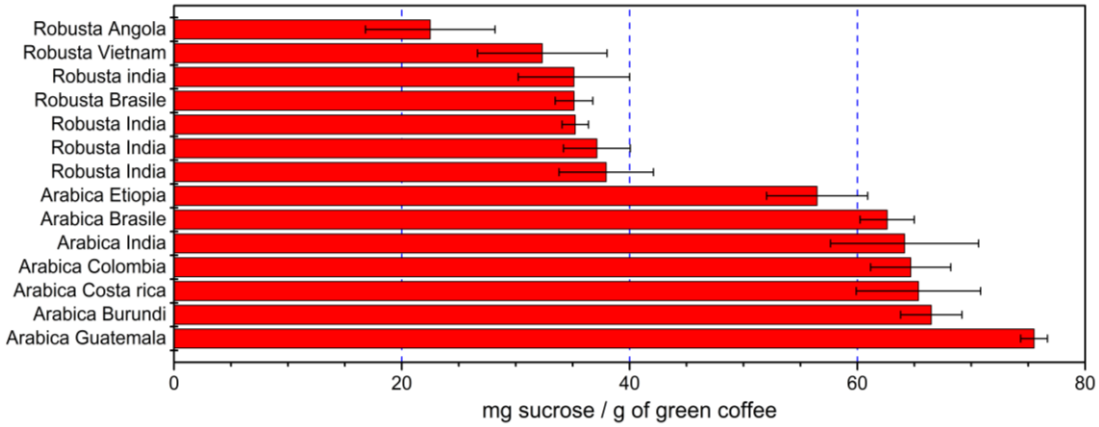

Figure 4.50. Sucrose content analysis on seven Arabica and seven Robusta coffee beans with different origins. All samples were analysed in triplicate and the mean value is reported together with the standard deviation as error bar.

From Figure 4.50, it follows that the intra-species variability is present with a relative standard deviation of 15% for Robusta and 9% in the case of Arabica, which can be

linked to different factors (such as moisture content, ripening state, origin and cultivation techniques). However, even considering the intra-species variability and the error associated with the measurement, a clear difference in sucrose content between Arabica and Robusta was observed and therefore the simple, fast and portable biosensor can be applied for accurate discrimination between the two commercially available species which is a crucial step for coffee roasters like illy that sells only 100% Arabica products.

Subsequently, considering the different factors that influence the quality of coffee beans, there is a scientific and economic interest in optimising all production stages from plantation to the brewing. In particular, it was decided to investigate the effects of different drying procedures on the final sucrose content of Arabica green beans from Brazil. When coffee cherries are harvested, the subsequent step is to dry them from a moisture content of 60% to 12% to be transported to the sellers without mould formation. Two main drying procedure can be used, the dry and wet method. In the dry method coffee cherries are harvest in an advanced mature state, and after being cleaned to eliminate any unwanted material such as leaves and branches, the whole cherry is left to dry naturally under the sun or artificially. The procedure is simple and straightforward, however since low care is taken during the harvesting and selection of ripe cherries the final coffee is usually of less quality. On the other hand, in the case of the wet method the cherries are individually harvested only when mature; subsequently, they are washed to eliminate any impurities and low-quality fruits. The selected cherries are then mechanically depulped and then the beans are subject to underwater-fermentation to remove the mucilage present. The fermentation process occurs naturally thanks to the presence of enzymes in the mucilage itself and it lasts 72 h. After this stage, the beans are washed again and finally dried naturally or artificially. A schematic summary and comparison of the two drying methodologies is presented in Figure 4.51, below.

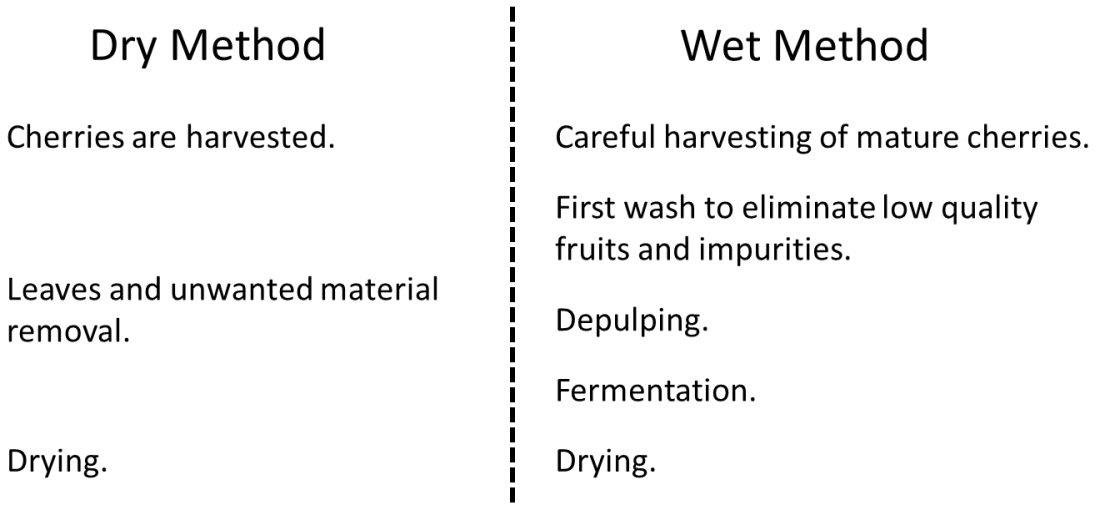

Figure 4.51.The comparison between two different post-harvesting procedures, the dry method and wet method.

The wet procedure leads to a higher quality coffee however it requires a higher amount of water to be performed and cannot be carried out in regions where water is not abundant. A recent study of Knopp S. *et al.* demonstrated that the dry and wet post-harvesting methodologies do not influence the content of sucrose in the final green coffee beans but the concentration of smaller carbohydrates such as glucose and fructose is reduced ten times when the wet procedure is employed.[106] illy Caffè is continuously investigating on improving coffee quality, and as part of this process also the drying methodologies are studied. In particular, during my placement, four different drying methods were investigated. Dry method 1 was done by taking the mature cherries and drying them under the sun (typical dry method). In the case of dry method 2, the cherries were immersed in water and only the floating cherries were selected and further processed. In the case of the two wet protocols, in 1 the mucilage is removed after the beans were desiccated while wet method 2 is the typical washed method that is described above (Figure 4.51). As part of the assessment of the coffee quality also the content of sucrose was determined and the results are reported in the Figure 4.52.

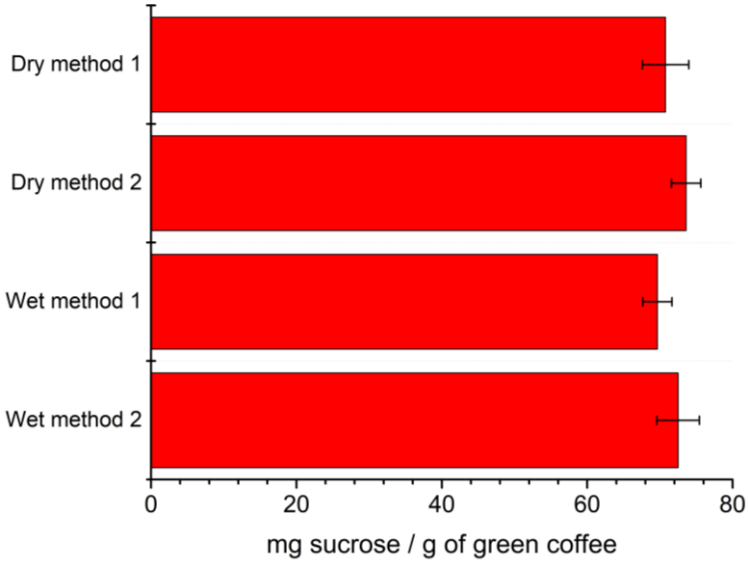

Figure 4.52. Effects of different drying methods on the sucrose content in green coffee beans. For each method three samples were analysed and the mean value was considered (the error bars represent the standard deviation measured).

From the data above, it can be observed that the different drying methods employed did not affect the final content of sucrose in the green beans, since the inter-samples deviation in concentration (4 mg/g of green coffee) is smaller than the intrasample deviation. Coffee quality is given by a combination of different compounds and therefore to conclude whether the drying protocols applied influenced the quality of the final brew a complete sensorial analysis has to be performed.

4.3.3 Conclusion

In conclusion, a more detailed investigation on the applicability of the omnilab sucrose biosensor for sucrose analysis in green coffee was done. This simple and portable device was found to be applicable not only to the most common coffee beans (Arabica and Robusta) but also for non-commercially available species. In addition, thanks to the wide difference in sucrose content between Arabica and Robusta the sensor can be used for accurate discrimination between these two species. Finally, the sensor provides an accurate and objective parameter to judge the quality of coffee beans and is helpful during the optimisation process of green beans quality.

4.4 Chapter conclusion and future work

In this chapter the applicability of fast, cost-effective and straightforward methods for the determination of caffeine, polyphenols and sucrose in different coffee preparations was described. All the sensing platforms were based on electrochemical methodologies, and were found to provide excellent results in terms of accuracy and simplicity of the assay. The applicability of electrochemical methods for coffee products analysis can be further explored thanks to the different screen-printed electrodes commercially available. In fact, different electrode material (carbon-paste, gold, platinum, boron doped diamond) are commercialised both as bare and modified electrodes with different modifiers (such as carbon nanotubes, graphene, graphene oxide, nanoparticles). The evaluation of the performance of different electrode material can help the identification of the most convenient material for the analysis of caffeinated products. In addition, the identification of a more sensitive electrochemical sensor for caffeine analysis will enlarge the applicability of the sensing platform to decaffeinated products (in which caffeine has been reduced to <1% of the initial content). Finally, studying the concentration of caffeine in biological samples (blood, urine and saliva) is also an appealing objective since the enzyme responsible for the metabolism of caffeine (CYP1A2) is also responsible for the metabolism of many marked drugs; among them common psychotics, antidepressant, no steroidal anti-inflammatory and cardiovascular drugs.[107,108] Interesting activity of this enzyme is strongly affected by external factors such as smoking, alcohol-drinking, diet, physical activity[109] which lead to an inter-individual variability up to 60 fold.[110] Recent studies proved that the metabolism of caffeine can be used as a safe probe to investigate the individual activity of CYP1A2.[111–114] Given the wide scientific attention in personalised medicine[115,116] and in studying the individual activity of enzymes involved in the clearance of drugs, the development of

simple and sensitive sensors for caffeine analysis in biological samples is of great economic and scientific interest.

4.5 Materials and methods

4.5.1 Chemicals and reagents

Caffeine, theophylline, theobromine, paraxanthine, glucose, sucrose, 5-caffeoylquinic acid, formic acid and acetonitrile were purchased from Sigma Aldrich with analytical grade purity. Double distilled water with resistivity above 18 MΩcm was employed in all experiments. Sulfuric acid (ACS reagent, 95.0-98.0%), nitric acid (ACS reagent, ≥ 69%), perchloric acid (ACS reagent, 70%) and orthophosphoric acid (ACS reagent, 85%) were tested as supporting electrolytes. Caffeine containing beverages (Coca-Cola, Pepsi-Cola, Red-Bull, Kofola) were purchased from the local store. Coffee samples were prepared by using medium roasting degree coffee (100% Coffea arabica L. blend, or idillyum blend) Iperespresso capsule (illycaffè S.p.A., Trieste, Italy). Green and roasted coffee beans from different origins and coffee species, were available at illy caffè S.p.A. and stored in plastic bags in dark environment at room temperature. Whatman filter paper, Grade 2W was employed for filtration and was purchased from VWR (Italy). Phenex NY 0.2 µm filters (Phenomenex, Italy) were employed to filter solutions before UHPLC analysis.

4.5.2 Apparatus

For caffeine determination using bare glassy carbon electrode, all electrochemical measurements were conducted in a three-electrode single compartment glass cell using Ag/AgCl (3 M KCl) as reference electrode, platinum as counter electrode and bare glassy carbon electrode (GCE, MetrohmAutolab B.V., The Netherlands) with 2 mm active surface area as working electrode. The experiments were performed using a small electrochemical analyser 910 PSTATmini (MetrohmAutolab B.V., The Netherlands).

The data were collected, handled and analysed using the PSTAT 1.0 (MetrohmAutolab B.V., The Netherlands) and OriginPro 7.5 (OriginLab Corporation, USA) software, respectively. In the case of the simultaneous determination of caffeine and polyphenol the μStat 400 potentiostat (Methrohm S.p.A. Italy) was employed in combination with the screen-printed carbon electrodes (DRP-110) (Dropsense Spain). A single drop of supporting electrolyte (100μL) over the three electrodes was employed to perform the experiments. The potentiostat was controlled using Dropview software (Dropsense Spain) and the obtained voltammograms were analysed using the same software and OriginPro 7.5 (OriginLab Corporation, USA). The Ominilab MINOR (Biorealis Ltd Slovakia) was employed for the measurement of sucrose content. The kit for sucrose analysis was purchased from Biorealis Ltd and included the disposable electrodes and mono-use reagent-mixture containing the supporting electrolyte and mediator for the analysis. For grounding green coffee beans and roasted beans, the mixer Mill MM 200 (Retsch GmbH Germany) was employed. For espresso preparation, Iperespresso coffee machine mod. X2 was employed (illycaffè S.p.A., Italy). The USC100TH ultrasonic bath (VWR, United Kingdom) was used for degassing when required. The Sorvall ST 8R Small Benchtop Centrifuge (Fisher Scientific, Italy) was employed for centrifugation of samples. Gilson micropipette (Gilson Inc Italy) were employed for the addition of volume ≤ 1mL, while for greater volumes glass pipettes were employed. Ultra High Performance Liquid Chromatography (UHPLC) was performed using a 1290 Infinity LC system with DAD detector, equipped with a 4.6 mm × 150 mm, 2.7 μm 120 SB-C18 Poroshell column. High Performance Liquid Chromatography (HPLC) was performed using a 1220 Infinity II LC system with DAD detector, equipped with a 4.6 mm × 150 mm, 2.7 μm 120 SB-C18 Poroshell column. For the analysis of the chromatograms LC Open lab was used (Agilent Technologies, Waldbronn, Germany).

4.5.3 Sample preparation

Espresso brews

Espresso brews coffee were prepared using illy iperespresso capsules and the X2 Iperespresso coffee machine with tap water (total hardness 18-20°f) according to the typical Italian cup volume known as *ristretto*, regular or *lungo*[94]. The samples were diluted ten times with distilled water before performing the analysis.

Green coffee extract for caffeine and polyphenols simultaneous analysis

Green beans were grounded using a ball mill with a frequency of 30 Hz for 30 seconds. 1 g of the obtained powder was dispersed in 100 mL of boiling distilled water in glass beakers. After 5 minutes the sample was centrifuged at 3,800 rpm for 5 min at 10 °C and filtered through filter paper to obtain a clear pale green solution.

Green coffee extract for sucrose analysis

Approximately, 20 green coffee beans were grounded using a ball mill at 30 Hz for 30 seconds. 0.50 g of the fine powder obtained was mixed with 10 mL of boiling distilled water in a plastic vial, and manually shaken for a couple of minutes. Subsequently, the mixture was let cooling to room temperature and the solid phase naturally deposit. The obtained clear green supernatant was analysed for sucrose determination.

Roasted coffee extract for caffeine analysis

The roasted coffee samples were prepared according to the ISO protocol 20481:2008 (https://www.iso.org/obp/ui/#iso:std:iso:20481:ed-1:v2:en). The sample preparation was performed by a qualified employee of illy caffè.

Caffeine analysis on soft and energy drinks

For carbonated soft drinks (i.e. Coca-Cola, Pepsi-Cola, Kofola, Red Bull) the samples were degassed for 3 minutes before analysis, using ultrasonic bath.

4.5.4 Electrochemical Measurements

Measurement procedures for caffeine determination using bare glassy carbon

Cyclic voltammetry (CV), differential pulse voltammetry (DPV) and Square Wave Voltammetry (SWV) techniques were used to study the electrochemical behaviour of caffeine and its reliable determination as well as for real sample analysis. In the case of Glassy Carbon, to get the active surface area clean, the standard procedure based on polishing with alumina (average grain size of 0.3 μm) was performed followed by electrochemical preconditioning of the electrode at +2.0 V for 30 s, before launching a measurement. To select the appropriate supporting electrolyte for caffeine sensing, three different inorganic acids in a concentration range from 0.01 up to 0.5 M were tested, including H_2SO_4, HNO_3 and $HClO_4$, with a fixed caffeine concentration of 5.46×10^{-4} M. Three consecutive cyclic voltammograms were recorded each time and the third measurement was the one used for comparison.

Different electrochemical pre-treatment were employed to study the effect on caffeine oxidation signal. A 5.46×10^{-4} M caffeine solution in 0.1 M H_2SO_4 was employed and the following pretreatmnet potentials were evaluated (+2, +1.75, +1, -2 V) for different lapses time (from 15 to 60 seconds).

The repeatability of the measurement was evaluated running 5 consecutive CVs, and a 1.25 mM caffeine solution in 0.1 M H_2SO_4.

For the optimisation of the DPV parameters, the pulse potential, pulse time and scan rate were investigated from 10 to 200 mV, from 5 to 150 ms and from 2 to 30 mV/s, respectively. In the case of SWV a range of pulse amplitude from 10 mV to 150 mV and pulse frequency from 1 Hz to 50 Hz were investigated for instrumental optimisation. A calibration curve was built by subsequent additions of an appropriate volume of caffeine stock solution (10 mM, in distilled water) in the electrochemical cell where 20 mL of

H_2SO_4 0.1 M were present as supporting electrolyte. The caffeine concentration range evaluated was from 3 to2725 μM, and for each addition three consecutive DPV or SWV experiments were done, and the mean value was considered.

Real samples analysis using glassy carbon

All samples were analysed without any previous filtration steps. The DPV measurements were performed in an electrochemical cell where 20 mL of supporting electrolyte were present and an appropriate volume of the particular beverage was added, i.e. four mL for soft drinks (Coca-Cola, Pepsi-Cola, Kofola), 1mL for Red-Bull, and 0.2 mL in the case of espresso brews. The content of caffeine was determined using standard addition method, by three consecutive additions of 0.8 mL of a standard stock solution of caffeine (10 mM in distilled water). After each addition five consecutive DP voltammograms were recorded and the mean signal intensities considered.

Measurement procedures for the simultaneous determination of polyphenols and caffeine.

CV was employed for the screening of the optimal supporting electrolyte, acetate buffer (pH 5), citric acid, sulfuric acid and orthophosphoric acid were evaluated and a range of concentrations from 0.01M up to 1 M was considered. In all cases a 4.06×10^{-4}M equimolar solution of the two analytes was employed and three consecutive voltammograms were performed using a scan rate of 100mV/s, the mean peak intensities were then considered. For each supporting electrolyte a new screen-printed carbon paste electrode was employed. H_3PO_4 0.1 M was selected as supporting electrolyte and used throughout all the following experiments.

The optimisation of DPV involved the searching of optimal pulse amplitude, pulse time and scan rate, while in the case of SWV the optimisation of pulse amplitude and frequency was done. The range for each instrumental parameter and the optimal value

for the simultaneous determination of 5-CQA and caffeine are reported in the following table.

Table 4.21. Instrumental settings optimisation for DPV and SWV analysis of 5-CQA and caffeine.

	DPV			SWV	
	Pulse amplitude (mV)	Pulse duration (ms)	Scan rate (mV/s)	Pulse amplitude (mV)	Pulse frequency (Hz)
Studied range	25 – 250	2.5 – 50	5 – 40	10 – 150	5 – 75
Optimal value	200	10	10	100	35

For the optimisation experiments a 2.34×10^{-4} M equimolar solution of the two analytes was employed three consecutive voltammograms recorded, and the mean value was considered for comparison. For the calibration curves a stock equimolar solution of the two analytes (2.81 mM in 0.1 M H_3PO_4) was prepared and from this solution, the following diluted stock solutions were prepared in 0.1 M H_3PO_4: $2.81 \times 10^{-4} M$, $2.81 \times 10^{-5} M$, $2.81 \times 10^{-6} M$. A 100 µL drop of 0.1 M H_3PO_4 was placed on the electrode, an aliquot of the stock solution added and the obtained drop was gently stirred with the tip of a Gilson micropipette. Prior to this using a different stock solution the electrode was washed with distilled water, gently dried with some lab paper and a new drop of only supporting electrolyte was deposited on the electrode active area. The aliquots of stock solution added and the concentration range evaluated for the calibration curve is reported in the following table.

Table 4.22. Calibration curve study. The amount of stock solution added and the concentration range investigated.

Stock solution (M)	Volume added (µL)	Final concentration (M)
2.81×10^{-6}	70	5.79×10^{-7}
2.81×10^{-6}	120	9.21×10^{-7}
2.81×10^{-5}	10	1.28×10^{-6}
2.81×10^{-5}	20	3.24×10^{-6}
2.81×10^{-5}	20	4.69×10^{-6}
2.81×10^{-5}	60	7.36×10^{-6}
2.81×10^{-5}	80	9.21×10^{-6}
2.81×10^{-4}	10	1.28×10^{-5}
2.81×10^{-4}	20	3.24×10^{-5}
2.81×10^{-4}	20	4.69×10^{-5}
2.81×10^{-4}	40	6.66×10^{-5}
2.81×10^{-4}	80	8.85×10^{-5}
2.81×10^{-3}	10	1.28×10^{-4}
2.81×10^{-3}	10	2.34×10^{-4}
2.81×10^{-3}	10	3.24×10^{-4}
2.81×10^{-3}	20	4.69×10^{-4}
2.81×10^{-3}	40	6.66×10^{-4}
2.81×10^{-3}	80	8.85×10^{-4}

Three consecutive SWVs were recorded and the mean value and standard deviation were employed to draw the calibration graphs. To evaluate the influence of one analyte over the other, stock solutions of caffeine (3.05×10^{-4} M and 3.05×10^{-3} M in 0.1M H_3PO_4) and 5-CQA (3.05×10^{-4}M and 3.05×10^{-3}M in 0.1M H_3PO_4) were prepared. Using the prepared stock solutions, two calibration curves were obtained by keeping fixed the concentration of one analyte (3.05×10^{-5} M) and adding the following equivalents of the second target compounds: 0, 0.1, 0.25, 0.5, 1, 2.5, 5, 7, 10.

The repeatability of the measurement was assessed by recording 23 consecutive voltammograms of a 3.05×10^{-4}M equimolar solution of the two analytes, and the relative standard deviation of the peak area was considered. The electrode-to-electrode reproducibility was evaluated by using three different screen-printed electrodes from the

same batch and recording 5 consecutive SWVs of a 3.05×10^{-4}M equimolar solution of the two analytes.

Real samples analysis using screen printed carbon electrode

Two stock solutions one of caffeine (2.80 mM) and one of 5-CQA (2.80 mM) were prepared in 0.1 M H_3PO_4. A 100 µL drop of supporting electrolyte was deposit over the active area of the electrode and an aliquot of sample added. The drop was then gently stirred with the plastic tip of a Gilson micropipette. The standard addition method was employed for accurate quantification of the target compounds. 5 consecutive SWVs were recorded after each addition and the mean peak charge was used for evaluation. A total of three additions of standard were made. The volumes of sample and standard solution added are listed below.

Table 4.23. Added volume of sample and standard for the quantitative analysis of the total polyphenol and caffeine content.

Sample		Volume of sample (µL)	Volume of 5-CQA standard (µL)	Volume of CAF standard (µL)
Roasted coffee beans	Idiyllum	30	0	2
	Regular	20	0	2
	LVU	20	0	2
Espresso	illy blend regular	5	3	3
	illy Blend *lungo*	5	3	3
	Idillyum blend regular	5	2	2
	Idillyum blend *lungo*	6	2	2
Green coffee beans	Arabica 1	10	5	2
	Arabica 2	8	5	2
	Robusta 1	6	5	2

The total concentration of polyphenols was calculated as equivalents of 5-CQA.

4.5.5 Comparative UHPLC and HPLC method

All chromatographic experiments were performed by a trained employee of illy caffè. The experimental conditions for the UHPLC analysis were the following: the mobile phases were aqueous formic acid (0.1%) and acetonitrile (flow rate equal to 1.2 mL/min), starting at 90% of aqueous phase, reaching 60% at 10 min, 50% at 12 min and then back to initial conditions. Caffeine concentration was determined by monitoring the absorbance at 273 nm. Chlorogenic acids were determined by measuring the absorbance at 324nm. For real sample analysis, all beverages were diluted with distilled water 1:10 (for energy and soft drinks), 1:50 (espresso), the diluted solution were filtered on Phenex NY 0.2 µm filters, prior analysis. For the accredited analysis of caffeine, the HPLC methodology described in the ISO protocol was employed (ISO protocol 20481:2008).

4.5.6 Measurement procedures for the determination of sucrose in green coffee beans.

A 3.42 g/L sucrose standard solution was prepared in distilled water. The amperometric measurements were performed in a 2 mL vial under stirring conditions following the procedure described in the manual provided by Biorealis Ltd and by adding 10 µL of sample and 10 µL of sucrose standard solutions when requested by the device. When the measurement was completed the device automatically calculated the concentration of sucrose in g/L.

4.5.7 Data analysis and statistical evaluation

The experimental results were evaluated using OriginPro 7.5 software and are reported with 95% confidence level interval. For the calibration curve, each point was obtained by the average peak intensity or charge of consecutive measurements, and the error bar was evaluated based on the standard deviation. The linearity was assessed using the least-square regression method. The limit of detection (LOD) and limit of quantification

(LOQ) were calculated using the 3σ and 10σ criterion, respectively. With regards to the real sample analysis, in the case of the electrochemical method, the caffeine and polyphenol content was determined by interpolation, following the standard addition methodology. The error on the analyte quantification was evaluated according to the following formula:

$$\boldsymbol{error = t_{n-1,\alpha} \times Standard\ Deviation/SQRT\ (n)} \qquad 4.4$$

with n=5, α=0.05, and $t_{4,0.05} = 2.13$.

For the paired t-test the QuickCalcs software (GraphPad Software Inc.) was employed. A more exhaustive description of the standard addition methodology and the statistical evaluation is presented elsewhere[48]. In the case of sucrose determination, the Omnilab sensor provided the concentration of sucrose in the sample as g/L, the precision was determined by measuring the sample in triplicate and the standard deviation was used to evaluate the error.

4.6 References

1 International Coffee Organization, *Coffee Market report-October 2016*, 2016.
2 S. Fenu and E. Acquas, *Behavioral Pharmacology of Caffeine*, Elsevier, 2013.
3 A. Santini, R. Ferracane, P. Mikušová, Š. Eged, A. Srobárová, G. Meca, J. Mañes and A. Ritieni, *Food Control*, 2011, **22**, 1240–1245.
4 I. Clark and P. H. Landolt, *Sleep Med. Rev.*, 2017, **31**, 70–78.
5 A. Atik, R. Harding, R. De Matteo, D. Kondos-Devcic, J. Cheong, L. W. Doyle and M. Tolcos, *Neurotoxicology*, 2017, **58**, 94–102.
6 A. Zulli, R. M. Smith, P. Kubatka, J. Novak, Y. Uehara, H. Loftus, T. Qaradakhi, M. Pohanka, N. Kobyliak, A. Zagatina, J. Klimas, A. Hayes, G. La Rocca, M. Soucek and P. Kruzliak, *Eur. J. Nutr.*, 2016, **55**, 1331–1343.
7 M. C. Costa, T. Goumperis, W. Andersson, J. Badiola, W. Ooms, S. Pongolini, C. Saegerman, M. Jurkovic, P. Tuominen, E. Tsigarida, J. Steinwider, C. Hölzl, N. Mikushinska, A. Gross-Bošković, P. Kanari, M. Christodoulidou, L. Babička, H. Korsgaard, S. Pesonen, A. M. Fillet, F. Foures, M. Lohman, P. Luber, M. Szabó, J. Cseh, H. P. J. M. Noteborn, K. Færden, Å. Fulke, T. Trnovec, N. G. Ilbäck, T. Andersson, T. Donohoe, C. Merten and T. Robinson, *Food Control*, 2017, **73**, 255–264.
8 F. Turak, R. Guzel and E. Dinc, *J. Food Drugs Anal.*, 2016, **25**, 285–292.
9 H. S. Ali, A. A. Abdullah, P. T. Pinar, Y. Yardim and Z. Senturk, *Talanta*, 2017,

170, 384–391.
10 J.-S. Jeon, H.-T. Kim, I.-H. Jeong, S.-R. Hong, M.-S. Oh, K.-H. Park, J.-H. Shim and A. M. A. El-Aty, *J. Chromatogr. B*, 2017, **1064**, 115–123.
11 J. Peris-Vicente, M. Rambla-Alegre, A. Durgavanshi, D. Bose, J. Esteve-Romero and S. Marco-Peiro, *J. Chromatogr. Sci.*, 2014, 1121–1126.
12 E. Schievano, C. Finotello, L. Navarini and S. Mammi, *Talanta*, 2015, **140**, 36–41.
13 O. Alharbi, Y. Xu and R. Goodacre, *Anal. Bioanal. Chem.*, 2015, **407**, 8253–8261.
14 L. A. Mercante, V. P. Scagion, F. L. Migliorini, L. H. C. Mattoso and D. S. Correa, *Trends Anal. Chem.*, 2017, **91**, 91–103.
15 S. Cinti and F. Arduini, *Biosens. Bioelectron.*, 2017, **89**, 107–122.
16 P. Y. Khashaba, H. R. H. Ali and M. M. El-Wekil, *R. Soc. Open Sci.*, 2017, **4**, 170324–170337.
17 Ľ. Švorc, *Int. J. Electrochem. Sci.*, 2013, **8**, 5755–5773.
18 G. K. Gnana, S. Amala and S. M. Gowtham, *RSC Adv.*, 2017, **7**, 36949–36976.
19 T. Xie, M. Zhang, P. Chen, H. Zhao, X. Yang, L. Yao, H. Zhang, A. Dong, J. Wang and Z. Wang, *RSC Adv.*, 2017, **7**, 38884–38894.
20 K. Tyszczuk-Rotko and I. Beczkowska, *Food Chem.*, 2015, **172**, 24–29.
21 M. Velmurugan, N. Karikalan, S. Chen and C. Karuppiah, *Microchim. Acta*, 2016, 2713–2721.
22 A. Yiğit, Y. Yardim, M. Çelebi, A. Levent and Z. Şentürk, *Talanta*, 2016, **158**, 21–29.
23 I. Sadok, K. Tyszczuk-rotko and A. Nosal-Wiercinska, *Sens. Actuators B Chem.*, 2016, **235**, 263–272.
24 J. M. Lim, M. Y. Ryu, J. H. Kim, C. H. Cho, T. J. Park and J. P. Park, *RSC Adv.*, 2017, **7**, 36562–36565.
25 L. Yu, P. Zhang, H. Dai, L. Chen, H. Ma and M. Lin, *RSC Adv.*, 2017, **7**, 39611–39616.
26 S. Amidi, Y. H. Ardakani, E. Ranjbari, Z. Sepehri and H. Bagheri, *RSC Adv.*, 2017, **7**, 40111–40118.
27 Ľ. Švorc, P. Tomcik, J. Svítková, M. Rievaj and D. Bustin, *Food Chem.*, 2012, **135**, 1198–1204.
28 A. Dekanski, J. Stevanovic, R. Stevanovic, Z. N. Branislav and V. M. Jovanovic, *Carbon N. Y.*, 2001, **39**, 1195–1205.
29 B. Uslu and S. A. Ozkan, *Anal. Lett.*, 2007, **40**, 817–853.
30 B. Brunetti, E. Desimoni and P. Casati, *Electroanalysis*, 2007, **19**, 385–388.
31 B. H. Hansen and G. Dryhurst, *J. Electroanal. Chem. Interfacial Electrochem.*, 1971, **30**, 407–416.
32 N. Spãtaru, B. V. Sarada, D. A. Tryk and A. Fujishima, *Electroanalysis*, 2002, **14**, 721–728.
33 S. Chalupczok, P. Kurzweil and H. Hartmann, *Int. J. Electrochem.*, 2003, **3**. 178-183.
34 N. Cheng, Q. Liu, J. Tian, Y. Xue, A. M. Asiri, H. Jiang, Y. He and X. Sun, *Chem. Commun.*, 2015, **51**, 1616–1619.
35 Y. Yi, G. Weinberg, M. Prenzel, M. Greiner, S. Heumann, S. Becker and R. Schlögl, *Catal. Today*, 2017, **295**, 32–40.
36 J. S. Dordević, A. M. Kalijadis, K. R. Kumrić, Z. M. Jovanović, Z. V. Laušević and T. M. Trtić-Petrović, *Cent. Eur. J. Chem.*, 2012, **10**, 1271–1279.
37 N. M. Truc, J. Mortensen, N. Ba and H. Anh, *Malaysian J. Anal. Sci.*, 2008, **12**, 586–592.

38 F. Li, J. Song, D. Gao, Q. Zhang, D. Han and L. Niu, *Talanta*, 2009, **79**, 845–850.
39 T. R. L. C. Paixão, L. Kosminsky and M. Bertotti, *Sens. Actuators, B Chem.*, 2002, **87**, 41–46.
40 W. H. Smyrl, R. T. Atanasoski, L. Atanasoska, L. Hartshorn, M. Lien, K. Nygren and E. A. Fletcher, *J. Electroanal. Chem.*, 1989, **264**, 301–304.
41 T. Nagaoka and T. Yoshino, *Anal. Chem.*, 1986, **58**, 1037–1042.
42 D. A. C. Brownson and C. E. Banks, in *The Handbook of Graphene Electrochemistry*, ed. S.-V. L. Ltd, Springer, 1st edn., 2014, pp. 1–201.
43 S. R. Sataraddi and S. T. Nandibewoor, *Der Pharma Chem.*, 2011, **3**, 253–265.
44 C. W. Huck, W. Guggenbichler and G. K. Bonn, *Anal. Chim. Acta*, 2005, **538**, 195–203.
45 L. López-Martínez, P. L. López-de-Alba, R. García-Campos and L. M. De León-Rodríguez, *Anal. Chim. Acta*, 2003, **493**, 83–94.
46 J. Pérez-Jiménez, V. Neveu, F. Vos and A. Scalbert, *Eur. J. Clin. Nutr.*, 2010, **64 Suppl 3**, S112–S120.
47 M. Filipiak, *Anal. Sci.*, 2001, **17**, 1667–1670.
48 J. N. Miller and J. C. Miller, *Statistics and Chemometrics for Analytical Chemistry*, Prentice Hall, 2005.
49 J. S. Jeon, H. T. Kim, I. H. Jeong, S. R. Hong, M. S. Oh, K. H. Park, J. H. Shim and A. M. Abd El-Aty, *J. Chromatogr. B Anal. Technol. Biomed. Life Sci.*, 2017, **1064**, 115–123.
50 J. Anissi, M. El Hassouni, A. Ouardaoui and K. Sendide, *Food Chem.*, 2014, **150**, 438–447.
51 M. Naveed, V. Hejazi, M. Abbas, A. A. Kamboh, G. J. Khan, M. Shumzaid, F. Ahmad, D. Babazadeh, X. FangFang, F. Modarresi-Ghazani, L. WenHua and Z. XiaoHui, *Biomed. Pharmacother.*, 2018, **97**, 67–74.
52 K. Hanhineva, R. Törrönen, I. Bondia-Pons, J. Pekkinen, M. Kolehmainen, H. Mykkänen and K. Poutanen, *Int. J. Mol. Sci.*, 2010, **11**, 1365–1402.
53 Y. Sato, S. Itagaki, T. Kurokawa, J. Ogura, M. Kobayashi, T. Hirano, M. Sugawara and K. Iseki, *Int. J. Pharm.*, 2011, **403**, 136–138.
54 B. Sarriá, S. Martínez-López, J. L. Sierra-Cinos, L. García-Diz, R. Mateos and L. Bravo-Clemente, *Eur. J. Nutr.*, 2016, **57**, 1–10.
55 G. I. Russo, D. Campisi, M. Di Mauro, F. Regis, G. Reale, M. Marranzano, R. Ragusa, T. Solinas, M. Madonia, S. Cimino and G. Morgia, *Molecules*, 2017, **22**, 1–9.
56 A. Crozier, I. B. Jaganath and M. N. Clifford, *Nat. Prod. Rep.*, 2009, **26**, 1001.
57 G. Grosso, U. Stepaniak, R. Topor-Madry, K. Szafraniec and A. Pajak, *Nutrition*, 2014, **30**, 1398–1403.
58 C. Taguchi, Y. Fukushima, Y. Kishimoto, N. Suzuki-Sugihara, E. Saita, Y. Takahashi and K. Kondo, *Nutrients*, 2015, **7**, 10269–10281.
59 H. M. Yahya, A. Day, C. Lawton, K. Myrissa, F. Croden, L. Dye and G. Williamson, *Eur. J. Nutr.*, 2016, **55**, 1839–1847.
60 N. Liang, W. Xue, P. Kennepohl and D. D. Kitts, *Food Chem.*, 2016, **213**, 251–259.
61 M. D. Del Castillo, J. M. Ames and M. H. Gordon, *J. Agric. Food Chem.*, 2002, **50**, 3698–3703.
62 A. Farah, T. De Paulis, L. C. Trugo and P. R. Martin, *J. Agric. Food Chem.*, 2005, **53**, 1505–1513.
63 G. Sacchetti, C. Di Mattia, P. Pittia and D. Mastrocola, *J. Food Eng.*, 2009, **90**, 74–80.

64 K. Chandrasekaran and D. Karunasagar, *J. Anal. At. Spectrom.*, 2014, **29**, 1720–1725.
65 Y. Sapozhnikova, *Food Chem.*, 2014, **150**, 87–93.
66 G. Baeza, B. Sarriá, L. Bravo and R. Mateos, *J. Agric. Food Chem.*, 2016, **64**, 9663–9674.
67 L. Regazzoni, F. Saligari, C. Marinello, G. Rossoni, G. Aldini, M. Carini and M. Orioli, *J. Funct. Foods*, 2016, **20**, 472–485.
68 P. Köseoğlu Yılmaz and U. Kolak, *J. Chromatogr. Sci.*, 2017, **55**, 712–718.
69 A. C. C. M. Castro, F. B. Oda, M. G. J. Almeida-Cincotto, M. G. Davanço, B. G. Chiari-Andréo, R. M. B. Cicarelli, R. G. Peccinini, G. J. Zocolo, P. R. V. Ribeiro, M. A. Corrêa, V. L. B. Isaac and A. G. Santos, *Food Chem.*, 2018, **246**, 48–57.
70 J. Fibigr, M. Majorová, H. Kočová Vlčková, P. Solich and D. Šatínský, *J. Pharm. Biomed. Anal.*, 2018, **151**, 291–300.
71 D. Soto-Cabrera, J. R. Salazar, I. Nogueda-Gutiérrez, M. Torres-Olvera, A. Cerón-Nava, J. Rosales-Guevara, T. Terrazas and H. Rosas-Acevedo, *Nat. Prod. Res.*, 2016, **30**, 1885–1889.
72 T. A. Catelani, R. N. M. J. Páscoa, J. R. Santos, L. Pezza, H. R. Pezza, J. L. F. C. Lima and J. A. Lopes, *Food Bioprocess Technol.*, 2017, **10**, 630–638.
73 G. Navarra, M. Moschetti, V. Guarrasi, M. R. Mangione, V. Militello and M. Leone, *J. Chem.*, 2017, **2017**, 1–8.
74 F. Wei, K. Furihata, F. Hu, T. Miyakawa and M. Tanokura, *Magn. Reson. Chem.*, 2010, **48**, 857–865.
75 N. Alpar, Y. Yardım and Z. Şentürk, *Sens. Actuators, B Chem.*, 2018, **257**, 398–408.
76 S. Khan and A. K. Narula, *New J. Chem.*, 2017, **41**, 8927–8939.
77 N. Mohammadi, M. Najafi and N. B. Adeh, *Sens. Actuators, B Chem.*, 2017, **243**, 838–846.
78 Y. Vlamidis, I. Gualandi and D. Tonelli, *J. Electroanal. Chem.*, 2017, **799**, 285–292.
79 I. Tomac, M. Šeruga and E. Beinrohr, *Food Anal. Methods*, 2017, **10**, 3924–3933.
80 I. G. David, D. E. Popa, M. Buleandra, Z. Moldovan, E. E. Iorgulescu and I. A. Badea, *Anal. Methods*, 2016, **8**, 6537–6544.
81 H. Karaosmanoglu, W. Suthanthangjai, J. Travas-Sejdic and P. A. Kilmartin, *Electrochim. Acta*, 2016, **201**, 366–373.
82 I. Tomac and M. Seruga, *Int. J. Electrochem. Sci.*, 2016, **11**, 2854–2876.
83 X. Ma, H. Yang, H. Xiong, X. Li, J. Gao and Y. Gao, *Sensors*, 2016, **16**, 1797.
84 I. Vasilescu, S. A. V. Eremia, A. Radoi, S. C. Litescu and G.-L. Radu, *RSC Adv.*, 2015, **5**, 261–268.
85 M. Chao and X. Ma, *J. Food Drug Anal.*, 2014, **22**, 512–519.
86 W. de J. R. Santos, M. Santhiago, I. V. P. Yoshida and L. T. Kubota, *Anal. Chim. Acta*, 2011, **695**, 44–50.
87 Y. Yardim, E. Keskin and Z. Şentürk, *Talanta*, 2013, **116**, 1010–1017.
88 G. Ziyatdinova, I. Aytuganova, A. Nizamova and H. Budnikov, *Food Anal. Methods*, 2013, **6**, 1629–1638.
89 J. Karpinska, R. Swisłocka and W. Lewandowski, *BioFactors*, 2017, **43**, 621–632.
90 I. Tomac and M. Šeruga, *Int. J. Electrochem. Sceince*, 2016, **11**, 2854–2876.
91 A. G. Pandolfo and A. F. Hollenkamp, *J. Power Sources*, 2006, **157**, 11–27.
92 E. P. Meier and J. Q. Chambers, *Anal. Chem.*, 1969, **41**, 914–918.
93 Paul Delhay, *Double Layer and Electrode Kinetics.*, John Wiley and Sons, Inc,

1st edn., 1965.
94 M. Ferrari, L. Navarini, L. Liggieri, F. Ravera and F. Suggi Liverani, *Food Hydrocoll.*, 2007, **21**, 1374–1378.
95 R. L. Prior, X. Wu and K. Schaich, *J. Agric. Food Chem.*, 2005, **53**, 4290–4302.
96 G. A. Agbor, J. A. Vinson and P. E. Donnely, *Int. J. Food Sci. Nutr. Diet.*, 2014, **8**, 147–156.
97 A. Farah, in *Coffee: Emerging Health Effects and Disease Prevention*, ed. C. Yi-Fang, Blackwell Publishing Ltd, 1st edn., 2012, pp. 21–58.
98 F. M. Borém, L. P. Figueiro, F. C. Ribeiro, J. H. S. Taveira, G. S. Giomo and T. J. G. Salva, *African J. Agric. Res.*, 2016, **11**, 709–717.
99 Y. Dessalegn, M. T. Labuschagne, O. Osthoff and L. Herselman, *Ethiophian J. Sci.*, 2007, 30, 77–82.
100 C. Geromel, L. P. Ferreira, F. Davrieux, B. Guyot, F. Ribeyre, M. Brígida dos Santos Scholz, L. F. Protasio Pereira, P. Vaast, D. Pot, T. Leroy, A. A. Filho, L. G. Esteves Vieira, P. Mazzafera and P. Marraccini, *Plant Physiol. Biochem.*, 2008, **46**, 569–579.
101 C. Campa, J. F. Ballester, S. Doulbeau, S. Dussert, S. Hamon and M. Noirot, *Food Chem.*, 2004, **88**, 39–43.
102 Y. Koshiro, M. C. Jackson, C. Nagai and H. Ashihara, *Eur. Chem. Bull.*, 2015, **4**, 378–383.
103 S. Smrke, I. Kroslakova, A. N. Gloess and C. Yeretzian, *Food Chem.*, 2015, **174**, 637–642.
104 C. L. Ky, S. Doulbeau, B. Guyot, S. Akaffou, A. Charrier, S. Hamon, J. Louarn and M. Noirot, *Plant Breed.*, 2000, **119**, 165–168.
105 M. Stredansky, L. Redivo, P. Magdolen, A. Stredansky and L. Navarini, *Food Chem.*, 2018, **254**, 8–12.
106 S. Knopp, G. Bytof and D. Selmar, *Eur. Food Res. Technol.*, 2006, **223**, 195–201.
107 L. Gabriel, M. Tod and S. Goutelle, *Clin. Pharmacokinet.*, 2016, **55**, 977–990.
108 J. A. Carrillo and J. Benitez, *Clin. Pharmacokinet.*, 2000, **39**, 127–153.
109 M. S. Faber, A. Jetter and U. Fuhr, *Basic Clin. Pharmacol. Toxicol.*, 2005, **97**, 125–134.
110 K. Haraya, M. Kato, K. Chiba and Y. Sugiyama, *Drug Metab. Pharmacokinet.*, 2016, **31**, 276–284.
111 F. Chen, Z.-Y. Hu, R. B. Parker and S. C. Laizure, *Biomed. Chromatogr.*, 2017, **1**, 115–141.
112 E. Urry, A. Jetter and H.-P. Landolt, *Nutr. Metab. (Lond).*, 2016, **13**, 66–75.
113 N. Y. Jordan, J. Y. Mimpen, W. J. M. van den Bogaard, F. M. Flesch, M. H. M. van de Meent and J. S. Torano, *J. Chromatogr. B*, 2015, **995**–**996**, 70–73.
114 E. Begas, E. Kouvaras, A. K. Tsakalof, M. Bounitsi and E. K. Asprodini, *Biomed. Chromatogr.*, 2015, **29**, 1657–1663.
115 R. L. Schilsky, *Nat. Rev. Drug Discov.*, 2010, **9**, 363–366.
116 E. A. Ashley, *Nat. Rev. Genet.*, 2016, **17**, 507–22.

CHAPTER 5
General conclusion and future work

This thesis describes the work on the synthesis of MIP as recognition element for the detection of caffeine and the applicability of bare carbon electrodes for caffeine determination in caffeinated beverages. The work was conducted in different research realities, both academic (UNITS and QMUL) and industrial (Biorealis Ltd and illy Caffè S.p.A.), as part of an industrial doctorate program (IPCOS). The interest towards the development of novel caffeine sensors is given by the wide consumption of caffeinated beverages and the important biological effect associated with caffeine intake. Two strategies were followed, the first one based on the use of MIPs and the development of a selective sensor for caffeine detection; while the second approach focuses on the development of a simple and cost-effective sensor. Both strategies led to interesting findings. With regards to the synthesis of MIPs for caffeine, a novel functional monomer with high affinity for caffeine was synthesised, besides, an accurate study on caffeine stability in the presence of radicals was conducted. Subsequently, the optimal conditions for the synthesis of the imprinted polymer in aqueous solutions were identified, and two MIPs synthesised. Due to the limited time available for this part of research, the obtained MIPs and their applicability for food sample analysis were not studied in details. Nevertheless, the preliminary results obtained are promising for investigating further the obtained materials and their applicability as selective sensor for caffeine. This is of great interest for the analysis of complex matrixes (for instance biological fluids) where interference problems may be encountered. In fact, in such samples the presence of similar compounds to caffeine (such as theophylline, theobromine and paraxanthine) can lead to interference and an inaccurate caffeine determination. Considering the important biological effects of caffeine, its determination also in biological fluids is of great scientific interest to further understand its effects in humans.

The computational study on caffeine self-association in solution (described in Chapter 2) is also connected to caffeine bioactive properties. The results showed that even small changes in the chemical structures of caffeine affect the formation of aggregates. This is of particular interest for the development of drugs based on caffeine structure, which are currently under investigation as a memory enhancer and for the treatment of neurogenerative diseases. In fact the speciation of a drug in solution (monomer or aggregate) will affect its biological activity. Given the excellent results achieved with the computational methodology described in Chapter 2, the applicability of this computational tool can be further explored in the drug development process of caffeine analogues.

The use of bare carbon electrodes as sensors for caffeine led to excellent results for caffeinated beverages analysis. The development of these sensors involves less parameters to be optimised, reducing the time costs. Despite these materials are not selective for caffeine, no interference problems were observed during the real sample analysis, and accurate quantification of caffeine content was possible. Moreover, these sensors represent a valid and more cost convenient alternative to chromatographic methods, and they are of particular interest for an industrial application. Given the strong collaboration and long secondments in the industrial research reality (18 months), simplicity and low costs were key features for the final caffeine sensor and were achieved during the research carried out at Bioralis and illy Caffè. In addition, a second sensor for the accurate determination of caffeine and polyphenols was developed and successfully applied for different coffee samples (green and roasted coffee beans, and espresso brews). Since new electrode materials are continuously under investigation, future research may focus on the applicability and comparison of different electrode's materials in terms of sensitivity, costs, and simplicity of use. In particular more sensitive devices

can be employed for the analysis of decaffeinated beverages, where some residual caffeine is still present and must be determined accurately.

In conclusion, the applicability of MIPs and bare carbon electrodes found interesting approaches. When interference problems may be encountered in the real sample analysis, the use of MIP is a powerful method to achieve selectivity and accurate caffeine determination. On the other hand, if no interfering problems are encountered, bare carbon electrodes are interesting solutions due to their simplicity, and low cost, which are key properties for an industrial application and a sensor for routine analysis.

Annex I
More details on the computational study presented in chapter 2

Computational studies using quantum mechanics

In the following annex a description of the theory behind the computational chemistry study reported in chapter 2 is presented. The explanation is divided into three sections: i) the theory behind quantum chemical calculations; ii) how chemical reactions in solution can be investigated; iii) how is it possible to study the self-aggregation of organic molecules using quantum mechanics simulations. This annex is only a brief and concise description of the theory behind the simulations presented in chapter 2, as more details are available in specialised books and reviews.[1–4]

Quantum Mechanics calculations

Quantum Mechanics simulations are based on quantum chemistry and particles (such as electrons and atoms) are considered quantum entities and obey to quantum physics. To calculate the energy of a molecule the Schrödinger's equation has to be solved, which is reported below.

$$H(R,r)\,\psi(R,r) = E(R,r)\,\psi(R,r) \qquad (1)$$

Where, $H(R,r)$ is called the Hamiltonian and is the operator to calculate the energy ($E(R,r)$) of the molecule ($\psi(R,r)$) which is assumed to be a wavefunction. R and r are the coordinates of the nuclei and electrons respectively. The Hamiltonian provides the total energy of the molecule, by considering: i) the kinetic energies for nuclei (T_n) and electrons (T_e); ii) the total potential energy arising from the interactions nuclei-nuclei (V_{nn}), nuclei-electron (V_{ne}) and electron-electron (V_{ee}). It is therefore possible to rewrite the Hamiltonian as follows:

$$H(R,r) = T_n + T_e + V_{nn}(R) + V_{ne}(R,r) + V_{ee}(r) \qquad (2)$$

Since both nuclei and electrons are charged particles, the potential energy is described by Coulomb law and for two generic charged entities (a and b) is equal to $\frac{Z_a Z_b}{d}$ where Z_X (X=a,b) is the charge of the particle a and b, and d is the distance between them. Given the relationship between potential energy and inter-particle distance, the potential energy depends upon the coordinates of the nuclei (R) and electrons (r). However, since both nuclei and electrons are constantly moving, it is impossible to solve exactly the Schrödinger equation since the electron-electron, nuclei-nuclei, and electron-nuclei interaction is not determined. Therefore, approximations have to be made in order to solve Schrödinger equation.

First, nuclei and electrons have different masses and therefore velocities, with the electrons being four orders of magnitude lighter than the nuclei and moving faster. As a consequence, electronic reactions (such as excitation, or bond formation) happen at a time scale that is shorter than nuclei's movement. An alternative point of view to understand this approximation is that upon a change in the nuclei positions, electrons rearrange instantaneously. This observation gives rise to the Born-Oppenheimer approximation, where nuclei are considered static, and the Schrödinger equation is solved to compute the energy of the system. Thanks to the high difference in masses and kinetic energies of nuclei and electrons, good results are still obtained when the Born-Oppenheimer approximation is employed. The resulting simplified Schrödinger equation is reported below, and the Hamiltonian, wavefunction and energy depend only on the coordinates of the electrons (r).

$$H(r)\,\psi(r) = E(r)\,\psi(r) \qquad (3)$$

With

$$H = T_e + V_{nn} + V_{ne}(r) + V_{ee}(r) \qquad (4)$$

The Hamiltonian is simplified since the kinetic energy of nuclei is null, interaction nuclei-nuclei is a constant, and the interaction nuclei-electrons depend only on the electrons coordinates. Using the Born-Oppenheimer approximation the Schrodinger equation can be solved only for the hydrogen atom since only one electron is present. For atoms and molecules where more than one electron is present, the electron-electron interaction is impossible to be calculated exactly since it depends upon all electrons coordinates. Further approximations are therefore necessary. For a generic molecule with *m* electrons (with *m* an integer number), the wavefunction will depend upon *m* coordinates of *m* electrons ($\psi(r_1, r_2, \dots, r_m)$). It is possible to divide this function into a product of single wavefunctions for each electron ($\varphi(r)$) as follow:

$$\psi(r_1, r_2, \dots, r_m) = \varphi(r_1)\varphi(r_2), \dots, \varphi(r_m) \qquad (5)$$

The Hamiltonian can also be rewritten as follows:

$$H(r_1, r_2, \dots, r_m) = \sum_{i=1}^{m} H(r_i) \qquad (6)$$

and the total energy of the system will be:

$$E(r_1, r_2, \dots, r_m) = \sum_{i=1}^{m} E_i \qquad (7)$$

The Hamiltonian contains all the terms as before (equation 4), however instead of depending upon *m* coordinates of *m* electrons, it will depend on one set of coordinates of one electron. In addition, the electron-electron potential energy (V_{ee}) is computed as the interaction between the electron (i^{th}) and the electron density created by all the other electrons. An illustrative example is reported in the figure below, where the balls represent the electrons, the red one is the i^{th} electron for which we want to solve the

Schrödinger equation. In principle, six individual electron-electron interactions should be considered (dashed gray lines) (Figure 1A). As stated before this is not possible since the position of all the particles are unknown. Therefore, a total electron density is defined around the investigated electron, and a single interaction is considered between the electron and the overall electron density (Figure B).

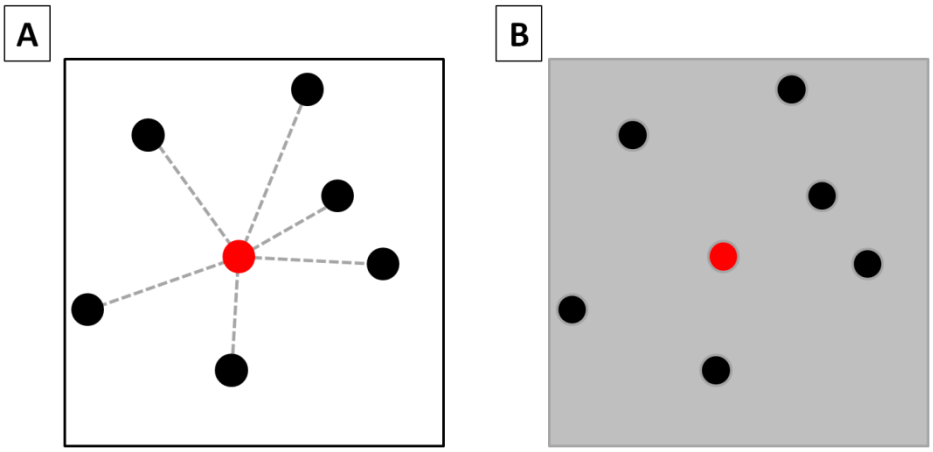

Figure 1. Graphical example of the independent model approximation to describe the electron-electron interaction. Figure A shows the interaction between an electron (i^{th}, in red) and 6 other electrons, leading to 6 interactions. Figure B shows the same system when the independent model approximation is applied and the electron-electron interaction is computed between the i^{th} electron (in red) and an electron density (grey space) arising from all the other electrons.

This approximation is called the independent model and a variety of mathematical methodologies to describe the electron-electron interaction have been developed and give rise to different quantum mechanical computational methodologies. For instance, Hartree-Fock (HF), Density Functional Theory (DFT), semiempirical methods, to name the most common ones. Among them, the most widely employed is Density Functional Theory (DFT), since it provides reliable results in terms of molecular geometry and energy at a reasonable computational cost.[1,2] A key component of DFT calculations is the functional that is employed, which is responsible for describing the physics of the system such as bond lengths and angles as well as chemical interactions (Van der Waals, ionic, hydrogen bonds interactions). A plethora of functionals are available in

conventional computational chemistry software, and the computational result will strongly depend on the functional employed. For example, some functionals provide excellent results for neutral organic molecules (such as caffeine) while they are not appropriate for metal clusters or charged chemical compounds. It is therefore essential to find an appropriate functional to be employed throughout the calculations and the selection is usually done by comparing computational and experimental data, or by looking at previous computational works if present in literature. The selection of the appropriate functional was a crucial step for obtaining accurate dimerisation energy of caffeine, and the selection process is described in chapter 2 (Assessment of the method). Two major types of functionals were employed: i) where the dispersion correction is not considered; ii) a second one with the inclusion of the dispersion correction. The dispersion correction is a mathematical correction to the functional which allows for the accurate reproduction of weak interactions such as Van der Waals, π-π stacking, hydrogen bonds, etc. This correction was originally developed by Grimme S., and is usually indicated in the functional by a capital d letter (for example B97-**D**)[5]. When the dispersion correction is included the time required to complete the computational simulation is longer and is therefore applied only when fundamental for obtaining accurate results.

To summarise, so far two approximations were defined, the Born-Oppenheimer (the nuclei are considered static) and the independent model (each electron is considered separately). The third approximation involves the wavefunction (φ) and how to express it mathematically. In fact, the analytical expression of a molecular orbital is unknown *a priori*, however, it can be approximated to a linear combination of simpler functions as follows:

$$\varphi = \sum_i^N c_i f_i \qquad (8)$$

Where c_i is the coefficient that weights the contribution of each function (f_i) to the wavefunction (φ). The sum of all c_i is equal to 1. N is the number of functions (f_i) available, which is called the size of the basis set. These functions (f_i), also called atomic orbitals, are usually Slater type, Gaussian or planewave functions, and this approximation is known as Molecular Orbital as Linear Combination of Atomic Orbitals (MO-LCAO). Although it may seem a complication to express a single function as a combination of functions, the result is calculated more rapidly when atomic orbitals are used, since the mathematical expression of the function is simpler. The more functions (f_i) are available the more accurate the final result will be, however the time required to compute the solution will increase exponentially with the size of the basis set ($computing\ time \propto N^4$). In order to reduce the computing time, without compromising significantly the results, different solutions have been developed. For instance, since most of chemical processes involve only the valence electrons, the core electrons are described less accurately compared to valence electrons. Instead of increasing the size of the basis set it is more convenient to use more than one basis set to describe one orbital (such basis sets are called double zeta, or triple zeta if two or three basis sets are employed). In addition, it is common practice to add additional functions, such as polarized functions or diffused functions, which improve the description of the orbital without affecting significantly the computing time. The final result of the computational simulation is considerably affected by the basis set selected and more accurate results are achieved by larger basis set (the exact solution is achieved ideally only with an infinite basis set). On the other hand, the computing time is exponentially increasing with larger basis set and therefore a compromise between accuracy of the method and time to perform the computational study is necessary. A simplified standard

notation to indicate the basis set employed is commonly used and an example is reported below:

6-311+G(d,p)

The first number (6) specifies the size of the basis set that is used to describe the core electrons. The following numbers indicate the size of the different basis sets used to describe the valence electrons; in this case each valence orbital is described by three basis sets, one with size 3 and two with size 1. The plus sign indicates that diffuse functions have also been employed for non- hydrogen atoms (+). G specifies that Gaussian-type functions are employed as atomic orbitals. In brackets the use of polarisation functions is specified, in the example polarised functions have been employed both for non-hydrogen atoms (d), and hydrogen atoms (p).

To summarise, three main approximation are employed to solve the Schrödinger equation: i) the nuclei are considered static (Born-Oppenheimer); ii) each electron is treated individually and interacts with an overall density charge arising from all the other electrons (independent model) iii) the molecular orbitals are expressed as linear combination of simpler functions called atomic orbitals (LCAO approximation). In particular these latest two approximations affect the computational result and therefore it is fundamental to specify the computational method employed (for instance, DFT), the functional employed (for instance B97-D) and the basis set (for instance 6-311+G(d,p)). A concise writing is commonly employed and an example is reported below:

B97-D/6-311+G(d,p)

Where the first term specifies the functional and after the symbol "/" the basis set employed is reported; the specific methodology used is also known as level of theory.

Quantum mechanics can provide the correct result when the Schrödinger equation is solved exactly. However, since there are no mathematical methods to solve this differential equation exactly, approximations have to be used and the more severe these approximations are, the less accurate the computational results will be. More precise calculations require longer time to be computed and usually a compromise between accuracy and time to perform the analysis is found. However, thanks to the continuous development of faster processors and computers, the precision of computational studies is increasing and accurate computational studies are nowadays possible. A second frontier of quantum mechanics simulations is that simulations are limited to systems with no more than 100 atoms, due to limitations on the computers commonly employed. As a consequence, biological systems such as proteins cannot be investigated using quantum mechanics-based studies. In addition, to study chemical processes in solution, solvents molecules cannot be explicitly considered but implicit solvent models need to be employed.

Computational studies of chemical processes in solution.

In an explicit solvation model, the solute molecule is enclosed by a massive number of solvents molecules. For instance, for a 10 mM caffeine aqueous solution 0.01 moles of caffeine are present in 1 litre of water and under the approximation that the density of caffeine aqueous solution is 1 kg/l, 1 L of solution equals 1000 g and therefore 55.56 moles of water are present ($\frac{1000}{18} = 55.56$). Therefore, the solvent-solute molecular ratio is:

$$\frac{Solvent\ molecules}{Solute\ molecules} = \frac{{}^{1000}/_{18}}{0.01} = 5556 \qquad (9)$$

It is therefore evident that by considering the solvent molecules explicitly, the number of atoms of the system under study rapidly increase, and quantum mechanics calculations

cannot be performed. To overcome this limitation and perform quantum chemical calculations for chemical reactions in solution, the implicit continuum solvation models was developed. In the continuum model the dielectric constant of the medium is changed. For instance, for simulation in vacuum the dielectric constant is 1 while in water this constant is set to 78, and as a consequence, ionic interactions that are strong in vacuum will be weaker in water. Moreover, around the solute molecule a pocket without solvent is created and the solute-solvent interactions are calculated by considering the functional groups of the solute molecules. For example, when water is employed as solvent, the ability of the solute molecule to form hydrogen bonds will be evaluated. A graphical comparison of the explicit and implicit solvent models is presented in the following figure, where a generic solute molecule (red circle) is enclosed with explicit solvent molecules (light blue circles, Figure 2A) or is studied using an implicit solvent model (Figure 2B) where the solute-solvent interactions (light blue arrows) are calculated based on the functional groups of the solute and solvent molecules.

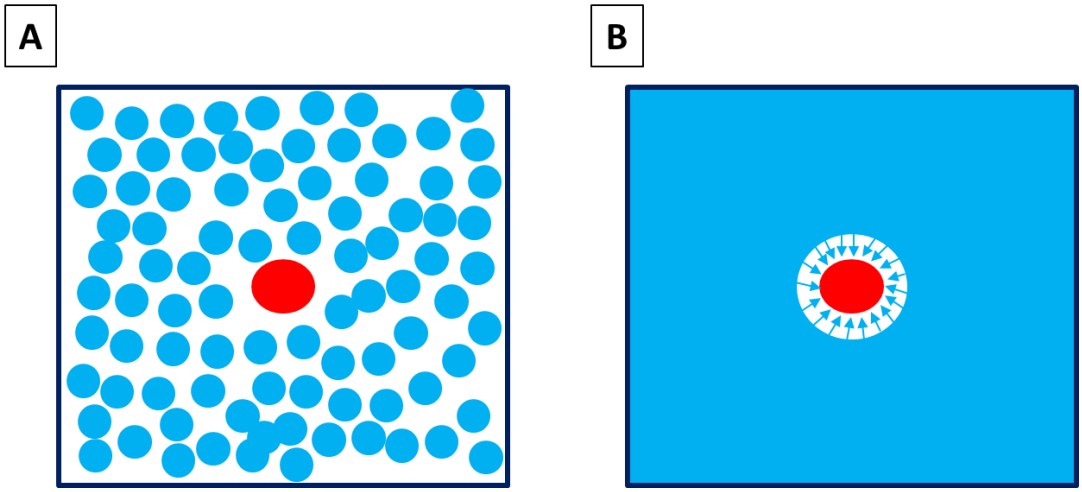

Figure 2. Comparison between explicit and implicit solvent model. Figure A shows an explicit model where solvent molecules (light blue circles) enclose the solute molecule (red circle). Figure B shows an implicit solvent model where the solute molecule (red circle) is immersed in a continuum environment with a constant permittivity. The arrows represent the solute-solvent interactions.

The explicit model provides a more accurate description of chemical processes in solution, since solvents molecules are explicitly present and interacts with solute molecule. Nevertheless, implicit solvation models are continuously optimised and, at the current state of art, it is possible to accurately reproduce solvent-solute interactions and obtain precise computational results for chemical processes in solution. In addition, in the case of explicit solvation models the computational studies are performed at a defined concentration since the ratio of solute-solvent molecules is defined. As a consequence, the result is dependent on the concentration considered in the study and very low concentrations (<1 mM) are commonly not performed because they required simulations with more than ten thousand molecules, which is at the far limit of any computational method. On the other hand, in the case of implicit model the system is studied without establishing a concentration and the results will not depend upon the concentration.

To summarise, quantum mechanical simulations are based on quantum physics and to calculate the energy of a molecule the Schrödinger equation has to be solved. In order to solve it three approximations are required: i) the nuclei are considered static (Born-Oppenheimer approximation); ii) the solution of a molecule with n electrons is obtained by solving n equations for each electron (independent model); iii) molecular orbitals are mathematically expressed as a linear combination of simpler functions (LCAO). In addition, solvent molecules cannot be considered explicitly and implicit solvation models are required to performed computational studies in solution. Although significant approximations are required, quantum mechanics simulations still provide reliable results thanks to the constant development of more accurate methods and the continuous improvement in computer's hardware which allow using always higher level of theory which limits the effects of the approximations employed.

Computational study on the self-association process of organic molecules.

In chapter 2 of this thesis, a quantum mechanics study was applied to investigate the self-association process of caffeine and of paraxanthine in aqueous solutions. To evaluate the self-association process it is required to calculate the thermodynamic stability of caffeine monomer (free caffeine molecules) and caffeine aggregates (dimer, trimer, etc). For example, for the dimerisation process the following chemical process can be written.

$$2CAF \leftrightarrows CAF_2 \qquad (10)$$

And the Gibbs free energy of dimerisation can be calculated as

$$\Delta G_{dim} = G_{CAF_2} - 2G_{CAF} \qquad (11)$$

For the trimerisation process two chemical processes are possible.

$$CAF + CAF_2 \leftrightarrows CAF_3 \qquad (12)$$

and

$$3CAF \leftrightarrows CAF_3 \qquad (13)$$

Which lead to two different Gibbs free energies of trimerisation:

$$\Delta G_{tri} = G_{CAF_3} - G_{CAF} - G_{CAF_2} \qquad (14)$$

$$\Delta G_{tri} = G_{CAF_3} - 3G_{CAF} \qquad (15)$$

Similar chemical processes can be considered for the formation of tetramer and higher order clusters. It is therefore evident from equations 11, 14 and 15 that to evaluate the self-association process it is essential to know the Gibbs free energies (G) of all the chemical species involved in the process (i.e. caffeine monomer, dimer, trimer, …). Quantum mechanical simulations can calculate the energy of a molecule by solving the

Schrödinger equation, provided that the geometry of the chemical species is known. In the case of caffeine monomer, the geometry of the molecule can be obtained from crystallographic data, and thanks to the rigidity of the conjugated aromatic rings only one conformation of caffeine is stable. As a consequence, the potential energy surface of caffeine monomer is characterised by only one minimum (Figure 3).

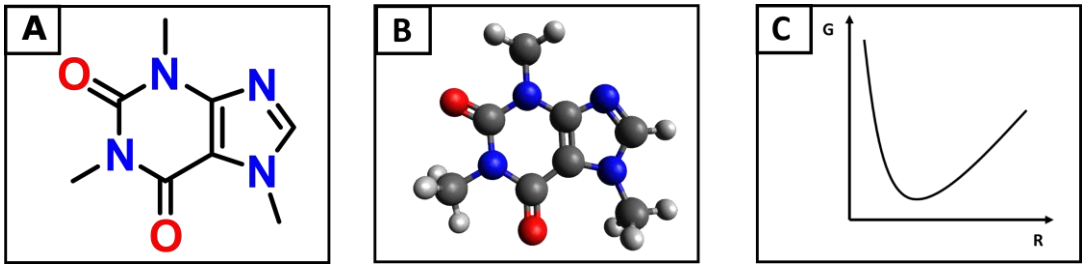

Figure 3. In Figure A The chemical structure of caffeine. B shows, the optimised geometry of caffeine monomer obtained using DFT calculations. Figure C the potential energy surface of caffeine monomer which is characterised by one minimum.

The potential energy surface (PES) is a representation of the energy (G) of a molecule and how it depends upon the position of all the atoms. In fact, bond lengths and angles do affect the energy and stability of a molecule, and in some cases, many minima can exist (i.e. many conformers) but for a rigid molecules, like caffeine, it is reasonable to think that only one stable geometry exists. In contrast, in the case of caffeine aggregates many interactions geometries are possible with the aromatic ring of caffeine molecules interacting with different geometries. Therefore, the PES of caffeine aggregates is characterised by different local minima, as shown in the following figure for caffeine dimer (the graph is an example to explain the complexity of the PES and does not represent the real profile of caffeine dimer).

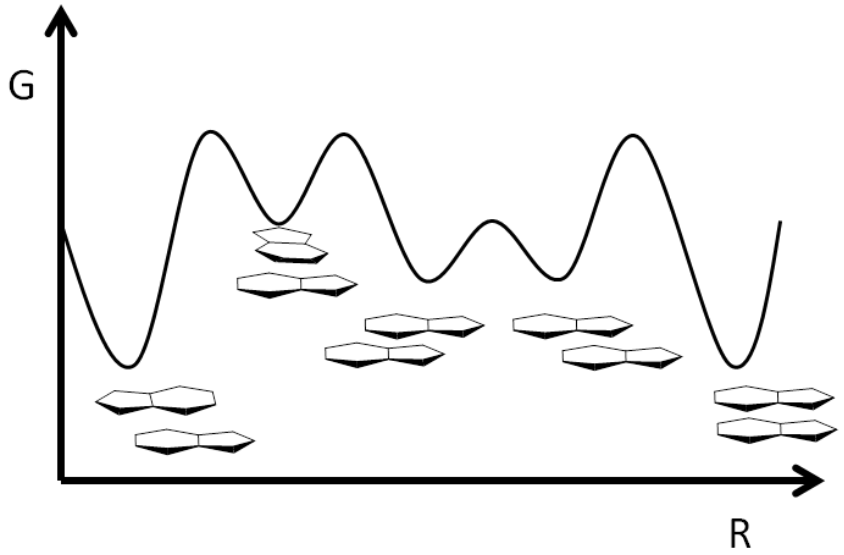

Figure 4. Graphical representation of the potential energy surface (PES) for caffeine dimer, where multiple local minima are possible.

As a consequence of the complex PES of caffeine aggregates, it is fundamental to accurately search for stable dimer configurations and evaluate their energy, to understand which dimer geometries are possible. In addition, if many configurations with similar energies are possible it is more representative to consider the energy of the dimer (G_{CAF_2}) as a Boltzmann distribution of all possible dimer configuration as follows:

$$G_{CAF_2} = \sum_{i=1}^{N} f_i G_i \qquad (16)$$

With G_{CAF_2} the Boltzmann averaged Gibbs free energy of dimerization, *i* runs from all the N possible dimer configurations, G_i is the Gibbs free energy of the i^{th} dimer structure and f_i is the Boltzmann factor and is defined as:

$$f_i = \frac{e^{-(G_i - G_0)/RT}}{\sum_{j=1}^{N} e^{-(G_j - G_0)/RT}} \qquad (17)$$

With $G_i - G_0$ the absolute difference in energy between the i^{th} structure and the energy of the most stable structure (G_0); R is the universal gas constant and T is the absolute temperature. The counter j run from all the N possible structures. Thanks to the

Boltzmann factor, the most stable dimeric configurations (in which $G_i - G_0$ is close to 0) will contribute more to the final Gibb free energy of caffeine dimer compared with less stable caffeine dimers (where $G_i - G_0$ is > 0). The procedure just described for the dimer of caffeine can be applied also for bigger caffeine aggregates in which case the complexity of the PES is increased since more molecules are present and therefore more interaction geometries are possible. Once the PES of caffeine aggregates is explored and the stable configuration are found, the calculation of the Gibbs free energy of aggregation can be easily computed using the previously described equations.

To summarise, for an accurate computational study on the self-association process of caffeine it is fundamental to: i) select a computational methodology able to correctly evaluate the stability of caffeine monomer and aggregates; ii) probe the PES of caffeine aggregates in order to find the most stable geometries for caffeine clusters. The detailed description of the methodology applied for calculating the stability of caffeine aggregates and investigating the PES of caffeine and paraxanthine clusters is described in chapter 2.

References

1 F. Jensen, *Introduction to computational chemistry*, John Willey & Sons, Ltd, Second., 2007.
2 W. J. Hehre, *A Guide to Molecular Mechanics and Quantum Chemical Calculations*, Wavefunction, Inc., 2003.
3 H. B. Schlegel, *J. Chem. Theory Comput.*, 2003, **24**, 1514–27.
4 A. Onufriev, *Annu. Rep. Comput. Chem.*, 2008, **4**, 125–137.
5 S. Grimme, *J. Comput. Chem.*, 2006, **27**, 1787–1799.

Annex II
Published articles and manuscript submitted

In this annex, the articles published during the research activity carried out as PhD student are reported. The manuscripts submitted and accepted by the relevant journal are here presented, while the published versions can be found using the following references:

- L. Redivo, M. Stredansky, E. De Angelis, L. Navarini, M. Resmini, Ĺ Švorc. Bare carbon electrodes as simple and efficient sensors for the quantification of caffeine in commercial beverages. R.Soc.opensci. 5:172146. (link).
- M. Stredansky, L. Redivo, P. Magdolen, A. Stredansky, L. Navarini. Rapid sucrose monitoring in green coffee samples using multienzymatic biosensor. Food chemistry, Volume 254, Pages 8-12, 2018. (link).

In addition, a third manuscript (L. Redivo, R. Anastasiadi, M. Pividori, F. Berti, M. Peressi, D. Di Tommaso, M. Resmini. Self-association of adenosine analogues: combined computational and isothermal titration calorimetry studies of caffeine and paraxanthine) has been submitted to Chemical Science.

This section is included for the benefit of the examiners.

Bare carbon electrodes as simple and efficient sensors for the quantification of caffeine in commercial beverages

Luca Redivo[a]*, Miroslav Stredanský[b], Elisabetta De Angelis[c], Luciano Navarini[c], Marina Resmini[a] and Ľubomír Švorc[d]

[a.]*Department of Chemistry and Biochemistry, School of Biological and Chemical Sciences, Queen Mary University of London, Mile End Road, London, E1 4NS, United Kingdom.*
[b.]*Biorealis s.r.o., Radlinského 9, 811 07 Bratislava, Slovak Republic.*
[c.]*illycaffè S.p.A, via Flavia 110, 34147, Trieste, Italy.*
[d.]*Institute of Analytical Chemistry, Faculty of Chemical and Food Technology, Slovak University of Technology in Bratislava, Radlinského 9, Bratislava, 812 37, Slovak Republic.*

Keywords: Glassy carbon electrode, Voltammetry, Food quality control, Caffeine.

1. Summary

Food quality control is a mandatory task in the food industry and relies on the availability of simple, cost-effective and stable sensing platforms. In the present work, the applicability of bare glassy carbon electrodes for routine analysis of food samples was evaluated as a valid alternative to chromatographic techniques, using caffeine as test analyte. A number of experimental parameters were optimized and a differential pulse voltammetry was applied for quantification experiments. The detection limit was found to be 2×10^{-5}M (3σ criterion) and repeatability was evaluated by the relative standard deviation of 4.5%. The influence of sugars, and compounds structurally related to caffeine on the current response of caffeine was evaluated and found to have no significant influence on the electrode performance. The suitability of bare carbon electrodes for routine analysis was successfully demonstrated by quantifying caffeine content in seven commercially available drinks and the results were validated using a standard ultra-high performance liquid chromatography method. This work demonstrates that bare glassy carbon electrodes are a simple, reliable and cost-effective platform for rapid analysis of targets such as caffeine in commercial products and they represent therefore a competitive alternative to the existing analytical methodologies for routine food analysis.

2. Introduction

Novel technological developments applicable to the area of food quality and safety are driven by strong public interests[1] as well as by the growing numbers of new regulations introduced by food agencies, to ensure that standards are withheld in commercialized products[2]. Most analytical techniques and protocols developed for these purposes allow sensitive and precise quantitative analysis, and rely on equipment-based systems such as capillary electrophoresis (CE)[3,4], gas chromatography (GC)[5,6], high-pressure liquid chromatography (HPLC)[7,8], infrared (IR)-Raman spectroscopy[9,10], surface-enhanced Raman spectroscopy (SERS)[11,12], nuclear magnetic resonance (NMR)[13,14] and UV spectroscopy[15,16]. These techniques are accurate and selective, but require expensive instruments and highly trained workers and in some cases additional steps due to sample pre-treatment[17]. As a result there is a strong demand for new systems characterised by minimal sample pre-treatment, short analysis time, long-time stability, and low costs while not requiring hazardous chemicals or specialised technical support, and maintaining high analytical performance[18,19].

Among the most promising approaches, electrochemistry has grown in interest, having been shown to satisfy most requirements[20–23]. In particular, the development of modified electrodes starting from bare carbon material (glassy carbon, boron doped diamond, graphene, and screen printed carbon electrodes) has led to important results

*Author for correspondence (l.redivo@qmul.ac.uk).
†Present address: Department of Chemistry and Biochemistry, School of Biological and Chemical Sciences, Queen Mary University of London, Mile End Road, London, E1 4NS, United Kingdom.

applications[24–27]. The surface modification is key in obtaining excellent performance in terms of sensitivity and specificity, although the significant additional costs, both in terms of added labour and final price of the device represent a limiting factor. Moreover, the short-term stability and the reproducibility of the preparation of modified electrodes has been highlighted recently as an important issue, which discourages further applications especially in industry[28–30]. Bare electrodes, without functionalization, represent an interesting alternative, in particular when high sensitivity is not required. This approach makes use of a simpler system, resulting in reduced costs for both production and use and a demonstrated long-term stability[31]. Among the different types of bare electrodes, glassy carbon electrodes (GCE) are the ones that have been extensively studied thanks to the relative low cost, chemical inertness and wide anodic potential window[32,33]. Some successful examples of an electrochemical sensor based on bare GCE were recently reported in the literature, in particular in the area of pharmaceutical formulation analysis[34–37].

In this work we explored the potential application of glassy carbon electrodes in quality controls applied to the food industry and for this purpose caffeine was identified as the model analyte. Caffeine (CAF) is mainly found in coffee, where its concentration varies significantly depending on the type of bean, the degree of roasting, the type of brewing and temperatures used[38,39]. However in recently years there has been a significant increase in the number of drinks commercially available, which contains caffeine, consumed not only by adults but by an increasing number of younger people. CAF is a physiological stimulant acting as adenosine A-receptor antagonist, which has been shown to have both positive and negative effects on health[40]. When the intake of CAF is moderate (less than 400 mg per day), there are positive effects, such as higher concentration and decreased tiredness[41], and in such doses its use has also been documented for the treatment of respiratory diseases[42]. However, in high dosage CAF may cause cardiovascular and calcium balance problems[43] and there is still a debate on what can be considered a safe amount of CAF intake, especially for children and young adults[44]. In other commercially available drinks the content of caffeine can vary significantly, ranging from 0.30 g/L in energy drinks, or 0.1 g/L in cola-based drinks orasactive ingredient in tables (usually 200 mg/tablet) or excipient (65 mg/tablet). Given the widespread presence, use and the biological effects of CAF, the routine analysis of its content in all commercialised drinks is a primary task for their manufacturers.

In the present work we demonstrate the validity of using bare GCE for the detection and quantification of CAF content in a variety of commercial samples. The assay is simple, innovative and efficient and most significantly is highly reproducible; the assay was validated with ultra-high performance liquid chromatography.

3. Materials and Methods

Chemicals and reagents

Caffeine, theophylline, theobromine, paraxanthine, glucose, sucrose, formic acid and acetonitrile were purchased from Sigma Aldrich with analytical grade purity. Double distilled water with resistivity above 18 MΩcm was employed in all experiments. Sulfuric acid (ACS reagent, 95.0-98.0%), nitric acid (ACS reagent, ≥ 69%), perchloric acid (ACS reagent, 70%) were tested as supporting electrolytes for CAF sensing. CAF containing beverages were purchased from the local store. Coffee samples were prepared by using medium roasting degree coffee (100% Coffea arabica L. blend) Iperespresso capsule (illycaffè S.p.A., Trieste, Italy). Iperespresso coffee machine (mod. X2, illycaffè S.p.A., Italy) and tap water (total hardness 18-20°f) were used to prepare three different types of espresso beverages according to the typical Italian cup volume known as ristretto, regular or lungo[45].

Apparatus

Electrochemical measurements were conducted in a three-electrode single compartment glass cell using Ag/AgCl (3 M KCl) as reference electrode, platinum as counter electrode and bare glassy carbon electrode (GCE, MetrohmAutolab B.V., The Netherlands) with 2 mm active surface area as working electrode. The experiments were performed using a small electrochemical analyzer 910 PSTATmini (MetrohmAutolab B.V., The Netherlands). The data were collected, handled and analyzed using the PSTAT 1.0 (MetrohmAutolab B.V., The Netherlands) and OriginPro 7.5 (OriginLab Corporation, USA) softwares, respectively. The USC100TH ultrasonic bath (VWR, United Kingdom) was used for degassing.

Measurement procedures

Cyclic voltammetry (CV) and differential pulse voltammetry (DPV) techniques were used for the study of the electrochemicalbehaviour of CAF and its reliable determination as well as for real sample analysis. Firstly, in order to get the active surface area of the GCE clean, the standard procedure based on using polishing with alumina (average grain size of 0.3 µm) was performed followed by a electrochemical preconditioning of the electrode at +2.0 V for 30 s, prior to launching a measurement.

To select the appropriate supporting electrolyte for CAF sensing, three different strong acids in a concentration range from 0.01 up to 0.5 M were tested, including H_2SO_4, HNO_3 and $HClO_4$, with a fixed CAF concentration of 0.546 mM.Two consecutive cyclic voltammograms were recorded each time and the second measurement was the one used. For the optimization of the DPV parameters, the pulse potential, pulse time and scan rate were investigated from 10 to 200 mV, from 5 to 150 ms and from 2 to 30 mV/s, respectively.

A calibration curve was built by subsequent additions of an appropriate volume of caffeine stock solution (10 mM, in milli Q-water) in the electrochemical cell where 20 mL of H_2SO_4 0.1 M were present as supporting electrolyte. The caffeine concentration range evaluated was from 3 to2725 µM, and for each addition three consecutive DPV experiments were done.

Real samples analysis

All samples were analysed without any previous dilution or filtration steps. For carbonated soft drinks (i.e. Coca-Cola, Pepsi-Cola, Kofola, Red Bull) the samples were degassed for 3 minutes prior to analysis, using ultrasonic bath. The DPV measurements were performed into an electrochemical cell where 20 mL of supporting electrolyte were present and an appropriate volume of the particular beverage was added, i.e. 4 mL for soft drinks (Coca-Cola, Pesi-Cola, Kofola), 1mL for Red-Bull, and 0.2 mL in the case of espresso brews. The content of CAF was determined using standard addition method, by three consecutive additions of 0.8 mL of a standard stock solution of caffeine (10 mM in milli-Q water). After each addition 5 consecutive DP voltammograms were recorded.

Comparative UHPLC method

Ultra-high performance liquid chromatography (UHPLC) was performed using a 1290 Infinity LC system with DAD detector, equipped with a 4.6 mm × 150 mm, 2.7 µm 120 SB-C18 Poroshell column, for the analysis of the chromatogram LC Open lab was used (Agilent Technologies, Waldbronn, Germany). The experimental conditions were the followings: the mobile phases were aqueous formic acid (0.1%) and acetonitrile (flow rate equal to 1.2 mL/min), starting at 90% of aqueous phase, reaching 60% at 10 min, 50% at 12 min and then back to initial conditions. CAF concentration was determined by monitoring the absorbance at 273 nm.

The calibration curve was obtained by analysing different CAF solution in milli-Q water, investigating a concentration range from 0.12 to 1.03 mM. A good linearity was found within the entire concentration range studied.

For real sample analysis, all beverages were diluted with Milli-Q water 1:10 (for energy and soft drinks), 1:50 (espresso),the diluted solution were filtered on Phenex NY 0.2 µm filters, prior analysis. The concentration of CAF was determined using the calibration curve, and each sample was analysed five times. The calibration curve equation and an example of the analysis of a caffeinated beverage are reported in the Supplementary Material (SM).

Data analysis and statistical evaluation

The experimental results were evaluated usingOriginPro 7.5 software, and are reported with 95% confidence level interval. For the calibration curve, each point was obtained by the average peak intensity of three consecutive measurements, and the error bar was evaluated based on the standard deviation. The linearity was evaluated using the least-square regression method. The limit of detection (LOD) and limit of quantification (LOQ) were calculated using the 3σ and 10σ criterion, respectively.

With regards to the real sample analysis, in the case of the electrochemical method, the CAF content was determined by interpolation, following the standard addition methodology. For UHPLC analysis, the data are presented as the mean value of 5 repetitions.The error on the CAF content was evaluated according to the following formula:

$$\boldsymbol{error = t_{n-1,\alpha} \times Standard\ Deviation/SQRT\ (n)}$$

with n=5, α=0.05, and $\boldsymbol{t_{4,0.05} = 2.13}$.

For the paired t-test the QuickCalcs software (GraphPad Software Inc.) was employed. A more exhaustive description of the standard addition methodology and the statistical evaluation is present elsewhere[46].

4. Results and Discussion

Electrochemical behaviour study

The first step in the development of an electrochemical sensor is to study the behaviour of the analyte on the electrode's material, and find the best experimental condition (solvent, ionic strength, pH). In particular, the electrochemical behaviour of CAF was previously reported, on bare and modified electrode surfaces elucidating that the process is highly irreversible, as evidenced by the absence of a reduction signal in the reverse scan [24,31,47]. The process is well known to involve the transfer of 4 electrons and 4 protons, leading to the formation of a trimethyl uric acid derivative[48,49]. Generally, an acid medium is employed for electrochemical sensing of CAF. Therefore, in the present work, three strong acids (H_2SO_4, HNO_3, $HClO_4$) at different concentrations were evaluated as supporting electrolytes. Fig. 1 shows the effect of changes in concentration of H_2SO_4 , used as supporting electrolyte, in the electrochemical oxidation of CAF using CV. The impact of the different concentrations of HNO_3 and $HClO_4$ is reported in the SM (Fig. S1 and S2). When different acids were evaluated all at the same concentration of 0.1M, perchloric and nitric acids performed similarly while in the case of sulfuric acid a narrower and sharper peak was obtained together with a higher S/N ratio (fig S3 supporting material). A possible explanation for the difference maybe found in the variation in ionic strength between the monoprotic acids and the diprotic sulfuric acid. A similar observation has been reported recently by Chalupczok S. et al.[50], using RuO_2 who conclude that changes in ionic strength have significant impact even when concentrations and pHs of the solutions are the same. As evidenced in Fig. 1, the favourable voltammetric peak of CAF with a maximum at +1.45 V was achieved using H_2SO_4 at a concentration of 0.1 M. Increases in H_2SO_4 concentration resulted in a higher peak for CAF, however increase in the background current was also noticed. H_2SO_4. Sulphuric acid was used at 0.1 M as the optimal concentration, as it gave the highest S/N ratio (data shown in table S1 and fig S4). In addition, at high acid concentration (i.e. 1 M and 0.5 M) a broad band was observed in the direct scan at 1.6 V (figure S4). This signal is likely due to the oxidation of carbon atoms from the GCE surface in highly acidic conditions. Previous works in the literature [51–53] have reported that a change in

morphology of glassy carbon can be observed when sulfuric acid is employed and long electrochemical pre-treatments applied. However, in this proposed work, no long pre-treatments were done and no electrochemical signals of the oxidation of glassy carbon were recorded, which suggest that oxidation of the glassy carbon electrode is negligible under the experimental conditions used for this work. Additionally, short electrochemical pre-treatment steps were done to improve the repeatability of the oxidation signal. Both positive and negative potentials (-2.00, +1.00, +1.75, +2.00 V) were tested for different lapses time (results not shown), and the best option was found by applying +2.0 V for 30 s.

GCE is well known for adsorbing molecules on its active surface during the electrochemical measurement, usually leading to a decline of the peak of the particular analyte due to the surface passivation by analyte and/or products of its electrode reaction. In our case, in order to assess whether the redox reaction of CAF is controlled by adsorption or diffusion on the GCE, the effect of different scan rates was studied. The scan rate value was examined from 10 up to 500 mV/s in 0.1 M H_2SO_4 containing 1.25 mM CAF. Fig. 2 reveals that by increasing the scan rate, the oxidation peak shifted towards higher potentials, which is a typical behaviour for electrochemically irreversible systems. The linear relationship between the peak current of CAF (in μA) and the square root of the scan rate (mV/s) was noticed (inset of Fig. 2) with the following regression equation (Eq. 1):

$$\boldsymbol{Peak\ Current}\ (\mu\boldsymbol{A}) = \mathbf{5.8}(\pm\mathbf{1.8}) + \mathbf{4.2}(\pm\mathbf{0.2}) \times \boldsymbol{square\ root\ of\ scan\ rate} \qquad \boldsymbol{R^2} = \mathbf{0.984}$$

The low intercept value and good linearity indicate that the redox process of CAF on GCE is predominantly driven by diffusion. In addition, a plot of the logarithm analysis (inset of Fig. 2, Eq. 2) was appeared to be linear, with the slope value of 0.41, in close conformity with the theoretical value (0.50) for a diffusion-controlled process[54].

$$\boldsymbol{Peak\ Current}\ (\mu\boldsymbol{A}) = \mathbf{0.89}(\pm\mathbf{0.06}) + \mathbf{0.41}(\pm\mathbf{0.03}) \times \boldsymbol{log_{10} scan\ rate} \qquad \boldsymbol{R^2} = \mathbf{0.975}$$

Thus, the effect of adsorption in electrochemical CAF sensing may be considered as minor, even when using GCE as the working electrode.

Analytical performance evaluation

Prior to constructing the calibration curve for the determination of CAF, the instrumental settings of differential pulse voltammetry (DPV) have to be optimized to achieve the favourable analytical performance. This optimization involves the searching for suitable values of pulse potential (from 10 to 200 mV), pulse time (from 5 to 150 ms) and scan rate (from 2 to 30 mV/s). The results showed that the best compromise between sharpness of the oxidation peak of CAF and measurement period was found with a scan rate of 30 mV/s. With regards to the pulse potential (Fig. 3), its increase gave rise to the growth and widening of the oxidation signal of CAF and at the same time the background current sharply increased. Hence, the best setting was found to be 50 mV. The effect of the pulse time was also studied (inset of Fig. 3) and 10 ms was found to be the best value, since further increases caused a decrease in the CAF signal.

Having optimized the instrumental parameters of DPV, the calibration curve for CAF was obtained. It was found that the DPV gave a significant linear relationship of peak current against CAF concentration from 28 to 479 μM (the origin studied range was from 3 up to 2725 μM) according to the following equation (Eq. 3):

$$\boldsymbol{Peak\ Current}\ (\mu\boldsymbol{A}) = \mathbf{1.583}(\pm\mathbf{0.499}) + \mathbf{0.091}(\pm\mathbf{0.008}) \times \boldsymbol{caffeine\ concentration}\ (\mu\boldsymbol{M}) \qquad \boldsymbol{R^2} = \mathbf{0.992}$$

The limit of detection (LOD) and limit of quantification (LOQ) were found to be $\mathbf{2 \times 10^{-5}}$ and $\mathbf{5 \times 10^{-5}}$ M, respectively. The DPV records, demonstrating the distinct oxidation peaks for the various concentrations of CAF with the particular calibration curve, are reported in Fig. 4. The reproducibility of the method was evaluated by measuring 5 consecutive CVs of a 1.25 mM CAF solution with the reached relative standard deviation of peak current of 4.5 %. The low RSD value reveals the fact that GCE used in this work provides the precise measurements for CAF sensing. Overall, the analytical performance obtained is suitable for the analysis of commercialized caffeinated products, where CAF content is in the mM range. In addition the long-term stability of the working electrode is ensured by the high chemical inertness of glassy carbon[32,33].

Numerous analytical techniques and protocols have been previously developed and reported for the detection and quantification of CAF. An overview of the most recent analytical methods for the determination of CAF is presented in the table below (table 1), together with the limit of detection reported for each case.

Liquid Chromatographic methods are the most employed techniques for CAF detection, thanks to the excellent analytical performance (i.e. low sensitivity, wide linear range, selectivity and robustness) and the possibility to be applied with a variety of matrices. Other analytical techniques were investigated for the detection of CAF, like Capillary Electrophoresis, Nuclear Magnetic Resonance, Surface-Enhanced Raman Scattering. All these methods were found suitable for the determination of CAF content and the sensitivity was found to be lower compared to the voltammetric sensor developed in this work. On the other hand, when the focus is on the application of a sensing platform for an industrial application the proposed Glassy Carbon based sensor has many advantages, compared with the other methodologies. In fact, our device is small, portable and non-expensive; no hazard or highly pure solvents are required; and no pre-treatments are necessary.

With regards to previously developed electrochemical sensors for CAF they are mostly based on modified GCE and a comprehensive review on this topic was written by Švorc Ľ[21]. The functionalization of the surface of GCE was investigated using different types of materials like Nafion[47], metallic nanoparticles[25,55], polymers[56]. Comparing

with our bare electrodes the surface modification enhance the performance in terms of Limit Of Detection (which can as low as $\mathbf{1 \times 10^{-9}}$ M[57]). This high sensitivity is necessary for the analysis of non-caffeinated beverages (were traces of caffeine are still present) or biological samples were the concentration of CAF is low (micromolar range). On the other hand the long-life stability of the sensing device is an issue, and in many case the analytical performance is not maintained after one month[26,58,59]. In addition, the chemical modification of the surface has a significant impact on its production and costs, resulting in an increased final price of the sensor, which can limit its widespread applicability.
Therefore in the case of industrial applications involving the routine analysis of commercialized caffeinated beverages, modified electrodes although sensitive and precise are not suitable choices in terms of long life stability and costs. On the other hand the proposed bare GCE is a suitable alternative to the currently employed techniques, thanks to its adequate sensitivity at the required concentrations, higher simplicity and high long-term stability. Furthermore, the electrode-based sensor has been used regularly over a period of several months for the quantification of caffeine content in coffee samples, and no significant variations in its performance were observed, suggesting that in the conditions employed any changes in the morphology and properties of the glassy carbon electrode are not significant.

Interference study

The next step in the work focused on the evaluation of the specificity of the electrode when operating in the presence of interfering agents frequently found in commercialized drinks. In fact, common caffeinated beverages, such as coffee and soft drinks, contain other chemical species, which may interfere with the signal of CAF, thus significantly affecting the reliability of method. The study focused on the effect of glucose and sucrose, as these compounds are commonly present in various beverages. Although these substances are not usually oxidized on bare carbon electrodes, however, they may be adsorbed onto the working electrode surface, thus considerably affecting the analyte signal. The results revealed that the peak potential and shape of CAF signal are not substantially influenced by the presence of these substances up to 100 times higher concentration (SM, Fig. S5 and S6). However, a moderate change in the background current was recorded, especially in the case of glucose, which is probably due to its adsorption on the surface of the working electrode.
Subsequently, selectivity studies to evaluate the specificity of the detection towards structurally related compounds, such as theophylline, theobromine and paraxanthine, were also performed. Fig. S7 and S8 display the effect of the presence of theophylline and paraxanthine (both from 1:1 up to 1:10 concentration ratio), respectively. It was found that the oxidation of these dimethyl xanthines occurred at a lower potential comparing with CAF (+1.26 and +1.22 V for theophylline and paraxanthine, respectively). This peak-to-peak separation (towards CAF) led to no differences in the shape and position of CAF signal. On the other hand, the peak current of CAF decreased by approximately 10% when an equimolar concentration ratio between CAF and theophylline was present. In the case of paraxanthine, the oxidation peak of CAF increased negligibly (2%). The selectivity observed thus far is promising and provides important preliminary data for the potential use of GCE for the simultaneous detection and quantification of CAF and paraxanthine and/or theophylline. Moreover, in the case of theobromine, an increase in the CAF signal was observed in an equimolar ratio (Fig. S9). The DPV scan of a solution of 333.3 µM theobromine (not shown here) shows that under the experimental conditions, theobromine rendered two oxidation peaks at +1.10 and +1.42 V, the second one overlapping with CAF signal. Overall, when the concentration ratio between the interfering xanthines and CAF was higher (up to 10:1), a partial overlapping of the signals was observed for theophylline; in the case of paraxanthine a decrease of 50% in the intensity was noticed. However, this limitation was not expected to affect the reliable determination of CAF in caffeinated beverages (coffee, soft drinks) where the concentration of theophylline, theobromine and paraxanthine is negligible[60,61] compared to the target analyte. On the other hand, in the case of coffee samples, polyphenols are usually present in similar amount as CAF (2.14 g/L in the final brew)[62]. These compounds are electrochemically active, however, their oxidation peak potential (around 0-600 mV), is different from CAF. Besides, their oxidation is strongly suppressed in acidic conditions[63]. As a consequence, no significant voltammetric peaks attributing to polyphenols and affecting the CAF signal were observed during the analysis of coffee samples (Fig. S10).

Method validation

The validation of the data obtained using bare glassy carbon electrodes was obtained by the analysis of four different commercially available caffeinated beverages and three different espresso brews. The standard addition method was applied for quantification of CAF in order to limit the matrix effect and to prove that the accuracy was within the expected limits. Fig. 5 reflects an illustrative example of analysis of Coca-Cola sample using the developed platform. The results were compared with a reference UHPLC method.
The data presented in Table 2 clearly indicate that the results obtained by the new method (DPV) are in good agreement with that obtained using the UHPLC method. The employed conditions for the chromatographic analysis are reported in the Material and Methods section. The calibration curve was obtained using solutions of caffeine prepared in Milli-Q water and the equation obtained is reported below.

$$\boldsymbol{Signal\ Area\ (a.u.) = 6.698 + 4.611 \times caffeine\ concentration\ (ng/\mu L)}$$

A good linearity was found in the concentration range between 0.12 to 1.03 mM, with an $\boldsymbol{R^2 = 0.9997}$.In addition, the chromatographic analysis of real samples showed a clear and isolated CAF signal with a retention time of 5.30 min. An illustrative example of the UHPLC analysis is reported in SM (Fig. S11, S12). Besides, according to the paired t-test[46] under 95% confidence level, no statistically significant differences were noticed between the values found by these methods since calculated t value (1.04) was lower than the tabulated one (2.45 for $\alpha = 0.05$ and number of measurements $n = 6$). To

summarize, no significant interference of the other compounds present in the analysed coffee and soft drink samples was recorded and the developed method provided good accuracy for the determination of CAF in caffeinated beverages. Moreover, the proposed procedure is simple and convenient, since it does not involve any pre-treatment of the samples and can be used as innovative alternative to conventional analytical methods in CAF assessment and assurance for routine beverage analysis.

5. Conclusion

In the present work, bare GCE was evaluated as alternative sensing platform to chromatographic methods for routine analysis in food samples, using CAF as the model analyte. The proposed sensor was shown to allow the precise and selective analysis of CAF content in commercial preparations. The wide applicability of the sensor was assessed by the analysis of seven commercially available caffeinated beverages and the data were found to be in agreement with a standard UHPLC method, routinely employed by a coffee company. The advantages of using the glassy carbon electrode instead of the more complex modified ones are related to the absence of any problems connected with storage and long-term stability. Furthermore, the use of this simple unmodified electrode avoids the use of costly and time-consuming surface functionalisation steps. Therefore, bare glassy carbon electrodes thanks to the chemical inertness, relative low costs and simplicity, can be considered good candidates for the development of accurate and innovative devices for routine quality analysis in the food industry.

Ethic Statement
Ethic issue were not relevant for this work

Data Accessibility
The datasets supporting this article have been uploaded as part of the Supplementary Material and are available at Dryad (doi:10.5061/dryad.vs656pd)

Competing Interests
We have no competing interests

Authors' Contributions
L.R., E.D.A. contributed with the acquisition of the data. L.R.,M.S., L.S. contributes to the conception and design of the work, and analysis of the data. L.R., M.S., E.D.A., M.R. and L.S. have contributed during the drafting and revision process, assuring accuracy and integrity of the whole work. All authors have read and approved the manuscript.

Funding Statement
This work has been supported by the European Union's Horizon 2020 research and innovation programme under the Marie Sklodowska-Curie grant agreement No 642014 (IPCOS). LS would like to acknowledge the Grant Agency of the Slovak Republic (grant No. 1/0489/16).

References

1. Wu MYC, Hsu MY, Chen SJ, Hwang DK, Yen TH, Cheng CM. 2017 Point-of-Care Detection Devices for Food Safety Monitoring: Proactive Disease Prevention. *Trends Biotechnol.* **35**, 288–300. (doi:10.1016/j.tibtech.2016.12.005)
2. Weng X, Neethirajan S. 2017 Ensuring food safety: Quality monitoring using microfluidics. *Trends Food Sci. Technol.* **65**, 10–22. (doi:10.1016/j.tifs.2017.04.015)
3. Peris-Vicente J, Rambla-Alegre M, Durgavanshi A, Bose D, Esteve-Romero J, Marco-Peiro S. 2014 Xanthine Derivatives Quantification in Serum by Capillary Zone Electrophoresis. *J.* 068)
11. Alharbi O, Xu Y, Goodacre R. 2015 Simultaneous multiplexed quantification of caffeine and its major metabolites theobromine and paraxanthine using surface-enhanced Raman scattering. *Anal. Bioanal. Chem.* **407**, 8253–8261. (doi:10.1007/s00216-015-9004-8)
12. Janci T, Valinger D, Gajdos Kljusuric J, Mikac L, Vidacek S, Ivanda M. 2017 Determination of histamine in fish by Surface Enhanced Raman Spectroscopy using silver colloid SERS substrates. *Food Chem.* **224**, 48–54. (doi:10.1016/j.foodchem.2016.12.032)
13. Kim L, Mitrevski B, Tuck KL, (doi:10.1098/rsos.170324)
21. Švorc Ľ. 2013 Determination of caffeine: A comprehensive review on electrochemical methods. *Int. J. Electrochem. Sci.* **8**, 5755–5773.
22. Gnana GK, Amala S, Gowtham SM. 2017 Recent advancement, key challenges and solution in non-enzymatic electrochemical glucose sensors based on graphene platforms. *RSC Adv.* **7**, 36949–36976. (doi:10.1039/C7RA02845H)
23. Xie T *et al.* 2017 A facile molecularly imprinted electrochemical sensor based on graphene : application to the selective determination of thiamethoxam in grain. *RSC Adv.* **7**, 38884–38894.

Chromatogr. Sci. , 1121–1126.
4. Omar MMA, Elbashir AA, Schmitz OJ. 2017 Capillary electrophoresis method with UV-detection for analysis of free amino acids concentrations in food. *Food Chem.* **214**, 300–307. (doi:10.1016/j.foodchem.2016.07.060)
5. Stupak M, Kocourek V, Kolouchova I, Hajslova J. 2017 Rapid approach for the determination of alcoholic strength and overall quality check of various spirit drinks and wines using GC-MS. *Food Control* **80**, 307–313. (doi:10.1016/j.foodcont.2017.05.008)
6. Jeon DB *et al.* 2017 Determination of volatile organic compounds, catechins, caffeine and theanine in Jukro tea at three growth stages by chromatographic and spectrometric methods. *Food Chem.* **219**, 443–452. (doi:10.1016/j.foodchem.2016.09.184)
7. Zaky AS, Pensupa N, Andrade-Eiroa Á, Tucker GA, Du C. 2017 A new HPLC method for simultaneously measuring chloride, sugars, organic acids and alcohols in food samples. *J. Food Compos. Anal.* **56**, 25–33. (doi:10.1016/j.jfca.2016.12.010)
8. Heeger A, Kosinska-Caganzzo A, Cantergiani E, Andlauer W. 2017 Bioactives of coffee cherry pulp and its utilisation for production of Cascara beverage. *Food Chem.* **221**, 969–975. (doi:10.1016/j.foodchem.2016.11.067)
9. Palo M, Kogermann K, Genina N, Fors D, Peltonen J, Heinämäki J, Sandler N. 2016 Quantification of caffeine and loperamide in printed formulations by infrared spectroscopy. *J. Drug Deliv. Sci. Technol.* **34**, 60–70. (doi:10.1016/j.jddst.2016.02.007)
10. Kobayashi Y, Mayer SG, Park JW. 2017 FT-IR and Raman spectroscopies determine structural changes of tilapia fish protein isolate and surimi under different comminution conditions. *Food Chem.* **226**, 156–164. (doi:10.1016/j.foodchem.2017.01.

Marriott PJ. 2013 Quantitative preparative gas chromatography of caffeine with nuclear magnetic resonance. *J. Sep. Sci.* **36**, 1774–1780. (doi:10.1002/jssc.201201081)
14. Monakhova YB, Kuballa T, Tschiersch C, Diehl BWK. 2017 Rapid NMR determination of inorganic cations in food matrices: Application to mineral water. *Food Chem.* **221**, 1828–1833. (doi:10.1016/j.foodchem.2016.10.095)
15. Frizzarin RM, Maya F, Estela JM, Cerdà V. 2016 Fully-automated in syringe dispersive liquid-liquid microextraction for the determination of caffeine in coffee beverages. *Food Chem.* **212**, 759–767. (doi:10.1016/j.foodchem.2016.06.032)
16. Martins AR, Talhavini M, Vieira ML, Zacca JJ, Braga JWB. 2017 Discrimination of whisky brands and counterfeit identification by UV-Vis spectroscopy and multivariate data analysis. *Food Chem.* **229**, 142–151. (doi:10.1016/j.foodchem.2017.02.024)
17. Dinovitser A, Valchev DG, Abbott D. 2017 Terahertz time-domain spectroscopy of edible oils Subject Category : Subject Areas : Author for correspondence : *R. Soc. Open Sci.* **4**, 170275–170284.
18. Mercante LA, Scagion VP, Migliorini FL, Mattoso LHC, Correa DS. 2017 Electrospinning-based (bio)sensors for food and agricultural applications: A review. *Trends Anal. Chem.* **91**, 91–103. (doi:10.1016/j.trac.2017.04.004)
19. Cinti S, Arduini F. 2017 Graphene-based screen-printed electrochemical (bio)sensors and their applications: Efforts and criticisms. *Biosens. Bioelectron.* **89**, 107–122. (doi:10.1016/j.bios.2016.07.005)
20. Khashaba PY, Ali HRH, El-Wekil MM. 2017 Development of a novel and cost-effective redox sensor for voltammetric determination of pantoprazole sodium during pharmacokinetic studies. *R. Soc. Open Sci.* **4**, 170324–170337.

(doi:10.1039/C7RA05167K)
24. Tyszczuk-Rotko K, Beczkowska I. 2015 Nafion covered lead film electrode for the voltammetric determination of caffeine in beverage samples and pharmaceutical formulations. *Food Chem.* **172**, 24–29. (doi:10.1016/j.foodchem.2014.09.056)
25. Velmurugan M, Karikalan N, Chen S, Karuppiah C. 2016 Core-shell like Cu2O nanocubes enfolded with Co(OH)2 on reduced graphene oxide for the amperometric detection of caffeine. *Microchim. Acta* , 2713–2721. (doi:10.1007/s00604-016-1914-4)
26. Yiğit A, Yardim Y, Çelebi M, Levent A, Şentürk Z. 2016 Graphene/Nafion composite film modified glassy carbon electrode for simultaneous determination of paracetamol , aspirin and caffeine in pharmaceutical formulations. *Talanta* **158**, 21–29. (doi:10.1016/j.talanta.2016.05.046)
27. Sadok I, Tyszczuk-rotko K, Nosal-Wiercinska A. 2016 Bismuth particles Nafion covered boron-doped diamond electrode for simultaneous and individual voltammetric assays of paracetamol and caffeine. *Sensors Actuators B Chem.* **235**, 263–272. (doi:10.1016/j.snb.2016.05.087)
28. Lim JM, Ryu MY, Kim JH, Cho CH, Park TJ, Park JP. 2017 An electrochemical biosensor for detection of the sepsis-related biomarker procalcitonin. *RSC Adv.* **7**, 36562–36565. (doi:10.1039/C7RA06553A)
29. Yu L, Zhang P, Dai H, Chen L, Ma H, Lin M. 2017 An electrochemical sensor based on Co3O4 nanosheets for lead ions determination. *RSC Adv.* **7**, 39611–39616. (doi:10.1039/C7RA06269A)
30. Amidi S, Ardakani YH, Ranjbari E, Sepehri Z, Bagheri H. 2017 Sensitive electrochemical determination of rifampicin using gold nanoparticles/poly-melamine nanocomposite. *RSC Adv.* **7**, 40111–40118. (doi:10.1039/C7RA04865C)

Table 1

Analytical Method	Limit of Detection	Application	Reference
Liquid Chromatography	Usually in the range of $\mathbf{10^{-7}}$M but can be as low as $\mathbf{10^{-9}}$M.	Different matrix from beverages to biological samples (blood, urine, saliva)	[64–66]
Capillary electrophoresis	$\mathbf{5 \times 10^{-5}}$M	Serum samples	[3]
Nuclear Magnetic Resonance	$\mathbf{7 \times 10^{-7}}$M	Salivary Samples	[67]
Surface-Enhanced Raman Scattering	$\mathbf{2 \times 10^{-6}}$M	Tertiary solid mixture of paraxanthine theobromine and caffeine	[11]
Voltammetry Based on bare Glassy Carbon Electrode	$\mathbf{2 \times 10^{-5}}$M	Caffeinated Beverages	This work

Table 2

Commercial caffeinated beverage	**Determined CAF content* (g/L)**	
	Proposed DPV	**Reference UHPLC**
Regular espresso coffee	3.047 ± 0.142	3.170 ± 0.195
Lungo espresso coffee	1.709 ± 0.178	1.672 ± 0.153
Ristretto espresso coffee	4.843 ± 0.291	5.326 ± 0.139
Coca-cola	0.098 ± 0.010	0.095 ± 0.008
Pepsi-cola	0.100 ± 0.006	0.110 ± 0.010
Kofola	0.070 ± 0.010	0.063 ± 0.005
Red Bull	0.361 ± 0.097	0.311 ± 0.028

* 95% confidence interval calculated according [mean ± $t_{n-1,\,\alpha}$ SD/sqrt(n)]; $t_{4;\,0.05} = 2.13$

Figures

For final submissions, figures should be uploaded as separate files.

Figure and table captions

Fig. 1.

The effect of different concentrations of sulfuric acid for electrochemical oxidation of 0.546·mM CAF on GCE using cyclic voltammetry (scan rate of 100 mV/s).

Fig. 2.

CV records of 1.25 mM CAF for different scan rates (v): (a) 10, (b) 25, (c) 50, (d) 75, (e) 100, (f) 200, (g) 300, (h) 400 and (i) 500 mV/s in 0.1 M H_2SO_4 on GCE. The peak current as a function of square root of the scan rate and logarithmic analysis are appended in the inset.

Fig. 3.

DPV records of 0.44 mM CAF in 0.1 M H_2SO_4 on GCE for various pulse potentials: (a) 10, (b) 25, (c) 50, (d) 100, (e) 150 and (f) 200 mV. The optimization of pulse time: (a) 5, (b) 10, (c) 25, (d) 50, (e) 100 and (f) 150 ms appears in the inset.

Fig. 4.

DPV records for various CAF concentrations: (a) 0; (b) 28; (c) 53; (d) 86; (e) 135; (f) 199; (g) 263; (h) 356; (i) 479; (j) 627; (k) 841; (l) 1112, (m) 1724 and (n) 2725 µM in 0.1 M H_2SO_4 on GCE. DPV parameters: pulse potential of 50 mV, pulse time of 10 ms and scan rate of 30 mV/s. The dependence between the peak current and CAF concentration is appended in the inset.

Fig. 5.
DPV records of analysis of Coca-Cola sample using the standard addition method in 0.1 M H_2SO_4 on GCE after addition of 4 mL of sample and after spiking of 80, 160 and 240 µL of 10 mM CAF solution. DPV parameters: pulse potential of 50 mV, pulse time of 10 ms and scan rate of 30 mV/s. The analysis by standard addition method is depicted in the inset.

Table 1 . Comparison of different analytical techniques for caffeine determination, based on recently reported work.
Table 2. Real samples analysis of seven different caffeinated beverages (n = 5).

Rapid sucrose monitoring in green coffee samples using multienzymatic biosensor

Miroslav Stredansky[a,d], Luca Redivo[b]*, Peter Magdolen[c], Adam Stredansky[d], Luciano Navarini[e]

[a] Department of Analytical Chemistry, Faculty of Chemical and Food Technology, Slovak University of Technology, Radlinskeho 9, 81237 Bratislava, Slovak Republic

[b]Department of Chemistry and Biochemistry, School of Biological and Chemical Sciences, Queen Mary University of London, Mile End Road, London, E1 4NS, United Kingdom

[c] Institute of Chemistry, Slovak Academy of Sciences, Dubravska cesta 9, 84538 Bratislava Slovak Republic

[d] Biorealis s.r.o., Radlinskeho 9, 81107 Bratislava, Slovak Republic

[e] illycaffè S.p.A., Via Flavia 110, 34147 Trieste, Italy

*E-mail: l.redivo@qmul.ac.uk

Abstract

Amperometric biosensor utilizing FAD-dependent glucose dehydrogenase (FAD-GDH) for a specific sucrose monitoring in green coffee is described. FAD-GDH was co-immobilized with invertase and mutarotase on a thin-layer gold planar electrode using chitosan. The biosensor showed a wide linearity (from 10 to 1200 μM), low detection limit (8.4 μM), fast response time (50 s), and appeared to be O2 independent. In addition the biosensors exhibited a good operational (3 days) and storage (1 year) stability. Finally, the results achieved from the biosensor measurements of sucrose in 17 samples of green coffee (Coffea arabica, C. canephora and C. liberica) were compared with those obtained by the standard HPLC method. The good correlation among results of real samples, satisfactory analytical performance and simple use of the presented biosensor make it suitable for application in coffee industry.

Keywords: Sucrose; Biosensor; Green coffee; Rapid analysis, Amperometry

1. Introduction

Coffee is the most commercialized food product and most widely consumed beverage in the world. In 2010, coffee production reached 8.1 million tons worldwide which represents more than 500 billion cups. The cup

quality is affected primarily by the composition of green coffee being influenced with agricultural practices, environmental factors, variety and maturity (Farah, 2012). Sucrose is one of the major constituent of green coffee and is responsible for coffee flavour and quality (Yigzaw Dessaleng et al., 2007). It is an important precursor of taste and aroma developed during the roasting process. Besides Borém et al. (2016) recently found that the level of sucrose is a good discriminant marker for the beverage quality. For instance, the higher sucrose content is one of the reasons for the superior aroma and overall flavour of Arabica coffee in comparison to Robusta one. In fact, Arabica contains from about 6 to 11 % and Robusta from 3 to 7 % of sucrose in green beans (Ky et al. 2001; Campa et al., 2004; Knopp et al., 2006; Farah, 2012).

Several methods have been used for determination of sucrose in green coffee, including high performance liquid chromatography (HPLC; O'Driscoll, 2014; Borém et al., 2016), anion-exchange chromatography coupled to pulsed amperometric detection (Ky et al., 2001), enzymatic spectrophotometric method (Alcázar et al., 2005), near infrared spectroscopy (Aluka et al., 2016; Santos et al., 2016). However, these methods require expensive laboratory equipment and educated personnel. Moreover, the HPLC analyses are time-consuming. Biosensors can represent an alternative method to overcome these drawbacks (Monošík et al. 2012a). They exhibit rapid response, high selectivity, cost effectiveness, and they provide an option to perform analysis in situ due to their ability to be miniaturized. Various enzymatic compositions and detection principles were described for the construction of sucrose biosensors. Sole invertase (INV) was used for the thermometric (Thavarungkul et al., 1999) or fluorescent (Bagal-Kestwal et al., 2015) biosensors. The combination of INV, glucose oxidase (GOX) and mutarotase (MUT) was employed for conductometric (Soldatkin et al., 2013; Pyeshkova et al., 2015) and amperometric (Surareungchai et al., 1999; Gouda et al., 2001; Majer-Baranyi et al., 2008). The simultaneous use of INV and fructose dehydrogenase (FDH) was presented, too. However, FDH is relatively expensive enzyme and the GOX based biosensors are susceptible to oxygen concentration in the measuring media, which can lead to a decrease in the signal, and underestimation of measured values in cases where artificial mediators are used (Tang et al., 2001). Recently we have proposed the implementation of FAD-dependent glucose dehydrogenase (FAD-GDH) in the biosensor for glucose analyses in various beverages (Monošík et al., 2012b). This commercially available convenient enzyme exhibits no dependency on oxygen and a high stability.

The aim of the present study was to develop a sucrose biosensor based on the combination of three enzymes (INV, MUT, FAD-GDH) suitable for the rapid and selective sucrose analysis in green coffee and compatible with the portable analytical device Omnilab currently serving beverage producers as an alternative to classic analytical methods.

2. Experimental

2.1. Materials

Glucose dehydrogenase FAD-dependent (GDH-FAD, 1160 U mg^{-1} solid) was purchased from Sekisui Diagnostic (Tokyo, Japan), and is reported to have been isolated for *Aspergillus sp.*, invertase and mutarotase from Sorachim (Lausanne, Switzerland). Meldola blue, Azure A, Azure C, methylene blue, thionine, N-methylphenazonium methyl sulfate, sucrose, trehalose and chitosan from shrimp shells (85% deacetylated) were supplied by Sigma-Aldrich (St. Louis, USA). Potassium phosphate monobasic and potassium phosphate dibasic were purchased from Riedel-de Haen (Seelze, Germany). Water deionized by a Millipore Milli-Q purification system was used. All chemicals used were of analytical grade. Gold planar electrodes with diameter of 1.6 mm equipped with Ag/AgCl reference electrode (diameter 2 mm, screen-printed) deposited on the planar glass-epoxy-laminate substrate were obtained from Biorealis (Bratislava, Slovakia).

Nine different samples of green *Coffea arabica* L. beans (geographical origin: El Salvador, India, Ethiopia, Brazil, Indonesia, Tanzania, Colombia), five different samples of green *C. canephora* Pierre ex Froehner var. robusta beans (geographical origin: Indonesia, Ivory Coast, Vietnam, Tanzania, Cameroon) and three different samples of green *C. liberica* Bull ex Hiern beans (geographical origin: Indonesia) from commercial lots were used. *C. arabica* sample from El Salvador was a Low Caffeine Bourbon (BLC) cultivar.

2.2. Apparatus

Electrochemical measurements were performed with electrochemical analyzers Autolab M101 (Methrom Autolab, Netherlands) and Omnilab from Biorealis (Bratislava, Slovakia)

Reference HPLC assays were run on Waters 600E HPLC System (Waters, Milford, USA) equipped with the refractometer detector (model PU 4026, Philips, Eindhoven, Netherlands).

2.3. Preparation of biosensors

The planar gold electrodes were cleaned with Milli-Q water and ethanol. The immobilization of the enzymes on the electrode surface was carried out by their sandwiching between (1 % w/w) chitosan layers. Each layer was deposited after the previous one was dried. All enzymes were dissolved in Milli-Q water before procedure. The prepared biosensors were stored at room temperature in a desiccator until use. The details on the quantities of enzymes are given in Results and Discussion.

2.4. Preparation of green coffee samples

Green coffee beans were ground to a fine powder using a mixer mill Retsch MM400 (Retsch GmbH., Germany). Then 2 g of each sample were deposited into a 100-mL flask, mixed with 40 ml of deionized water, heated up to the boiling point agitated and left slowly until laboratory temperature. The extracts were subsequently filtered through a fine paper.

2.5. Amperometric measurements

Electrochemical measurements were performed with electrochemical analyzers Autolab M101 (Methrom Autolab, Netherlands) and Omnilab from Biorealis (Bratislava, Slovakia). Chronoamperometry was performed by applying selected constant potential (vs. Ag/AgCl) after inserting the biosensor in volume of a measuring solution either 1 mL in microtube or 10 mL in beaker under stirring at laboratory temperature. Values from -300 mV to +300 mV were tested for the optimization of working potential. The pH values of a 0.1 M phosphate buffer solution (PBS) were optimized from pH 5.0 to 8.0. Similarly, the suitable concentrations of electrochemical mediators (from 0.1 to 2 mM) in the working media were also investigated. The biosensors were stored after measurements in 0.1 M PBS of pH 6.0 at laboratory temperature (up to 10 hours) or at 4 °C (for longer operational stability studies). The biosensors were kept dry in a desiccator at laboratory temperature for the storage stability studies.

2.6. HPLC analysis

Reference HPLC assays of sucrose were run on Waters 600E HPLC System (Waters, Milford, USA) equipped with the refractometer detector (model PU 4026, Philips, Eindhoven, Netherlands). The analytical conditions were as follows: column Polymer IEX in H^+ form 250 mm x 8 mm, 8µm in diameter (Watrex, Bratislava, Slovakia); column temperature 80 °C and pressure 300 Psi; mobile phase Milli-Q water; flow rate 1.0 mL min^{-1}. Data were collected and processed by Clarity chromatography station DataApex (Prague, Czech Republic). Samples were diluted in a mobile phase and filtered through 0.22 µm Chromafil AO filters, Macherey-Nagel (Dűren, Germany) prior to analysis. Sugars were identified by comparison with retention times and co-elution of authentic standard solutions.

3. Results and discussion

The principle of the presented biosensor is illustrated in Figure 1. It is based on the amperometric detection of reduced electron acceptor, further referred to as mediator (Med), which is generated during the course of the

GDH-FAD-catalyzed oxidation of β-D-glucose formed from sucrose by the co-immobilized INV and MUT. The GDH-FAD enzyme was previously employed in the development of glucose specific biosensor and its specificity is reported in the work by (Monošík R. *et al*., 2012b). From this study, the high specificity for β-D-glucose of GDH-FAD enzyme was proved against other sugars, alcohols, and acids. The reduced mediator is oxidized on the electrode surface and the resulting current proportional to the analyte concentration is measured. Gülce et al. (1995) reported that phosphate ions used in the medium at a high concentration catalyse the conversion of α-glucose to β-glucose, eliminating the need for MUT. When we applied the high level of phosphates instead of MUT the biosensor response became sluggish. Another possible principal problem of the used enzyme cascade comes from the fact that glucose presented in real samples could cause an interference, but its content in green coffee is negligible in comparison with sucrose (Knopp et al., 2006; Smrke et al., 2015). Besides small amounts of glucose in coffee samples did not influence the results obtained by the sucrose biosensor because differential measurements were applied and the signal obtained by the biosensor without invertase (measuring only glucose) was subtracted from the signal of the sucrose biosensor (measuring sucrose + glucose).

3.1. Optimization of biocatalytic layer

The quantities of enzymes on the electrode surfaces were optimized from 0.5 to 15 U. The optimal amounts of 6.0 U of FAD-GDH, 1.75 U of MUT, and 2.5 U of INV were found for immobilization on the electrode. Higher enzyme loadings induce the significant current decrease, which is probably caused by a partial blocking of the electrode surface with the large mass of protein. By contrary, lower enzyme quantities led to the decline of biosensor sensitivities and narrow linear ranges. The enzymes were immobilized on the electrode surface by their sandwiching between chitosan layers. Similarly, to our previous works (Monošík et al., 2012b; Monošík et al., 2013), the chitosan concentration of 1 % (w/w) showed the best results. Finally, the addition of 1.5% of trehalose in the solution of enzymes before their spreading on the electrodes improved the sensibility and stability of the biosensors. The use of trehalose is a common practice to improve the long-term stability and activity of enzymes, especially in the dried state, which is the condition for the storage of the biosensor. The long-term storage stability results in an improved enzyme functionality and therefore sensor sensitivity. The mechanism of action of trehalose is explained in more details in other works (Kaushik & Bhat, 2003; Olsson, Jansson, & Swenson, 2016).

3.2. Optimization of working conditions

The pH of working media is a very important factor affecting the biosensor performance, particularly in the case of multienzymatic biosensors. The pH dependence of the presented biosensor was investigated over the range from 5.0 to 8.0 in 0.1 M PBS. The highest relative response was obtained at pH 5.75 which corresponds to the optimum of FAD-GDH (Monošík et al. 2012b) and it is the compromise between the optimum values of INV (3.5-4.0) and MUT (7.4) given by their supplier. The concentration of the PBS showed a low effect in the range from 0.025 to 2.0 M, and next experiments were performed in 0.1 M PBS.

The selection of a good electrochemical mediator is important for the good functionality, sensitivity and selectivity of the amperometric biosensors. The suitable mediator accelerates an electron transport from the enzyme to the electrode surface and determines the working potential. The possibility to apply low potential allows a substantial reduction of eventual interferences coming from electroactive compounds presented in real samples, such as polyphenols, ascorbate, etc. Green coffee contains a very high quantity of polyphenols (various chlorogenic acids), up to 12% of its dry weight (Farah, 2012). Chlorogenic acids showed oxidation peaks about +225 mV against Ag/AgCl reference electrode (Šeruga & Tomac, 2014). It means lower working potentials should be used to eliminate this interfering current of the oxidation of chlorogenic acids during sucrose measurements with biosensors. The use of mediators from groups of phenothiazine or phenoxazine dyes allows working at low potentials. Monošík et al. (2012b) utilized N-methylphenazonium methyl sulfate at +50 mV for the glucose biosensor based on FAD-GDH. Here we tested the following dyes: N-methylphenazonium methyl sulfate, Meldola blue, Azure A, Azure C, methylene blue and thionine. All of them showed the highest biosensoric responses between -200 and +50 mV (vs. Ag/AgCl). The best results derived from the use of 0.5 mM Azure C at -100 mV, which we chose for next study. No interferences from green coffee extracts were observed at these conditions using the bare electrode without enzymes. Therefore, this potential permits satisfactory sucrose measurement sensitivities and simultaneously avoids undesirable interferences.

3.3. Analytical performance

The analytical studies were performed at the optimal working conditions in 1 mL of PBS in microtube under stirring (at laboratory temperature) by additions of 10 mM sucrose solution. The resulting calibration plot (Figure 2) was linear over the range from 10 to 1200 μM with a correlation coefficients R^2 = 0.998 (n=11) (the equation is reported below).

$$y = 7.030\ (\pm 4.772) + 0.647\ (\pm 0.008) \times Sucrose\ concentration\ (\mu M)$$

The biosensor showed a detection limit of 8.4 μM with the sensitivity of 0.65 nA μM^{-1}. Limit of detection is based on signal/noise = 5. The time required to reach steady-state response was 50s. These results are comparable to those obtained with the amperometric biosensors reported previously (Surareungchai et al., 1999; Gouda et al., 2001; Majer-Baranyi et al., 2008; Vargas et al., 2013; Antiochia et al., 2014).

3.4. Reproducibility and stability

The reproducibility of the biosensor measurements was carried-out by consecutive addition of 10 μL of standard sucrose solution (10mM) in 1 mL PBS solution. The average response of the biosensor was 71.3 ± 1.8 nA (n=10, R.S.D.= 2.28%). This finding confirms the reliability of the biosensor for analysis of real samples.

Long-term storage stability of biosensors is one of the most important parameters in case of their potential commercial use. Humidity and high temperatures are the most negative factors, which can affect the storage stability of enzymatic biosensors. The presented biosensors held in a desiccator at room temperature without use, kept more than 90% of the initial response ability at least after 12 months. Moreover, they were resistant against 50 °C heat for at least 5 days, which proves the stability of the sensor for shipment also in summer. The stability monitoring yet continues. Among the described sucrose biosensors only the one reported by Antiochia et al. (2014) showed the comparable stability retaining 80% of the original response after 4 months.

Operational stability is also required for the evaluation of biosensor performance because describes the stability of the biosensor during routine analysis. To assess the capability of the sucrose biosensor for routine analysis standard sucrose solutions were measured in various intervals to simulate a real use. Between measurements, biosensors were stored in PBS at laboratory temperature and overnight at 4°C. The biosensors did not show any loss of activity after 60 analyses in a row and after 24 hours of use. All of them exhibited response ability above 75% after 4 days. Some sucrose biosensors based on combination of INV and GOX (Gülce et al., 1995; Surareungchai et al., 1999) or FDH (Vargas et al., 2013; Antiochia et al., 2014) showed comparable or better operational stabilities. But these biosensors are constructed using classical disc electrodes (Pt, Au, carbon paste) which are not convenient for a low-cost mass production. On the other hand, the here presented biosensor, have a simple concept, and is based on commercially available cheap planar electrodes, which are easily processable, and the enzyme and chitosan layers could be deposited onto the planar substrate by well-known printing techniques. Thus, a more frequent sensor exchange is acceptable.

3.5. Sucrose analysis in green coffee

Although the biosensor showed good analytical performance when using pure sucrose solutions, it was necessary to assess the performance of the biosensor with respect to more complex real samples and to compare the results with those obtained by a standard analytical method. It is an important step for a verification of biosensor's accurateness to measure real samples. Considering the linear range of the biosensor and the sugar levels in green coffee, the extraction by the 20-fold amount of water allowed direct biosensoric analyses without further dilution and any other pre-treatment. The sucrose determination was performed by successive injecting 10 μL of sample and calibration solution in 1 mL of PBS of pH 5.75 containing 0.5 mM Azure C. The measurements of 17 green coffee (*C. arabica*, *C. canephora* and *C. liberica*) samples were performed simultaneously with the standard HPLC method (Table 1). A satisfactory correlation was obtained between the biosensor and the HPLC techniques results. Figure 3 compares the performance of the proposed biosensor against the HPLC method. The obtained correlation equation and its linearity are reported below.

$$y = 0.059(\pm 0.311) + 0.995(\pm 0.047)x \qquad R^2 = 0.965$$

The correlation between the two set of data is good, as evident from the slope of the fitted line very close to 1 and the low intercept value. These data confirm the validity of the proposed biosensor for accurate and reliable sucrose analysis in green coffee beans.

As expected, no interferences coming from green coffee constituents were observed at the selected measuring conditions. This opens the possibility to adopt the rapid, easy and convenient application of the presented sucrose biosensor by coffee industry. The content of fructose and glucose measured by HPLC in the used samples was negligible. Only some African green coffee samples (Ethiopia, Cameroon, Tanzania, and Ivory Coast) contained slightly higher amounts of glucose (from 0.23 to 0.42 %) and fructose (from 0.24 to 0.95 %). These data were confirmed also by measuring with the glucose and fructose specific biosensors, described previously by our group (Monošík et al., 2012b; 2013).

4. Conclusions

A novel multienzymatic biosensor selectively quantifying sucrose in green coffee based on commercially available materials is reported. INV, MUT and FAD-GDH were co-immobilized between chitosan layers on the surface of thin-layer planar gold electrodes. The simple and effective immobilization technique provided long-term storage stability, low fabrication costs, and good analytical performance. The biosensor exhibited a wide linear range (10-1200 μM), low detection limit (8.4 μM), high sensitivity (0.65 nA μM^{-1}), short measuring time

(50 s) and interference-free measurements. It was successfully applied to sucrose analysis in green coffee samples, and validated through comparison with the reference HPLC method. Performance characteristics of this useful analytical tool make it appropriate for coffee industry, as valid alternative of standard analytical techniques. The developed biosensor is fully compatible with the small commercial biosensoric devices Omnilab and is now commercially available.

Acknowledgements

This work was supported by the Competence Center for SMART Technologies for Electronics and Informatics Systems and Services, ITMS 26240220072, funded by the Research&Development Operational Programme from the ERDF. LR would like to acknowledge the European Union's Horizon 2020 research and innovation programme under the Marie Sklodowska-Curie grant agreement No 642014 (IPCOS).

References

Alcázar, A., Jurado, J. M., Martín, J., Pablos, F. & González, A. G. (2005). Enzymatic-spectrophotometric determination of sucrose in coffee beans. *Talanta*, *67*, 760-766

Aluka, P., Davrieux, F., Ngugi, K., Omaria, R., Gerard, F., Leroy, T., Dufour, M. & Fabrice, P. (2016). The diversity of green bean biochemical compounds in robusta coffee (*Coffea canephora* Pierre ex A. Froehner) as evaluated by near infrared spectroscopy. *American Journal of Experimental Agriculture*, *12*, 1-13.

Antiochia, R., Gorton, L. & Mannina, L. (2014). Rapid determination of sucrose in fruit juices: A new sensitive carbon nanotube paste osmium-polymer mediated biosensor. *Journal of Food Research*, *3*, 101-112.

Bagal-Kestwal, D., Kestwal, R. M. & Chiang, B.-H. (2015). Invertase-nanogold clusters decorated plant membranes for fluorescence-based sucrose sensor. *Journal of Nanobiotechnology*, *13*, 30-40.

Borém, F. M., Figueiredo L. P., Ribeiro F. C., Taveira J. H. S., Giomo G. S. & Salva T. J. G. (2016). The relationship between organic acids, sucrose and the quality of specialty coffees. *African Journal of Agricultural Research*, *11*, 709-717.

Campa, C., Ballester, J.F., Doulbeau, S., Dussert, S., Hamon S. & Noirot M. (2004). Trigonelline and sucrose diversity in wild Coffea species. *Food Chemistry*, *88*, 39-43.

Farah, A. (2012). Coffee: Emerging Health Effects and Disease Prevention. In Yi-Fang Chu (Eds.). *Coffee constituents* (pp. 21-58). John Wiley & Sons, Inc. Blackwell Publishing Ltd.

Gouda, M. D., Thakur, M. S. & Karanth, N. G. (2001). Optimization of the multi-enzyme system for sucrose biosensor by response surface methodology. *World Journal of Microbiology & Biotechnology*, *17*, 595-600.

Gülce, H., Çelebi, S. S., Özyörük, H. & Yildiz, A. (1995). Amperometric enzyme electrode for sucrose determination prepared from glucose oxidase and invertase co-immobilizedin poly(vinylferrocenium). *Journal of Electroanalytical Chemistry*, *397*, 217-223.

Kaushik, J. K., & Bhat, R. (2003). Why is trehalose an exceptional protein stabilizer? An analysis of the thermal stability of proteins in the presence of the compatible osmolyte trehalose. *Journal of Biological Chemistry*, *278*, 26458–26465.

Knopp, S., Bytof, G. & Selmar, D. (2006). Influence of processing on the content of sugars in green Arabica coffee beans. *European Food Research Technology*, *223*, 195-201.

Ky, C.-L., Louarn, J., Dussert, S., Guyot, B., Hamon, S. & Noirot, M. (2001). Caffeine, trigonelline, chlorogenic acids and sucrose diversity in wild *Coffea arabica* L. and *C. canephora* P. accessions. *Food Chemistry*, *75*, 223-230.

Majer-Baranyi, K., Adányi, N. & Váradi, M. (2008). Investigation of a multienzyme based amperometric biosensor for determination of sucrose in fruit juices. *European Food Research Technology*, *228*, 139-144.

Monošík, R., Stredansky, M., Tkáč, J., & Šturdík, E. (2012a). Application of enzyme biosensors in analysis of food and beverages. *Food Analytical Methods*, *5*, 40-53.

Monošík, R., Stredansky, M., Lušpai, K., Magdolen, P. & Šturdík, E. (2012b). Amperometric glucose biosensor utilizing FAD-dependent glucose dehydrogenase immobilized on nanocomposite electrode. *Enzyme and Microbial Technology*, *50*, 227-232.

Monošík, R., Magdolen, P., Stredansky, M. & Šturdík, E. (2013). Monitoring of monosaccharides, oligosaccharides, ethanol and glycerol during wort fermentation by biosensors, HPLC and spectrophotometry. *Food Chemistry*, *138*, 220-226.

O'Driscoll, D. J. (2014). Analysis of coffee bean extracts by use of ultra-performance liquid chromatography coupled to quadrupole time-of-flight mass spectrometry. *MethodsX*, *1*, 264-268.

Olsson, C., Jansson, H., & Swenson, J. (2016). The Role of Trehalose for the Stabilization of Proteins. *Journal of Physical Chemistry B, 120*, 4723–4731.

Pyeshkova, V. M., Dudchenko, O. Y., Soldatkin, O. O., Kasap, B. O., Lagarde, F., Kurç, B. A. & Dzyadevych, S. V. (2015). Application of silicalite-modified electrode for the development of sucrose biosensor with improved characteristics. *Nanoscale Research Letters*, *10*, 149-155.

Santos, J. R., Viegas, O., Páscoa, R. N. M. J., Ferreira, I. M. P. L. V. O., Rangel, A. O. S. S. & Lopes, J. A. (2016). In-line monitoring of the coffee roasting process with near infrared spectroscopy: Measurement of sucrose and colour. *Food Chemistry*, *208*, 103-110.

Šeruga, M. & Tomac, I. (2014). Electrochemical behaviour of some chlorogenic acids and their characterization in coffee by square-wave voltammetry. *International Journal of Electrochemical Science*, *9*, 6134-6154.

Smrke, S., Kroslakova, I., Gloess, A. N. & Yeretzian, C. (2015). Differentiation of degrees of ripeness of *Catuai* and *Tipica* green coffee by chromatographical and statistical techniques. *Food Chemistry*, *174*, 637-642.

Soldatkin, O.O., Peshkova, V.M., Saiapina, O. Y., Kucherenko, I. S., Dudchenko, O. Y., Melnyk, V. G., Vasylenko, O. D., Semenycheva, L. M., Soldatkin, A. P. & Dzyadevych, S. V. (2013). Development of conductometric biosensor array for simultaneous determination of maltose, lactose, sucrose and glucose. *Talanta*, *15*, 200-207.

Surareungchai, W., Worasing, S., Sritongkum, P., Tanticharoen, M. & Kirtikara, K. (1999). Dual electrode signal-subtracted biosensor for simultaneous flow injection determination of sucrose and glucose. *Analytica Chimica Acta*, *380*, 7-15.

Tang, Z. R., Louie, R. F., Lee, J. H., Lee, D. M., Miller, E. E. & Kost, G. J. (2001). Oxygen effects on glucose meter measurements with glucose dehydrogenase- and oxidase-based test strips for point-of-care testing. *Critical Care Medicine*, *29*, 1062-70.

Thavarungkul, P., Suppapitnarm, P., Kanatharana, P. & Mattiasson, B. (1999). Batch injection analysis for the determination of sucrose in sugar cane juice using immobilized invertase and thermometric detection. *Biosensors & Bioelectronics*, *14*, 19-25.

Vargas, E., Gamella, M., Campuzano, S., Guzmán-Vázquez de Prada, A., Ruiz, M.A., Reviejo, A.J. & Pingarrón, J.M. (2013). Development of an integrated electrochemical biosensor for sucrose and its implementation in a continuous flow system for the simultaneous monitoring of sucrose, fructose and glucose. *Talanta*, *10*, 593-100.

Yigzaw Dessaleng, Labuschagne, M. T., Osthoff, G. & Herselman, L. (2007). Variation for green bean caffeine, chlorogenic acid, sucrose and trigolline contents among Ethiopian arabica coffee accessions. *Ethiopian Journal of Science*, *30*, 77-82.

Figure Captions

Figure 1: Sucrose bioelectrode reaction scheme.

Figure 2: Calibration curve obtained for the sucrose biosensor. Experimental conditions: 0.5 mM Azure C, 0.1 M phosphate buffer, pH 5.75, applied potential -100 mV vs. Ag/AgCl.

Figure 3: Graphical comparison between the sucrose determination in 17 green coffee sample, performed using the proposed electrochemical biosensor and the comparative HPLC methodology.

Figure 1

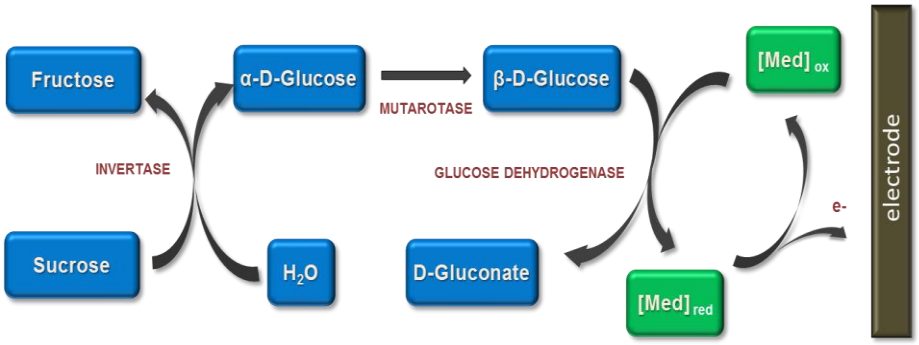

Figure 2

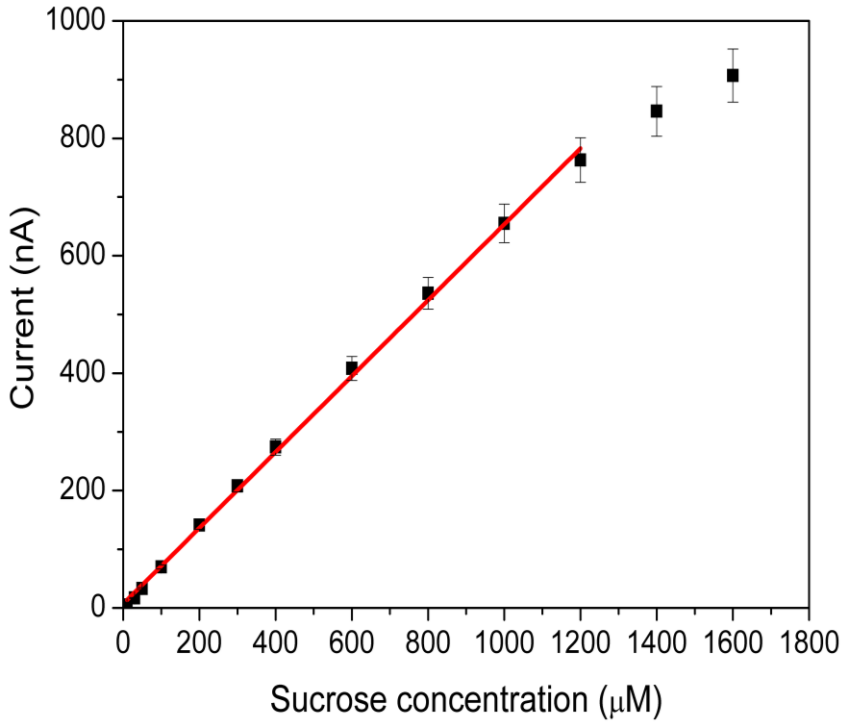

Figure 3

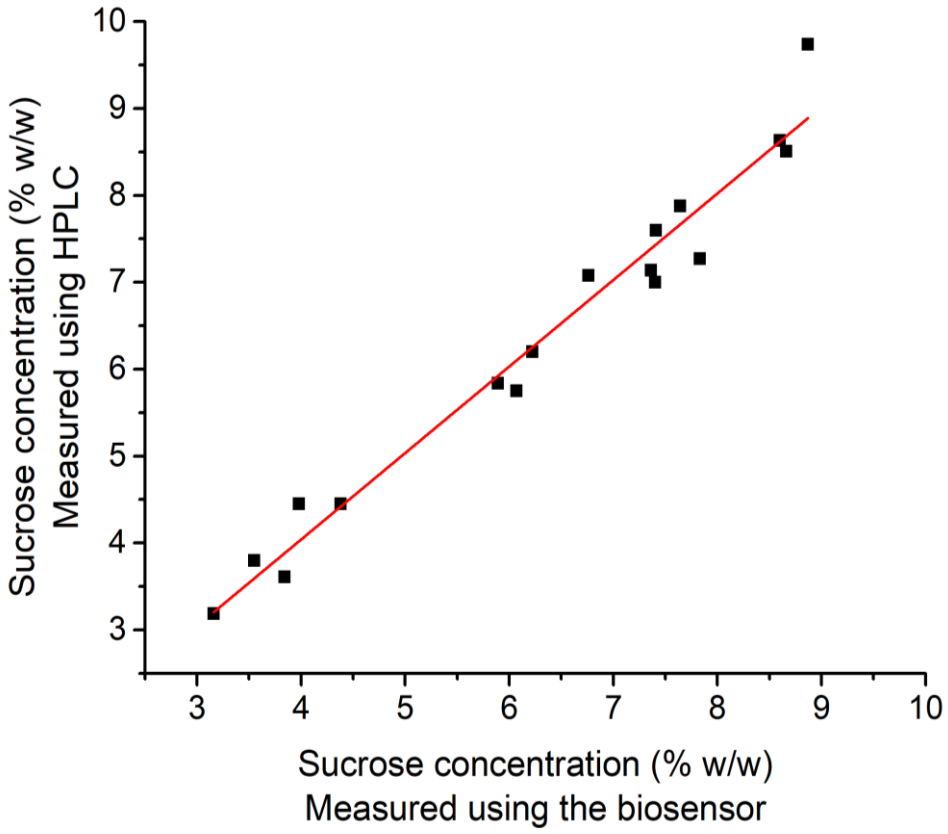

Table 1 Sucrose content analysis in 17 different green coffee beans using the developed biosensor and a comparative HPLC method.

Green coffee sample	Sucrose by biosensor (% w/w)	Sucrose by HPLC (% w/w)
Arabica BLC	8.66 ± 0.22	8.51 ± 0.30
Arabica India	7.36 ± 0.18	7.14 ± 0.25
Arabica Ethiopia	8.60 ± 0.31	8.63 ± 0.31
Arabica Brazil 1	8.87 ± 0.78	9.74 ± 0.35
Arabica Brazil 2	6.07 ± 0.18	5.75 ± 0.21
Arabica Brazil 3	7.41 ± 0.80	7.60 ± 0.27
Arabica Indonesia	7.83 ± 0.38	7.27 ± 0.25
Arabica Tanzania	7.64 ± 0.23	7.88 ± 0.28
Arabica Colombia	7.40 ± 0.62	7.00 ± 0.24
Robusta Indonesia	3.98 ± 0.26	4.45 ± 0.18
Robusta Ivory Cost	3.84 ± 0.16	3.61 ± 0.15
Robusta Vietnam	3.16 ± 0.14	3.19 ± 0.13
Robusta Tanzania	4.38 ± 0.19	4.45 ± 0.19
Robusta Cameroon	3.55 ± 0.21	3.80 ± 0.15
Liberica Indonesia 1	5.89 ± 0.44	5.84 ± 0.22
Liberica Asia	6.76 ± 0.25	7.08 ± 0.25
Liberica Indonesia 2	6.22 ± 0.12	6.20 ± 0.23

Journal Name

ARTICLE

Prediction of self-assembly of adenosine analogues in solution: a computational approach validated by isothermal titration calorimetry

Received 00th January 20xx,
Accepted 00th January 20xx

DOI: 10.1039/x0xx00000x

www.rsc.org/

Luca Redivo,[‡a] Rozalia-Maria Anastasiadi,[‡a] Marco Pividori,[b] Federico Berti,[c] Maria Peressi,[d] Devis Di Tommaso,[*a] Marina Resmini[*a]

The recent discovery of the role of adenosine-analogues as neuroprotectants and cognitive enhancers has sparked an interest in these molecules as new therapeutic drugs. Understanding the behavior of these molecules in solution and predicting their ability to self-assemble will accelerate new discoveries. We developed a density functional theory based approach to determine the structure and thermodynamic stability of molecular clusters of adenosine analogues in solution, using caffeine as a model. The work evaluated the behavior in solution at concentrations comparable to the ones found in biological samples. The method was validated as a tool for the prediction of the impact of small structural variations on self-assembly using paraxanthine. The computational results were supported by isothermal titration calorimetry experiments. The thermodynamic parameters enabled the quantification of the actual percentage of dimer present in solution as a function of concentration. The data suggest that both caffeine and paraxanthine are present in biological samples predominantly as monomers (99.95%).

Introduction

Adenosine is a naturally occurring purine nucleoside present in human cells and known to play a key role in a number of pathologies, including neurological disorders, cardiovascular and autoimmune diseases.[1–3] The role of adenosine and its interactions with the different receptors have been studied extensively[4–6] with consequent interests in adenosine analogues with agonist and antagonist activity[7] and methods that allow fast screening.[8] Among the different adenosine analogues, caffeine has been the most extensively studied compound. Research carried out on the health implications of caffeine intake has established important beneficial links to a number of illnesses, including depression,[9,10] type 2 diabetes, liver disease, Parkinson's disease[11] and stroke risk.[12] Caffeine is rapidly absorbed in the stomach and it is metabolised to three primary compounds: paraxanthine (82%), theophylline (11%) and theobromine (4%).[13–16] Studies have demonstrated that the key physiological effects of caffeine[17] are the result of interactions effect on the A_1 and A_2 subtypes of the adenosine receptor.[18] The role of caffeine as a cognitive enhancer[19] and also as a neuroprotectant[20] have also been reported recently. Caffeine used in combination with melatonin was shown to have antiamyloidogenic action, for the treatment of neurodegenerative diseases.[21] Borota *et al.* have demonstrated recently that caffeine enhances consolidation of long-term memory in humans.[22] There is considerable interest in understanding the mechanism by which caffeine and more generally adenosine analogues can interact with the different receptors, as this may subsequently lead to the identification of new compounds with drug-like activity. In this context, information on a new molecule's behaviour in solution and its potential for self-assembly, in particular its degree of complexation (*i.e.* dimers, trimers, tetramers) and relative distribution, is a key requirement. The self-association of caffeine has been studied experimentally using a variety of techniques including NMR[23–25] and FTIR spectroscopies,[26] dynamic light scattering (DLS),[27,28] osmometry,[29] fluorescence,[30] thermal analysis and differential scanning calorimetry (DSC).[31,32] These methods provide some characterisation although the experimental approach is time consuming and the data analysis is often model-dependent. Approaches based on computational studies have been explored widely to provide a useful tool to understand the behaviour of caffeine and adenosine analogues. Recent molecular dynamics (MD) simulations of aqueous caffeine solutions conducted by Tavagnacco *et al.* showed extensive aggregation, with caffeine molecules 'stacking their flat faces

[a] School of Biological and Chemical Sciences, Queen Mary University of London, Mile End Road, London, United Kingdom, E1 4NS.
[b] Dipartimento di Fisica, Università degli Studi di Trieste, via A. Valerio 2, Trieste, Italy, 34149.
[c] Dipartimento di Scienze Chimiche e Farmaceutiche, Università degli Studi di Trieste, via L. Giorgieri 1, Trieste, Italy, 34149.
[d] Istituto Officina dei Materiali, Consiglio Nazionale delle Ricerche, S.S. 14 km 163.5, Trieste, Italy.
[‡] These authors contributed equally.
Electronic Supplementary Information (ESI) available: See DOI: 10.1039/x0xx00000x

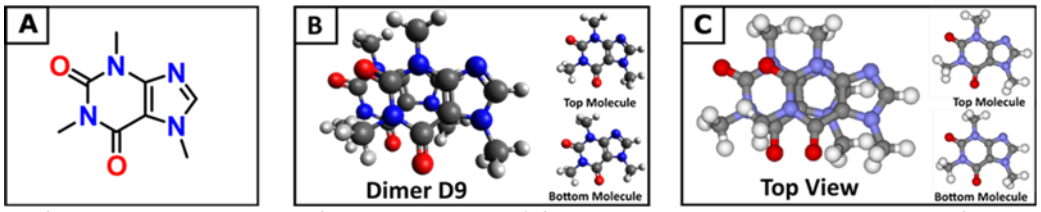

Fig.1 A) The skeletal chemical structure of caffeine. B) The most stable dimer structure (D9) in water as calculated using the proposed computational approach. C) The dimer structure of caffeine as found in the solid state.[47,48] For clarity the reciprocal orientations of the top and bottom molecules in the dimer in (B) and (C) are reported separately.

against one another like coins'.[33–35] These simulations were, however, conducted at the limit of solubility of caffeine in water (about 16 mg/mL) which is approximately five orders of magnitude higher than the concentration range at which caffeine is present in biological systems (0.002 mg /mL in plasma).[36–38] Such low concentrations would require simulation at the limit of MD techniques, containing hundreds of millions of solvent molecules. The continuum solvation method is an alternative technique for the determination of the structure and thermodynamic stability of molecular aggregates in solution,[39] where the solute (monomer, dimer, trimer, etc.) is treated at the density functional theory (DFT) level and the solvent is described using a polarizable continuum solvation model. Using this approach Senthilnithy *et al.*[40] and Bradley and Hendson[41] report highly positive (+12 kcal.mol^{-1}) dimerization free energies. However, the B3LYP density functional employed in these studies does not allow dispersion interactions to be described fully,[42] which can affect accuracy. The availability of a computational approach that can accurately predict changes in free energies, as a result of small structural alterations, would accelerate the identification of new candidate drugs. In this work, we present the a quantum mechanical continuum solvation approach as a computational tool that allows to predict the behaviour in solution of adenosine-analogues (AA) by determining the structure and thermodynamic stability of their molecular clusters $(AA)_n$ (n = 2-4), in solution, at concentrations comparable to the ones found in biological samples. Caffeine was initially used as model molecule; the same tool was then employed to predict the effect of small structural variations in the thermodynamics of molecular aggregation by studying paraxanthine (1,7-dymethylxanthine). The computational approach was then validated experimentally by using isothermal titration calorimetry, (ITC) to determine the association enthalpies for both molecules. The thermodynamic data were then used to assess the presence and distribution of potential clusters.

Results and Discussion

Caffeine dimers. Dimers are the first aggregates that can form during the process of self-association and their structure often corresponds to the building unit of the crystal that grows from solution.[43–46] The chemical nature of the intermolecular interactions in the caffeine dimer $(CAF)_2$ can therefore be expected to control its aggregation. The rearrangement of the electronic charge of the face-to-face and face-to-back dimeric configurations found in the X-ray crystalline structure of caffeine[47,48] (Figures S.4.b and S.4.b') confirms the presence of six C-H···O and C-H···N intermolecular hydrogen bonds between the two caffeine molecules.[49–52] Although the difference in electronegativity between C and H is small, the weak hydrogen bonds between caffeine molecules play an important role, together with the π-π stacking of the aromatic rings, in controlling the self-association process.[53]To evaluate all possible interactions, a computational approach based on probing the potential energy surface of caffeine dimers was applied. Nine low energy configurations for the caffeine dimer (**D1**-**9**) were identified (Figure S5) using this approach, five of which had never been reported before.[40,49] All these structures present the CH_3···X (X = N, O) interactions between the two caffeine molecules, therefore confirming their key role. Overall, the gas-phases energy (ΔE) and Gibbs free energy (ΔG°_{gas}) of dimerization were found to be negative. However, in aqueous solution the formation of dimers **D1**-**8** is thermodynamically unfavourable (Table S3). The exception is represented by dimer **D9** (Figure 1B), whose liquid-phase reaction is slightly exoergonic (ΔG^{*}_{dis} = –0.4 kcal.mol^{-1}). This therefore suggests that dimer **D9** can exist in aqueous solutions. There is much debate on the structural relationship between the most populated dimers in solution and the structural motifs found in solid state forms.[44,52,54] Figures 1B and 1C highlight how the structure of the most stable caffeine dimer in water (**D9**), obtained computationally, correlates very well with the structural synthon found in the X-ray crystal structure (Figure 1C). On this basis, it can be affirmed that the aggregation of caffeine obeys the so-called "link hypothesis",[52] according to which the transfer of structural information from the liquid- to the solid state-phase is linked to the presence in solution of stable "face-to-back" dimers. The effect of changes to the solvation environment on caffeine dimerization was also investigated by computing the formation of $(CAF)_2$ in three different systems: (i) methanol, a polar protic solvent with a static dielectric constant (ε) lower than water; (ii) acetone, a polar aprotic solvent, and (iii) chloroform, an apolar aprotic solvent. The Boltzmann averaged Gibbs free energy of dimerization (ΔG_D) obtained for all three systems (Table S.4) shows an inverse correlation between ΔG_D and the dielectric constants.

Caffeine clusters. Given the existing literature data on higher order clusters for caffeine, the next step focused on the stability of these systems.[28,35] The configuration of the

tetramer was obtained by stacking two dimers of type D9 (the most stable in water) on top of each other. The configuration of the trimer was then obtained by removing one caffeine molecule from the $(CAF)_4$. The optimised structures of the higher order clusters $(CAF)_3$, and $(CAF)_4$ are reported in Figure 2. Two reaction schemes were used to compute the thermodynamic stability of the trimer in solution: i) the condensation of D9 with an additional caffeine molecule, $(CAF)_{D9} + CAF \rightarrow (CAF)_3$; ii) the aggregation of three isolated CAF molecules, $3CAF \rightarrow (CAF)_3$. For the tetrameter (CAF_4), we considered the condensation of two D9 dimers, $2\ CAF_{D9} \rightarrow (CAF)_4$, as well as the association of one caffeine molecules to the trimer structure $(CAF)_3 + CAF \rightarrow (CAF)_4$. The energetics of formation of the caffeine trimer and tetramer are listed in Table S5 and show that the free energies of formation of these two species are approximately +2 kcal.mol^{-1}. Trimers and tetramers are unstable in water, compared to both monomer and dimer **D9**, and unlikely to be present in caffeine aqueous solutions at the concentrations found in biological samples.

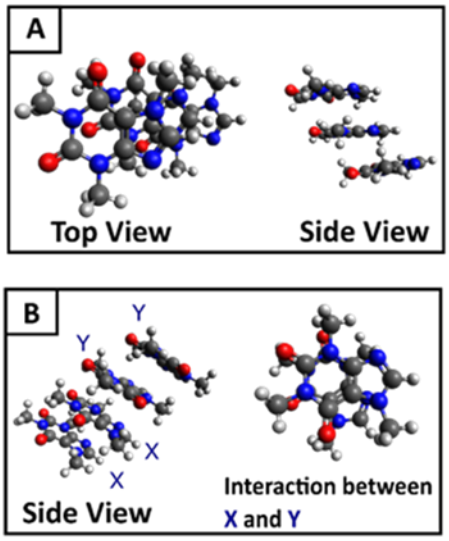

Fig. 1. Optimized structures of trimer (A) and tetramer (B) of caffeine. For the trimer a top and a side view are reported, which show that the reciprocal orientation of the molecules is retained. In the case of the tetramer, the first two neighbor molecules have an identical orientation while the second two caffeine are rotated, leading to a final geometry of the type (XX-YY). The interaction geometry between X and Y is reported.

Paraxanthine dimers. Understanding the molecular structure of the analogues and their self-association behaviour is an important requirement for the evaluation of interactions with biological receptors.[55] Paraxanthine (1,7-dimethylxanthine) is the major primary metabolite of caffeine, and although the two molecules are very similar in structure, the removal of one methyl group results in a tenfold decrease in the limit of solubility in water.[56] Compared with the nine low energy dimeric configurations of caffeine, the DFT tool identified 20 stable paraxanthine dimers (Figure S.6), showing the significant effect of small structural changes in caffeine analogues to the process of self-association. Two types of structures can be identified: (i) dimers D1, D2, D4 and D13, where the two paraxanthine units are linked by two lateral H-bonds; (ii) all remaining $(PX)_2$ structures, where the interaction is controlled by π-π stacking. Dimers D4 and D7 correspond to the synthons in the crystallographic structure of paraxanthine (Figure 3). The agreement between the simulated building units of paraxanthine in solution and its solid-state structure confirms the efficiency of the computational tool here adopted to identify possible dimeric structures of caffeine-analogues. In the gas phase most dimers are thermodynamically stable but in aqueous solution only the configurations forming π-π stacking interactions have a negative free energy of formation ($-1.0 < \Delta G_D < -0.1$ kcal.mol^{-1}) (Table S8). In water the Boltzmann averaged value for the dimerization of paraxanthine is –0.11 kcal.mol^{-1}. The comparison of the computed thermodynamic stability of the dimers of caffeine and paraxanthine shows that, despite their very small structural difference, the free energy of formation of $(PX)_2$ is 1.1 kcal.mol^{-1} lower than $(CAF)_2$. ITC experiments were conducted to obtain the enthalpy and equilibrium constant of dissociation of caffeine and paraxanthine in aqueous solution (Table S.9). The raw calorimetric data are characterised by positive heat peaks (Figures S8 and S10) indicating that the dissociation for both caffeine and paraxanthine is an endothermic process ($\Delta H_{diss} > 0$). Fitting of these data to a dimer dissociation model provides constants for both caffeine ($K_{diss} = 0.112 \pm 3.3x10^{-3}$ M) and paraxanthine ($K_{diss} = 0.03 \pm 1.8$ m $x10^{-3}$ M). In both cases, the Gibbs free energy of association ($\Delta G_{ass} < 0$) is negative. The ΔG_{ass} value obtained using ITC measurements (–1.3 kcal.mol^{-1}) is in excellent agreement with a previously reported DSC study ($\Delta G_{ass} = -1.5$ kcal.mol^{-1} at 25 °C).[57] The free energies of dimerization obtained computationally for caffeine (+0.92 kcal.mol^{-1}) and paraxanthine (-0.11kcal.mol^{-1}) are in agreement with the experimental data, when the standard deviation is taken into account (Table S9). The small values obtained in both cases (< 2 kcal.mol^{-1}) further confirm that the monomer and dimer can coexist in solution. The difference in the Gibbs free energies of association of caffeine and paraxanthine ($\Delta\Delta G_{ass} = \Delta G_{ass}^{CAF} - \Delta G_{ass}^{PX}$) obtained by ITC (0.6 kcal.mol^{-1}) and DFT (1.1 kcal.mol^{-1}) is also in excellent accordance, providing strong evidence for the use of our computational approach to predict the self-association behaviour in solution of adenosine-analogues. Having demonstrated that at low concentrations both caffeine

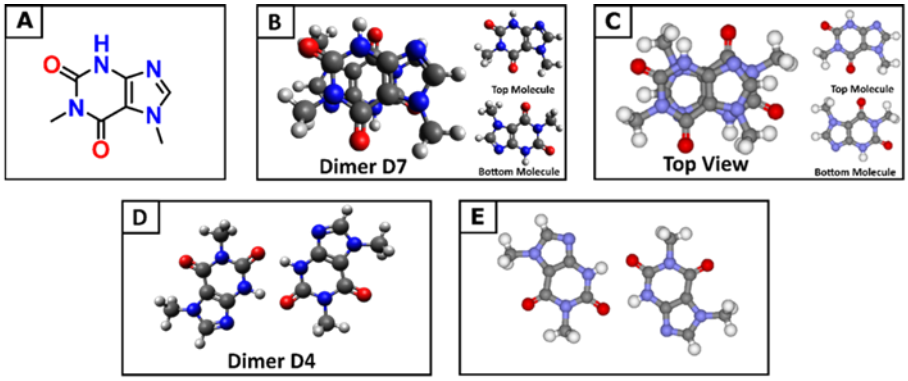

Fig.3 A) The skeletal chemical structure of paraxanthine. B) A stable dimer structure in gas phase as calculated using the proposed computational approach. C) The π-π stacking dimer synthon of paraxanthine as found in X-Ray structure. For the dimer structures (B, C) the top and bottom molecules are also reported separately to clarify the reciprocal orientation. D) A stable dimer structure linked only by H-bond interactions as calculated using the proposed computational approach. E) The later dimer synthon of paraxanthine as found in X-Ray structure.

and paraxanthine are potentially present in solution only as a combination of monomers and dimers, the experimental and computational values of ΔG_{ass} were used in the monomer-dimer model (equation 9 SI) to estimate the percentage of dimer in solution as a function of total concentration.[58]

Figure 4 shows the computational and experimental profiles of the dimer percentage in solution for caffeine and paraxanthine in the concentration range 5μM-50μM, which is close to the one found in biological samples. The computational data consistently suggest a lower percentage of dimer in solution compared to ITC for both paraxanthine and caffeine. This is due to the value of ΔG_{ass} (DFT), for both moelcules, being slightly more positive than ΔG_{ass} (ITC). For both approaches, computational and ITC, paraxanthine is found to be present as dimer in higher concentrations compared to caffeine, which

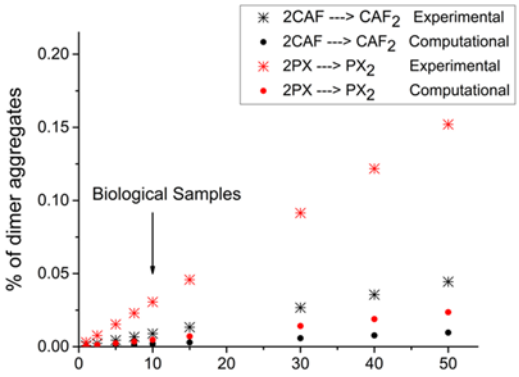

Fig.1 Comparison between the computational and experimental profiles of the population of dimers in solution at different total concentrations of caffeine and paraxanthine (μM). The computational points were determined using the Gibbs free energy of dimerization in water of the most stable dimers: caffeine (black circles) and paraxanthine (red circles). The experimental points were calculated using the Gibbs free energy of association determined using ITC experiments: caffeine: (black star) and paraxanthine (red star).

may be related to the differences in solubility of the two molecules (PX = 5mM, CAF 82mM). This behaviour is observed not only at very low concentrations, but also towards the limit of solubility (Figure S12). The results therefore indicate that both paraxanthine and caffeine, when evaluated at the concentrations found in biological samples (10μM[36]), are predominantly present as monomers, with less than 0.05% dimer in solution.

Conclusions

We presented a DFT-based computational tool that allowed the study of the self-assembly behaviour in solution of two adenosine-analogues like caffeine and paraxanthine, and we demonstrated that for both molecules the formation of higher order clusters is thermodynamically disfavored. The results were validated experimentally by ITC measurements, which provided values for the Gibbs free energy of association consistent with the DFT results. Significantly we showed how the computational approach allows to predict the effect of small structural changes on the chemical structure and thermodynamic stability of clusters resulting from self-assembly. In low concentration solutions, both caffeine and paraxanthine are mainly present as monomers, with less than 0.05% dimer present in 10μM solutions. The computational method used here is a valid tool to quantify the speciation of adenosine-analogues and predict accurately their behaviour in solution, which can provide a standardised and faster approach to the evaluation of potential new drug leads.

Conflicts of interest

There are no conflicts to declare.

Acknowledgements

This work has been supported by the European Union's Horizon 2020 research and innovation programme under the Marie Sklodowska-Curie grant agreement No 642014 (IPCOS). The authors would like to acknowledge Dr L. Navarini for helpful discussions. This research utilized Queen Mary's Apocrita HPC facility, supported by QMUL Research-IT.

References

1 G. Haskó, J. Linden, B. Cronstein and P. Pacher, *Nat. Rev. Drug Discov.*, 2008, **7**, 759.
2 E. S. Hayes, *Cardiovasc. Toxicol.*, 2003, **3**, 71–88.
3 T. W. Stone, S. Ceruti and M. P. Abbracchio, In Adenosine Receptors in Health and Disease; Wilson, C. N. Mustafa, S. J., Eds.; *Springer Berlin Heidelberg*, 2009; 535–587.
4 C. Cekic, D. Sag and Y. Li, *J. Immunol.*, 2012, **188**, 198–205.
5 P. Fishman, S. Bar-yehuda, L. Madi, I. Cohn, P. Tikva, I. C. Biopharma and P. Tikva, *Anticancer. Drugs*, 2002, **13**, 437–443.
6 A. K. Dhalla, J. C. Shryock and R. S. Belardinelli, *Current Topics in Medicinal Chemistry*, 2003, **1**, 369–385.
7 S. Crunkhorn, *Nat. Rev. Drug Discov.*, 2010, **9**, 21-26.
8 K. R. Jones, U. Choi, J. L. Gao, R. D. Thompson, L. E. Rodman, H. L. Malech and E. M. Kang, *Sci. Rep.*, 2017, **7**, 1–10.
9 S. Hall, B. Desbrow, S. Anoopkumar-Dukie, A. K. Davey, D. Arora, C. McDermott, M. M. Schubert, A. V. Perkins, M. J. Kiefel and G. D. Grant, *Food Res. Int.*, 2015, **76**, 626–636.
10 I. A. Ludwig, M. N. Clifford, M. E. J. Lean, H. Ashihara and A. Crozier, *Food Funct.*, 2014, **5**, 1695–1717.
11 J. V. Higdon and B. Frei, *Crit. Rev. Food Sci. Nutr.*, 2006, **46**, 101–123.
12 S. Ruiz-Crespo, J. M. Trejo-Gabriel-Galan, M. Cavia-Saiz and P. Muñiz, *Neurochem. Res.*, 2012, **37**, 1085–1090.
13 M. S. Caubet, W. Elbast and M. C. Dubuc, J. L. Brazier, *J. Pharm. Biomed. Anal.* 2002, **27**, 261–270.
14 M. S. Caubet, B. Comte and J. L. Brazier, *J. Pharm. Biomed. Anal.* 2004, **34**, 379–389.
15 V. Perera, A. S. Gross and H. Xu, A. J. McLachlan, *J. Pharm. Pharmacol.*, 2011, **63**, 1161–1168.
16 N. Y. Jordan, J. Y. Mimpen, W. J. M. Van den Bogaard, F. M. Flesch, M. H. M. Van de Meent and J. S. Torano, *J. Chromatogr. B*, 2015, **995**, 70–73.
17 M. A. Heckman, J. Weil and E. G. De Mejia, *J. Food Sci.*, 2010, **75**, R77–R87.
18 B. B. Fredholm, K. Bättig, J. Holmén, A. Nehlig and E. E. Zvartau, *Pharmacol. Rev.* 1999, **51**, 83–133.
19 A. Nehlig, A. *J. Alzheimer's Dis.*, 2010, **20**, S85–S94.
20 V. L. Batalha, D. G. Ferreira, J. E. Coelho, J. S. Valadas, R. Gomes, M. Temido-Ferreira, T. Shmidt, Y. Baqi, L. Buée and C. E. Müller, *Sci. Rep.* 2016, **6**, 31493–33157.
21 L. F. Zhang, Z. W. Zhou, Z. H. Wang, Y. H. Du, Z. X. He, C. Cao and S. F. Zhou, *Drug Des. Devel. Ther.*, 2015, **9**, 241–272.
22 D. Borota, E. Murray, G. Keceli, A. Chang, J. M. Watabe, M. Ly, J. P. Toscano and M. A. Yassa, *Nat. Neurosci.* 2014, **17**, 201–203.
23 I. Horman, B.Dreux and *Helv. Chim. Acta*, 1985, **68**, 72–75.
24 D. B. Davies, D. A. Veselkov, L. N. Djimant and A. N. Veselkov, *Eur. Biophys. J.*, 2001, **30**, 354–366.
25 N. D'Amelio, L. Fontanive, L. F. Uggeri, F. Suggi-Liverani and L. Navarini, *Food Biophys.*, 2009, **4**, 321–330.
26 M. Falk, M. Gil and N. Iza, *Can. J. Chem.*, 1990, **68**, 1293–1299.
27 S. Banerjee, D. Bhowmik, P. K. Verma, R. K. Mitra, A. Sidhhanta, G. Basu and S. K. Pal, *J. Phys. Chem. B*, 2011, **115**, 14776–14783.
28 L. Tavagnacco, Y. Gerelli and A. Cesàro, J. W. Brady, *J. Phys. Chem. B*, 2016, **120**, 9987–9996.
29 E. L. Farquhar and M. Downing, S. J. Gill, *Biochemistry*, 1968, **7**, 1224–1225.
30 S. Banerjee, P. K. Verma, R. K. Mitra and G. Basu, S. K. Pal, *J. Fluoresc.*, 2012, **22**, 753–769.
31 H. Bothe and H. K. Cammenga, *Thermochmica Acta*, 1983, **69**, 235–252.
32 A. Cesàro and G. Starec, *J. Phys. Chem.*, 1980, 84, 1345–1346.
33 L. Tavagnacco, S. Di Fonzo, F. D'Amico, C. Masciovecchio, J. Brady and A. Cesàro, *Phys. Chem. Chem. Phys.*, 2016, **123**, 13478–13486.
34 L. Tavagnacco, O. Engström, U. Schnupf, M. L. Saboungi, M. Himmel, G. Widmalm, A. Cesàro and J. W. Brady, *J. Phys. Chem. B*, 2012, **116**, 11701–11711.
35 L. Tavagnacco, P. E. Mason, G. W. Neilson, M. Saboungi, A. Cesàro, J. W. Brady, *J. Phys. Chem. B*, 2018, **122**, 5308–5315.
36 E. Schievano, C. Finotello and L. Navarini, S. Mammi, *Talanta*, 2015, **140**, 36–41.
37 V. Perera, A. S. Gross and A. J. McLachlan, *Biomed. Chromatogr.* 2010, **24**, 1136–1144.
38 F. Chen, Z. Y. Hu, R. B. Parker and S. C. Laizure, *Biomed. Chromatogr.*, 2017, **1**, 115–141.
39 R. F. Ribeiro, A. V. Marenich, C. J. Cramer and D. G. Truhlar, *Phys. Chem. Chem. Phys.*, 2011, **13**, 10908–10922.
40 R. Senthilnithy, M. S. S. Weerasingha and D. P. Dissanayake, *Comput. Theor. Chem.*, 2014, **1028**, 60–64.
41 E. S. Bradley, C. H. Hendon, *Food Funct.*, 2017, **8**, 1037–1042.
42 E. G. Hohenstein, S. T. Chill and C. D. Sherrill, *J. Chem. Theory Comput.*, 2008, **4**, 1996–2000.
43 S. Parveen, R. J. Davey, G. Dent and R. G. Pritchard, *Chem. Commun.*, 2005, **12**, 1531–1533.
44 R. J. Davey, S. L. Schroedera and J. H. Terhorst, *Angew. Chemie - Int. Ed.*, 2013, **52**, 2167–2179.
45 E. Gaines, K. Maisuria and D. Di Tommaso, *CrystEngComm.*, 2016, **18**, 2937-2945.
46 A. J. Cruz-Cabeza, R. J. Davey, S. S. Sachithananthan, R. Smith, S. K. Tang, T. Vetter and Y. Xiao, *Chem. Commun.*, 2017, **53**, 7905–7908.
47 C. W. Lehmann and F. Stowasser, *Chem. A Eur. J.*, 2007, **13**, 2908–2911.
48 J. D. Sutor, *Acta Crystallogr.*, 1965, **19**, 453–458.
49 V. I. Poltev, T. I. Grokhlina, E. González, A. Deriabina, A. Cruz, L. Gorb, J. Leszczynski, L. N. Djimant and A. N. Veselkov, *J. Mol. Struct.*, 2004, **709**, 123–128.
50 M. Karthika, L. Senthilkumar and R. Kanakaraju, *Comput. Theor. Chem.*, 2012, **979**, 54–63.
51 J. D. Sutor, *J. Chem. Scociety*, 1963, **1**, 1105–1110.
52 R. J. Davey, G. Dent, R. K. Mughal and S. Parveen, *Cryst. Growth Des.* 2006, **6**, 1788–1796.
53 E. A. Meyer, R. K. Castellano and D. François, *Angew. Chemie Int. Ed.* 2003, **42**, 1210–1250.
54 D. Di Tommaso, *CrystEngComm*, 2013, **15**, 6564–6577.
55 M. B. Patrascu, E. Malek-Adamian, M. J. Damha and N. Moitessier, *J. Am. Chem. Soc.*, 2017, **139**, 13620–13623.
56 Inc S. C. B. Paraxanthine technical Information https://www.scbt.com/scbt/product/paraxanthine-611-59-6.
57 S. J. Gill, M. Downing and G. F. Sheats, Biochemistry, 1967, **6**, 272–276.
58 T. Krishnan, W. C. Duer, S. Goldman and J. L. Fortier, *Can. J. Chem.*, 1979, **57**, 530–537.